Proceedings of the

6th Patras Workshop on Axions, WIMPs and WISPs

PATRAS 2010

July 5–9, 2010

Zürich, Switzerland

Editors: Laura Baudis, Marc Schumann

Verlag Deutsches Elektronen-Synchrotron

Impressum

Proceedings of the 6th Patras Workshop on Axions, WIMPs and WISPs (PATRAS 2010)
July 5–9, 2010, Zürich, Switzerland

Conference homepage
`http://axion-wimp2010.desy.de/`

Slides at
`http://axion-wimp2010.desy.de/e30/`

Online proceedings at
`http://www-library.desy.de/confprocs.html`

Editors:
Laura Baudis and Marc Schumann
November 2010
DESY-PROC-2010-03
ISBN 978-3-935702-48-5
ISSN 1435-8077

Published by
Verlag Deutsches Elektronen-Synchrotron
Notkestraße 85
22607 Hamburg
Germany

Organizing Committee

Laura Baudis and Marc Schumann
Physik Institut,
University of Zurich
Winterthurerstr. 190
8057 Zurich
Switzerland

Joerg Jaeckel,
Institute for Particle Physics Phenomenology (IPPP),
Durham University,
South Road
Durham DH1 3LE
United Kingdom

Axel Lindner and Andreas Ringwald,
Deutsches Elektronen Synchrotron (DESY),
Notkestraße 85
D-22607 Hamburg,
Germany

Konstantin Zioutas,
Department of Physics,
University of Patras,
26504 Rio,
Greece

Conference Secretary and Local Organization

Carmelina Genovese,
Physik Institut,
University of Zurich
Winterthurerstr. 190
8057 Zurich
Switzerland

Barbara Wittmann,
Deutsches Elektronen Synchrotron (DESY),
Notkestraße 85
D-22607 Hamburg,
Germany

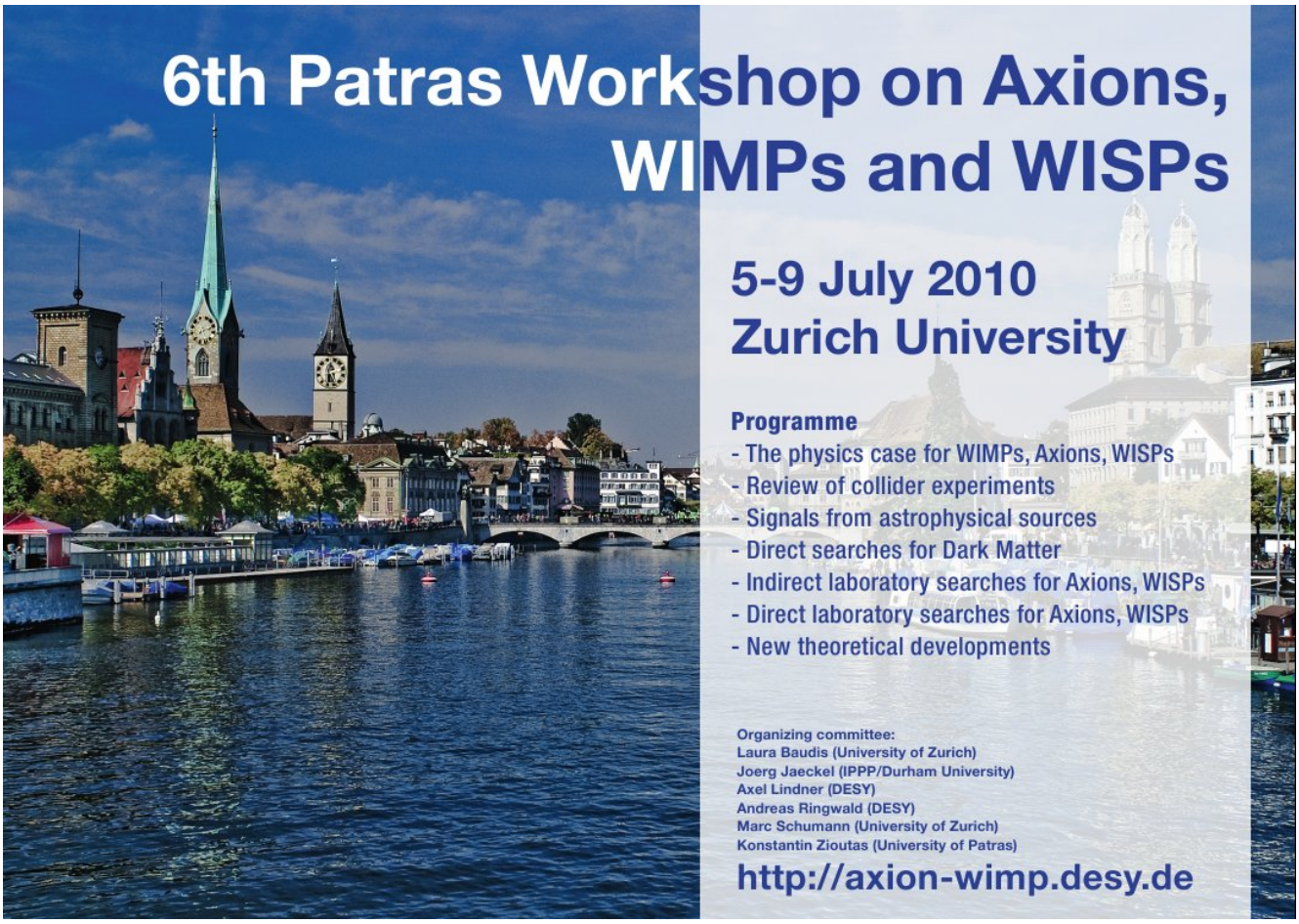
6th Patras Workshop on Axions, WIMPs and WISPs
5-9 July 2010
Zurich University
Programme
- The physics case for WIMPs, Axions, WISPs
- Review of collider experiments
- Signals from astrophysical sources
- Direct searches for Dark Matter
- Indirect laboratory searches for Axions, WISPs
- Direct laboratory searches for Axions, WISPs
- New theoretical developments
Organizing committee:
Laura Baudis (University of Zurich)
Joerg Jaeckel (IPPP/Durham University)
Axel Lindner (DESY)
Andreas Ringwald (DESY)
Marc Schumann (University of Zurich)
Konstantin Zioutas (University of Patras)
http://axion-wimp.desy.de

Preface

The 6th Patras Workshop on Axions, WIMPs, and WISPS took place from July 5–9, 2010, at the University of Zurich, Switzerland. We are more than happy that the number of participants has increased again. A total number of 76 participants from all around the world gathered together to discuss the most recent experimental and theoretical progress on the following questions:

- What do we know about the Dark Universe?
- How do we directly search for Axion, WIMPs and WISPs?
- Can we constrain or detect these particles by indirect astrophysical observations?
- What can we learn from neutrinos and collider experiments, in particular from the LHC?
- Are there new, "crazy" ideas out there?

A session dedicated to visions for the future, including statment from the large laboratories CERN, DESY, and LNGS, where some of this research is performed, and the annual *Axion Strategy Workshop* completed the meeting.
We express our gratitude to the scientists from the many countries who followed our invitation and contributed to the success of this meeting, as well as to our scientific co-organizers.
From the beginning, the idea of the Patras workshops has been to bring together theorists and experimentalists working in the wide field of axions, WIMPs and WISPs in a fruitful and inspiring atmosphere, which allows plenty of time for discussions and exchange of ideas. This aim has been successfully achieved once more, and we are looking forward to the 7th Patras Workshop, which will be held on the Greek island Mykonos from June 26–July 1, 2011, organized by the University of Patras.

Laura Baudis and Marc Schumann

Acknowledgements

The organizers would like to thank the Dean of Natural Sciences at Univerity of Zurich, DESY, CERN, the IPPP Durham, and the University of Patras for support. Special thanks also to the local conference secretary Carmelina Genovese (UZH) and to Barbara Wittmann (DESY) for creating the online presence of the conference.

The organizing committee

Contents

Chapter 1

Axions, WIMPs, WISPs, and Neutrinos in the Universe

Fundamental physics from astronomical observations

Raul Jimenez[1]

[1]ICREA & Institute for Sciences of the Cosmos (ICC), University of Barcelona, Spain

DOI: http://dx.doi.org/10.3204/DESY-PROC-2010-03/jimenez_raul

Current and forthcoming astronomical observations are providing enough data as to address some of the fundamental questions in physics, such as: what is the mass of neutrinos, are neutrinos Majorana or Dirac and what is the nature of the dark matter particle? In this talk I will provide an overview of how these questions can be answered by astronomical observations.

1 Introduction

Astronomy is a peculiar science, as one does not do experiments, it simply observes the sky. The amount of information contained in the sky is finite, thus one can wonder if observations can extract all such information, and if so, what can be learned about fundamental physics. It turns out we already have one example where all information in the sky has been extracted. This is the case of the Planck satellite and the temperature of the cosmic microwave background. This satellite has performed a cosmic variance limited observation of the full sky; nobody ever will need to repeat it. Unfortunately, we have not reached the same status with other interesting probes, such as the polarization of the cosmic microwave background and the angular postions and redshifts of galaxies. However, it is not farfetched to think that at the end of this century we will have extracted all information in the sky at most wavelengths of the electromagnetic spectrum. In any event, even today, we have already obtained significant constraints on fundamental physics using astronomical observations. Here I will describe what our current robust limits are on the mass of neutrinos, how we can discover if they are Majorana or Dirac and what can be said about the nature of dark matter. Most of the material has been presented elsewhere [1, 2, 3] and I refer the interested reader to those papers for full details.

2 Robust neutrino masses

In [1] we have shown that probes of the cluster mass function and increased precision on the Hubble constant can break key degeneracies with CMB observations and yield excellent constraints on both the number of species and sum of the masses of cosmological neutrinos. When the expansion history is fixed to ΛCDM, current constraints on H_0 [4] and the cluster mass function [5] constrain $\sum m_\nu < 0.4$ eV at 95% confidence. This bound relaxes to 0.5 eV in the two extended models we considered: wCDM, and the dark coupling model of [6], which allowed curvature, w, and coupling strength ξ to vary. Probing the mass function using X-ray

clusters, [7] combine their data with WMAP5+BAO+SN and find $\sum m_\nu < 0.33$ eV in a wCDM cosmology, though the systematic errors still must be clearly quantified. The optimistic upper bound available from current data, $\sum m_\nu \sim 0.3$ eV, almost excludes the scenario in which the neutrino masses are quasi-degenerate. The constraint on the number of relativistic species $N_{\rm rel}$ from probes of the cluster mass function has not been widely explored so far. We find that the combination of WMAP5, [4] H_0, and the maxBCG cluster mass function constraint provides an excellent constraint: $N_{\rm rel} = 3.76^{+0.63}_{-0.68}$. However, we point out that this constraint does not improve when BAO and SN data are also included; those data sets have been shown to have excellent constraining power on both Ω_k and w.

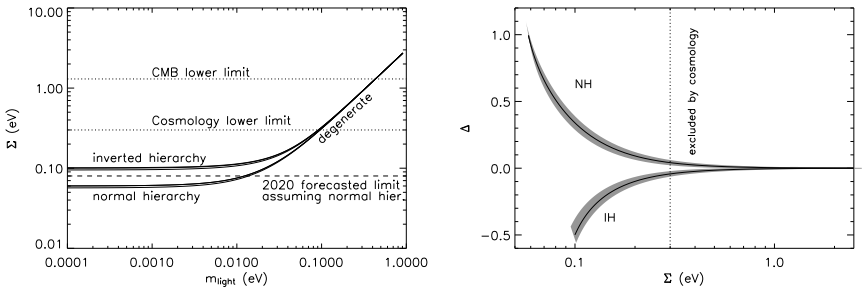

Figure 1: Left: constraints from neutrino oscillations and from cosmology in the m-Σ plane. Right: constraints from neutrino oscillations (shaded regions) and from cosmology in the Σ-Δ plane. In this parameterization the sign of Δ specifies the hierarchy.

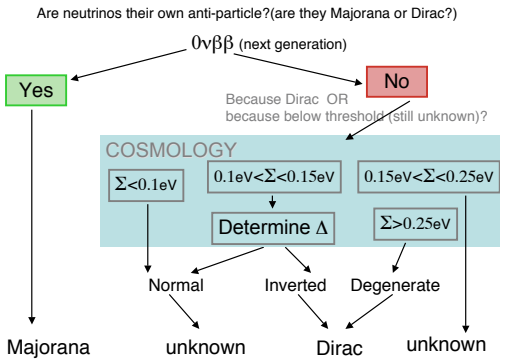

Figure 2: Future neutrinoless double beta decay ($0\nu\beta beta$) experiments and future cosmological surveys will be highly complementary in addressing the question of whether neutrinos are Dirac or Majorana particles. Next generation means near future experiments whose goal is to reach a sensitivity to the neutrinoless double beta decay effective mass of 0.01 eV. We can still find two small windows where this combination of experiments will not be able to give a definite answer, but this region is much reduced by combining $0\nu\beta beta$ and cosmological observations.

3 Measuring neutrino hierarchy

The shape of the matter power spectrum contains information, in order of decreasing sensitivity, about the sum of neutrino masses, the amplitude of the mass splitting and the hierarchy (i.e., the mass splitting order). In [2] we introduced a novel parameterization of the neutrino mass hierarchy, Δ, that has the advantage of changing continuously between normal, degenerate and inverted hierarchies and whose sign changes between normal and inverted. The absolute value of Δ describes the maximum mass difference between the eigenstates. We stress that, current constraints from neutrino oscillations have ruled out large part of the parameter space given by the sum of the masses and the Δ parameter, leaving two narrow regions: for a fixed value of the total mass, the value of Δ for the normal hierarchy is related to that of the inverted one and $\Delta_{\rm NH} \simeq -\Delta_{\rm IH}$. It is the allowed region that cosmology should explore.

We found that the information about Δ accessible from the power spectrum shape yields a degeneracy: parameters values Δ and $-\Delta$ yield nearly identical power spectra and therefore that the likelihood surface in Δ is bimodal. This was not noted in the literature before and not taking this into account when using the Fisher matrix-approach to forecast future surveys performance may lead to spurious indications of a surveys ability to determine the hierarchy.

Detecting the signature of the hierarchy in the sky is therefore extremely challenging, and therefore we asked: can cosmology in the cosmic-variance limit, and for an ideal experiment, distinguish the neutrino heirarchy? or in other words, is there enough information in the sky to measure the neutrino hierarchy? To address these questions we considered ideal, full-sky, cosmic variance-limited surveys and found that substantial Bayesian evidence can be achieved assuming a minimal LCDM base model. Increasing the parameter space by including e.g. effective number of neutrino species, non-inflationary motivated shape of the primordial power spectrum, etc. weakens the constraints and makes a determination of the hierarchy not possible, even though the constraint on the total neutrino mass are less affected and remain still at an interesting level. Are such surveys feasible in the next $5-10$ years? There are two candidates for such surveys: a full extragalactic survey in the optical/ infrared like Euclid[1] and a full 21cm survey by the SKA[2]. Euclid will make an all sky Hubble-quality map for weak lensing and will directly trace the dark matter using this technique. The 21cm surveys provide the most un-biased indirect tracer of the dark matter distribution in the Universe and have negligible shot noise.

For the degenerate and inverted mass spectra, the next generation neutrinoless double beta decay experiments can determine if neutrinos are their own anti-particle. For the normal hierarchy, the effective electron-neutrino mass may even vanish. However, if the large-scale structure cosmological data, improved data on the tritium beta decay, or the long-baseline neutrino oscillation experiments establish the degenerate or inverted mass spectrum, the null result from such double-beta decay experiments will lead to a definitive result pointing to the Dirac nature of the neutrino mass. This is summarized in Fig. 2. If the small mixing in the neutrino mixing matrix is negligible, cosmology might be the most promising arena to help in this puzzle. Our work shows that depending on the total neutrino mass, there might be substantial evidence by cosmological data to infer the neutrino hierarchy.

[1] sci.esa.int/euclid
[2] www.skatelescope.org

4 Constraining beyond the standard model physics

Cosmological observations provide constraints on different distance measures: luminosity distance (as provided e.g., by supernovae), angular diameter distance (as provided e.g., by baryon acoustic oscillations) and even on the expansion rate or the Hubble parameter as a function of redshift z. Both luminosity distance and angular diameter distance are functions of the Hubble parameter. While combining these measurements helps to break parameter degeneracies and constrain cosmological parameters, comparing them helps to constrain possible deviations from the assumptions underlying the standard cosmological model (e.g. isotropy), or to directly constrain physics beyond the standard model of particle physics (e.g. couplings of photons to scalar or pseudo-scalar matter). The Etherington relation implies that, in a cosmology based on a metric theory of gravity, distance measures are unique: the luminosity distance is $(1+z)^2$ times the angular diameter distance. This is valid in any cosmological background where photons travel on null geodesics and where, crucially, photon number is conserved.

More exotic sources of photon conservation violation involve a coupling of photons to particles beyond the standard model of particle physics. Such couplings would mean that, while passing through the intergalactic medium, a photon could disappear or even (re)appear! interacting with such exotic particles, modifying the apparent luminosity of sources. In [3] we considered the mixing of photons with scalars, known as axion-like particles, and the possibility of mini-charged particles which have a tiny, and unquantised electric charge. Photon-conservation can be violated by simple astrophysical effects which give uniform attenuation such as gray dust. We have reported updated constraints on this effect.

More exotic sources of photon-conservation violation involve a coupling of photons to particles beyond the standard model of particle physics. We have focused on axion-like particles, new scalar or pseudo scalar elds which couple to the kinetic terms of photons, and mini-charged particles which are hidden sector particles with a tiny electric charge. Photons passing through intergalactic magnetic fields may be lost by pair production of light mini-charged particles. If the mixing between axion-like particles and photons is signicant, then interactions in the intergalactic magnetic elds will also lead to a loss of photons due to conversion into ALPs. However if the coupling between photons and ALPs is sufficiently strong, one-third of any initial ux will be converted into ALPs, and two-thirds into photons, resulting in a redshift-independent dimming of supernovae which we cannot constrain or exclude with cosmic opacity bounds.

The improved measurement of the cosmic opacity found in [3] leads to improved bounds on these exotic physics scenarios which are summarised in Fig. 13 of [3]. Future measurements of baryon acoustic oscillations, and an increase in the number of observations of high redshift supernovae will lead to further improvements in the constraints on physics beyond the standard model.

References

[1] Reid B. A., Verde L., Jimenez R., Mena O., 2010, JCAP, 1, 3
[2] Jimenez R., Kitching T., Peña-Garay C., Verde L., 2010, JCAP, 5, 35
[3] Avgoustidis A., Burrage C., Redondo J., Verde L., Jimenez R., 2010, arXiv, arXiv:1004.2053
[4] A. G. Riess et al., 2009, ApJ, 699, 539
[5] E. Rozo et al., 2010, ApJ, 708, 645
[6] M. B. Gavela, D. Hernandez, L. Lopez Honorez, O. Mena, S. Rigolin, 2009, JCAP, 7, 34
[7] A. Vikhlinin et al., 2009, ApJ, 692, 1060.

Motivation for Weakly Interacting SubeV Particles

Ignatios Antoniadis[*1]

[1]Department of Physics, CERN - Theory Unit, CH-1211 Geneva 23, Switzerland

DOI: http://dx.doi.org/10.3204/DESY-PROC-2010-03/antoniadis_ignatios

We review sources and physics of WISPs (weakly interacting subeV particles) from theories beyond the Standard Model, such as string theory or models involving non-trivial anomaly cancellation. In particular, we discuss extra short range forces, axion-like particles (ALPs) and extra $U(1)$s.

WISPs appear in several theories beyond the Standard Model. In particular, they are generic in string compactifications but have varying properties in different classes of models, such as supersymmetric compactifications with high string scale or models with low string scale and large extra dimensions. Examples of WISPs are: light pseudoscalars, extra $U(1)$s, light scalars, as well as their possible superpartners, giving rise to axions or in general ALPs[1], and extra short range forces.

Indeed, string compactifications lead to scalar moduli whose vacuum expectation values (VEVs) parametrize the geometry of the internal compactified space, such as the size of cycles, shapes, the string coupling itself, etc. These VEVs are arbitrary because moduli have no potential (at least) at the classical level, which creates a serious problem since all low energy couplings are functions of moduli. In supersymmetric compactifications the moduli are complexified with pseudoscalars coming from internal components of higher-rank antisymmetric tensors present in the low energy spectrum. The moduli stabilization is a long outstanding problem, necessary to provide moduli masses (avoiding experimental conflict from long range forces and cosmology) and to fix their VEVs (allowing computation of the low energy couplings). A moduli potential can be generated either by non-perturbative effects or by turning on fluxes for the internal components of the higher-rank gauge potentials, generalizing ordinary magnetic fields.

Another source of light ALPs and extra $U(1)$s is related to non-trivial anomaly cancellation. In fact, theories in which fermions have chiral couplings with gauge fields are known to suffer from *anomalies* – a phenomenon of breaking of gauge symmetries of a classical theory at one-loop level. Anomalies make a theory inconsistent (in particular, its unitarity is lost). The only way to restore its consistency is to arrange for an exact *cancellation* of anomalies between the various chiral sectors. This happens, for example, in the Standard Model (SM), where the cancellation occurs between quarks and leptons within each generation [1]. Another well studied example is the Green-Schwarz anomaly cancellation mechanism [2] in string theory. In this case the cancellation arises between the anomalous contribution of chiral matter of the closed string sector with that of the open string.[2]

*On leave from CPHT (UMR CNRS 7644) Ecole Polytechnique, F-91128 Palaiseau.

[1]ALPs are axion like particles with no particular relation between their mass and decay constant ($m_a f_a = m_\pi f_\pi$ for ordinary axions).

[2]Formally, the Green-Schwarz anomaly cancellation occurs due to the anomalous Bianchi identity for the field

Particles involved in anomaly cancellation may have very different masses. For example, the mass of top quark in the SM is much higher than the masses of all other fermions. However, gauge invariance should pertain at all energies, including those which are smaller than the mass of some particles involved in anomaly cancellation. The usual logic of field theory is that interactions, mediated by heavy fermions running in loops, are suppressed by the masses of these fermions [4]. The case of anomaly cancellation presents a notable counterexample to this famous "decoupling theorem" – the contribution of *a priori* arbitrary heavy particles should remain unsuppressed at low energies. As it was pointed out in [5], this is possible because anomalous (i.e. gauge-variant) terms in the effective action have topological nature and therefore are scale independent. As a result, they are not suppressed even at energies much smaller than the masses of the particles producing these terms via loop effects. This gives a hope to see at low energies some signatures of new physics.

In the following, we first discuss sources of new short range forces and microgravity experiments, then axion like particles and finally effects of non-trivial anomaly cancellation involving extra $U(1)$s.

1 5th force and microgravity experiments

Theories with large extra dimensions predict modifications of gravitation in the sub-millimeter range, which can be tested in "table-top" experiments that measure gravity at short distances. There are three categories of such predictions:
(i) Deviations from the Newton's law $1/r^2$ behavior to $1/r^{2+n}$, which can be observable for $n = 2$ large extra dimensions of sub-millimeter size.
(ii) New scalar forces in the sub-millimeter range, related to the mechanism of supersymmetry breaking, and mediated by light scalar fields φ with masses [6, 7]:

$$m_\varphi \simeq \frac{m_{susy}^2}{M_P} \simeq 10^{-4} - 10^{-6}\ \text{eV}\,, \tag{1}$$

for a supersymmetry breaking or string scale $m_{susy} \simeq 1 - 10$ TeV; they correspond to Compton wavelengths of 1 mm to 10 μm. A universal attractive scalar force is mediated by the so-called radion modulus field. Such a force can be tested in microgravity experiments and should be contrasted with the change of Newton's law due the presence of extra dimensions that is observable only for $n = 2$ [9, 10]. The resulting bounds from an analysis of the radion effects are [11]: $M_* \gtrsim 6\,\text{TeV}$.
(iii) Non universal repulsive forces much stronger than gravity, mediated by possible abelian gauge fields in the bulk [12, 13]. Such fields acquire tiny masses of the order of M_s^2/M_P, as in (1), due to brane localized anomalies [13]. Although their gauge coupling is infinitesimally small, $g_A \sim M_s/M_P \simeq 10^{-16}$, it is still bigger that the gravitational coupling E/M_P for typical energies $E \sim 1$ GeV, and the strength of the new force would be $10^6 - 10^8$ stronger than gravity.

In Fig. 1 we depict the actual information from previous, present and upcoming experiments [10, 8]. The solid lines indicate the present limits from the experiments indicated. The excluded regions lie above these solid lines. Measuring gravitational strength forces at short

strength of the closed 2-form. However, this modification of Bianchi identity arises from the 1-loop contribution of chiral fermions in the open string sector. A toy model, describing microscopically Green-Schwarz mechanism was studied e.g. in [3].

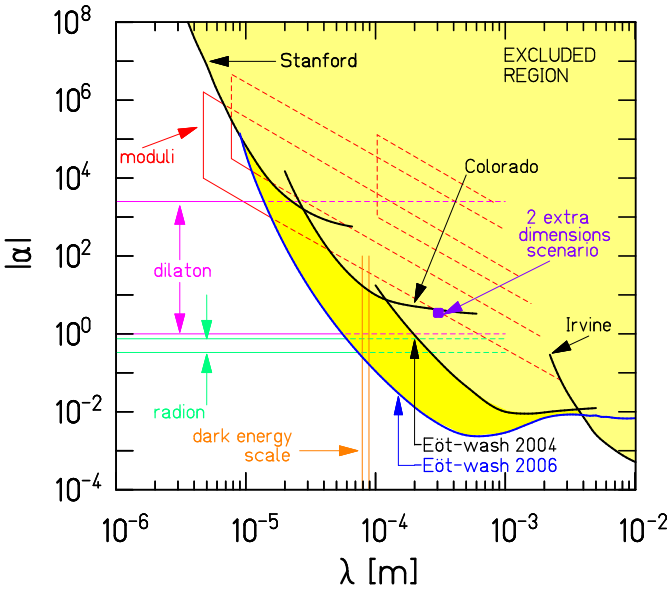

Figure 1: Present limits on new short-range forces (yellow regions), as a function of their range λ and their strength relative to gravity α.

distances is challenging. The horizontal lines correspond to theoretical predictions, in particular for the graviton in the case $n = 2$ and for the radion.

2 Axion Like Particles

As mentioned in the introduction pseudoscalar partners of moduli (Poincarée duals to two-index antisymmetric tensors in four dimensions) are often associated to perturbative shift symmetries and are thus candidates for axions or in general ALPs. Their common characteristic is the $\vec{E}\cdot\vec{B}$ type coupling to gauge fields, such as the photon:

$$\mathcal{L}_{a\gamma\gamma} = \frac{a}{4f_a}\epsilon_{\mu\nu\lambda\rho}F^{\mu\nu}F^{\lambda\rho} = -\frac{1}{2f_a}\epsilon^{\mu\nu\lambda\rho}\left(\partial_\mu a\right)A_\nu\,.F_{\lambda\rho} \tag{2}$$

Their mass m_a may be related to new strong interactions scales, or setup by the string scale, or suppressed by the compactification volume, or related to the supersymmetry breaking scale as in eq. (1). Similarly, their decay constant f_a may be related to a different physical scale independently of m_a but in general is strongly constrained from astrophysics to be $f_a \gtrsim 10^{10}$ GeV. Indeed the experimental bounds in the two-parameter space are shown in Fig. 2.

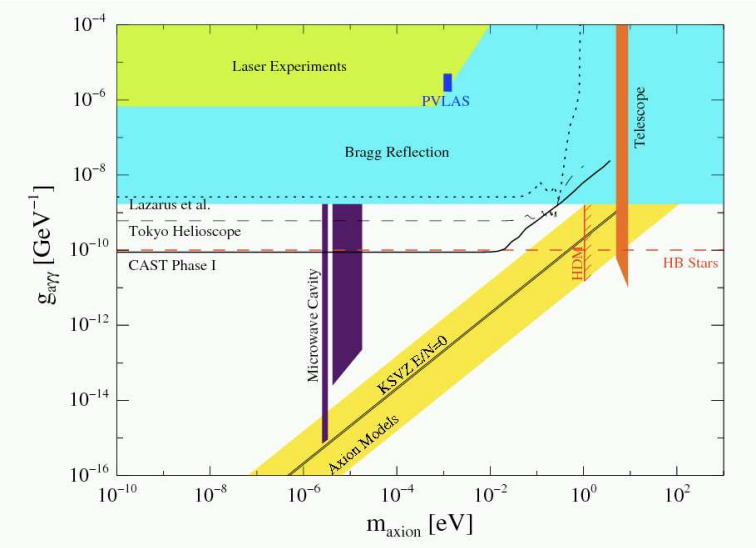

Figure 2: Present experimental bounds on ALPs.

3 Extra $U(1)$s and mixed anomaly involving photon

As discussed previously, non-trivial anomaly cancellation generically should involve at least one gauge field beyond the SM gauge sector. To reconcile this with existing experimental bounds, such an anomaly cancellation should take place between SM and "hidden" sector, with new particles appearing at relatively high energies. Here we concentrate on the case of one additional Abelian group. Extra $U(1)$ fields appear in many extensions of the Standard Model (see e.g. [14] and refs. therein). For example, additional $U(1)$s appear naturally in models in which $SU(2)$ and $SU(3)$ gauge factors of the SM arise as parts of unitary $U(2)$ and $U(3)$ groups (as e.g. in D-brane constructions of the SM [15, 16, 17, 18]). A common feature of these models is a non-trivial cancellation of anomalies between various sectors of the theory.

If the mixed anomaly cancellation between several groups of fermions involves the photon field A_μ, terms (often called *Generalized Chern-Simons*) can appear in the action

$$\mathcal{L}_{\rm CS} = -\frac{\kappa}{2}\epsilon^{\mu\nu\lambda\rho} X_\mu A_\nu F_{\lambda\rho} \tag{3}$$

where X_μ is an extra $U(1)$. Here κ is a dimensionless coupling constant. The Chern-Simons-like interaction (3) appears in various models (see e.g. [15, 18, 19, 20, 21, 22]). This term resembles an axion coupling to photon (2), under the identification of a derivatively coupled pseudo-scalar with the longitudinal part of the massive vector field X_μ, $\partial_\mu a \longrightarrow m_X X_\mu$, where m_X is the mass of this new vector boson. An analog of Peccei-Quinn scale f_a is played in this theory by the combination

$$f_a \leftrightarrow \frac{m_X}{\kappa} \tag{4}$$

Notice, that by making the coupling κ small, one can have $f_a \gg m_X$.

The simplest model involving the interaction term (3) is given by the effective action (with the masses generated via the Stückelberg mechanism):

$$S = \int d^4x \left(-\frac{1}{4}F_{\mu\nu}^2 - \frac{1}{4}X_{\mu\nu}^2 + \frac{m_X^2}{2}X_\mu^2 + \frac{m_\gamma^2}{2}A_\mu^2 + \frac{\kappa}{2}\epsilon^{\mu\nu\lambda\rho}X_\mu A_\nu F_{\lambda\rho} \right) \tag{5}$$

Here $X_{\mu\nu} = \partial_\mu X_\nu - \partial_\nu X_\mu$ is the field strength of the massive vector field X_μ. The Chern-Simons-like term is not gauge invariant under the electromagnetic gauge transformation $U(1)_{\rm QED}$. To amend this drawback, we introduced a mass to the photon (m_γ), consistent with all existing restrictions (see e.g. [23] for current bounds on the photon mass). Alternatively, one can impose an additional constraint in the theory: $F_{\mu\nu}X_{\lambda\rho}\epsilon^{\mu\nu\lambda\rho} = 0$ [19].

For optical experiments the phenomenology of the theory (5) is similar to that of ALPs with (4) and ($m_X \leftrightarrow m_a$). However, at higher energies the phenomenology of the theory (5) can get significantly different. Indeed, if a massive vector field couples to a conserved current, all the processes involving the longitudinal degree of freedom are suppressed at energies much greater than its mass m_X. On the other hand, if the current is *not conserved*, for $E \gg m_X$ the longitudinal polarization behaves as a derivatively coupled scalar (the so called *Goldstone boson equivalence theorem* [24]).

This is what may happen in theory (5). Although the theory can be written in a formally gauge invariant form under the $U(1)_X$ gauge symmetry by introducing a Stückelberg field θ_X, the symmetry is realized by simultaneous gauge transformations of the X-field and θ_X-shifts. As a result, the field X_μ couples to a *non-conserved current* ($j_X^\mu \equiv \delta\mathcal{L}/\delta X_\mu$) and therefore its longitudinal polarization behaves as an axion (for $E \gg m_X$).

However, the theory (5) is an effective field theory, valid up to a certain energy scale Λ. This scale $\Lambda \lesssim \frac{m_X}{\kappa}$, as one can easily find by analyzing the unitarity bound in tree-level processes with outgoing longitudinally polarized X. It may naturally happen that for $E \gtrsim \Lambda$ the theory gets modified in such a way that the current j_X^μ becomes conserved. Then, all processes involving emission or absorption of the longitudinal polarization of X_μ get suppressed as $\left(\frac{m_X}{E}\right)^2$. As we are interested in the situation where the field X_μ can be produced at laboratory energies (e.g. in laser experiments), its mass should be $m_X \lesssim E_{lab} \sim$ eV.

The stringent constraints on ALPs come from stellar observations (see e.g. [25, 26]). The ALPs, created in stellar interior via the interactions (2), can significantly change burning cycles and life-times of stars (see [25]). To change the situation, as compared to a standard axion with energy-independent coupling, the scale of new physics Λ should be in the keV region $\Lambda \sim E_\star \sim$ keV. The conservation of the current j_X^μ implies a suppression of emission of longitudinal vector boson by *at least* $\sim (E_{lab}/E_\star)^2 \sim 10^{-6}$. Taking into account the astrophysical constraints, one finds $\kappa \lesssim 10^{-10}\,\text{eV}/m_X$. Thus, the theory with Chern-Simons (CS) interaction (5) does not resemble the theory of ALPs. In particular, the production of X_μ is strongly suppressed by the small value of the dimensionless CS coupling κ.

To illustrate this idea, assume that there is an additional fermion with mass M_f, interacting with the fields of the theory (5) and giving rise to an effective action of the following (schematic) form:

$$\mathcal{L} = -\frac{1}{4}F_{\mu\nu}^2 - \frac{1}{4}X_{\mu\nu}^2 + \frac{m_X^2}{2}(D_\mu\theta_X)^2 + \frac{\kappa}{2}\epsilon^{\mu\nu\lambda\rho}X_\mu A_\nu F_{\lambda\rho} + \left(M_f^2\theta_X - \partial_\mu X^\mu\right)\frac{\kappa}{\Box + M_f^2}F\tilde{F} \tag{6}$$

where we introduced the notation $F\tilde{F} = \frac{1}{2}\epsilon^{\mu\nu\lambda\rho}F_{\mu\nu}F_{\lambda\rho}$. For simplicity of the presentation we work with the non-local action (6), but one can find an example of a renormalizable field theory

which shares these properties in Ref. [20]. Recall that we add to this theory the constraint $\epsilon^{\mu\nu\lambda\rho}F_{\mu\nu}X_{\lambda\rho}=0$ to make it gauge invariant with respect to $U(1)_A$ transformations.

Let us now demonstrate that this theory possesses the desired properties: At *low energies* (for $E<M_f$) one obtains the action (5) (formally taking $M_f\to\infty$). To analyze the theory at high energies ($E\gg M_f$), one can formally take $M_f\to 0$ and neglect the interaction term proportional to θ_X in the action (6). As a result at high energies, the field X_μ couples to the *conserved* current

$$j^\mu_X=\frac{\kappa}{2}\epsilon^{\mu\nu\lambda\rho}A_\nu F_{\lambda\rho}-\kappa\frac{\partial^\mu}{\Box}(F\tilde{F})\ . \tag{7}$$

Therefore, at energies $E\gg M_f$ the production of the longitudinally polarized X_μ-field in theory (6) is suppressed. Of course, for $E>M_f$ the current (7) should be computed directly in the microscopic theory producing the non-local terms in (6), containing additional particles, rather than in the non-local effective theory. However, the conclusion remains the same.

The effect of decoupling of the longitudinal polarization of the vector boson at high energies, significantly changes the phenomenology. Most interestingly, it allows to reconcile the stellar constraints on ALPs (see e.g. [25, 26]) with a possible signal in the high precision optical experiments, outside the standard axion parameter space.

Notice, that such a model requires fermions with masses $E_{lab}\lesssim M_f<E_\star$, i.e. in the range from $\sim$ 1 eV to $\sim$ 1 keV. There are various restrictions on the charges q_f of such fermions. First, laboratory bounds, coming from the contribution to the Lamb shift and invisible orthopositronium decay [27] (based on the results of [28]) give $q_f<10^{-4}$. A stronger bound on millicharged fermions ($q_f<10^{-6}$) with sub-eV masses comes from the requirement that such fermions do not distort the CMB spectrum too much [29]. However, this restriction is not applicable in our case as the fermion masses are assumed to be above $M_f>E_{lab}\sim 1$ eV.

Finally, the strongest bound ($q_f<10^{-14}$) on the charges of fermions with mass below $\lesssim$ 30 keV comes from limiting the contribution of these particles to the energy transfer in stars [30] (see also [25]). To satisfy this bound, the vector field X_μ should be extremely light with $m_X\sim 10^{-10}$ eV and $\kappa\sim 10^{-28}$ [20] (which is a possibility). However, these bounds can be avoided in our model because the paraphoton field X_μ acquires a kinetic mixing with the photon due to the loop corrections coming from light fermions. Therefore, the mechanism of additional suppression of the coupling of fermions with the photon in stars, proposed in [31], is possible. The restriction then becomes $q_f\lesssim 10^{-14}\left(\frac{E_\star}{m_X}\right)^2$, i.e. the stellar bound of [30, 27] is weakened by *at least* six orders of magnitude, making the model compatible with existing observations (see [20] for details).

If a non-trivial anomaly cancellation *involves the electromagnetic* $U(1)$ *gauge group* observable effects may be present in optical experiments. Indeed, such high precision experiments (e.g. those measuring the change of polarization of light propagating in a strong magnetic field) could in principle see the anomalous terms, proportional to $\tilde{F}\cdot F=4\vec{E}\cdot\vec{H}\neq 0$. There exists a significant experimental activity searching for such signals, as various ALPs are expected to couple to $\tilde{F}_{\mu\nu}F^{\mu\nu}$ and produce interesting signatures in parallel electric and magnetic fields. A different type of experiment using static fields, which may test effects caused by non-trivial anomaly cancellation in the electromagnetic sector, was suggested in [32].

Acknowledgements: Work supported in part by the European Commission under the ERC Advanced Grant "MassTeV" ERC-2008-AdG 20080228 and the ITN contract "UNILHC" PITN-GA-2009-237920.

References

[1] D. J. Gross, and R. Jackiw, *Phys. Rev.* **D6**, 477–493 (1972); C. Bouchiat, J. Iliopoulos, and P. Meyer, *Phys. Lett.* **B38**, 519–523 (1972); H. Georgi, and S. L. Glashow, *Phys. Rev.* **D6**, 429 (1972).

[2] M. B. Green, and J. H. Schwarz, *Phys. Lett.* **B149**, 117–122 (1984).

[3] A. Boyarsky, J. A. Harvey, and O. Ruchayskiy, *Annals Phys.* **301**, 1–21 (2002), `hep-th/0203154`.

[4] T. Appelquist, and J. Carazzone, *Phys. Rev.* **D11**, 2856 (1975).

[5] E. D'Hoker, and E. Farhi, *Nucl. Phys.* **B248**, 59 (1984); *ibid.* 77.

[6] N. Arkani-Hamed, S. Dimopoulos and G. R. Dvali, *Phys. Lett.* B **429** (1998) 263 [arXiv:hep-ph/9803315]; I. Antoniadis, N. Arkani-Hamed, S. Dimopoulos and G. R. Dvali, *Phys. Lett.* B **436** (1998) 257 [arXiv:hep-ph/9804398].

[7] I. Antoniadis, S. Dimopoulos and G. Dvali, *Nucl. Phys.* B **516** (1998) 70; S. Ferrara, C. Kounnas and F. Zwirner, *Nucl. Phys.* B **429** (1994) 589.

[8] I. Antoniadis, K. Benakli, A. Laugier and T. Maillard, *Nucl. Phys.* B **662** (2003) 40 [arXiv:hep-ph/0211409].

[9] D. J. Kapner, T. S. Cook, E. G. Adelberger, J. H. Gundlach, B. R. Heckel, C. D. Hoyle and H. E. Swanson, Phys. Rev. Lett. **98** (2007) 021101.

[10] J. C. Long and J. C. Price, *Comptes Rendus Physique* **4** (2003) 337; R. S. Decca, D. Lopez, H. B. Chan, E. Fischbach, D. E. Krause and C. R. Jamell, *Phys. Rev. Lett.* **94** (2005) 240401; R. S. Decca et al., arXiv:0706.3283 [hep-ph]; S. J. Smullin, A. A. Geraci, D. M. Weld, J. Chiaverini, S. Holmes and A. Kapitulnik, arXiv:hep-ph/0508204; H. Abele, S. Haeßler and A. Westphal, in 271th WE-Heraeus-Seminar, Bad Honnef (2002).

[11] E. G. Adelberger, B. R. Heckel, S. Hoedl, C. D. Hoyle, D. J. Kapner and A. Upadhye, Phys. Rev. Lett. **98** (2007) 131104.

[12] N. Arkani-Hamed, S. Dimopoulos and G. Dvali, *Phys. Rev.* D **59** (1999) 086004.

[13] I. Antoniadis, E. Kiritsis and J. Rizos, *Nucl. Phys.* B **637** (2002) 92.

[14] J. L. Hewett, and T. G. Rizzo, *Phys. Rept.* **183**, 193 (1989).

[15] I. Antoniadis, E. Kiritsis, and T. N. Tomaras, *Phys. Lett.* **B486**, 186–193 (2000), `hep-ph/0004214`.

[16] L. E. Ibanez, F. Marchesano, and R. Rabadan, *JHEP* **11**, 002 (2001), `hep-th/0105155`.

[17] I. Antoniadis, E. Kiritsis, J. Rizos, and T. N. Tomaras, *Nucl. Phys. B* **660**, 81–115 (2003).

[18] P. Anastasopoulos, M. Bianchi, E. Dudas, and E. Kiritsis, *JHEP* **11**, 057 (2006a), `hep-th/0605225`; C. Coriano, N. Irges, and E. Kiritsis, *Nucl. Phys.* **B746**, 77–135 (2006), `hep-ph/0510332`; C. Coriano, M. Guzzi, and S. Morelli (2008a), `arXiv:0801.2949[hep-ph]`; C. Coriano, and M. Guzzi (2007), `0711.3424[hep-ph]`; `0709.2111`.

[19] I. Antoniadis, A. Boyarsky, and O. Ruchayskiy (2006), `hep-ph/0606306`.

[20] I. Antoniadis, A. Boyarsky, and O. Ruchayskiy, *Nucl. Phys.* **B793**, 246–259 (2008a), `0708.3001`.

[21] I. Antoniadis, A. Boyarsky, S. Espahbodi, O. Ruchayskiy, and J. D. Wells, *Nucl. Phys.* **B824**, 296–313 (2010), `0901.0639`.

[22] P. Anastasopoulos, et al., *Phys. Rev.* **D78**, 085014 (2008), `0804.1156`; J. A. Harvey, C. T. Hill, and R. J. Hill, *Phys. Rev.* **D77**, 085017 (2008), `0712.1230`; E. Dudas, Y. Mambrini, S. Pokorski, and A. Romagnoni (2009), `0904.1745`.

[23] C. Amsler, et al., *Phys. Lett.* **B667**, 1 (2008).

[24] J. M. Cornwall, D. N. Levin, and G. Tiktopoulos, *Phys. Rev.* **D10**, 1145 (1974).

[25] G. G. Raffelt, *Stars as laboratories for fundamental physics*, UofC Press, Chicago, USA, 1996.

[26] K. Zioutas, et al., *Phys. Rev. Lett.* **94**, 121301 (2005), `hep-ex/0411033`.

[27] S. Davidson, S. Hannestad, and G. Raffelt, *JHEP* **05**, 003 (2000a), `hep-ph/0001179`.

[28] T. Mitsui, et al., *Phys. Rev. Lett.* **70**, 2265–2268 (1993).

[29] A. Melchiorri, A. Polosa, and A. Strumia, *Phys. Lett.* **B650**, 416–420 (2007), `hep-ph/0703144`.

[30] S. Davidson, B. Campbell, and D. C. Bailey, *Phys. Rev.* **D43**, 2314–2321 (1991).

[31] E. Masso, and J. Redondo, *Phys. Rev. Lett.* **97**, 151802 (2006), `hep-ph/0606163`.

[32] A. Boyarsky, O. Ruchayskiy, and M. Shaposhnikov, *Phys. Lett.* **B626**, 184–194 (2005b).

Neutrino Astronomy and IceCube

Teresa Montaruli[1] *for the IceCube Collaboration*

[1]Dep. of Physics, University of Wisconsin - Madison, 1150 University Ave, 53706, WI, USA

DOI: http://dx.doi.org/10.3204/DESY-PROC-2010-03/montaruli_teresa

Understanding cosmic acceleration mechanisms, such as jet formation in black holes, star collapses or binary mergers, and the propagation of accelerated particles in the universe is still a 'work in progress' and requires a multi-messenger approach, exploiting the complementarities across all possible probes: ultra-high energy cosmic rays (UHECR), gamma-rays and neutrinos. In this report the IceCube results concerning searches for astrophysical neutrino point sources and diffuse fluxes from populations of sources widely distributed in the sky or from the GZK cut-off will be summarized. The results to other Neutrino Telescopes and to astrophysical models of neutrino production in sources will be compared.

1 Introduction

The IceCube Neutrino Observatory will be composed of a deep array of 86 strings holding 5,160 light sensors (PMTs) deployed between 1.45 and 2.45 km below the surface of the South Pole ice. The strings are typically separated by about 125 m with PMTs separated vertically by about 17 m along each string. IceCube construction started with a first string installed in the 2005–6 season and will be completed in the austral summer of 2010–11. Eight of the strings in the final detector, six of which use higher quantum efficiency PMTs with respect to the others, are at smaller spacing (about 70 m horizontally and 7 m vertically). Together with seven standard strings they make up DeepCore, designed to enhance the physics performance of IceCube below 1 TeV such as Dark Matter searches. The observatory also includes a surface array, IceTop, for extensive air shower measurements on the composition and spectrum of CRs. PMTs detect the Cherenkov light induced by relativistic charged particles passing through the ice sheet. Direction of events can be reconstructed using the time of hit PMTs and the amplitude as well, and the energy can be inferred exploiting the stochastic energy loss properties of muons and the charge measurement.

2 Astrophysical diffuse fluxes of neutrinos

Unlike gamma and proton astronomy, neutrino astronomy can access the entire universe, probe cosmological sources and sources opaque to photons. The generic neutrino and comic ray (CR) source can be envisaged as an engine that accelerates protons and possibly magnetic fields confine them in the accelerator region. If protons attain sufficient energy, they can interact with radiation and produce neutrons that can escape the accelerating region before interacting. Subsequently, neutron decay can give rise to the observed cosmic ray flux, gamma rays, and yet unobserved neutrinos. These conditions together define an optically thin source [1]. From

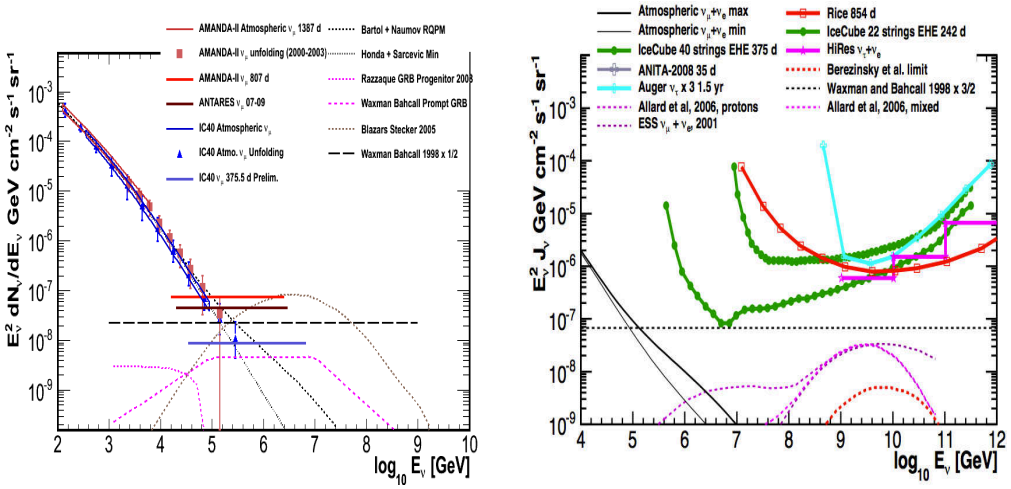

Figure 1: *On the left:* The measured flux of atmospheric $\nu_\mu + \bar{\nu}_\mu$ measured by AMANDA-II (squares) [4] and two independent analyses with 40 strings of IceCube (an unfolding of the spectrum - triangles [5] and a forward folding [6]) is compared to a combination of conventional (from π's and K's) and prompt (from charmed mesons) ν models that approximately indicate the theoretical uncertainty [7]. Horizontal lines are 90% c.l. upper limit to an E^{-2} muon neutrino flux for AMANDA-II [4] (807 d), ANTARES (334 d with 9-12 line configurations) [8] and 40 strings of IceCube (375.5 d). The WB limit [2] is shown together with some models on GRBs [2, 9] and an example of an AGN model [10] rejected at 5σ c.l. by the 40 string limit. *On the right:* 90%c.l. differential upper limits for experiments sensitive to all-ν flavors (for experiments sensitive to < 3 flavors the applied correction factor is given): PAO, HiRes, RICE [12] and IceCube (the 22 string limit and the preliminary 40 string one [11]) are shown. At low energies the region of predictions of $\nu_e + \nu_\mu$ is shown too [7]. At higher energy cosmogenic neutrino models are shown [13] and the limit on the cosmogenic neutrino flux (ankle model) calculated using the Fermi-LAT extragalactic γ-ray background [14].

the measured Ultra-High Energy CR (UHECR) flux above 10^{18} eV the power required for a population of sources to generate the energy density in CRs can be inferred. This hints to active galactic nuclei (AGNs) and gamma-ray bursts (GRBs) as best candidate sources. The result is the Waxman & Bahcall (WB) upper limit for optically thin sources shown in Fig. 1 (on the left). It is extrapolated to lower energies than the UHECR region assuming a proton injection spectrum of E^{-2} [2] resulting from Fermi acceleration mechanism in shocks and $p-\gamma$ interactions that produce a Δ-resonance. The limit also assumes that magnetic fields in the universe do not affect the observed CR spectrum. It has been divided by a factor of 2 to account for mass neutrino oscillations. The upper bound applies as well to $p-$*nucleon* interactions since it is likely that the energy fraction of the protons transferred to pions is even less than for $p-\gamma$ [2] but can be much higher at lower energies than 10^{16} eV assuming a 10% contribution of an extragalactic source of protons between the measured galactic component. The experimental limits exclude this option. It should be noted that if the injected CR spectrum from extragalactic sources include heavier nuclei than protons, then the upper bound and the cosmogenic neutrino fluxes [13] would be lower than for the assumed proton case [3].

A search dedicated to EHE events has been performed using the data of 333.3 d of 22 strings of IceCube and 375.5 d of 40 strings [11]. Upper limits are shown in Fig. 1 (on the right). Models predict between 2 and 24.5 neutrino events (WB upper bound with z evolution of sources [2]) in 3 yrs of the full detector. The search uses a zenith dependent cut of the total charge released in the detector.

3 Searches for Point Sources and Dark Matter

An unbinned likelihood method that compares the signal and the signal plus atmospheric muon and neutrino background hypotheses has been applied to look for emissions of neutrinos from point like sources. The method uses the reconstructed direction and energy of events and can use also time for time-dependent emission searches [15]. As a matter of fact events would cluster around the point source with an error that we measure to be less than 1.2° for 50% of the events with $E_\nu \in [10, 100]$ TeV and less than 0.6° for 50% of the events with $E_\nu \in [1, 10]$ PeV. Moreover, as discussed above, neutrino signal from sources is expected to have a harder spectrum ($\sim E^{-2}$) compared to atmospheric muon and neutrinos produced in the meson decays in atmospheric showers ($\sim E^{-3.7}$ for $\gtrsim 500$ GeV).

The search for the 40 string configuration has been conducted on a data sample of 36,900 events collected during 375.5 d of livetime: 14,121 from the northern sky, mostly muons induced by atmospheric neutrinos and 22,779 from the southern sky, mostly high energy atmospheric muons. A zenith-dependent energy proxy cut has been implemented to prevent that the large background of atmospheric muons overwhelms the IceCube sensitivity to hard-spectrum neutrino sources in the southern sky in the sub-PeV energy region. The sensitivity is at least a factor of two better than previous searches (depending on declination), with 90% c.l. muon neutrino flux upper limits between $E^2 dN/dE \sim 2 - -200 \times 10^{-12} \mathrm{TeV\,cm^{-2}\,s^{-1}}$ in the northern sky and between $3 - -700 \times 10^{-12} \mathrm{TeV\,cm^{-2}\,s^{-1}}$ in the southern sky. A comparison with some models is shown in Fig. 2 (on the left).

The absolute pointing has been confirmed by the Moon shadow detection, initially reported in [16], at the level of 6.76σ for 14 lunar cycles during the 40-string configuration.

Indirect detection of neutrinos from the annihilation of dark matter eventually trapped in celestial bodies like the Sun is extremely promising. Being the Sun rich in H the limits set by IceCube are of interest with respect to direct detection experiments (see Fig. 2 on the right). While the limit begins to touch the region of the MSSM not excluded by direct detection experiments, IceCube with DeepCore will probe an interesting fraction of the parameter space.

References

[1] Ahlers M *et al.*, Phys. Rev. D **72**:023001 (2005).

[2] Waxman E, Bahcall JN, *Phys. Rev.* D **59**:023002 (1999).

[3] K. Murase and J. F. Beacom, Phys. Rev. D **81**, 123001 (2010) [arXiv:1003.4959 [astro-ph.HE]].

[4] R. Abbasi *et al.* [IceCube Coll.], Astrop. Phys. **34**, 48 (2010).

[5] R. Abbasi *et al.* [IceCube Coll.], subm. to Phys. Rev. D (2010) [arXiv:1010.3980].

[6] S. Grullon *et al.* [IceCube Coll.], arXiv:1005.4962 [astro-ph.HE].

[7] G. D Barr *et al.*, Phys. Rev. D **70**, 023006 (2004); M. Honda *et al*, Phys. Rev. D **75**, 043006 (2007); R. Enberg *et al.*, Phys. Rev. D **79**, 053006 (2009); E. V. Bugaev *et al.*, Nuovo Cim. C **12**, 41 (1989).

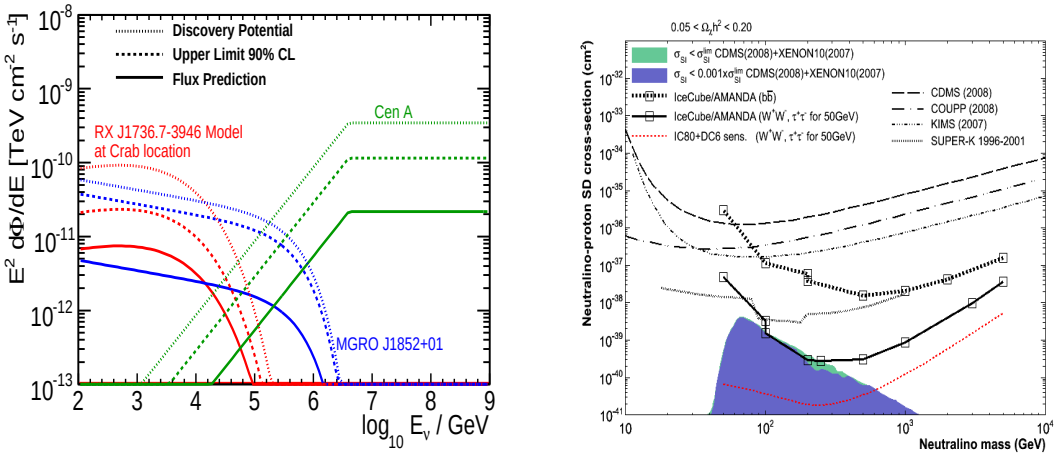

Figure 2: *On the left:* Differential flux for three theoretical models shown with the IceCube 40-string upper limit (90% CL) and discovery potential in each case. Shown are the ν_μ predictions of for SNR RX J1713.7-3946 but moved to the location of the Crab Nebula, for MGRO J1852+01, and for Cen A with the optimistic condition that protons have a spectral index $\alpha_p = 3$ (references in order in [17]). *On the right:* 90% c.l. limits on the spin dependent p-neutralino cross section in the Sun vs the neutralino mass for the 22 string configuration summed to the AMANDA-II result for two annihilation channels. The darkened regions represent MSSM parameter scans. All references for other experiments and the description of IceCube analysis are in [18].

[8] J.A. Aguilar *et al.* [ANTARES Coll.], "Search for a diffuse flux of high-energy ν_μ with the ANTARES neutrino telescope", subm. to Phys. Lett. B (2010).

[9] S. Razzaque *et al.*, Phys. Rev. D **68**, 083001 (2008).

[10] F. W. Stecker, Phys. Rev. D **72**, 107301 (2005).

[11] R. Abbasi *et al.* [IceCube Coll.], accept. by PRD [arXiv:1009.1442v1]; A. Hishiara *et al.* [IceCube Coll.], "Searches for the Highest Energy Neutrinos with IceCube", talk at the COSMO/CosPa Conf., Tokyo (2010).

[12] J. Abraham *et al.* [Pierre Auger Coll.], Phys. Rev. D **79**, 102001 (2009); Abbasi RU *et al.* [HiRes Coll.], subm. to ApJ [arXiv:0803.0554]; P. W. Gorham *et al.* [ANITA Coll.], Phys. Rev. D **82**, 022004 (2010); Kravchenko I *et al.* [RICE Coll.], Phys. Rev. D **73**:082002 (2006).

[13] Allard D *et al.*, JCAP **0609**, 005 (2006); Engel R *et al.*, Phys. Rev. D **64**, 093010 (2001).

[14] V. Berezinsky *et al.*, [arXiv:1003.1496].

[15] J. Braun *et al.*, Astrop. Phys. **29**, 299 (2008) and Astrop. Phys. **33**, 175 (2010).

[16] D. J. Boersma *et al.*, *Moon Shadow Observation by IceCube*, Proc. of ICRC2009, Lodz, Poland (2009) [arXiv:1002.4900v2].

[17] G. Morlino *et al.*, Astrop. Phys. **31**, 376 (2009); F. Halzen *et al.*, Phys. Rev. D **78**, 063004 (2008); H. B. J. Koers and P. Tinyakov, Phys. Rev. D **78**, 083009 (2008).

[18] R. Abbasi *et al.*, Phys. Rev. Lett. **102**, 201302 (2009).

Neutrino properties from experiments

Gustav Wikström

DPNC, University of Geneva, 24 Quai Ernest-Ansermet, 1211 Geneva, Switzerland

DOI: http://dx.doi.org/10.3204/DESY-PROC-2010-03/wikstrom_gustav

The neutrino field has recently received much attention and several new experiments are ready to take or analyze data which have a potentially large impact on the standard model of particle physics. An overview of current neutrino physics is here followed by a summary of the latest results, and finally a list of important results anticipated in the near future is given.

1 Open issues

It is by now well established that neutrinos oscillate between the three weak states ν_e, ν_μ, ν_τ. That flavor changes are possible over time shows that neutrinos have non-equal masses, and that the interaction states are not equal to the mass states ν_1, ν_2, ν_3. The relation between interaction state i and mass state j is written with a mixing matrix U as $\nu_i = \sum_j (U_{ij}\nu_j)$. The matrix U is characterized by three mixing angles $\theta_{12}\theta_{13}, \theta_{23}$ relating the mass states, a CP-violation phase δ_{CP}, and two Majorana phases α, β.

The probability of passing from a weak state to another is a function of the squared mass difference and the mixing angle (and the distance to energy ratio L/E), and these are therefore the quantities that experiments have measured. Current best values are $\Delta m^2_{21} \sim +8 \cdot 10^{-5} eV^2, \Delta m^2_{32} \sim 2 \cdot 10^{-3} eV^2, \theta_{12} \sim 32°, \theta_{23} \sim 45°, \theta_{13} < 7°$.

These five values represent what we currently know about neutrinos, and thus the pieces missing and sought after are the following: the sign on Δm_{32} (*Mass hierarchy*), the value of δ_{CP} (*CP-violation*), values of α, β (*Dirac/Majorana*), absolute values of m_1, m_2, m_3 (*Absolute mass scale*), the value of θ_{13} (*Non-zero* θ_{13}). To this list of open issues we can add the existance of sterile neutrinos, and the asymptotic form of the mixing matrix. Apart from these unknowns, the parameters $\Delta m^2_{32}, \theta 23$ and the νN cross-sections also need to be better understood.

2 Methods of measurement

The study of oscillation parameters needs powerful neutrino sources, which apart from extraterrestial natural sources can be either nuclear reactors ($\bar{\nu_e}$) or neutrino beams (ν_μ or $\bar{\nu_\mu}$). Reactor neutrinos are produced at MeV scale and are emitted isotropically, whereas neutrino beams (from protons on target $p + N \rightarrow \pi^+ \rightarrow \mu^+ + \nu_\mu$) are directed and can be produced at GeV energies.

Studying a neutrino beam over long distances, the probability that a ν_μ disappears from the beam depends mainly on $\Delta m^2_{32}, \theta_{23}$ (*disappearance search*) and the probability that a ν_e appears mainly depends on $\Delta m^2_{32}, \theta_{23}, \theta_{13}$ (*appearance search*), meaning that both oscillations can be

studied. The presence of CP-violations would imply that the probabilities for the transitions $\nu_\mu \to \nu_e$ and $\bar{\nu}_\mu \to \bar{\nu}_e$ are different. Measuring appearances with ν_μ and $\bar{\nu}_\mu$ beams thus gives a handle on δ_{CP}.

Looking instead at reactor neutrinos over much shorter distances, the probability that a $\bar{\nu}_e$ disappears depends mainly on $\Delta m^2_{32}, \theta_{13}$. The lower neutrino energy makes L/E comparable to beam neutrinos, near oscillation maximum, while still exploiting the high flux near the reactors.

The search for the absolute scale of neutrino masses can be addressed by the study of β-decay spectra, where the endpoint of the observed electron spectrum, studied in a sensitive spectrometer, depends on the value of m_{ν_e}.

Whether neutrinos are Majorana particles can be tested by searching for ν-less double β-decay events. In this process, a β-decay in a nucleus is followed by an inverse β-decay in the same nucleus. For this to be possible the $\bar{\nu}_e$ from the first reaction must act as a ν_e in the second, requiring $\bar{\nu}_R = \nu_R$ and the Lorentz transition $\nu_R \to \nu_L$, of which the former is only possible for Majorana particles. The process is commonly studied in Ge-detectors, where the detector acts at once as source and target.

3 Recent results

Several interesting oscillation results have recently been presented.

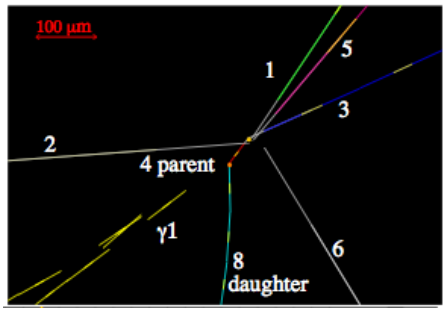

Figure 1: Tau event from a ν_μ beam observed in OPERA [1] viewed in the transverse plane of the neutrino direction. Track 4 is identified as a τ decaying to a μ (track 8).

OPERA [1], using a ν_μ beam from CERN to Gran Sasso (730 km), has presented one observed τ event (see Fig refopera) appearing in the detector, consisting of lead plates interlayered with emulsion plates. While disappearance has long been studied, this result is the very first evidence of neutrino flavour appearance. The result is reported as a 2.1σ effect, and is thus not enough to firmly exclude neutrino decay or decoherence models, but certainly strengthens the oscillation case.

MINOS [2] has new disappearance results using ν_μ and $\bar{\nu}_\mu$ beams from Fermilab to the Soudan mine (735 km). A near detector, made of steel and scintillator plates) close to the start of the beam measures the neutrino flux, which then is compared to the flux observed in the far detector, a larger version of the near detector. The derived parameters for ν_μ (see Fig 2) nicely match earlier measurements using atmospheric neutrinos by Super-K, but a comparison with the parameters derived from the $\bar{\nu}_\mu$ beam (see Fig 2) shows only a small overlap of confidence regions. The uncertainty is dominated by statistics and precision is therefore expected to

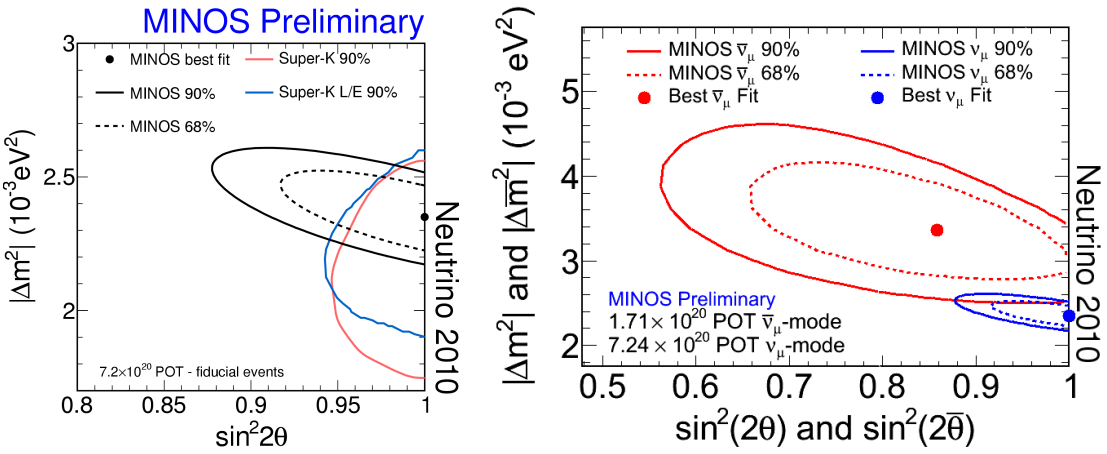

Figure 2: MINOS 90% confidence regions for ν_μ (left) and $\bar{\nu}_\mu$ (right) disappearance [2].

improve in the near future. It is worth to note here that a non-agreement of ν_μ and $\bar{\nu}_\mu$ parameters implies CPT-violation, a much unexpected scenario.

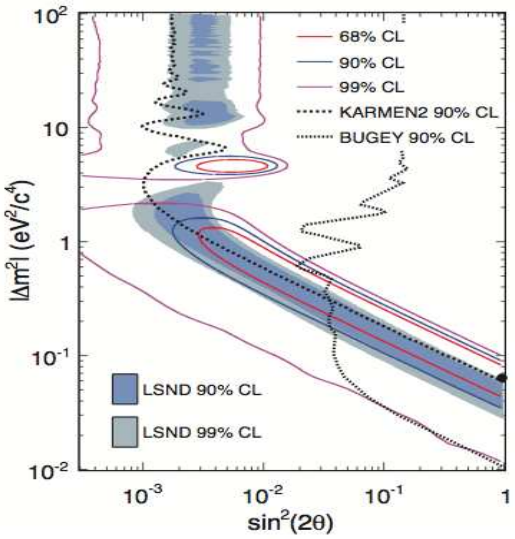

Figure 3: MiniBooNE confidence regions for $\bar{\nu}_\mu \rightarrow \bar{\nu}_e$ appearance [3]. The black dot shows the best fit and shaded areas show the LSND allowed regions [4].

MiniBooNE [3] has studied a $\bar{\nu}_\mu$ beam at 0.5 km and has found an excess in the search for appearing $\bar{\nu}_e$, see Fig 3 with low significance. The fit of appearance parameters agrees with the previous LSND excess [4]. An excess is not observed using a ν_μ beam. The derived oscillation parameters are not consistent with the other three oscillations and would therefore require new transitions to one or more sterile neutrinos. MiniBooNE has no near detector and has therefore

a lesser control of systematic effects compared to *e.g.* MINOS.

4 Anticipated results

Several important experimental quests, aimed at answering the fundamental questions listed above, are in a start-up phase.

The T2K experiment, using a ν_μ beam from J-PARC to Kamioka (295 km), [5] has started taking data early 2010. Its near and far detectors, ND280 and Super-K, respectively, are placed 2.5° off-axis to allow an optimal neutrino energy distribution. ND280 is a composite tracking detector expected to give a precise flux prediction and also measure background rates and νN cross-sections for Super-K. T2K is designed to measure $\Delta m^2_{32}, \theta_{23}$ with high precision, and θ_{13} for which the expected $5y$ sensitivity from ν_e appearance is $\sin 2\theta_{13} < 0.02$.

Double Chooz [6], using $\bar{\nu}_e$ from the two Chooz reactors, will consist of two identical water-Cherenkov detectors at 400 m and 1.05 km. Measurements in the far detector has started in 2010, and the near detector is planned to start in 2012. The expected 90% sensitivity after three years of full detector running is $\sin 2\theta_{13} < 0.03$.

Precise νN cross-sections is being studied at GeV-scale by Minerva, which is placed on the MINOS ν_μ beamline. Muon information from MINOS will be used in Minerva to reconstruct events. The results from Minerva will be an important input for oscillation experiments, *e.g.* T2K.

EXO has started a search for ν-less double β-decay, using a liquid Xe TPC, in 2010. The detector is equipped with Ba^{2+}-tagging, making it able to count the resulting nuclei. In two years time the sensitivity to Majorana masses is expected to reach down to the level of 0.1 eV.

The large electron spectrometer KATRIN studies tritium β-decay in the search for the absolute neutrino mass. After five years running, starting in 2012, the expected 90% sensitivity is $m_\nu < 0.2eV$.

5 Summary

Over the last few years neutrino physics has evolved into a test bench for various exciting physics scenarios (CP-violation, CPT-violation, lepton number violation, sterile particles) that now come in reach of experimenters. The oscillation model is now firmly established and the neutrino community enter a region of precision measurements. In parallell to this detailed knowledge, several essential parameters are waiting to be measured for the first time.

References

[1] N. Agafonova *et al.*, arXiv:1006.1623v1 (2010).

[2] P. Vahle for the MINOS collaboration, presented at Neutrino 2010.

[3] A. A. Aguilar-Arevalo *et al.*, arXiv:1007.1150v3 (2010).

[4] A. Aguilar *et al.*, Phys. Rev. **D** 64, 112007 (2001).

[5] T. Kobayashi for the T2K collaboration, presented at Neutrino 2010.

[6] A. Cabrera for the Double Chooz collaboration, presented at Neutrino 2010.

Chapter 2

Laboratory experiments searching for WISPs

Low energy laboratory searches for WISPs

Joerg Jaeckel

Institute for Particle Physics Phenomenology, Durham University, Durham DH1 3LE, UK

DOI: http://dx.doi.org/10.3204/DESY-PROC-2010-03/jaeckel_joerg

We present an overview over the current status of laboratory experiments searching for (very) weakly coupled slim particles (WISPs). These experiments at the high precision frontier explore new physics beyond the standard model in a complementary way to high energy accelerators. The multitude of active and planned experiments shows a lively field and promises interesting new data in the near future.

1 Introduction

Exploring new physics in its very meaning requires that we go beyond the boundaries of what is known. For example the Large Hadron Collider (LHC) will push the high energy frontier into the multi-TeV range, exploring untested regions with the promise of exciting discoveries. At the same time there is actually a wide range of experiments pushing in a different, complementary direction by going to high precision. In this note we will briefly review a range of these high precision experiments, in particular those looking for new light, (very) weakly interacting particles, called weakly interacting slim particles (WISPs).

When searching for new particles the natural question to ask is: why haven't we already seen them? The high energy and the high precision frontier follow from the two different possible answers to this question. One possible answer is that the particles are very massive. Then we simply do not have enough energy to produce them. The solution are high energy experiments. Alternatively the particles interact only very weakly with ordinary matter, then we have a hard time producing and detecting them, even if they are very light. In this case high precision searches are more promising.

For the high energy frontier we have a lot of circumstantial evidence that points us towards the existence of new physics at the TeV scale explored at the LHC. But do we also expect new physics at low energies? The answer to this question is yes. Indeed we already have observed puzzling phenomena connected to very low energy scales:

- Neutrinos have masses (or more precisely mass splittings Δm^2) of the order of meV.
- The energy density of dark energy (at best very weakly coupled to ordinary matter) is of the order of $(\text{meV})^4$.
- The total energy density of the universe (of which dark energy is about 70 %) is of the order of $(\text{meV})^4$, too[1].

[1]The surprising thing about this is that the matter density is of the same order of magnitude as the dark energy density at the present time. This is the so-called coincidence problem.

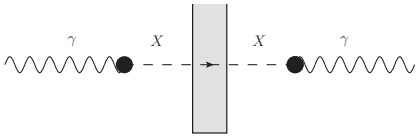

Figure 1: Schematic of a "light-shining-through a wall" experiment. An incoming photon γ is converted into a new particle X which interacts only very weakly with the opaque wall. It passes through the wall and is subsequently reconverted into an ordinary photon which can be detected.

Moreover, there is quite often an interesting connection between underlying physics happening at very high energy scales, to low masses and very weak couplings (see, e.g., [1]). A prime example for this connection are (pseudo-)Goldstone bosons arising from spontaneous symmetry breaking of a global symmetry. If M is the scale at which the symmetry is broken their (effective) couplings are typically suppressed by powers of $1/M$. For true Goldstone bosons the masses vanish and for pseudo-Goldstone bosons the mass is again suppressed by the symmetry breaking scale, $\sim \Lambda^2/M$. The classic example of such a pseudo-Goldstone particle, originating from a spontaneously broken U(1) symmetry proposed to solve the strong CP problem, is the axion [2]. The axion is still one of the prime WISP candidates and finding it is a strong motivation for many of the experiments discussed below.

With this motivation in mind let us now return to the main topic of this note. How can we search for WISPs with their feeble interactions? In the following sections we will present an overview of the techniques and existing experiments to search for WISPs. For brevity we will focus on a particular class of WISPs interacting with photons (for 5th forces experiments see [3]).

2 Light shining through walls

Light shining through walls (LSW) [4, 5, 6] (for a review see [7, 8]) is one of the main techniques to search for WISPs in the laboratory. The basic process (shown in Fig. 1) really does what the name suggests, it allows photons to traverse a completely opaque wall. The photon basically avoids the wall by converting into particle(s) which interact only very weakly with ordinary matter.

The power of this approach becomes immediately evident when considering the following numbers. A laser with a wavelength of 1064 nm and a power of only 20 W produces of the order of 10^{20} photons per second. On the other side, detecting 1 photon per second is quite doable. Therefore even such a simple experiment can test probabilities for the process $\gamma \to X \to \gamma$ of the order of $P_{\gamma\to X\to\gamma} \sim 10^{-20}$. This makes it quite clear that we are able to test very weak couplings. The price to pay is that the energy to produce a particle X is typically of the order of the energy of the incoming photon and therefore $\sim$ eV. In other words we can only produce very light particles with masses $\lesssim$ eV.

So what can the particle X be? And how do we achieve the conversion? Let us consider here only the two simplest possibilities. A (pseudo-)scalar ϕ could couple to two photons via a term $\sim g/4\phi(F^{\mu\nu})^2$ ($\sim g/4\phi F^{\mu\nu}\tilde{F}_{\mu\nu}$). This allows the conversion of photons into these so-called axion-like particles (ALPs) in the presence of a background magnetic field. Alternatively we could have spin-1 gauge bosons just like the ordinary photon but hidden by the fact that all ordinary matter particles carry no charge under this "hidden photon". The interaction then takes place via a kinetic mixing term [4, 9] in the Lagrangian $\sim \chi F^{\mu\nu}X_{\mu\nu}$ where $X^{\mu\nu}$ is the

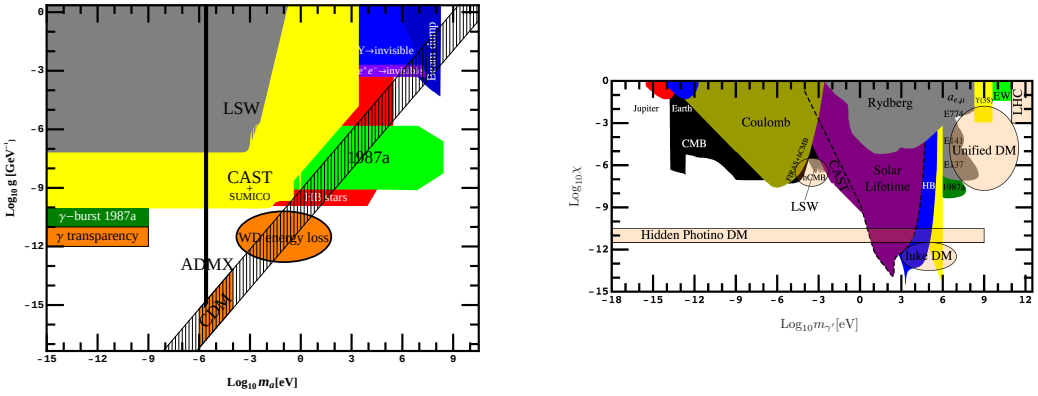

(a) (b)

Figure 2: Summary of constraints for axion-like particles (left panel) and hidden photons (right panel). Both compilations taken from [7] where also details can be found. The mass region, where the axion is a natural dark matter candidate is marked in orange and labeled "CDM". Also other areas which are especially interesting are marked in orange (transparent in (b)).

field strength corresponding to this hidden photon and χ gives the mixing angle[2]. If the hidden photons have a small mass (this can be generated either via a Higgs or via a Stueckelberg mechanism) then we have photon – hidden photon oscillation which are completely analogous to neutrino oscillations.

Experimentally the last few years have brought enormous progress. After the pioneering BFRT experiment in the early 1990s the last three years have brought a flurry of activity and significant improvements with a large number of experiments ALPS, BMV, GammeV, LIPSS and OSQAR taking data, publishing results and improving their setup on the time-scale of month [12, 13, 14]. Since unfortunately no light shining through walls was found the results are in the form of upper bounds which are summarized in Fig. 2 for ALPs and hidden photons. We can see that these experiments are indeed sensitive to tiny couplings!

¿From Fig. 2 the challenges for the future are clear. In particular for ALPs the helioscope bounds (discussed below) are still significantly better. So one of the goals will be to improve the sensitivity of LSW experiments beyond this. Moreover, it would also be desirable to extend the reach towards larger masses in order to come closer to the predicted region for the QCD axion (the hatched diagonal band in Fig. 2(a)). The first goal might be facilitated by using more magnets [15] and by employing optical cavities in both the production as well as in the regeneration region [16, 18]. This "resonant regeneration" enhances the number of photons reaching the detector by a factor proportional to the number of passes the light does in each cavity $N_{\mathrm{pass,\,prod}} N_{\mathrm{pass,\,reg}}$ (the ALPS experiment already pioneered the use of an optical cavity in the production region [12]). Moreover, improvements in detection sensitivity will further help. Higher masses can be reached using suitable configurations of several magnets and other tricks [6, 19]. However, to reach the axion line further improvements may be necessary.

For hidden photons the situation is significantly better in that already the current experiments provide the best bounds for masses in the interesting region of a meV. The improvement discussed above will significantly increase the probed area of parameter space providing huge discovery potential for new physics.

[2]Such a mixing arises quite naturally in both field [9] and string theory [10, 11].

The idea of resonant regeneration might work even better with "light" in the microwave region. Here the light can be reflected up to 10^{11} times inside the cavity, promising interesting sensitivities [18]. Again several groups are planning and or building such an experiment [20] and two test setups have already yielded first data [21].

Modified LSW setups, so called afterglow experiments can be used to search for chameleons (a special type of scalar ALP connected to dark energy). Chameleons are different from ordinary ALPs in that dense regions of ordinary matter, like mirrors or a wall also represent barriers for the chameleon. Therefore, chameleons produced in a vacuum tube closed with transparent windows on both sides, remain trapped in it. The experiment then works as follows. First a laser is shone through the tube, effectively "charging" it with chameleons. Then the laser is switched off. The trapped chameleons then slowly reconvert into ordinary photons which can leave the tube through the windows and be detected. An experiment searching for this "afterglow" [22] has been performed by the GammeV collaboration producing new bounds on chameleons [23]. Moreover, the ADMX collaboration did a test run in the microwave regime [24].

3 Helioscopes

Helioscopes [25] follow the same principle as LSW experiments. The difference is that on the production side the laser photons are replaced by the photons in the core of the sun. For ALPs the conversion of these photons is stimulated by the electromagnetic fields of the ions in the plasma (as discussed above such fields are not necessary for hidden photons; nevertheless the conversion is affected by the plasma due to the modified photon propagation). On earth one then has a reconversion region (oriented towards the sun) just as in an ordinary LSW experiment. Everything between the solar core and this regeneration region effectively can be considered part of a very thick wall.

Due to the enormous number of photons inside the solar core this is a very powerful technique. Indeed, as can be seen from Fig. 2(a) the CAST experiment is setting the best limits on ALPs for masses below 10 meV [26]. This is currently many orders of magnitude better then the LSW experiments, thereby setting the benchmark for the next generation of those experiments. In addition the SUMICO collaboration has produced interesting bounds for masses around 1 eV [27]. For hidden photons the situation is very good in that the helioscopes yield complementary bounds to the LSW experiments at somewhat higher masses (cf. Fig. 2(b)). Dedicated hidden photon helioscopes such as the proposed SHIPS may even compete with LSW experiments in the meV range [28].

Unfortunately, helioscopes are also still somewhat shy of the axion region. Future improvements can include a stronger magnet and a wider aperture. The former enhances the regeneration probability for ALPs. The latter generally increases the WISP flux that can be used for reconversion and hence also increases the sensitivity for hidden photons.

At higher masses sensitivity is lost, because the axion wave and the regenerated photon wave[3] have slightly different wavelengths. After some distance newly regenerated photons have opposite phase to those produced at an earlier point and interfere destructively, effectively reducing the number of regenerated photons. This problem can be solved by changing the wavelength of the photons to match those of the WISP. This can be achieved by filling the regeneration region with a buffer gas with a refractive index such that $(n-1) = -m_\phi^2/(2\omega^2)$. In the X-ray regime (photons in the solar core have X-ray energies) refractive indices smaller

[3] In LSW experiments the same happens on the production side.

than 1 can indeed occur in ordinary gases like helium. To reach higher masses the CAST and SUMICO collaborations therefore fill their regeneration regions with such a gas [29, 27]. Higher masses will require more gas in the beam line[4].

4 Haloscopes - Searching for axion dark matter

True QCD axions (and perhaps to some degree also general axion-like particles) can form all or a part of dark matter (it is actually one of the most favorite dark matter candidates [30]). In the axion mass range (1-100)μeV production of a sufficient number of suitably cold axions is indeed a natural expectation (orange "CDM" region in Fig. 2(a)). This provides a plentiful source of these particles and therefore another opportunity to find them.

Having the dark matter axions all around us we only need to reconvert them and detect the produced photons. This is the idea of a haloscope [25]. In a sense such an experiment would convert dark matter into electricity! The advantage of such an experiment is that we pay the price of the small coupling only for the reconversion. (The disadvantage is that we rely on the additional assumptions that axions are indeed contributing to dark matter.)

Since dark matter axions are assumed to have very small velocities their energy is basically determined by the rest mass. Therefore, regenerated photons are in the microwave regime. As in the LSW experiments the regeneration probability can be enhanced by employing a high quality cavity. For this enhancement to be effective the regenerated photons which have energy $\approx m_a$ must be resonant in the cavity. Since the mass of the axion is unknown such an experiment must scan through the masses changing the resonance frequency of the cavity in each step.

An experiment of this type is currently being performed by the ADMX collaboration. The data collected in the last few years yields already an absolutely impressive sensitivity [31], currently being the only laboratory experiment testing true QCD axions. The price to pay is that the mass range is somewhat limited. However, currently ADMX is implementing improvements in the detector sensitivity which will greatly enhance the scanning speed. This will then allow to scan about a decade in axion masses in a few years. The CARRACK collaboration is developing microwave detectors based on Rydberg atoms [32] which could improve the (already impressive) sensitivity to detect microwave radiation even further.

5 Laser polarization experiments

In all the experiments above, detection was based on reconverting the WISPs (produced in the laboratory or from a source like dark matter) into photons. In that sense they are direct detection or appearance experiments. But in principle we could also do a disappearance experiment. This is the principle with which laser polarization experiments can search for WISPs.

The basic idea is that as polarized light passes through an interaction region, the real or virtual production of WISPs can leave traces in the polarization of the laser light. This is most easily understood in the case of (pseudo-scalar) ALPs. Here the interaction is given by $\sim g\phi\mathbf{E}\cdot\mathbf{B}$. In a background magnetic field $\mathbf{B}$ the photons provide the $\mathbf{E}$ field necessary for the interaction. We can immediately see that only those photons with an $\mathbf{E}$ field parallel to the magnetic field interact. When an ALP is produced, the corresponding photon is absorbed.

[4]It should be noted that at higher masses more and more tuning steps are required making this increasingly difficult.

Consequently, we have a selective absorption of photons parallel to the magnetic field. This is a so-called dichroism, and leads to a rotation of the polarization direction. Similarly, virtual production causes a polarization dependent effective refractive index (birefringence) which leads to a phase shift between the two polarizations turning an initially linear polarized laser beam into one with an elliptic polarization.

To allow the different polarization directions to be affected differently we need a preferred direction in space. Typically this is provided by a background magnetic field. Therefore polarization experiments are typically not sensitive to hidden photons which do not interact with this magnetic field. However, in presence of additional hidden matter this can change [33].

Measurements of this type have already been performed [34] by the BFRT, PVLAS, Q&A and BMV collaborations and OSQAR [14] is also setting up such an experiment. The sensitivity of polarization experiments is somewhat limited due to difficult to control experimental backgrounds (at least for the rotation signature the theoretical backgrounds are very low [35]). Nevertheless, these experiments provide a useful platform to develop optical techniques such as Fabry-Perot cavities. Moreover, and maybe even most importantly they also have an additional physical goal: They want to test the QED prediction of vacuum magnetic birefringence created by virtual electron positron loops.

6 Tests of Coulomb's law

Tests of Coulomb's law can also be a very sensitive probe for WISPs. In particular, hidden photons cause a small Yukawa contribution $\sim \alpha\chi^2 \exp(-m_{\gamma'} r)/r$ to the Coulomb potential which allows for a very powerful test of these particles as can be seen from Fig. 2(b).

The yellow "Coulomb" region in Fig. 2(b) originates [36] from an experiment performed at a scale of 10s of cm already 39 years ago [37]. Therefore, it seems very plausible that with current technology significant improvements are possible.

Tests of Coulomb's law can also be performed at other length scales. Indeed at large length scales the bounds "Jupiter" and "Earth" in Fig. 2(b) arise from "Coulomb's law" tests on the magnetic fields of Jupiter and Earth. Similarly one can use atomic spectra to probe Coulomb's law at very small length scales, labelled "Rydberg" [36, 38] in Fig. 2(b). As a test of hidden photons these bounds are particularly model-independent[5] [39].

7 Searches at higher masses

Over the last few years, a variety of dark matter experiments and astrophysical observations have provided interesting hints towards hidden photons with somewhat higher masses in the MeV-GeV range[6] (labelled "Unified DM" [40] in Fig. 2(b)). Similarly, hidden photons with masses in this range could also provide an explanation [38] for the deviation of $(g-2)_\mu$ from the standard model prediction [41]. Moreover, masses in this range could arise quite naturally in supersymmetric [42] or string theory setups [11].

[5] For example, the fixed target experiments discussed below typically assume that hidden photons with mass greater than the electron threshold dominantly decay into electrons (and perhaps muons). This can be different in models with hidden matter.

[6] These masses are still below the current high energy frontier ∼TeV and particles in this range must have (moderately) small couplings to the standard model in order to be viable. Accordingly experiments searching for them must be sufficiently precise and we include them in our discussion of the high precision frontier.

Hidden photons (and typically also ALPs) at masses above the electron threshold, $2m_e \approx 1\,\mathrm{MeV}$, can be nicely probed in fixed target experiments [43]. Here a high current beam of electrons (possibly also protons) is shot onto a target, typically a sheet or even a block of metal. Hidden photons are then produced, e.g. via hidden photon Bremsstrahlung. Depending on the size of the kinetic mixing the hidden photons can then travel a significant distance before they decay into electron-positron pairs (or if sufficiently massive muons) which can be detected.

A wide range (see [44] for an overview) of these experiments is currently in planning, testing or early operation states at various accelerator facilities such as DESY (HIPS), MAMI and Jefferson Lab (APEX, HPS and DarkLight) [45].

Moreover, these "heavyish WISPs" can also be searched for in meson experiments [38, 46].

8 Conclusions

High precision experiments at low energies have great potential to search for new light, but very weakly coupled particles. Thereby, they can shed light on the so-called "hidden sector" and deliver complementary information to high energy collider experiments.

A multitude of active and near future experiments will explore this high precision frontier in the next years, bringing a wealth of new information on the nature of fundamental physics and hopefully exciting discoveries.

Acknowledgements

The author would like to thank L. Baudis, M. Schumann and the local organizing team of the 6th Patras-Axion-WIMP-WISP workshop for creating a wonderful atmosphere. Moreover, he would like to thank J. Redondo and A. Ringwald for helpful comments.

References

[1] J. Jaeckel, AIP Conf. Proc. **1274**, 30 (2010).

[2] R. D. Peccei and H. R. Quinn, Phys. Rev. Lett. **38**, 1440 (1977); S. Weinberg, Phys. Rev. Lett. **40**, 223 (1978); F. Wilczek, Phys. Rev. Lett. **40**, 279 (1978); J. E. Kim, Phys. Rev. Lett. **43**, 103 (1979); M. Dine, W. Fischler, and M. Srednicki, Phys. Lett. **B104**, 199 (1981); M. A. Shifman, A. I. Vainshtein, and V. I. Zakharov, Nucl. Phys. **B166**, 493 (1980); A. R. Zhitnitsky, Sov. J. Nucl. Phys. **31**, 260 (1980).

[3] S. Hoedl, Talk at the 6th Axion-WIMP-WISP Workshop in Zurich, `http://axion-wimp.desy.de`. (2010); E. G. Adelberger *et al.*, Prog. Part. Nucl. Phys. **62**, 102 (2009).

[4] L. B. Okun, Sov. Phys. JETP **56**, 502 (1982).

[5] A. A. Anselm, Yad. Fiz. **42**, 1480 (1985).

[6] K. Van Bibber *et al.*, Phys. Rev. Lett. **59**, 759 (1987).

[7] J. Jaeckel and A. Ringwald, (2010), arXiv:1002.0329.

[8] J. Redondo and A. Ringwald, DESY 10-175 (2010).

[9] B. Holdom, Phys. Lett. **B166**, 196 (1986).

[10] K. R. Dienes, C. F. Kolda, and J. March-Russell, Nucl. Phys. **B492**, 104 (1997); S. A. Abel and B. W. Schofield, Nucl. Phys. **B685**, 150 (2004); S. A. Abel *et al.*, Phys. Lett. **B666**, 66 (2008); S. A. Abel *et al.*, JHEP **07**, 124 (2008); M. Bullimore, J. P. Conlon, and L. T. Witkowski, (2010), arXiv:1009.2380.

[11] M. Goodsell *et al.*, JHEP **11**, 027 (2009).

[12] K. Ehret *et al.*, Nucl. Instrum. Meth. **A612**, 83 (2009); Phys. Lett. **B689**, 149 (2010).

[13] M. Fouche *et al.*, Phys. Rev. **D78**, 032013 (2008); A. S. . Chou *et al.*, Phys. Rev. Lett. **100**, 080402 (2008); A. Afanasev *et al.*, Phys. Lett. **B679**, 317 (2009); Phys. Rev. Lett. **101**, 120401 (2008).

[14] P. Pugnat *et al.*, Phys. Rev. **D78**, 092003 (2008).

[15] A. Ringwald, Phys. Lett. **B569**, 51 (2003).

[16] F. Hoogeveen and T. Ziegenhagen, Nucl. Phys. **B358**, 3 (1991);

[17] P. Sikivie, D. B. Tanner, and K. van Bibber, Phys. Rev. Lett. **98**, 172002 (2007).

[18] F. Hoogeveen, Phys. Lett. **B288**, 195 (1992); J. Jaeckel and A. Ringwald, Phys. Lett. **B659**, 509 (2008).

[19] P. Arias *et al.*, (2010), arXiv:1009.1519; (2010), arXiv:1009.1519.

[20] P. Slocum, F. Caspers and P. Williams, separate talks at the 6th Axion-WIMP-WISP Workshop in Zurich, `http://axion-wimp.desy.de`. (2010).

[21] R. Povey, J. Hartnett, and M. Tobar, Phys. Rev. **D82**, 052003 (2010); A. Wagner *et al.*, (2010), arXiv:1007.3766.

[22] M. Ahlers *et al.*, Phys. Rev. **D77**, 015018 (2008); H. Gies, D. F. Mota, and D. J. Shaw, Phys. Rev. **D77**, 025016 (2008).

[23] A. S. Chou *et al.*, Phys. Rev. Lett. **102**, 030402 (2009); J. H. Steffen *et al.*, (2010), arXiv:1010.0988.

[24] G. Rybka *et al.*, Phys. Rev. Lett. **105**, 051801 (2010).

[25] P. Sikivie, Phys. Rev. Lett. **51**, 1415 (1983).

[26] S. Andriamonje *et al.*, JCAP **0704**, 010 (2007).

[27] Y. Inoue *et al.*, Phys. Lett. **B668**, 93 (2008).

[28] D. Cadamuro and J. Redondo, (2010), arXiv:1010.4689.

[29] E. Arik *et al.*, JCAP **0902**, 008 (2009).

[30] H. Baer, A. D. Box, and H. Summy, JHEP **10**, 023 (2010).

[31] S. J. Asztalos *et al.*, Phys. Rev. **D69**, 011101 (2004); Phys. Rev. Lett. **104**, 041301 (2010).

[32] M. Tada *et al.*, Nucl. Phys. Proc. Suppl. **72**, 164 (1999).

[33] H. Gies, J. Jaeckel, and A. Ringwald, Phys. Rev. Lett. **97**, 140402 (2006); M. Ahlers *et al.*, Phys. Rev. **D76**, 115005 (2007).

[34] R. Cameron *et al.*, Phys. Rev. **D47**, 3707 (1993); E. Zavattini *et al.*, Phys. Rev. **D77**, 032006 (2008); S.-J. Chen, H.-H. Mei, and W.-T. Ni, Mod. Phys. Lett. **A22**, 2815 (2007); F. Bielsa *et al.*, (2009), arXiv:0911.4567.

[35] M. Ahlers, J. Jaeckel, and A. Ringwald, Phys. Rev. **D79**, 075017 (2009).

[36] V. Popov, Tr. J. of Physics **23**, 943 (1999).

[37] E. R. Williams, J. E. Faller, and H. A. Hill, Phys. Rev. Lett. **26**, 721 (1971).

[38] M. Pospelov, Phys. Rev. **D80**, 095002 (2009).

[39] S. G. Karshenboim, Phys. Rev. Lett. **104**, 220406 (2010); J. Jaeckel and S. Roy, (2010), arXiv:1008.3536.

[40] N. Arkani-Hamed *et al.*, Phys. Rev. **D79**, 015014 (2009).

[41] K. Hagiwara *et al.*, Phys. Lett. **B649**, 173 (2007).

[42] E. J. Chun and J.-C. Park, JCAP **0902**, 026 (2009); C. Cheung *et al.*, Phys. Rev. **D80**, 035008 (2009); D. E. Morrissey, D. Poland, and K. M. Zurek, JHEP **07**, 050 (2009). M. Baumgart *et al.*, JHEP **04**, 014 (2009); Y. Cui *et al.*, JHEP **05**, 076 (2009).

[43] J. D. Bjorken *et al.*, Phys. Rev. **D80**, 075018 (2009).

[44] S. Andreas and A. Ringwald, (2010), arXiv:1008.4519.

[45] J. Mnich, Talk at the 6th Axion-WIMP-WISP Workshop in Zurich, `http://axion-wimp.desy.de` (2010); A. Denig, Talk at the BOSON 2010, `http://conferences.jlab.org/boson2010/` (2010); R. Essig *et al.*, (2010), arXiv:1001.2557; T. Maruyama and J. Thaler and J. Fisher, separate talks at the SLAC - Dark Forces Workshop. `http://www-conf.slac.stanford.edu/darkforces2009/` (2009).

[46] M. Reece and L.-T. Wang, JHEP **07**, 051 (2009); B. Batell, M. Pospelov, and A. Ritz, (2009), arXiv:0911.4938; S. Andreas *et al.*, JHEP **08**, 003 (2010).

Improving the Discovery Potential of Future Light-Shining-through-a-Wall Experiments

Paola Arias[1], *Joerg Jaeckel*[2], *Javier Redondo*[3], *Andreas Ringwald*[1]

[1]Deutsches Elektronen-Synchrotron, Notkestraße 85, D-22607 Hamburg, Germany
[2]Institute for Particle Physics Phenomenology, Durham University, Durham DH1 3LE, UK
[3]Max Planck-Institut für Physik, Föhringer Ring 6, D-80805 München, Germany

DOI: http://dx.doi.org/10.3204/DESY-PROC-2010-03/arias_paola

Planning for the next generation of light-shining-through-wall experiments has started. It is therefore timely to investigate possible ways to optimize their setups. The goals are to improve the sensitivity towards smaller couplings and increase the mass range to which the experiments are sensitive. We discuss possible magnet arrangements and the effects of the unavoidable gaps in the magnetic field profile. Furthermore, we discuss requirements on the diameter of the laser beam and aperture of the magnets in order to achieve high-quality cavities.

Several well motivated extensions of the Standard Model predict the existence of very weakly interacting slim particles (dubbed WISPs). In particular, top-down models arising from compactifications in string theory suggest plenty of them [1], such as axions [2], axion-like particles (ALPs), hidden U(1) gauge bosons [3] and mini-charged particles [4]. Optical precision experiments are a powerful tool to search for these particles. In particular, a class of very simple and effective laser experiments is based on photon – WISP – photon oscillations: the so called *light-shining-through-a-wall* (LSW) experiments.

The sensitivity of LSW experiments has grown considerably over the last few years. In this work we will concentrate on ALPs, whose coupling to two photons has been recently constrained, using the LSW technique, to be smaller than $g \sim \text{few} \times 10^{-7}\,\text{GeV}^{-1}$ [5]. The goal of the next generation of LSW experiments should be to surpass the present limits of $g \sim \text{few} \times 10^{-10}\,\text{GeV}^{-1}$ obtained by CAST, the CERN Solar Axion Telescope [6]. The most straightforward way to increase the sensitivity for ALPs is to enlarge the product BL of the magnetic field strength (B) and the length of the magnetic region (L), since the probability of $\gamma \to \text{ALP} \to \gamma$ conversion, at small masses, scales as $\propto (BL)^4$. Nearly all of the current generation of LSW experiments (ALPS [5, 7, 8], GammeV [9], LIPSS [10] and OSQAR [11]), recycle one or two of the long superconducting dipole magnets from accelerator rings, such as the ones from HERA, Tevatron or LHC. Additional improvements can be achieved by: using a larger number of these magnets [12], progress in laser and detector technology, and the introduction of matched optical resonators in both, production and regeneration regions [13]. Implementing these advances, sensitivities in the $g \sim \text{few} \times 10^{-12}$ GeV^{-1} range seem achievable for light ALPs, thus opening great opportunities for discoveries.

However, using an array of magnets to increase the magnetic field region modifies the production/regeneration form factors and high quality cavities must have a minimum diameter in order to avoid excessive clipping losses, in turn requiring magnets with sufficiently large

aperture. We will discuss these effects and ways to profit from them or at least minimize their negative impact. Finally, we want to find an optimal configuration, based on existing technology, that maximizes the sensitivity of the experiment for a wide range of ALPs masses.

1 Oscillation probability for realistic magnet arrangements

To start with, let us recall that the probability of a laser photon of frequency ω converting into an ALP of mass m_ϕ - and vice versa - after traveling a distance L, is given by

$$P_{\gamma\to\phi} = P_{\phi\to\gamma} = \frac{1}{4}\frac{\omega}{k_\phi}\left(gBL\right)^2 |F(qL)|^2,$$

where $q \equiv |k_\gamma - k_\phi|$ is the difference of the photon and ALP momenta which for small m_ϕ is approximately $q \approx m_\phi^2/(2\omega)$. The function F, sometimes called form-factor, characterizes the profile of the magnetic field, which we wrote as $\vec{B}(\vec{x}) = \vec{e}_z B f(x)$, along the photon trajectory,

$$F(qL) \equiv \frac{1}{L}\int_0^L dx' f(x')\; e^{iqx'}.$$

In the current generation of LSW experiments, exploiting single dipole magnets with homogeneous B, both on the generation and regeneration side, the form factor takes the familiar form $F_{\rm single}(qL) = (2/(qL))\sin(qL/2)$. The maximum conversion probability $P_{\gamma\to\phi} = g^2B^2L^2/4$ is achieved in vacuum for small momentum transfer, $qL/2 \ll 1$, corresponding to small masses, where the form factor takes its maximum value, $F_{\rm single}(qL) = 1$. Thus, the goal is to optimize the setup such that $F(qL)$ is as close to 1 as possible, for a wide range of $m_\phi \ll \omega$.
The setup foreseen for the next generation of LSW experiments will exploit series of N dipole magnets (see e.g. [7, 9]), including a natural and probably unavoidable "gap", with no magnetic field in between each magnet. Therefore, we should re-write the form factor for a longitudinal profile corresponding to N equally spaced magnets, each of length ℓ, separated from each other by a fixed length Δ. In fact, a short calculation results in

$$F_{N,\Delta}(qL) = \frac{1-e^{iqN(\ell+\Delta)}}{1-e^{iq(\ell+\Delta)}} \times \frac{F_{\rm single}(q\ell)}{N} = \frac{2}{qL}\sin\left(\frac{qL}{2N}\right)\frac{\sin\left(\frac{qN}{2}\left(L/N+\Delta\right)\right)}{\sin\left(\frac{q}{2}\left(L/N+\Delta\right)\right)}, \qquad (1)$$

with $L = N\ell$ the total length of the magnetic field. The effect of the gap in between the magnets acts as a phase added to a single magnet just as the *phase shift plates* proposed in [14], but with the advantage that the gaps introduce no optical losses. Besides the usual zeros of $F_{\rm single}(qL)$, located at $m_\phi^2 = 4k\pi\omega/\ell$, with $k \in \mathbb{Z}^+$, other zeros (gap dependent) appear in $F_{N,\Delta}(qL)$, given by $m_\phi^2 = 4k\pi\omega/\left(N\left(\ell+\Delta\right)\right)$. Therefore, in this setup, the loss of the coherent photon-ALP conversion occurs already at somewhat smaller masses.

The latter issue can be ameliorated by considering an array on N identical magnets of length ℓ, segmented into n subgroups of alternating polarity [15], such that the total magnetic length is given by $L = N\ell$. Including a fixed gap in-between the magnets, as we did before, we find that again the form factor is modified with an extra oscillation mode,

$$F_{N,n,\Delta}(qL) = \begin{cases} \frac{2}{qL}\sin\left(\frac{qL}{2N}\right)\frac{\sin\left(\frac{qN}{2}(L/N+\Delta)\right)}{\sin\left(\frac{q}{2}(L/N+\Delta)\right)}\tan\left(\frac{qN}{2n}(\frac{L}{N}+\Delta)\right), & n \text{ even}, \\ \frac{2}{qL}\sin\left(\frac{qL}{2N}\right)\frac{\cos\left(\frac{qN}{2}(L/N+\Delta)\right)}{\sin\left(\frac{q}{2}(L/N+\Delta)\right)}\tan\left(\frac{qN}{2n}(\frac{L}{N}+\Delta)\right), & n \text{ odd}. \end{cases} \qquad (2)$$

In the limit $\Delta \to 0$, the formulas from [15] are recovered.
We can now maximize Eqs. (1) or (2) varying the gap length. We are then able – in principle – to optimize the sensitivity for given values of m_ϕ changing the size of the gap, scanning optimally the ALP parameter space. For instance, maximization of Eq. (1) gives $(q\ell/2)\,(1+\Delta_{\rm opt}/\ell) = k\pi$, with $k \in \mathbb{Z}$. Unfortunately, using this equation, a full scan of the parameter region it is not possible experimentally, because Δ is limited by the length of the setup, and in particular also by the maximal length of the cavity (see below).[1]

2 Discovery potential

To estimate the sensitivity of next generation LSW experiments, we have chosen a benchmark set of reasonably realistic input parameters (summarized in Table 1). Here, $\mathcal{P}_{\rm prim}$ is the primary laser power, $\mathcal{F}_{g,r}$ are the finesses of the generation and regeneration cavities, τ is the measurement time, and η is the spatial overlap integral between the ALP mode and the electric field mode.

ℓ	14.3 m (6×6)
B	9.5 T
$\mathcal{P}_{\rm prim}$	30 W
$\mathcal{F}_g = \mathcal{F}_r$	$\pi \times 10^5$
ω	1.17 eV
τ	50 h
η	0.95

Table 1: Benchmark values for a next generation of LSW experiment.

For instance, let us assume a 6+6 LHC setup (i.e. 6 magnets in the production and in regeneration side, respectively) and the benchmark parameters given by Table 1. Using the estimated number of photons in the regeneration cavity, given in Ref. [16], such configuration can reach a limit of $g \sim 5\times10^{-12}$ GeV^{-1} for small masses.[2] Figure 1 a) shows the impact of considering a realistic configuration with gaps in-between the magnets versus neglecting them. As we can see, enlarging the magnetic region of LSW experiment by placing a series of superconducting magnets modifies the probability of photon-ALP-photon conversion. Nonetheless, the unavoidable gaps in-between the magnets can represent an improvement in the setup, since they appear as a *free* parameter, adding an extra oscillation mode.

However, care must be taken: the enlargement of the resonant cavity is strongly dependent on the diameter of the laser beam and therefore, the aperture of the magnet. A rough estimate of the optimum cavity length, as a function of the aperture of the magnet (a) and the wavelength of the laser (λ), gives $L_{\rm opt} = (0.42)^2\,(\pi a^2)/(2\lambda)$ [17]. For instance, using LHC magnets ($a \approx$ 28 mm) the optimum cavity length is $L_{\rm opt} \sim 204$ m.

Finally, in Fig. 1 b) we display the projected sensitivity on ALPs for the next generation of LSW experiments. With six magnets on each side of the experiment we can produce four different symmetric configurations: $\uparrow\uparrow\uparrow\uparrow\uparrow\uparrow$, $\uparrow\downarrow\uparrow\downarrow\uparrow\downarrow$, $\uparrow\uparrow\downarrow\downarrow\uparrow\uparrow$, $\uparrow\uparrow\uparrow\downarrow\downarrow\downarrow$. Moreover, we have calculated the sensitivity for seven different gap sizes. We infer that, using these alternating field configurations, we are able to restore the sensitivity almost completely up to masses of order $m \sim 5 \times 10^{-4}$ eV.

3 Conclusions

We have shown the modifications on the form factor, when a series of magnets with gaps in-between is exploited in LSW experiments. With a setup of $6+6$ LHC magnets, a sensitivity of $g \sim 5 \times 10^{-12}$ GeV^{-1} seems realistic, for $m_\phi \leq 5 \times 10^{-4}$ eV. The next generation of

[1] As can be seen from the maximization condition, for small $q\ell$ the size of the gap grows.
[2] We have assumed negligible dark count rate in the detector, therefore the sensitivity to g grows as $\tau^{-1/4}$.

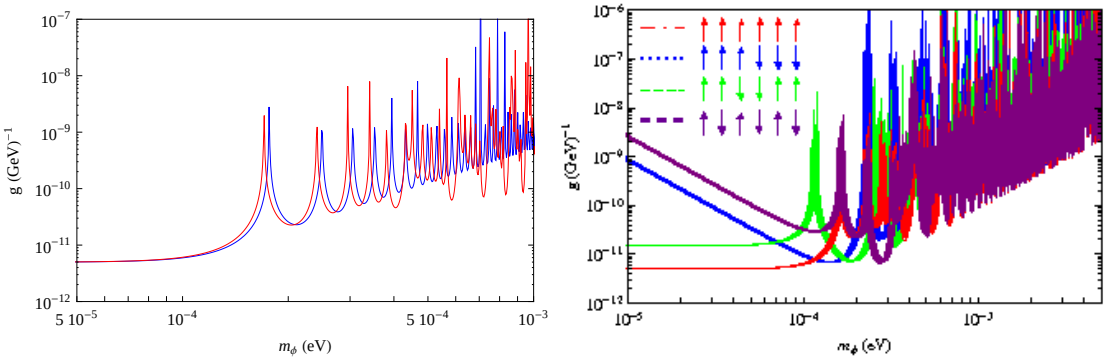

Figure 1: a) Solid line represents the sensitivity of a setup without taking into account the gap in-between the magnets ($F(qL) = F_{\rm single}(qL)$). Dashed line corresponds to the same setup, considering $\Delta = 1$ m. b) The four configurations complement each other, fullfilling the sensitivity for small masses. With $\Delta[m] = \{3.83, 3.30, 2.80, 2.33, 1.89, 1.47, 1.08\}$.

LSW experiments may therefore indeed explore territory in parameter space that has not been excluded yet by astrophysics and cosmology. Moreover, it may probe ALP interpretations of hints for cosmic photon regeneration [18] and for an anomalous energy loss in white dwarfs [19].

References

[1] E. Witten, Phys. Lett. B **149**, 351 (1984); J. P. Conlon, JHEP **0605**, 078 (2006); P. Svrcek and E. Witten, JHEP **0606**, 051 (2006); A. Arvanitaki *et al.*, arXiv:0905.4720 [hep-th]; M. Goodsell, J. Jaeckel, J. Redondo and A. Ringwald, JHEP **0911** (2009) 027 [arXiv:0909.0515 [hep-ph].

[2] R. D. Peccei and H. R. Quinn, Phys. Rev. Lett. **38**, 1440 (1977) ; S. Weinberg, Phys. Rev. Lett. **40**, 223 (1978) ; F. Wilczek, Phys. Rev. Lett. **40**, 279 (1978).

[3] L. B. Okun, Sov. Phys. JETP **56**, 502 (1982) [Zh. Eksp. Teor. Fiz. **83**, 892 (1982)].

[4] B. Holdom, Phys. Lett. B **166**, 196 (1986).

[5] K. Ehret *et al.*, Phys. Lett. B **689** (2010) 149 [arXiv:1004.1313 [hep-ex]].

[6] T. Papaevangelou, "CAST, Recent Results and Future Outlook", `http://axion-wimp.desy.de` and these proceedings.

[7] K. Ehret, "ALPS at DESY", `http://axion-wimp.desy.de` and these proceedings.

[8] K. Ehret *et al.* [ALPS collaboration], Nucl. Instrum. Meth. A **612**, 83 (2009) [arXiv:0905.4159].

[9] W. Wester, "GammeV, Results and Future Plans at FermiLab", `http://axion-wimp.desy.de` and these proceedings.

[10] A. Afanasev, "Searches for Dark Matter Candidates with Electron Beams at JLAB", `http://axion-wimp.desy.de` and these proceedings.

[11] A. Siemko, "Status of the OSQAR Experiment", `http://axion-wimp.desy.de` and these proceedings.

[12] A. Ringwald, Phys. Lett. B **569**, 51 (2003) [arXiv:hep-ph/0306106].

[13] F. Hoogeveen and T. Ziegenhagen, Nucl. Phys. B **358**, 3 (1991); P. Sikivie, D. B. Tanner and K. van Bibber, Phys. Rev. Lett. **98**, 172002 (2007).

[14] J. Jaeckel and A. Ringwald, Phys. Lett. B **653** (2007) 167 [arXiv:0706.0693 [hep-ph]].

[15] K. Van Bibber *et al.*, Phys. Rev. Lett. **59**, 759 (1987).

[16] G. Mueller *et al.*, Phys. Rev. D **80**, 072004 (2009) [arXiv:0907.5387 [hep-ph]].

[17] P. Arias, J. Jaeckel, J. Redondo, A. Ringwald, work in preparation.

[18] M. Roncadelli, "Evidence for an axion-like particle from blazar spectra?", `http://axion-wimp.desy.de` and these proceedings.

[19] J. Isern, "White dwarf axions", `http://axion-wimp.desy.de` and these proceedings.

Superconducting RF Cavity Search for a Hidden Sector Photon

Peter H. Williams

Cockcroft Institute & STFC Daresbury Laboratory, Warrington, WA4 4AD, UK

DOI: http://dx.doi.org/10.3204/DESY-PROC-2010-03/williams_peter

Using a pair of high-quality superconducting niobium-titanium cavities we will search for hidden sector photons with coupling $\chi < 10^{-8}$ in the 1-30 μeV range. The experiment is the radio frequency analogue of the classic "light shining through a wall" technique. We present the proposed experimental setup and discuss the anticipated physics reach.

1 Introduction

Generically, extensions of the Standard Model (SM) of particle physics contain extra $U(1)$ gauge bosons. If these have direct Yukawa couplings to SM matter they are referred to as Z' bosons. Negative collider searches have constrained the mass of these to greater than a few hundred GeV. However, in many cases (notably string based extensions), SM matter is uncharged in the additional $U(1)$ symmetry. Then the only renormalizable interaction between the additional $U(1)$ gauge boson and visible matter is via mixing between it and the photon [1]. Collider experiments are not sensitive to this, particularly if the mass of the hidden sector photon (HSP) is in the sub-eV range. In the μeV to meV range the current bounds arise from Cavendish type tests of Coulomb's law [2, 3] and from constraints on distortions in the cosmic microwave background that would be produced by resonant production of HSPs [4, 5]. In the meV to eV range bounds have recently been extended by light shining through a wall (LSW) experiments using both optical lasers [6, 7] and intense, accelerator based infrared free-electron lasers [8]. In the eV to keV range bounds arise from considerations of the solar lifetime [9] and the non-observation of photon regeneration in helioscopes such as CAST [10].

2 Proposed experimental setup

We intend to use superconducting RF cavities in a light shining through a wall configuration to extend the limits on the existence of the HSP by more than an order of magnitude. This relies on exploiting the high-quality nature of the cavities developed for the international linear collider ($Q \sim 10^8$) [11] and existing high power microwave infrastructure at Daresbury Laboratory [12]. Initially, two frequency matched cavities will be mounted in separate cryostats and cooled to 2 K. One cavity, termed the emitter, will be powered in it's first dipole transverse magnetic mode (TM110) at 3.9 GHz. From a non-observance of this power in the second, receiver cavity one can construct a bound on the mixing parameter between photon and HSPs that would mediate a transmission between the two cavities if it exists.

Figure 1 shows the existing vertical test facility cryostat that will hold the emitter cavity. This is a fully shielded experimental environment, being buried below ground level in a concrete pit. This is designed to allow high field running of cavities within the cryostat without risk of personnel exposure to field emission X-rays, but also ensures isolation from external RF interference. Cryogenic connections to an in-situ LHe dewer ensure that multi-hour running at 2K is possible. Our intention is to install a second cryostat to hold the receiver cavity next to the existing one in an underground access tunnel. At a later stage this could be replaced with a dilution refrigerator, permitting operation of the receiver cavity in the millikelvin regime. Doing this would further improve sensitivity to the coupling through the virtual elimination of thermal noise.

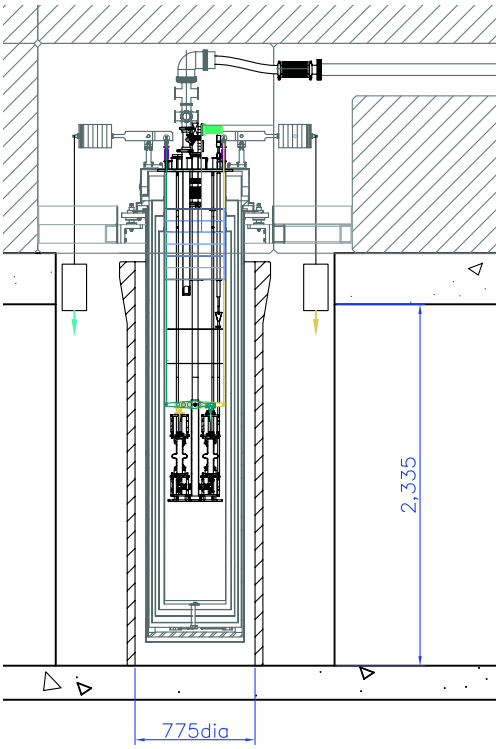

Figure 1: Vertical test facility

The sensitivity of the experiment relies on the suppression of regular microwave leakage between the cavities by many orders of magnitude (roughly an attenuation of 300dB is required). We intend to achieve this by employing a "box in a box" technique [13] that also allows leakage to be exactly quantified. This involves generating not only the fundamental driving frequency, but also a number of sidebands. One of these is mixed with the signal from the receiver cavity and FFT analysed to determine existence of the signal. The others are deliberately leaked into the outer receiver box and general external environment. These can also then be FFT analysed and compared with the signal to determine the amount of shielding achieved. Each box will have minimal RF connections to ensure a near perfect Faraday cage. The two internal boxes will be the cavities themselves, the outer boxes will be the cryostats. For the emitter, one connection is required to feed in the fundamental 3.9 GHz RF from a solid-state amplifier. For the receiver, the only RF connection allowed is that of the sideband leakage monitor. The signal output and power for the internal low noise amplifier (LNA) will be fed using electro-optic conversion equipment.

With high-Q cavities it is important to ensure that they remain mutually on tune for the duration of the experiment. For the emitter this is simple, one merely measures the reflected power continuously and re-tune periodically if required. For the receiver this will require the periodic switching in of a reference signal, correction, then re-establishing of full RF isolation. With the expected stability of the LHe, we can expect that the cavity will then remain on tune for many minutes before the process needs to be repeated. This is analogous to the Dicke procedure of eliminating electronic gain fluctuations in radio astronomy.

3 Expected physics reach

The probability for photon-HSP mixing is given by

$$P = \chi^4 Q_1 Q_2 \frac{m_{\gamma'}^8}{\omega_0^8} |G|^2 ,$$

where χ is the photon-HSP kinetic mixing fraction, Q_i are the cavity quality factors, $m_{\gamma'}$ is the HSP mass, ω_0 is the resonant frequency of the cavities and

$$G(k/\omega_0) \equiv \omega_0^2 \int_{V'} \int_{V} d^3\mathbf{x}\, d^3\mathbf{y} \frac{\exp(ik|\mathbf{x}-\mathbf{y}|)}{4\pi|\mathbf{x}-\mathbf{y}|} A_{\omega_0}(\mathbf{y}) A'_{\omega_0}(\mathbf{x})$$

is a dimensionless factor that encodes the geometrical setup of the cavities. Figure 2 shows the geometric factor for a pair of pillbox cavities in the TM110 mode with the configuration envisaged for our setup. We have also evaluated the TM310 mode at 6.4 GHz which could be excited in the emitter given a suitable solid state amplifier. The performance of the crab cavities has been measured whilst operating at 4K. Using a standard extrapolation to 2K we can expect that the cavities will exhibit $Q = 1.6 \times 10^8$ when critically coupled (i.e. a ring time of tens of milliseconds). The emitter will achieve this, however to accommodate the output coupling the receiver will have $Q = 1.0 \times 10^6$. Assuming a noise temperature for the LNA of 2K and a power gain of 17 dB, and a stored power in the emitter of 0.1 W for four hours of data taking we expect to obtain the 3σ exclusion limits indicated in Fig. 3 (green shaded regions). This is compared to the existing bounds espoused in Section 1. We consider these bounds to be conservative as there are methods of improving a number of the parameters from the values assumed in this paper. For example, signal to noise ratios can be improved by moving from a solid state LNA to a SQUID device, and through cooling the receiver to millikelvin temperatures. Additionally, more power could be stored in the emitter, and if LHe stability is as expected running could be extended over many days.

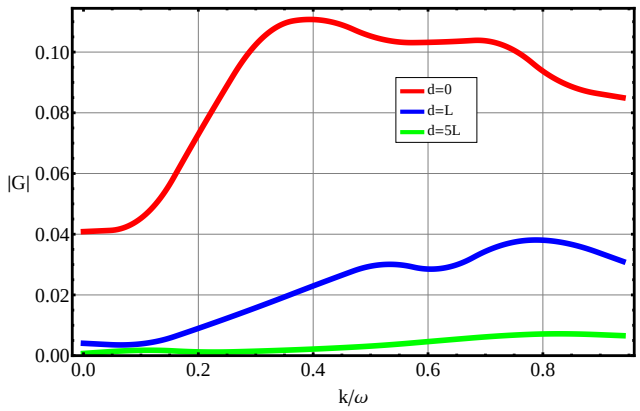

Figure 2: Geometric factor for a pair of pillbox cavities in the TM110 mode, d indicates the cavity separation in units of cavity length.

4 Conclusion

The high electric fields and quality factors attainable by the superconducting microwave cavities we propose to use in this experiment opens up a method to search for μeV particles with unprecedented sensitivity.

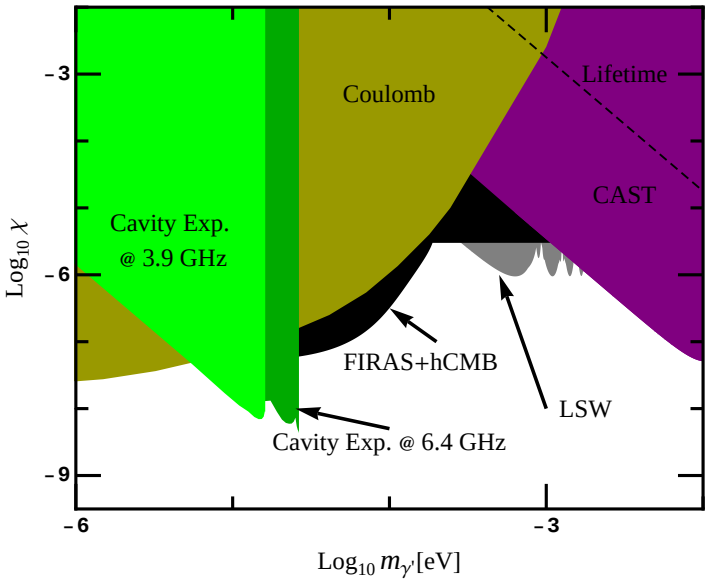

Figure 3: Anticipated SCRF cavity experiment 3σ exclusion limits on the photon-HSP kinetic mixing fraction with 4 hours running compared to existing bounds.

Acknowledgements

The author wishes to thank P. Goudket, S. Jamison & A. Moss of Daresbury Lab., A. Dexter & G. Burt of U. Lancaster, J. Dainton of U. Liverpool. Also thanks to F. Caspers and J. Jäckel for discussions and encouragement.

References

[1] J. Jäckel and A. Ringwald, Phys. Lett. B **659** (2008) 509 [arXiv:0707.2063 [hep-ph]].

[2] E. R. Williams, J. E. Faller and H. A. Hill, Phys. Rev. Lett. **26** (1971) 721.

[3] D. F. Bartlett and S. Loegl, Phys. Rev. Lett. **61** (1988) 2285.

[4] J. Jaeckel, J. Redondo and A. Ringwald, Phys. Rev. Lett. **101** (2008) 131801 [arXiv:0804.4157 [astro-ph]].

[5] A. Mirizzi, J. Redondo and G. Sigl, JCAP **0903** (2009) 026 [arXiv:0901.0014 [hep-ph]].

[6] A. S. Chou *et al.*,Phys. Rev. Lett. **100** (2008) 080402 [arXiv:0710.3783 [hep-ex]].

[7] K. Ehret *et al.*, Phys. Lett. B **689** (2010) 149 [arXiv:1004.1313 [hep-ex]].

[8] A. Afanasev *et al.*, Phys. Lett. B **679** (2009) 317 [arXiv:0810.4189 [hep-ex]].

[9] J. Redondo, JCAP **0807** (2008) 008 [arXiv:0801.1527 [hep-ph]].

[10] E. Arik *et al.* JCAP **0902** (2009) 008 [arXiv:0810.4482 [hep-ex]].

[11] P. Ambattu, G. Burt, A. Dexter, P. Goudket, C. Lingwood, P. McIntosh and I. Tahir, ICFA Beam Dyn. Newslett. **51** (2010) 48.

[12] P. A. Corlett *et al.*, *In Proceedings of 11th European Particle Accelerator Conference (EPAC 08), Magazzini del Cotone, Genoa, Italy, 23-27 Jun 2008, pp MOPP125.*

[13] F. Caspers, J. Jaeckel and A. Ringwald, JINST **4**, P11013 (2009) [arXiv:0908.0759 [hep-ex]].

High-Intensity Probes of Axion-Like Particles

Babette Döbrich and Holger Gies

Theoretisch-Physikalisches Institut, Friedrich-Schiller-Universität Jena
& Helmholtz Institute Jena, Max-Wien-Platz 1, D-07743 Jena, Germany

DOI: http://dx.doi.org/10.3204/DESY-PROC-2010-03/dobrich_babette

With continuously increasing intensities, modern laser systems can become a valuable tool for the search for axions and axion-like particles. As conventional setups of axion searches cannot easily accommodate the usage of a high-intensity laser system, we propose a novel, purely laser-based setup in which the occurrence of a frequency shift is an observable for the axion-photon interaction.

1 Motivation

Optical probes of the axion-like particle (ALP) parameter space, such as polarimetric measurements or "Light-shining-through-walls" setups, are enhanced by applying strong external (electro-)magnetic fields B over a large spatial extent L. Conventionally, dipole magnets are used to modify the propagation of probe beams. But with the remarkable increase in available laser intensity over the past years, multi-terawatt laser systems have become competitive with dipole magnets in providing $B \times L$ and can be expected to eventually exceed them. Still, the limited temporal and spatial extent of pulsed high-intensity beams disfavors standard setups used for ALP search and requires different observables which are particularly useful for purely laser-based experiments. Such an observable can, e.g., be a diffraction pattern [1], or a frequency shift [2, 3]. The latter will be the subject of this contribution.

2 Photon-Axion dynamics

As we are interested in the effects of the nonlinear interaction of laser photons due to the presence of an axion or ALP, we start from the equations of motion for the two fields:

$$\partial_\mu \partial^\mu \phi + m^2 \phi - \frac{1}{4} g F_{\mu\nu} \tilde{F}^{\mu\nu} = 0 \quad (1)$$

$$\partial_\mu F^{\mu\nu} - g(\partial_\mu \phi) \tilde{F}^{\mu\nu} = 0 \,. \quad (2)$$

For the following discussion, we split the field strength tensor $F_{\mu\nu}$ into contributions of a probe field $F^{\rm in}_{\mu\nu}$ and two external high-intensity beams $F^{\rm ext}_{\mu\nu}$, and linearize in the probe field. Coupling to the first external beam in Eq. (1), the probe photons can be converted into ALPs, denoted by ϕ. Successively, by means of Eq. (2), the ALPs can be reconverted into photons through the second external field. For simplicity, the following discussion will be limited to a one-dimensional setup where the probe photons propagate along the positive z axis. Then, the above equations of motion can be solved using a Green's function approach [2, 4].

In order to motivate the findings for a purely laser-based setup we first review the probe photon dynamics for static or slowly varying external fields spanning a length L as e.g. provided by a dipole magnet. In this case, employing an incoming plane wave probe beam of frequency ω_{in} in Eq. (1) yields via Eq. (2) an outgoing wave that carries the original frequency ω_{in} after the intermediate propagation as an ALP, necessitating the use of a light-blocking wall or polarimetric measurements. In addition, the outgoing wave's amplitude picks up two factors of $\sin(\Delta k \frac{L}{2})/\Delta k$ with $\Delta k = -\omega_{\text{in}} + \sqrt{\omega_{\text{in}}^2 - m^2}$ arising in the conversion and back-conversion processes, respectively, causing it to be maximal at $\Delta k \simeq 0$. From this it follows that the ALP search with dipole magnets is most sensitive for small ALP masses, cf. also Fig. 2.

From another perspective, the sensitivity for small axion masses being maximal is related to momentum conservation as reflected by the requirement $\Delta k \simeq 0$ for both the photon-axion conversion and back-conversion process.

3 Photon-Axion conversion in high-intensity laser fields

From the preceding consideration it becomes obvious that employing lasers as external fields will modify the momentum balance as they carry a further frequency scale. This changes the sensitivity characteristics with respect to the ALP mass. Moreover, in accordance with energy conservation, the frequency of the outgoing photon will in general be modified. This happens in close analogy to the processes of sum-frequency generation (SFG) and difference-frequency generation (DFG) known from nonlinear optics. The frequency of the outgoing electromagnetic wave will be the sum or difference of the incident frequencies and, analogous to the phase matching conditions within SFG and DFG, the wave vectors of the external beams (being different in general) enter the requirements[1] $\Delta k \simeq 0$. In summary, we thus suggest the measurement of a frequency shift $\omega_{\text{out}} \neq \omega_{\text{in}}$ of probe beam photons as an observable of photon-ALP interaction, which is feasible for unsuppressed interaction amplitudes, i.e. $\Delta k \simeq 0$ for the conversion and back-conversion process. This perfectly accommodates the features of the high-intensity beam making the use of a light-blocking wall or polarimetric measurements superfluous. With hindsight, we choose a configuration in

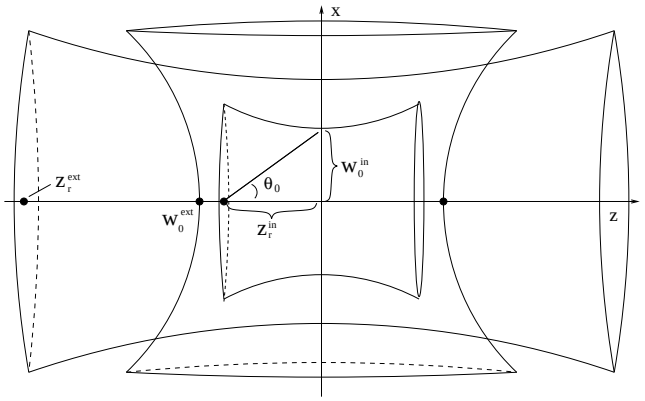

Figure 1: Overlap of Gaussian laser beams. The innermost probe beam is embedded into two external beams propagating orthogonally and transversally to it, respectively. The waist size w_0^{ext} as well as the Rayleigh lengths z_r^{in} and z_r^{ext} determine the extent of the beam foci.

[1] Introducing high-intensity lasers as external fields changes also the functional form of the conversion amplitude since one has to employ a Gaussian beam form [5]. Also, the length scale L will be substituted by the natural spatial extent of Gaussian beams, being the waist size w_0 and the Rayleigh length z_r of the beams.

which the photon-axion conversion is mediated by an external beam of frequency $\omega_\perp$ propagating orthogonally to the z axis, while the back-conversion process from the ALP to a photon is due to a counter-propagating beam with $\omega_\parallel$, cf. Fig. 1.

Then, as within SFG and DFG, one obtains from Eq. (1) ALP partial waves carrying frequencies $\omega_{\rm ax}^{\pm} = \omega_{\rm in} \pm \omega_\perp$, while the corresponding 'phase matching condition' becomes

$$\Delta k_\perp^{\pm} = -\omega_{\rm in} + \delta_{\rm T}\sqrt{(\omega_{\rm in} \pm \omega_\perp)^2 - m^2} \stackrel{!}{\simeq} 0 \ , \tag{3}$$

with $\delta_{\rm T} = \pm 1$ in case of transmission and reflection of the ALP wave, respectively.

Above, $\Delta k_\perp^+ = 0$ is realized in the case of transmission (i.e. $\delta_{\rm T} = +1$) for $m = m_\parallel \equiv \sqrt{\omega_\perp^2 + 2\omega_{\rm in}\omega_\perp}$, whereas $\Delta k_\perp^- = 0$ cannot satisfy the requirement of a non-negative ALP frequency $\omega_{\rm ax}$. Thus, only the 'SFG solution' $\omega_{\rm ax}^+ = \omega_{\rm in} + \omega_\perp$ is kept in the following.

Note that, since the wave vector of the external $\perp$ beam has no component along z, it does not enter *explicitly* in the momentum conservation in Eq. (3). This is different for the back-conversion process mediated by the $\parallel$ beam. The outgoing electromagnetic partial waves now carry frequencies $\omega_{\rm out} = \omega_{\rm in} + \omega_\perp \pm \omega_\parallel$, whilst momentum conservation requires that

$$\Delta k_\parallel^{\pm} = -\sqrt{(\omega_{\rm in} + \omega_\perp)^2 - m^2} + \delta_{\rm T}(\omega_{\rm in} + \omega_\perp \pm \omega_\parallel) \pm \omega_\parallel \stackrel{!}{\simeq} 0 \ . \tag{4}$$

As argued above, Eqs. (3) and (4) have to hold simultaneously for a feasible sensitivity while we demand $\omega_{\rm out} \neq \omega_{\rm in}$ as an observable for the photon-ALP conversion. Requiring positivity of all frequencies, it can be checked that this is only possible for DFG and transmission of the wave, i.e. $\delta_{\rm T} = +1$ in Eq. (4). In particular, choosing $\omega_\perp = 2\omega_\parallel$, we see that $\Delta k_\parallel^- = \Delta k_\perp^+ = 0$ for axion masses $m = m_\parallel$ yielding $\omega_{\rm out} = \omega_{\rm in} + \omega_\parallel$. This constitutes an observable of the ALP-photon interaction[2]. As the resonant masses $m_\parallel$ and $m_\perp$ are of the same order of magnitude as the laser frequency scales being $\mathcal{O}$(eV), purely laser-based searches are *complementary* to standard dipole setups. Of course, to facilitate the detection of the frequency shift requires $\omega_{\rm out}$ to lie feasibly outside the spectral widths $\Delta\omega$ of all interacting beams.

At last, it is worth emphasizing that the condition $\omega_\perp = 2\omega_\parallel$ is in fact an enormous experimental advantage since second harmonic generation is a standard technique even for high-intensity lasers, thus requiring the employment of only *one* external high-intensity beam.

4 Discovery potential

An estimate of the ALP discovery potential for purely laser-based searches is given in Fig. 2, see [2] for details. Here, the black wedge-like curves and the black line correspond to a feasible setup at IOQ [8] employing the multi-TW class laser JETI as probe and the PW class laser POLARIS as external beam, which could be realized in the near future. For the estimate, single-photon detection is assumed for the frequency-shifted photons[3]. The wedge-like structures of the bounds around $m_\parallel$ and $m_\perp$ are a consequence of the fixed frequencies within the setup.

Using optical parametric amplification (OPA) for the probe beam, a larger range of the mass-coupling plane can be explored, as indicated by the black line. However, as OPA limits

[2] In the discussed setting, the photon-ALP conversion can also be induced by the ($\perp$) oriented field and back-conversion can be due to the counter-propagating ($\parallel$) field as the interaction order is not assessable for synchronized pulses. The conversion process with the opposite order $\perp \leftrightarrow \parallel$ results in $\omega_{\rm out} = \omega_{\rm in} - \omega_\parallel$ for axion masses around $m_\parallel = 2\sqrt{\omega_{\rm in}\omega_\parallel}$ and $\omega_\perp = 2\omega_\parallel$, thus defining a second 'resonant mass' besides $m_\perp$ [2].

[3] For higher photon statistics the number of shots $N_{\rm shot}$ can be increased ($\mathcal{O}$(100) per day at IOQ [8]).

intensity, the sensitivity to the ALP coupling is decreased. Nevertheless, we see that a setup at IOQ could provide the strongest model-independent [6] bounds for ALP masses at $\mathcal{O}$(eV).

Even smaller ALP coupling values can potentially be probed at the future exawatt class facility ELI [7]. Already with single shot measurements it can be possible to almost complement the currently best laboratory bounds provided by ALPS [9] in the $\mathcal{O}$(eV) mass range as shown by the red dotted line in Fig. 2. In order to surpass even the CAST [10] bounds on solar axions, one would require $N_{\rm shot} N_{\rm in} \approx 10^{26}$ at ELI (dash-dotted line). This constitutes a rather ambitious aim, but would allow for a direct probe of the QCD axion parameter space (given as a yellow band in Fig. 2), making it a worthwhile task for the future.

5 Conclusions

The rapid increase in available laser intensity strongly suggests to investigate the potential of high-intensity lasers for axion and ALP search. As argued, a possible observable in this context is the measurement of a probe beam frequency shift. This is particularly useful since the limited temporal and spatial extent of the pulses disfavors conventional setups such as polarimetric measurements and Light-shining-through-walls. In summary, high-intensity probes of ALPs can constitute a new tool in the general quest [11] for weakly interacting slim particles. B.D. thanks the organizers of the 6th Patras Workshop for the opportunity to present this work. Support by the DFG through grants SFB/ TR18, GRK1523, and Gi328/5-1 is gratefully acknowledged.

References

[1] D. Tommasini and H. Michinel, Phys.Rev.A **82**, 011803 (2010), [arXiv:1003.5932 [hep-ph]].

[2] B. Dobrich and H. Gies, JHEP **1010**, 022 (2010), [arXiv:1006.5579 [hep-ph]].

[3] K. Homma *et al.*, arXiv:1006.4533 [quant-ph].

[4] S. L. Adler *et al.*, Annals Phys. **323**, 2851 (2008).

[5] L.W. Davis, Phys. Rev. A **19**, 1177-1179 (1979).

[6] J. Jaeckel *et al.*, Phys. Rev. D **75**, 013004 (2007), [arXiv:hep-ph/0610203].

[7] http://www.extreme-light-infrastructure.eu/

[8] http://www.physik.uni-jena.de/inst/ioq//start-Engl.html

[9] K. Ehret *et al.* , Phys. Lett. B **689**, 149 (2010), [arXiv:1004.1313 [hep-ex]].

[10] E. Arik *et al.* , JCAP **0902**, 008 (2009), [arXiv:0810.4482].

[11] J. Jaeckel and A. Ringwald, arXiv:1002.0329 [hep-ph].

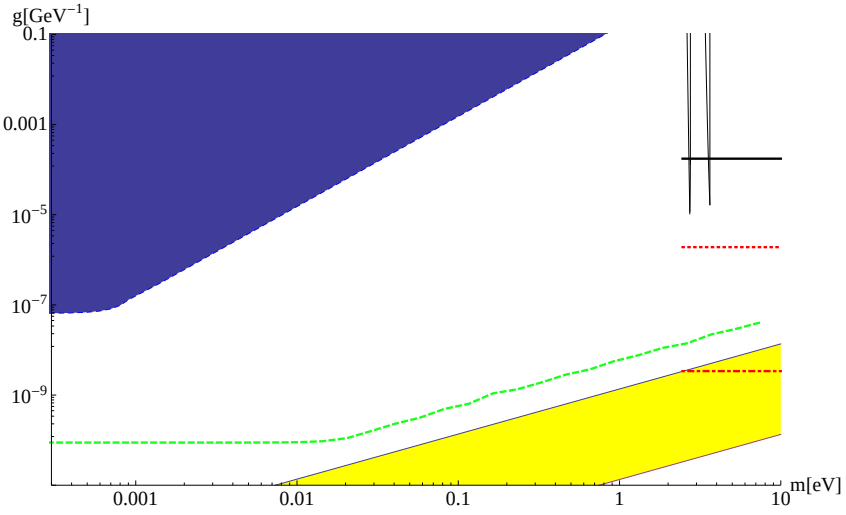

Figure 2: ALP exclusion bounds for ALPS [9] (blue-shaded area), and CAST [10] (green-dashed line) in comparison to a setup involving the laser systems available in Jena [8], denoted by black wedges. The black line indicates the principle exclusion bounds at this setup employing a conventional OPA system, while the red-dotted line gives an analogous estimate for ELI [7]. The red dot-dashed line suggests the requirements at ELI for entering the parameter regime of typical QCD axion models which are given by a yellow band.

Status of sub-GeV Hidden Particle Searches

Sarah Andreas and Andreas Ringwald

Deutsches Elektronen-Synchrotron DESY, Notkestraße 85, D-22607 Hamburg, Germany

DOI: http://dx.doi.org/10.3204/DESY-PROC-2010-03/andreas_sarah

Hidden sector particles with sub-GeV masses like hidden U(1) gauge bosons, the NMSSM CP-odd Higgs, and other axion-like particles are experimentally little constrained as they interact only very weakly with the visible sector. For masses below the muon threshold, we present constraints from meson decays, $g-2$ as well as beam-dump and reactor experiments. The NMSSM CP-odd Higgs and generally any pseudoscalar is required to be heavier than 210 MeV or couple to fermions much weaker than the SM Higgs. Hidden photons are less constrained and can be searched for at future fixed-target experiments, e.g. HIPS at DESY.

1 Motivation for a sub-GeV dark sector

Hidden sectors are frequently proposed as part of the physics beyond the standard model. Since their interactions with the visible sectors are very weak, so are the current experimental bounds. In fact, motivated both from a bottom-up and a top-down perspective, those sectors might even contain light particles with masses in the sub-GeV range that have so far escaped detection. Among those weakly interacting slim particles (WISPs) are hidden U(1) gauge bosons, the CP-odd Higgs of the NMSSM, and other axion-like particles (ALPs).

Such particles are of great interest in many models that seek to interpret recent terrestrial and astrophysical anomalies in terms of dark matter (DM). The rise in the positron-fraction with energy as observed by PAMELA (cf. [1]) and the deviation from the power-law in the $e^+ + e^-$ spectrum measured by FERMI (cf. [2]) together with the absence of an excess in anti-protons require the DM candidate to annihilate dominantly into leptons *(leptophil)* with a cross section much larger than the one giving the correct relic abundance. Different direct detection measurements like the annual modulation observed by DAMA/LIBRA [3] and the null results of CDMS and XENON [4, 5] seem somewhat contradicting. Consistency might still be possible if either the DM candidate is light ($m \sim 5 - 10$ GeV) with elastic scattering or heavy with excited states (mass splitting $\Delta m \sim 100$ keV) generating inelastic scattering. Those properties are challenging for standard DM candidates and alternative scenarios like hidden sectors with light messenger particles have been considered because of the following advantageous features. A long range attractive force mediated by such a light messenger generates a so called Sommerfeld enhancement of the annihilation cross section. Dark matter annihilation proceeding through this messenger – if light enough – is naturally leptophilic due to kinematics. Inelastic scattering on nuclei can also be mediated by such a light particle. Possible examples of messenger particles that have already been studied are ALPs like the NMSSM CP-odd Higgs [6] and hidden U(1) photons of a generic hidden sector [7, 8, 9, 10] or of asymmetric mirror worlds [11].

From a top-down perspective, hidden sectors appear naturally in various supersymmetric models descending from string theory. Mediator particles are generally weakly coupled to the visible sector and can also be light. Specifically in [12] it was found that the heterotic string can

reproduce the NMSSM in a Peccei-Quinn limit with a light Pseudo-Goldstone boson, an axion-like particle. The breaking of larger groups down to the SM gauge group can in general yield hidden U(1) symmetries which may remain unbroken down to small energy scales. Their hidden photon may be light and couple weakly to the visible sector through kinetic mixing [13, 14].

In the following we present various constraints on the NMSSM CP-odd Higgs as representative of an axion-like particle and the hidden photon for masses below the muon threshold.

2 NMSSM CP-odd Higgs

The extension of the MSSM with an additional scalar field S to the NMSSM has been motivated as it solves the μ-problem by replacing the μ-parameter with a SM singlet S [15]. Additionally, the enlargement of the particle content by an additional CP-odd Higgs A^0 alleviates the little hierarchy problem if A^0 is light by opening an additional Higgs decay channel $h \to 2A^0$, thereby reducing the LEP limit on the Higgs mass. We focus our analysis on the Z_3-symmetric NMSSM, a special version without direct μ-term, with superpotential

$$W = \lambda S H_u H_d + \frac{1}{3}\kappa S^3.$$

In the limit $\kappa \to 0$, the Higgs potential possesses an approximate Peccei-Quinn symmetry and a naturally light pseudoscalar A^0 arises with $m^2_{A^0} \simeq \kappa \cdot \mathcal{O}(\text{EW scale})^2$ where $\kappa \ll 1$. In the heterotic string example of [12], κ can be as small as 10^{-6} resulting in a 100 MeV pseudoscalar. Its couplings to fermions are according to [16] given by

$$\Delta\mathcal{L} = -i\frac{g}{2m_W}\, C_{Aff} \left(m_d\, \bar{d}\gamma_5 d + \frac{1}{\tan^2\beta} m_u\, \bar{u}\gamma_5 u + m_l\, \bar{l}\gamma_5 l \right) A^0.$$

We treat C_{Aff} as free parameter focusing on the range $10^{-2} \lesssim C_{Aff} \lesssim 10^2$ to avoid violation of perturbativity and/or finetuning and summarize the constraints derived in [17] in the following.

Different meson-decays set bounds for two distinct cases depending on the lifetime of A^0. If it is sufficiently long lived to escape the detector, invisible decays $X \to Y + A^0 \to Y +$ inv. place limits requiring $\Gamma^{X\to YA^0}/\Gamma^{\text{tot}} < \mathcal{B}^{\text{exp}}_{\text{inv}}$. Larger values of C_{Aff} for which A^0 decays within the detector are constrained by visible decays $X \to Y + A^0 \to Y + e^+e^-$ demanding $\text{BR}^{\text{X}\to\text{YA}^0}\text{BR}^{\text{A}^0\to\text{e}^+\text{e}^-} < \mathcal{B}^{\text{exp}}_{\text{e}^+\text{e}^-}$. Together with the limit from a search for a peak in the π^+ momentum spectrum in $K^+ \to \pi^+ + X$, meson decays cover most of the parameter space in Fig. 1.

Complementary constraints arising from the pion-decay $\pi^0 \to e^+e^-$ and the muon anomalous magnetic moment a_μ completely close the available parameter space. The former process which proceeds in the SM through loop diagrams receives a tree level contribution from A^0 and sets a limit requiring $\Gamma^{\pi^0 \overset{A^0}{\to} e^+e^-}/\Gamma^{\text{tot}} < \mathcal{B}^{\text{exp}}_{\pi^0\to e^+e^-}$. As there are several NMSSM contributions to a_μ of both signs, even though the negative loop-contribution from A^0 worsens the current discrepancy $a^{\text{exp}}_\mu > a^{\text{SM}}_\mu$, we derive a constraint demanding A^0 not to worsen it beyond 5σ.

Additional constraints can be derived from beam-dump and reactor experiments (lines and shaded regions, respectively, in Fig. 1, right) searching for the decay $A^0 \to e^+e^-$. Like any ALP, A^0 can be emitted in the former via bremsstrahlung from an e- or p-beam and in the latter in place of photons in transitions between nuclear levels.

In summary, for masses below the muon threshold, the CP-odd Higgs is excluded or required to couple to matter at least 4 orders of magnitude weaker than the SM Higgs which can hardly be achieved in the NMSSM. Those constraints as they are plotted in Fig. 1 apply in general to the coupling of a light pseudoscalar to matter.

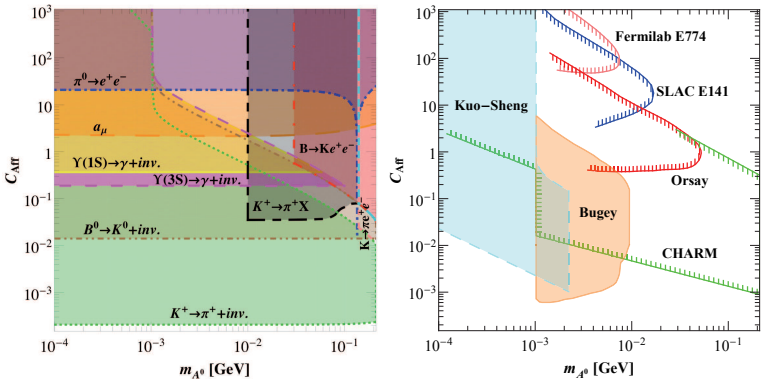

Figure 1: Excluded regions for the NMSSM CP-odd Higgs [17].

3 Hidden U(1) gauge boson

Many SM extensions contain additional U(1) symmetries in the hidden sector under which the SM is neutral. The corresponding gauge boson, the hidden photon γ' and the ordinary photon kinetically mix [13, 18] induced by loops of heavy particles charged under both U(1) groups.

The most general Lagrangian is

$$\mathcal{L} = -\frac{1}{4}F_{\mu\nu}F^{\mu\nu} - \frac{1}{4}X_{\mu\nu}X^{\mu\nu} + \frac{\chi}{2}X_{\mu\nu}F^{\mu\nu} + \frac{m^2_{\gamma'}}{2}X_\mu X^\mu$$

where $F^{\mu\nu}$ is the usual electromagnetic field strength and $X^{\mu\nu}$ the one corresponding to the hidden gauge field X^μ. The kinetic mixing χ is typically of the size of a radiative correction $\sim \mathcal{O}(10^{-4} - 10^{-3})$. Kinetic mixing allows γ' to couple and decay to SM fermions thereby making it accessible for experimental searches, the constraints of which are presented in the following.

Similarly to the CP-odd Higgs, limits arise from one-loop contributions of the hidden photon to the muon and electron anomalous magnetic moment [19]. Also beam-dump experiments in which γ' is emitted through bremsstrahlung from an e-beam can set constraints by searching for the decay $\gamma' \to e^+e^-$ [20]. The resulting limits (shaded in Fig. 2) leave an unexplored region in the parameter space which is best explored by fixed-target experiments [20, 21]. Dedicated proposals are being developed at DESY (HIPS, see also [22]), JLab (APEX [23, 24], HPS [25], DarkLight [21, 26]), and Mainz (MAMI, MESA [27]), with complementary sensitivities (cf. lines in Fig. 2, right).

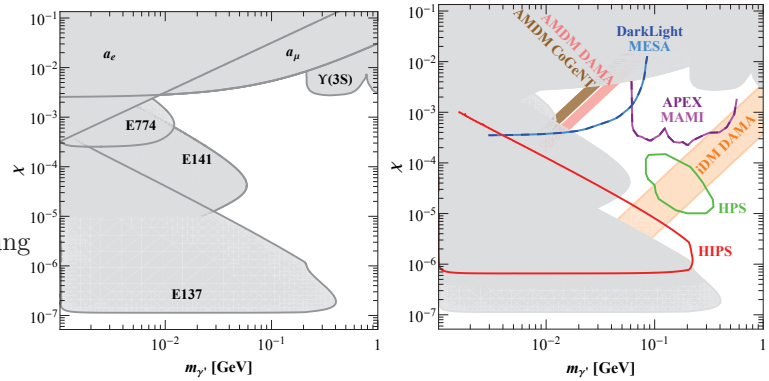

Figure 2: Exclusion regions *(left)* as well as projected sensitivities and phenomenological motivations *(right)* for the hidden photon.

The whole allowed parameter range in Fig. 2 is phenomenologically interesting for DM with

dark photons of a generic hidden U(1) [7] or mirror photons in asymmetric mirror DM models (AMDM) [11]. The former can reproduce DAMA for inelastic DM [28] (orange "iDM" band) and achieve naturally the leptophilic DM annihilation required for PAMELA [29], while the latter is able to explain the DAMA and CoGeNT measurements with mirror neutrons as DM [30] (colored "ADMD" bands).

4 Conclusions

Hidden sectors are well motivated by DM, SM extensions, and string theory. They might contain light particles that despite their very weak couplings to the SM can be constrained experimentally. In particular, the NMSSM CP-odd Higgs has to be heavier than 210 MeV or couple much weaker to fermions than the SM Higgs. Hidden photons on the contrary are less constrained and can be searched for in complementary experiments at DESY, JLab and Mainz.

References

[1] R. Sparvoli, "Understanding Cosmic Rays and searching for DM with PAMELA," these proceedings.

[2] L. Strigari, "Search for Dark Matter with Fermi," these proceedings.

[3] R. Cerulli, "Results of the DAMA/LIBRA experiment," these proceedings.

[4] D. Balakishiyeva, "CDMS," these proceedings.

[5] U. Oberlack, "WIMP Dark Matter Search with XENON and DARWIN," these proceedings.

[6] D. Hooper and T. M. P. Tait, Phys. Rev. D **80** (2009) 055028 [arXiv:0906.0362].

[7] N. Arkani-Hamed et al., Phys. Rev. D **79** (2009) 015014 [arXiv:0810.0713].

[8] C. Cheung, J. T. Ruderman, L. T. Wang and I. Yavin, Phys. Rev. D **80** (2009) 035008 [arXiv:0902.3246].

[9] D. E. Morrissey, D. Poland and K. M. Zurek, JHEP **0907** (2009) 050 [arXiv:0904.2567].

[10] T. Cohen, D. J. Phalen, A. Pierce and K. M. Zurek [arXiv:1005.1655].

[11] H. An, S. L. Chen, R. N. Mohapatra and Y. Zhang, JHEP **1003** (2010) 124 [arXiv:0911.4463].

[12] O. Lebedev and S. Ramos-Sanchez, Phys. Lett. B **684** (2010) 48 [arXiv:0912.0477].

[13] B. Holdom, Phys. Lett. B **166** (1986) 196.

[14] M. Goodsell, J. Jaeckel, J. Redondo and A. Ringwald, JHEP **0911** (2009) 027 [arXiv:0909.0515].

[15] J. R. Ellis, J. F. Gunion, H. E. Haber, L. Roszkowski and F. Zwirner, Phys. Rev. D **39** (1989) 844.

[16] R. Dermisek and J. F. Gunion, Phys. Rev. D **81** (2010) 075003 [arXiv:1002.1971].

[17] S. Andreas, O. Lebedev, S. Ramos-Sanchez and A. Ringwald, JHEP **1008** (2010) 003 [arXiv:1005.3978].

[18] D. Cadamuro and J. Redondo, "Hidden Photons from the Sun," these proceedings [arXiv:1010.4689].

[19] M. Pospelov, Phys. Rev. D **80** (2009) 095002 [arXiv:0811.1030].

[20] J. D. Bjorken, R. Essig, P. Schuster and N. Toro, Phys. Rev. D **80** (2009) 075018 [arXiv:0906.0580].

[21] M. Freytsis, G. Ovanesyan and J. Thaler, JHEP **1001** (2010) 111 [arXiv:0909.2862].

[22] J. Mnich, "Axions, WIMPs and WISPs at DESY," these proceedings.

[23] R. Essig, P. Schuster, N. Toro and B. Wojtsekhowski, [arXiv:1001.2557].

[24] A. Afanasev, "Searches for Dark Matter candidates with electron beams at JLAB," these proceedings.

[25] T. Maruyama, talk given at the SLAC - Dark Forces Workshop, 2009.

[26] J. Thaler and P. Fisher, talk given at the SLAC - Dark Forces Workshop, 2009.

[27] A. Denig, talk given at the JLab Workshop - Searching for a New Gauge Boson at JLab, 2010.

[28] R. Essig, P. Schuster and N. Toro, Phys. Rev. D **80** (2009) 015003 [arXiv:0903.3941].

[29] P. Meade et al., Nucl. Phys. B **831** (2010) 178 [arXiv:0905.0480].

[30] H. An et al., Phys. Rev. D **82** (2010) 023533 [arXiv:1004.3296].

Measurements in Search for 0.1 meV Axion–Like Particles and Hidden Sector Photons using Copper Resonant Cavities

P. L. Slocum, O. K. Baker, J. L. Hirshfield, Y. Jiang, G. Kazakevitch, S. Kazakov, M. A. LaPointe, A. Martin, S. Shchelkunov, A. Szymkowiak

Yale University, 260 Whitney Avenue, New Haven, CT 06457

DOI: http://dx.doi.org/10.3204/DESY-PROC-2010-03/slocum_penny

We present preliminary measurements from the electronics chain in the 34 GHz photon regeneration experiment at Yale. The experiment is a search for the coupling ($g = 10^{-6}$/GeV) of two photons to a light neutral boson (LNB) in the presence of a strong axial magnetic field. The final setup will consist of two side by side Cu resonant cavities, one of which will be coupled to the pulsed, ∼1 MW 34.29 GHz magnicon at Yale. Using the same apparatus, we will look for mixing between photons and hidden sector photons (χ=10^{-7}). The experiment will also have limited sensitivity to galactic halo axions. Preliminary tests of the electronics chain have yielded results that are consistent with original estimates.

1 Introduction

Several proposed extensions to the standard model of elementary particles have motivated a wide array of searches for new particles with sub–eV masses. For example, the axion [1] and other axion–like particles (ALPs) have been postulated to account for broken symmetries and should behave as weakly interacting sub–eV particles (WISPs) (see e.g. [2]). Additional *hidden sector* particles with very low masses arise from supersymmetry and interact only rarely with standard model particles [3][4]. In each case the discovery of a new low–mass neutral particle could also be a possible cosmological Dark Matter candidate.

Many searches for new sub–eV particles in the laboratory have relied upon their coupling with low energy photons. In particular the *light shining through walls* (LSW) experiments (e.g. [5][6][7][8][9]) and resonant cavity searches for galactic halo axions [10] have placed stringent limits on the photon coupling constants, predominantly below 1 meV. In this work we discuss preliminary tests of a LSW experiment utilizing two resonant cavities, one of which will be driven at 34 GHz by the high–power *magnicon* microwave source at Yale [11] [12].

2 Experiment

The apparatus [13] will consist of two side by side Cu resonant cavities, one of which will be driven by the 34 GHz microwave source. The second (signal) cavity will be electromagnetically isolated from the drive cavity, and cooled to below 10 K in a He gas flow cryostat. The cavities and cryostat will sit inside the bore of a 7 T magnet.

The electronics chain begins with a cryogenic low noise HEMT amplifier inside the cryostat and is followed by a room temperature microwave receiver. Tests of the room temperature components are summarized in the next section.

2.1 Receiver

The receiver [14] is a triple heterodyne with a total gain of approximately 130 dB. The room temperature segment of the electronics chain is shown in Figure 1. It is preceded by a cryogenic HEMT amplifier with a typical noise figure of 22 K. The 34 GHz RF signal is mixed down to 4.09 GHz, amplified and filtered, then is mixed down to 590 MHz. After further amplification the signal is mixed down to a few MHz in in–phase (I) and quadrature (Q) paths, where a 4 MHz low pass filter precedes the final voltage preamplifier.

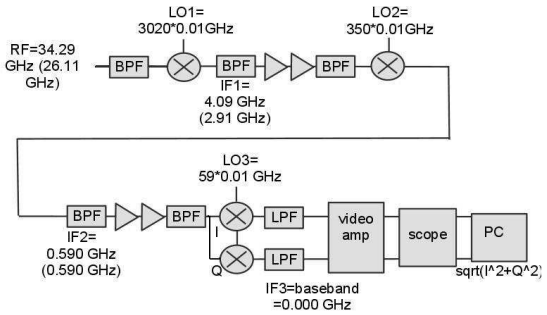

Figure 1: Block diagram of the room temperature electronics chain. Quantities in parentheses are the image frequencies LO–IF.

The first test of the electronics chain was to place a 50Ω terminator at the RF input to the first room temperature mixer. The middle column of Table 1 shows the resulting noise power measured at each component along the receiver chain. The right column denotes the expected power based on the assumption of a flat thermal noise spectrum, and on the specified gains and noise figures of the components cascaded to the point of the measurement. The table indicates good agreement between the measured and expected values.

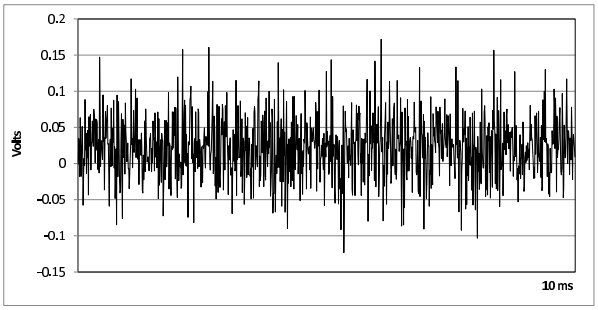

Figure 2: Oscilloscope trace showing the output of the voltage preamplifier with a 50Ω terminator at the input to the first mixer in the room temperature electronics chain.

The final component of the receiver is a pair of broadband voltage amplifiers each with gain adjustable

component	measured (dBm/Hz)	expected (dBm/Hz)
300K 50Ω term.		-174
(IF1=4.09 GHz)		
mixer 1	<-150	-173
BPF	<-150	-173
IF1 amp	-112	-112
BPF	-112	-112
(IF2 590 MHz)		
mixer 2	-116	-118
BPF	-118	-119
IF2 amp	-85	-85
BPF	-87	-86
(IQ mixer)		
LPF (I)	-92	-95
LPF (Q)	-94	-95
(V amp in)		
input (I)	-95	-95
input (Q)		-95

Table 1: Measured power and expected power along the room temperature components of the receiver chain using a 50 Ω terminator at the input to the first mixer. The "measured" values of the voltage amplifier inputs are reconstructed from the oscilloscope trace shown in Figure 2.

from 5× through 625× and maximum output of 1 volt. Figure 2 shows an oscilloscope trace of one amplifier's output in the I path, using a room temperature 50 Ω terminator at the RF input to the first 34 GHz mixer.

The trace shown in Figure 2 is related to the power at the output of the IQ mixer. First the standard deviation of the voltage fluctuations σ_V is calculated as

$$\sigma_V = \sqrt{\frac{\sum_i (V_i - \mu)^2}{N}}$$

where V_i is the ith voltage sample on the trace, μ is the mean voltage, and N is the number of points on the trace. The power P_N at the input is then

$$P_N = \sigma_V^2 / G^2 / R / B$$

where G is the voltage gain of the amplifier (5×) and R is its input impedance (50Ω). B is the 4 MHz bandwidth of the low pass filter. Table 1 contains the power reconstructed at the input in the I path (-95 dBm/Hz).

3 Outlook

3.1 Halo Axions

Like the photon regeneration experiments, the sensitivity of the apparatus to galactic halo axions is limited by the thermal noise power

$$\begin{aligned} P_N &= k_B T_N B \\ &= (10^{-23}\ \text{J/K})(20\ \text{K})(3.4\ \text{MHz}) \\ &\approx 10^{-15}\ \text{W}. \end{aligned}$$

where T_N is the typical noise temperature of the cooled HEMT amplifier and B is the bandwidth of the cavity in the TE011 mode, $B = f/Q$ =34 GHz/10^4.

The signal power P_S is estimated to be

$$P_S = \rho V \Pi Q E.$$

The halo axion concentration ρ is taken to be 0.45 GeV/cm^3 [15], or 10^{13}/cm^3 at 34 GHz. The probability of conversion Π is estimated by $(1/4)(gBL)^2$[16][17]. For g∼10^{-4}/GeV P_S is approximately 10^{-17} W or 1% of the noise power. This sensitivity could and should be improved, for example, with a lower noise amplifier, a cavity with a higher Q, or by implementing an experiment with more than one cavity (e.g. [18]). In the meantime the current apparatus can be useful for a measurement that is less sensitive but is still valuable as a proof of concept.

3.2 LSW experiment

Tests of the room temperature electronics chain and data acquisition are complete and the results are consistent with expected values. Fabrication and testing of the resonant cavities is ongoing, and the cryostat is being cooled routinely to temperatures below 10 K. The next steps will be to check the output of the electronics with a cold resonant cavity and HEMT amplifier at the input. Sensitivity of the experiment is expected to be on the order of g>10^{-6}/GeV for LNBs and χ>10^{-7} for HSPs [13].

Acknowledgments

This work was supported by the U.S. Office of Naval Research at Yale University. The authors are also very grateful to W. Guinon, J. Jaeckel, and S. Weinreb for many helpful and detailed discussions about this work.

References

[1] R. D. Peccei and H. R. Quinn, Phys. Rev. **D16** 1791 (1977).

[2] J. Jaeckel and A. Ringwald, Ann. Rev. of Nuc. and Part. Sci., **60** doi: 10.1146/annurev.nucl.012809.104433 (2010).

[3] M. Ahlers *et. al.*, Phys. Rev. **D77** 095001 (2008).

[4] J. Jaeckel and A. Ringwald, Phys. Lett. **B659** 509 (2008).

[5] K. V. Bibber *et al.*, Phys. Rev. Lett **59** 759 (1987).

[6] A. Afanasev *et al.*, Phys. Lett **B679** 317 (2009).

[7] A. Afanasev *et al.*, Phys. Rev. Lett **101** 120401 (2008).

[8] F. Caspers, J. Jaeckel, and A. Ringwald, JINST **4** P11013 (2009) doi: 10.1088/1748-0221/4/11/P11013

[9] K. Ehret et al. [ALPS collaboration], Nucl. Instrum. Meth. A **612** 83 (2009).

[10] P. Sikivie, Phys. Rev. **48** 1156 (1982).

[11] O. A. Nezhevenko, *Gyrocons and magnicons: Microwave generators with circular deflection of the electron beam*, IEEE Trans. Plasma Sci. **22** 756 (1994).

[12] O. A. Nezhevenko, M. A. LaPointe, V. P. Yakovlev, and J. L. Hirshfield, *Commissioning of the 34–GHz, 45–MW Pulsed Magnicon*, IEEE Trans. Plasma Sci., **32**, 994 (2004).

[13] P. L. Slocum et al., Axions, WIMPs and WISPs. Proceedings, 5th PatrasWorkshop, PATRAS09, Durham, UK, July 13-17, 2009,

[14] W. Guinon, private communication (2009).

[15] E. I. Gates, G. Gyuk, and M. S. Turner, Astrophys. J. Lett. **L123** 449 (1995).

[16] R. Cameron *et al.*, Phys. Rev. **D47** 3707 (1993).

[17] E. Zavattini et al., Phys. Rev. Lett. **96** 110406 (2006).

[18] K. V. Bibber, seminar at Yale Physics Dept., (2010).

GammeV: Search for WISPs at Fermilab

*William Wester**

Fermilab, MS209, Batavia IL, USA
presented on behalf of the GammeV *and* GammeV-CHASE *Collaborations*

DOI: http://dx.doi.org/10.3204/DESY-PROC-2010-03/wester_william

The GammeV experiment has searched for Weakly Interacting Slim Particles (WISPs) and has previously published exclusion plots for axion-like particles and a first exclusion of chameleons that couple to photons. Recently, a new experiment, GammeV-CHASE, has obtained improved preliminary results in the search for chameleons. Members of the collaboration are also involved in R&D in long baseline optical cavities that might be required for a photon resonnant regeneration experiment or a search for holographic noise.

1 Introduction

Physics beyond the Standard Model might include Weakly Interacting Slim Particles (WISPs) that would address fundamental questions such as what is the nature of dark matter or even shed insight into the underlying nature of dark energy. WISPs are a general class of particles that include axions, axion-like particles, hidden sector photons, milli-charged particles, chameleons etc. The GammeV experiment originated in 2007 in order to test an anomalous axion-like particle signal by the PVLAS experiment [1] which was not evident in subsequent data [2]. The GammeV experiment utilized a laser and an accelerator magnet in a light shining through a wall (LSW) [3] configuration where a photon propagating in a magnetic field could oscillate into a WISP, traverse an opaque barrier, and have a small probabilty for reconverting back into a detectable photon. GammeV excluded the WISP interpretation of the anomalous result. Beyond this result, it has been found that the parameter space of a variety of other WISP candidates is both largely unexplored and is accessible by modest experiments employing lasers and possibly accelerator magnets. GammeV data has also been used to set limits on possible hidden sector photons [4]. Further work by the GammeV team has focused on a reconfiguration of the apparatus to be sensitive to chameleon particles including a new result presented here. In order to extend sensitivity for searches beyond what has been achieved, new techniques employing optical cavities are under development.

2 Axion-like particle search

The GammeV apparatus consists of a 3W pulsed Nd:YAG laser frequency doubled to 532 nm shown into the warm bore of a Tevatron dipole magnet operating at 5 T. Two novel aspects have been employed in order to increase sensitivity over the region of interest. A plunger is

*This work is supported by the U.S. Department of Energy under Contract No. DE-AC02-07CH11359

constructed so that it can place the "wall" either in the middle or toward one end of the magnet in order to remove regions of insensitivity of mass where the oscillation probability vanishes. The second aspect is to utilize time correlated single photon counting techniques in order to have high efficiency for signal and very low noise. The chance of a random PMT pulse being in time with a laser pulse is very small compared with the possible rate of regenerated photons. No signal above background is observed and 3σ exclusion limits for the coupling of scalar and pseudoscalar axion-like particles to photons in milli-eV mass region have been published [6] and are consistent with the results obtained by other experiments [7].

Figure 1(a) shows an enhanced LSW experiment that employs phased locked optical cavities on both the generation and regeneration side of the wall [9]. The "**R**esonnantly **E**nhanced **A**xion **P**hoton **R**egeneration" (REAPR) possible project is in an R&D phase to develop the phase locking scheme between the cavities and to explore the achievable finessee, $\mathcal{F}$, of long baseline cavities. The sensitivity to the $g_{a\gamma\gamma}$ coupling constant scales as the fourth root of the product of the two $\mathcal{F}$'s and linearly with the magnetic field length. With at least 12 Tevatron magnets in length and $\mathcal{F} \sim 10^5$, a sensitivity of $g_{a\gamma\gamma} < \sim 10^{-11}$ would be achievable, exceeding current experimental bounds on the coupling of axion-like particles to photons.

R&D on long baseline optical cavities is expected to continue for the next couple of years at Fermilab. During this time, clarification on the required infrastructure to support a long magnet string will be obtained. In the meantime, design work for optical feedback and control for the two phased matched cavities will continue with collaborators at the University of Florida. The R&D on long baseline optical cavities is also relevant at Fermilab for a laser interferometer experiment that might be sensitive to "holographic noise" [10] - a possible jitter in space-time due to Planck scale effects. The status is that a 40m long vacuum system is being constructed in an otherwise unused and vacant beam tunnel at Fermilab. Two service vacuum vessels are connected by valves, bellows, and about 40m of vacuum tubes with a diameter of 6 inches. Baffles have been developed that will reduce the clear apparature to about 4 inches but will greatly reduce the chance of scattered light from adding phase noise into the cavity. A laser table will allow for the launch of a laser beam into one service vessel where the light in vacuum will then move through a power recycling mirror, through one end mirror, down the 40m of length, and reflect upon the end mirror on the far service vessel. Sensitive photodiodes will be employed for monitoring and feedback of the cavity. Specially coated optics with small losses have been ordered. The piezo actuated control system including using a Pound-Drever-Hall locking scheme is also being developed. First results on the achievable finesse of this cavity are expected in early 2011.

3 Chameleon search

Chameleons are WISPs that usually take the form of a scalar particle coupled to the stress energy tensor in a potential such that their properties depend on their environment. In particular, a chameleon acquires an effective mass proportional to its local matter density. The original GammeV apparatus was reconfigured such that a laser is shown through the chamber (no wall) with photons that might oscillate into chameleons and reflect off of the exit vacuum windows or vacuum walls estenially building up a gas of chameleon particles within the vacuum region. The laser is turned off and the PMT is turned on to look for an expontential signal decay above background as chameleons reconvert back into photons resulting in a detectable afterglow.

GammeV searched for chameleons and no afterglow was observed. Fig. 2 shows the exclu-

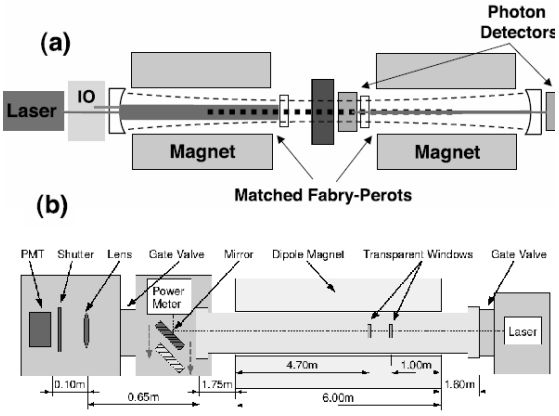

Figure 1: Schematic of the (a) resonnant regeneration light shining through a wall proposal and (b) the GammeV-CHASE experiment.

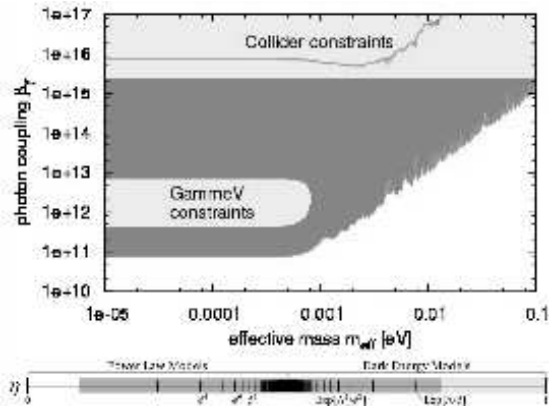

Figure 2: (a) The exclusion region of the coupling normalized to the Planck mass to photons versus the effective chameleon massas published for the GammeV reconfiguration (small region) and the results from GammeV-CHASE.

sion region in the chameleon coupling to photons vs effective chameleon mass obtained under the assumption that the chameleon potential had a characteristic mass dependence on matter density $m_{eff} \propto \rho^{\alpha}$ with $\alpha > 0.8$ [11].

A new effort, **GammeV - CHASE** (**CH**ameleon **A**fterglow **SE**arch), has been mounted during the past year. In this reincarnation, shown in Fig. 1(b), improvements to the original chameleon search have been addressed. Data taking at reduced magnetic field allows for a probe for very strong chameleon couplings to photons. A lower noise PMT helps improve the sensitivity for weak couplings. A "dish rack" that holds optical windows such that the 6 m magnetic field region is divided into regions of approximately 4.7 m, 1.0 m, and 0.3 m, probes higher effective masses. Finally, removing a mechanical pump and utilitizing very low vacuum enabled by cryopumping allows for sensitivity of an extended range of $\alpha > 0.1$ such that potentials consistent with various chameleon dark energy models can be probed [12].

For both scalar and pseudoscalar configurations, data was recorded at magnetic fields from 0.05 T to 5 T in science runs. A laser-on time of 10 minutes was followed by a rapid transition using gate valves and shutters to a laser-off period when the PMT was exposed to the apparatus to search for afterglow. During this $\sim$ 15 min period, the shutter was alternatively opened and closed in $\sim$ 15s periods to allow for a background subtraction. For small couplings to photons, longer runs at the maximum field strength were employed. Two runs for each of the polarizations consisted of approximately 5 hours of filling and 45 minutes of data collection. Calibration runs are acquired before and after science runs. These runs have no magnetic field and showed two systematic effects. The first was a 1.15 ± 0.08 Hz of photons present in the shutter open data which is thought to be dominated by small light given off of ion pumps (note ion gauges, which give off quite a bit of light, are turned off during the data collection periods). This small effect demonstrates the ability of the apparatus to be sensitive to a small rate of photons at a level of $\sim$ 1 Hz. The second systematic effect has been dubbed "orange glow" as it appears when using several 40nm-wide orange wavelength filters. The glow is observed as a steeply falling rate of

excess photons present shortly after the laser is turned off. The excess rate after the laser is turned off has most of the rate disappearing after a few 10s of seconds; however, a small residual amount lasts beyond 120s. The rate depends heavily on temperature with an initial amplitude of several hundred Hz when the magnet and cold bore are near 4K, a few 10s of Hz when the magnet is cooled to liquid N_2 temperatures, and just a few Hz when the magnet is at room temperature. The working assumption is that impurities in the dish rack windows get optically excited or other phosphoresent contaminates are present despite no evidence in RGA scans of our vacuum. Further investigation will continue and since this observation at no magnetic field is not consistent with a chameleon, limits are derived from a non-observation of excess rate after these two systematics are subtracted. Figure 2 shows the preliminary exclusion region for the photonic coupling versus effective mass. An exclusion region of the matter coupling versus photonic coupling for a variety of potential models has also been obtained [13].

4 Conclusions

A new research program at Fermilab has obtained published results for axion-like particle and chameleon searches. Next generation experiments have started or are undergoing R&D. The possibility that WISPs or other phenomenon might be observable using relatively inexpensive experimental optical set-ups allows for searches of physics beyond the Standard Model. Who knows, such crazy experiments might just reveal a new weirdness of nature.

References

[1] E. Zavattini *et al.* [PVLAS Collaboration], Phys. Rev. Lett. **96**, 110406 (2006) [arXiv:hep-ex/0507107].

[2] E. Zavattini *et al.* [PVLAS Collaboration], arXiv:0706.3419 [hep-ex].

[3] K. Van Bibber, N. R. Dagdeviren, S. E. Koonin, A. K. Kerman and H. N. Nelson, Phys. Rev. Lett. **59**, 759 (1987).

[4] M. Ahlers, H. Gies, J. Jaeckel, J. Redondo and A. Ringwald, Phys. Rev. D **77**, 095001 (2008) [arXiv:0711.4991 [hep-ph]].

[5] R. Cameron *et al.*, Phys. Rev. D **47**, 3707 (1993).

[6] A.S. Chou *et al.* [GammeV Collaboration], Phys. Rev. Lett. **100**, 080402 (2008). Additional description may be found at: `http://gammev.fnal.gov`.

[7] M. Fouche *et al.* [BMV Collaboration], Phys. Rev. D **78**, 032013 (2008) [arXiv:0808.2800 [hep-ex]].
K. Ehret *et al.* [ALPS Collaboration], Phys. Lett. B **689**, 149 (2010).
A. Afanasev *et al.* [LIPSS Collaboration], Phys. Rev. Lett. **101**, 120401 (2008) [arXiv:0806.2631 [hep-ex]].
P. Pugnat *et al.* [OSQAR Collaboration], Phys. Rev. D **78**, 092003 (2008) [arXiv:0712.3362 [hep-ex]].

[8] P. Sikivie, Phys. Rev. Lett. **51**, 1415 (1983) [Erratum-ibid. **52**, 695 (1984)]. P. Sikivie, Phys. Rev. D **32**, 2988 (1985) [Erratum-ibid. D **36**, 974 (1987)].

[9] G. Mueller, P. Sikivie, D. B. Tanner and K. van Bibber, Phys. Rev. D **80**, 072004 (2009) [arXiv:0907.5387 [hep-ph]].

[10] C. J. Hogan, arXiv:0905.4803 [gr-qc]. See also:
`www.fnal.gov/directorate/program_planning/Nov2009PACPublic/holometer-proposal-2009.pdf`.

[11] A. S. Chou *et al.* [GammeV Collaboration], Phys. Rev. Lett. **102**, 030402 (2009) [arXiv:0806.2438 [hep-ex]].

[12] A. Upadhye, J. H. Steffen and A. Weltman, Phys. Rev. D **81**, 015013 (2010) [arXiv:0911.3906 [hep-ph]].

[13] J. H. Steffen *et al.*, arXiv:1010.0988 [astro-ph.CO].

ALPS – WISP Search at DESY

Klaus Ehret[1] *for the ALPS Collaboration*

[1]DESY, Notketraße 85, 22607 Hamburg, Germany

DOI: http://dx.doi.org/10.3204/DESY-PROC-2010-03/ehret_klaus

The ALPS experiment at DESY performs a *light shinning through the wall* experiment to search for *Weakly Interacting Slim Particles (WISPs)*. Resonant laser power build-up with a large-scale optical cavity boosts the available power for WISP production and facilitates the experiment to provide the most stringent laboratory constraints on WISP production. Resent results as well as plans for the next phase are presented.

1 Low Energy Frontier: ALPs and other WISPs

In the last years it has been realized, that extensions of the Standard Model may manifest itself also at low energy scales. They predict very *weakly interacting slim particles (WISPs)*. Potential WISP candidates are *axion-like particles (ALPs)* or *hidden sector photons (HPs)*. The low energy frontier is a rich complement to the conventional high-energy particle physics landscape [1, 2, 3]. There exist several hints from astrophysics pointing to new physics in the sub-eV range and a QCD axion in the sub-meV would be a cold Dark Matter candidate.

There are prediction from theory which can be tested in dedicated high precision lab experiments and the search for these new particles initiated experimental activities around the world [2]. *Light shining through a wall (LSW)* experiments, cf. Fig. 1, are an old intriguing simple idea [4, 5, 6] to perform direct WISP searches with an enormous sensitivity [1, 3].

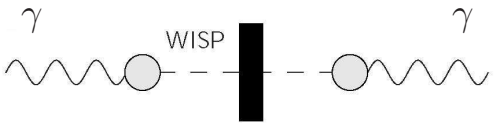

Figure 1: Sketch of a LSW experiment. Photons, typically from a laser, are shone on a light tight wall. Some photons may be converted into WISPs which traverse the wall. Behind the wall some of these WISPs reconvert into ordinary photons, with the same properties as the initial photons, which are observed with a detector.

The conversion of the incident photons to an axion-like particles ϕ and its reconversion in the presence of a magnetic field is governed by the Primakoff effect. Assuming that the mass m_ϕ and two photon coupling g of the ALPs are uncorrelated the LSW probability in a symmetric setup is given by

$$P_{\gamma\to\phi\to\gamma} = \frac{1}{16\beta_\phi^2}(gBL)^4 \left(\frac{\sin(qL/2)}{qL/2}\right)^4 ,$$

with B the magnetic field strength, L the length of the conversion region, β_ϕ denoting the velocity of the ALP and $q = p_\gamma - p_\phi$.

For $qL << 1$ the oscillation is coherent along the full length and the transition probability reaches its maximum $P_{\gamma\to\phi\to\gamma} = 1/(16\beta_\phi^2)\cdot(gBL)^4$. For a larger ALP mass m_ϕ the momentum p_ϕ decreases, i.e. the wavelength rises and runs out of phase compared to the photon wave

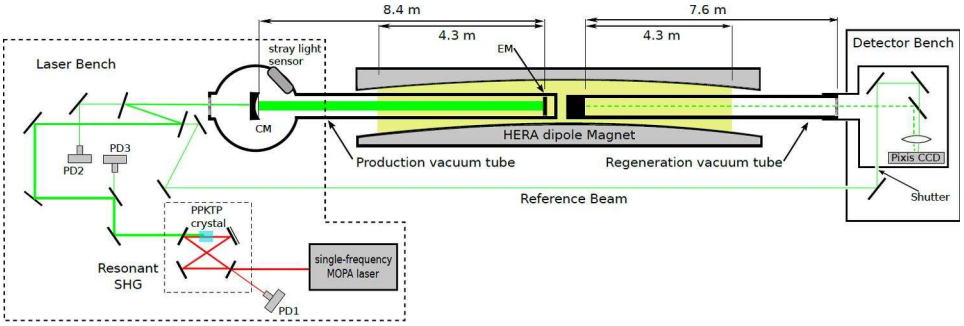

Figure 2: Sketch of the ALPS experiment. PD denotes various photo detectors, CM the coupling mirror and EM the end mirror of the resonant cavity. See the text and references for details.

function, causing a lower conversion probability, cf. Fig. 3. The sensitivity of LSW experiments is mainly determined by the number of incident photons, $B \cdot L$ of the magnet and the capability of the detector, cf. Tab. 1. The polarization of the beam allows to distinguish between scalar and pseudo scalar ALPs.

2 The ALPS Experiment at DESY

The **A***ny* **L***ight* **P***article* **S***earch (ALPS)* experiment located at DESY in Hamburg uses a spare superconducting HERA dipole magnet with a field $B \approx 5$ T and exploits resonant laser power build-up in a large-scale optical cavity to perform a *light shining through a wall* experiment [4, 5, 6] for direct WISP searches. The ALPS collaboration comprises besides DESY the Albert Einstein Institute in Hannover, the Laser Zentrum Hannover and the Hamburg observatory.

Figure 2 shows a sketch of the experimental setup. The opaque wall sits in the middle of the magnet. Inside the dipole magnet two beam tubes are placed, which bound the $\gamma - \phi$ conversion and reconversion regions and are operated under vacuum conditions. On the left side is the laser setup, providing the incident photons. On the right is the detector bench with the commercial CCD camera PIXIS 1024B, which is attached light-tight to the detector tube. Operated at -70 ^{o}C it features a very low dark current of 0.001 e^-/pixel/s as well as a low read-out noise of 3.8 e^-/pixel RMS and a very high quantum efficiency of more than 95% for green light. The beam spot is focused onto one defined 42×42 μm^2 bin of 9 pixels. Usually one hour frames are taken in order to minimize the impact of read-out noise, providing a sensitivity to a photon flux of a few mHz. For details of the ALPS setup refer to [7, 8]. ALPS also exploits successfully a new method to cover the gaps in the sensitivity for higher masses, where the ALP wave runs out of phase w.r.t. the phase of the laser beam. Introducing Ar gas at a pressure of 0.18 mbar changes the photon momentum and the $\gamma-$ALP relative phase velocity increases thereby to have an extra half oscillation length. Even if the sensitivity is lowered compared to vacuum conditions this helps to cover the high mass gaps, cf. Fig. 3.

The most sophisticated part of the ALPS experiment is the laser system and the resonant photon generation. ALPS is the first experiment, which successfully exploit a large-scale optical resonator for WISP searches. A LIGO-type single frequency laser system which allows a frequency shift of $\pm$100 MHz is used to produce 1064 nm laser light. In order to optimize the detection efficiency, the frequency of the laser beam is doubled to green light in a folded ring shaped resonator build around a nonlinear crystal. The length of the resonator is constantly changed in order to keep it resonant with the incident infrared laser light. The 532 nm laser beam is then redirected into the production vacuum tube in which photon-WISP conversions could occur. An optical resonator inside this pipe is used to buildup the laser power, enhancing

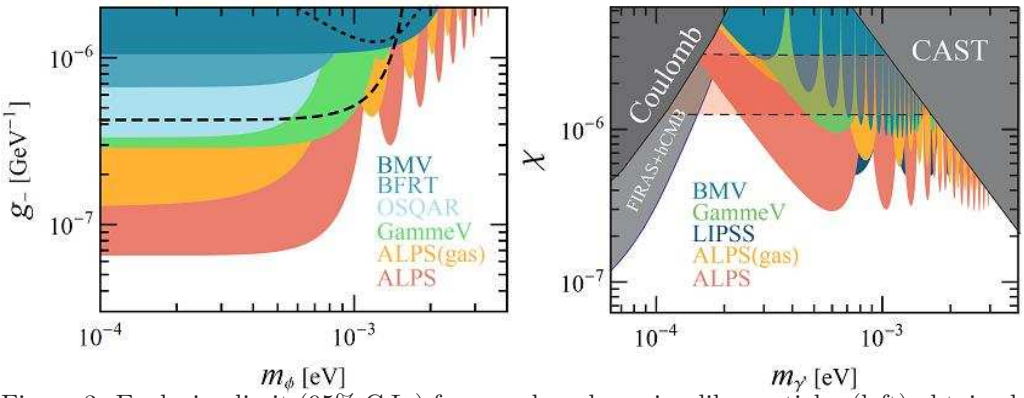

Figure 3: Exclusion limit (95% C.L.) for pseudoscalar axion-like particles (left) obtained by the ALPS experiment from vacuum and gas runs and for hidden photons (right) together with the results from various other LSW experiments, for details and references see [8].

proportionally the WISP flux. The frequency of the infrared laser is adopted in order to lock the cavity. Variations of the resonator frequency are dominated by length fluctuations of the setup. To avoid loses of the circulating laser light the complete cavity with both mirrors is housed inside the vacuum, cf. Fig. 2. This boosts the power build-up to $PB \approx 300$. During the measurement period in the year 2009 the green laser power feed into the cavity was kept below 5 W to minimize potential degradation of the cavity mirrors, resulting in a continuously circulating power inside the ALPS production region of around 1.2 kW.

ALPS took around 50 data sets (1 h frames) under different experimental conditions: with magnet on or off, laser polarization parallel or perpendicular to the magnetic field and different gas pressures. Details on the methodology and analysis are described in [7, 8]. From the non observation of any WISP signal a 95 % confidence level on the conversion probabilty was obtained, ranging between $P_{\gamma\to\phi\to\gamma} = 1...10 \times 10^{-25}$ for the different experimental setups. Fig. 3 shows the ALPS results for pseudoscalar axion-like particles and for hidden photon search together with the results obtained from other experiments.

3 Summary and Prospects for ALPS II

The ALPS experiment at DESY demonstrated successfully the feasibility of large scale optical cavities to boost the power available for WISP production. ALPS provides now the most stringent laboratory constraints on the existence of WISPs. This success is based on a close collaboration between particle physicist, laser physicists from the gravitational wave detector community and the infrastructure and support of a high-energy physics laboratory. Based on this background a detailed planing of a future large scale LSW experiments which improves the sensitivity by orders of magnitudes has started, aiming to surpass present day limits from astrophysics on the coupling of ALPs to photon [11]. This requires a sensitivity in the photon-ALP coupling of $g < 10^{-10}\text{GeV}^{-1}$, an improvement of 3 orders of magnitude with respect to the ALPS results. Table 1 summarizes the dependence of the sensitivity in g on experimental parameters together with possible improvements. The sensitivity in g improves linearly with the magnetic field strength and length. Instead of half an HERA dipole magnet one may use e.g. six magnets on each side providing a $BL \approx 280$ Tm. Furthermore it looks feasible to increase the

Table 1: Dependence of the photon-ALP coupling g on experimental parameter together with the prospects of the ALPS II experiment w.r.t. the actual ALPS setup, see text for details.

Parameter	g dependence	ALPS	ALPS II	gain
Magnetic field	$g \propto BL^{-1}$	$BL = 23$ Tm	$BL = 300$ Tm	13
Laser power	$g \propto P^{-\frac{1}{4}}$	$P = 1$ kW	$P = 100$ kW	3.2
Detector sensitivity	$g \propto \epsilon^{\frac{1}{4}}$	$\epsilon = 2$ mHz	$\epsilon = 0.02$ mHz	3.2
Measurement time[1]	$g \propto t^{-\frac{1}{8}}$	$t = 10$ h	$t = 1000$ h	1.8
Resonant regeneration	$g \propto PB^{-\frac{1}{4}}$	$PB = 1$	$PB = 10000$	10

incident laser power to the cavity by a factor of 10 and to improve the power build-up in the resonant cavity by an additional factor of 10. Single photon counting techniques, e.g. with cryogenic transition edge sensors may provide in addition a factor up to 100 improvement in the sensitivity. This results in two orders of magnitude improvement in the sensitivity for g. More statistics, i.e. longer measurement time, will not really help.

An old idea from the 1990's was recently rediscovered, namely to set up similar to the generation part an additional optical cavity for resonant axion photon regeneration, which enhances the small electromagnetic photon component of a potential WISP wave behind the wall [9, 10]. The technical details are rather challenging, e.g. one can obviously not use laser light of the same wavelength for locking and for the WISP production. ALPS II intend to use 1064 nm laser light for the WISP production and frequency doubled laser light with 532 nm for the locking of the regeneration cavity [12]. A power build of $PB \approx 10000$ seems to be possible, which would increase the sensitivity to g by another order of magnitude, enabling ALPS II to surpass present day limits on g from astrophysics.

References

[1] J. Jaeckel and A. Ringwald, arXiv:1002.0329 [hep-ph].

[2] J. Jaeckel, *Lab Searches for WISPs*, http://axion-wimp.desy.de and these proceedings.

[3] K. Ehret [ALPS Collaboration], arXiv:1006.5741 [hep-ex].

[4] L. B. Okun, Sov. Phys. JETP **56** (1982) 502 [Zh. Eksp. Teor. Fiz. **83** (1982) 892].

[5] A. A. Anselm, Yad. Fiz. **42** (1985) 1480.

[6] K. Van Bibber *et al.* Phys. Rev. Lett. **59** (1987) 759.

[7] K. Ehret *et al.* [ALPS collaboration], NIM A **612** (2009) 83 [arXiv:0905.4159 [physics.ins-det]].

[8] K. Ehret *et al.* [ALPS Collaboration], Phys. Lett. B **689** (2010) 149 [arXiv:1004.1313 [hep-ex]].

[9] F. Hoogeveen and T. Ziegenhagen, Nucl. Phys. B **358** (1991) 3.

[10] G. Mueller, P. Sikivie, D. B. Tanner and K. van Bibber, Phys. Rev. D **80** (2009) 072004 [arXiv:0907.5387 [hep-ph]].

[11] P. Arias, J. Jaeckel, J. Redondo and A. Ringwald, arXiv:1009.4875 [hep-ph] and these proceedings..

[12] T. Meier [ALPS Collaboration], AIP Conf. Proc. **1274** (2010) 156 [arXiv:1003.5867 [physics.optics]].

[1] For detectors limited in their sensitivity by background counting rates.

Engineering aspects of microwave axion generation and detection experiments using RF cavities

Fritz Caspers

CERN, CH-1211, Genve 23, Switzerland

DOI: http://dx.doi.org/10.3204/DESY-PROC-2010-03/caspers_fritz

Using microwave cavities one can build a resonant microwave-shining-throughwalls experiment to search for hidden sector photons and axion-like particles, predicted in many extensions of the standard model. This talk presents a feasibility study of the sensitivities which can be reached using state of the art technology.

1 Motivation and Introduction

Axions, axion-like particles (ALPs), hidden photons and similar weakly interacting slim particles (WISPs) often occur in models beyond the standard model and may be dark matter candidates. Laser-light-shining-through-the-wall (LSW) experiments like ALPS at DESY are currently the most sensitive probes of WISPs. ALPS exploits a resonant optical cavity in order to enhance the power available for photon – WISP conversion.

The idea is to exploit microwave cavities instead of optical resonators [1, 2, 3]. With current technology increased sensitivity in certain mass range can be expected. The first test experiments have already been done (Livermore; Perth), or are being set-up (Daresbury; Yale).

2 Two Cavity setup with very high isolation

A crucial ingredient for a LSW (Laser-light-shining-through-the-wall) experiment is to achieve sufficient shielding. For the intended sensitivity one has to achieve a shielding of roughly 300 dB (a factor 10^{30} in power) between the emitter and the receiver cavity.

Both, the emitting and receiving cavity will be shielded. For the transmitter leakage a good reference level is the ambient electromagnetic parasitics level (cell phones, radio and TV stations etc.) which is usually many orders of magnitude above the thermal noise level. As we cannot keep this background noise below a certain level, the more critical shielding part will be on the receiver side.

One can obtain and measure realistically and in a straightforward manner a shielding value of about 100 dB in a single shell (box) by conventional means in the RF and microwave range (of course higher values are possible). These kind of shielding shells are usually demountable and not soldered. Many examples for this can be found in stochastic cooling systems but also all kind of modern microwave electronics and RF systems in particle accelerators.

The receiving side demands higher requirements and the box-in-the-box concept can be applied, summing up the attenuation of the individual shielding shells in logarithmic scale (i.e.

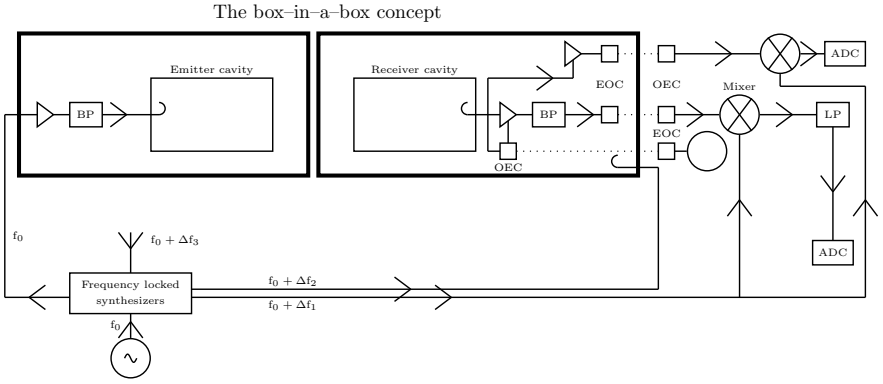

Figure 1: The box-in-a-box concept [3].

multiplying in linear scale) [3]. The innermost shielding layer is provided by the receiving cavity itself.

However, in order to provide sound test data, the shielding between those boxes needs to be constantly monitored and recorded over the full lifetime of the experiment. This makes sure that one is not fooled by electromagnetic leakage (the shielding might degrade due to bad and ageing contacts).

Test tones with the frequency f_0 are emitted between the particular shielding shells [3]. They are small signals in the μW range on different frequencies ($f_0 + \Delta f_2$, $f_0 + \Delta f_3$). Inside the first shell of the receiving setup, the signals are detected by a pick up antenna (PU). The amplitude of the test tone $f_0 + \Delta f_3$ allows the quantification of any potential leakage through the outermost shielding layer. This PU antenna will also see – if there is leakage from the transmitting cavity – signals at f_0 (which would be a veto condition for the measurement). The same principle is used to monitor the second shell with the signal $f_0 + \Delta f_2$ emitted in the first shielding box and detected inside the receiving cavity. By looking for the test signals in our signal spectrum we can evaluate the leaked signals and determine the amount of shielding achieved (of course in the desirable case where we observe no signal at this frequency we know the minimal amount of shielding).

The detected signals are then fed into a mixer where it is combined, i.e., multiplied with the local oscillator on $f_0 + \Delta f_1$ (superheterodyne concept). It is about 20 to 30 kHz offset from the carrier f_0 since the desired intermediate frequency is in the audio range (otherwise we could get too much data for a 2 weeks signal observation and to avoid frequencies from DC to a few kHz in order to eliminate 1/f noise). It then passes through a low frequency band pass filter, is converted into a digital data with an analog digital converter (ADC) and is then recorded. The last bandpass filter reduces the total amount of noise by eliminating the noise from high frequencies where we do not expect a signal. The recorded signal will then be analyzed with a FFT method. A proper signal should appear at frequency Δf_1 in the Fourier analysis.

We have to transport signals and small amounts of DC power for preamplifiers and signal converters through those shells (receiver side) without degrading the performance of the shield-

ing. The number of cables going in and out of the cavity needs to be minimized. It is likely that the only reliable way to do this is using optical transmission for RF/microwave signals, but also of getting in a (needs clarifying) few Watt of DC power for feeding the small signal amplifiers and mixers. We then use an electro optical converter (EOC) to change the signal into an optical signal which is then transmitted to the outside of the box by a glass fibre (dotted lines) where it is reconverted with an opto-electrical converter (OEC). In a similar way the power to the amplifier is fed in with an EOC-OEC set.

2.1 Optical Link on Receiver side

Such DC power transmission using optical fibers (with LEDs at one end and photocells on the other side) was been developed about 30 years ago to supply DC power to small electronic units on high voltage potential in HV transmission systems. Commercial systems for optical fiber based DC power transmission (5 Watt) are available from industry [7], but there is a question mark about how well they would work at cryo-temperatures and / or in very strong magnetic fields.

3 A mHz range observation bandwidth setup

One advantage of the microwave-shining-through-walls setup is that the frequency of the detected signal is exactly at the same frequency as used to produce the new particles. This can be used to suppress noise – and therefore improve signal to noise – by using a narrowband detection method.

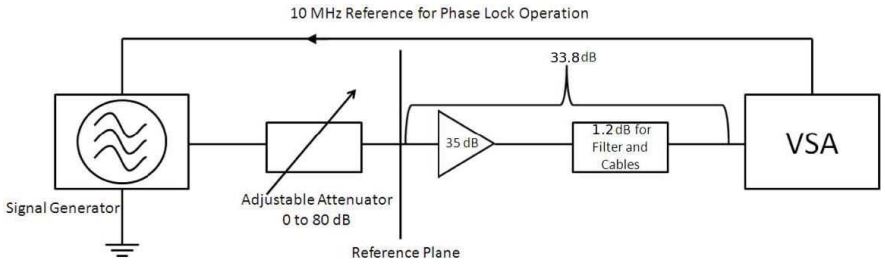

Figure 2: Measurment scheme [4]

A simple test experiment has been performed with standard RF instrumentation in order to crosscheck feasibility of very low observation bandwidth implementation [4]. Using a commercially available vector spectrum analyzer (Agilent 9020 MXA) and a standard low-noise amplifier a sensitivity for a detection of $10^{-22}W$ with 10 measurements of 300 s each has been demonstrated at room temperature [4]. A weak signal is generated in the signal generator and is then further attenuated down to -190 dBm = $10^{-22}W$. This signal is then amplified by a total of 33.8 dB and combined (i.e. mixed) with the reference signal in the vector spectrum analyzer which also records the signal and performs the FFT. In the lower panel the observed signal averaged over 10 measurements (this smoothes out the fluctuations of the envelope of the narrowband filtered and peak detected noise) is shown (the resolution bandwidth is 3 mHz).

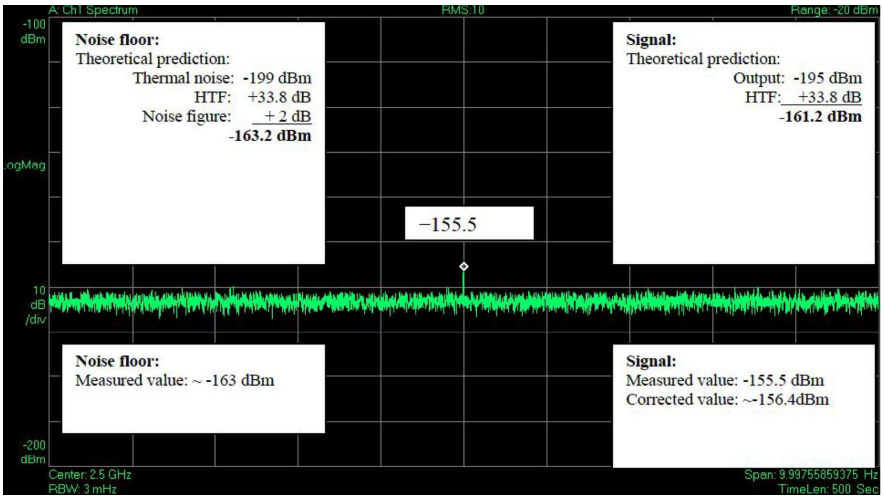

Figure 3: Measured results [4]

A narrow signal line is observed which is clearly distinct from thermal background (-199 dBm) plus the noise from the amplifier (2dB).

In a more advanced setup at cryogenic temperatures we can assume noise temperatures of the order of 10 K. Combining this with integration times of the order of 1000 s we theoretically achieve a sensitivity of $1.4 \cdot 10^{-25} W$. At a frequency of 5 GHz this corresponds to a tiny flux of 0.04 photons per second [3].

Thus by reducing the observation bandwidth down to the mHz or μHz range, we can gain a lot on thermal noise background reduction, provided that the frequency of our converted axions is defined with the same resolution.(i.e. RF cavity generation and receiver concept).

4 Rectangular waveguide TE_{10n} resonator in a LHC magnet

So far, much of the discussion over the last years on axion emitter and receiver cavities has been focused on single mode type cavities (e.g. TM_{010} mode in a pillbox and a solenoid magnet around). Essentially we are aiming for a situation where the RF electric field is parallel to the DC magnetic field over a volume as large as possible. When going to higher frequencies with single mode cavities the volume is getting inevitably smaller and thus also the receiver cross-section and sensitivity for a given distance between emitter and receiver cavity. For a single mode cavity we cannot expect a very strong directionality in the antenna diagram since the maximum linear dimension of the radiating volume (and accordingly by reciprocity for the receiver antenna) is comparable to a single free space wavelength. Higher order mode (with a well defined mode pattern) radiating and receiving structures should exhibit an axion radiation pattern with much better antenna directivity as compared to an elementary dipole. This raises the idea to use the a TE_{101} mode waveguide in the bore of an LHC Magnet.

For the waveguide in the LHC magnet, z would be along the beam axis and y in the direction

of the static magnetic field (up to 8 Tesla).

The Q values of different types of waveguide and coaxial line resonators as a function of frequency are given in [5]. For the TE_{101} resonator (rectangular waveguide with aspect ratio 2/1) we can assume an unloaded Q value of about 8000 for 10 GHz (X-band) at room temperature and no magnetic field. At cryogenic temperatures assuming copper with a RRR value of 100 the Q would be 10 times higher, but due to the magneto-resistance in the end probably just better by a factor of 3.5.

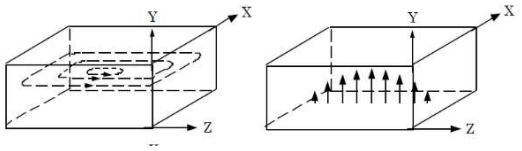

Figure 4: TE_{101} mode pattern in a rectangular waveguide.

Rectangular waveguide dimensions from L-band up to X-band (8.2 to 12.4 GHz) can be found in [5]. The CW power handling capability of an X-band waveguide in air is roughly 200 kW. A X-band waveguide would nicely fit into the beam-screen of an LHC magnet. For higher frequencies i.e. around 100 GHz one may consider a package of say up 20 waveguide in parallel.

The losses for (non overmoded) metallic waveguides increase dramatically towards higher frequencies and accordingly the power handling capability decreases. One can gain about a factor of 10 in losses by using overmoded waveguides (tallguide). As an alternative, above 50 GHz dielectric waveguides with a metallic shielding become interesting since they have much lower losses compared to conventional metallic structures of the same size.

We may consider using an anti-cryostat for the axion transmitter part, thus we would no longer be restricted by the cryo power dissipation limit of 2 Watt per meter of the LHC main dipole beam screen. We could also apply water cooling along the 15 meter long waveguide and possibly dissipate a CW power of 10 kW maybe even 100 kW. Of course this does not make sense for the receiver cavity since low-noise temperature is required. An anti-cryostat has been designed and successfully tested inside a LHC dipole magnet for the purpose of performing magnetic measurements [6]. Its internal temperature was 300 K.

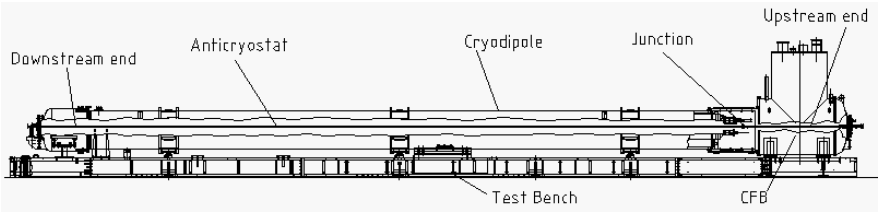

Figure 5: Anti-cryostat.

Another important point is the medium inside the waveguide on the (warm) transmitter side. Air can be better than vacuum as multipacting has to be considered. A quick analysis with the ESA (European Space Agency) multipactor calculator [8] shows that in vacuum and without magnetic field we are all ready for 10 kW power from the generator in a critical region. (But those results need to be re-checked with a magnetic field present)

5 Axion radiation patterns

The waveguide inside the LHC magnet can serve as a phased array antenna. These kind of slotted atennas are widely used e.g. in maritime radars but also for final approach landing radar on airports and of course for all kind of military applications. There is a strong analogy to the axion radiation (and reception) pattern. The slots allow the concentration of the electromagnetic radiation towards the receiving cavity. They are not centered, in order to cut through wall currents and thus provide an electric and magnetic polarization of each slot. This kind of antenna structure (often at higher frequencies than shown here) can be used in standing and in travelling wave mode.

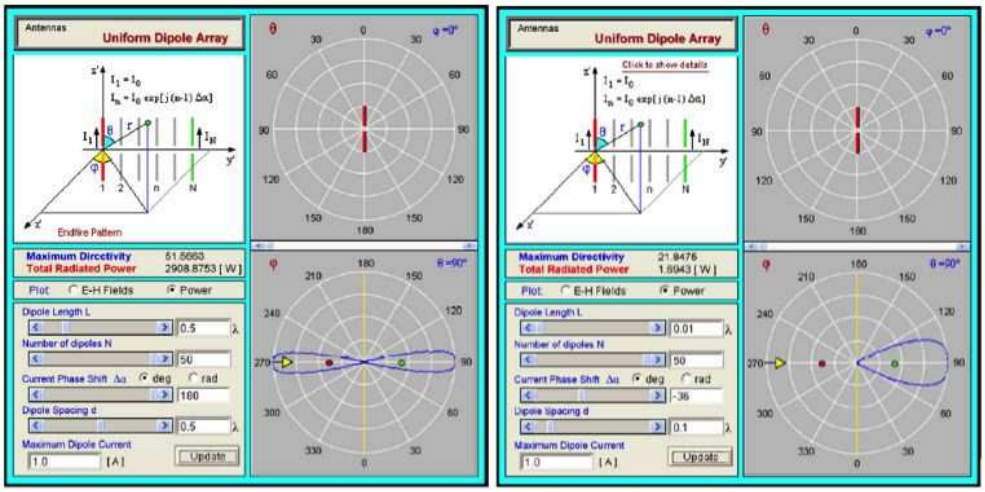

Figure 6: Axion antenna diagrams.

Both is shown in Figure 6. On the left we see nicely the forward and backward radiation lobe ($\phi = 90$ and 270 degree respectively). This case corresponds to the standing wave pattern of a laser beam or coaxial line without dielectric material. As a reminder, the basic law of antenna design: The radiation characteristic of a group of radiating elements in this example is equal to the characteristic of the group (isotropic radiators) to be multiplied with the characteristic of the individual radiator (e.g. dipole). The directional diagram of an empty coaxial line is the same as the Fabry Perot resonator like it is used for axion search in CAST. Thus one might consider using the other bore of the CAST magnet for such a TEM line with about 40 mm outer diameter and operate it in the travelling wave or standing wave mode. A sensitive microwave radiometer used as broadband detector in the range of 2 to 4 GHz bandwidth could detect microwave noise temperature differences in the order of a few μK depending on the orientation of the sun, or any other potential celestial axion source, to the CAST magnet.

On the right side we have the radiation pattern of a travelling wave antenna (end-fire antenna). Note that the relative spacing of the radiating elements is smaller than in the last slide i.e. the antenna is shorter and thus the directional diagram becomes wider. This case corresponds to the travelling wave pattern of a laser beam (v=c).

6 Conclusion and Outlook

In this note we have argued that microwave cavity experiments can provide a powerful tool to search for weakly interacting sub-eV particles, in particular for hidden sector photons and axion-like particles.

The electromagnetic interference problem, in particular for the receiver cavity is an important issue for microwave axion detection experiments. Here the combination of the box-in-the-box concept, together with optical fiber powered diagnostic equipment in the space between the first shielding and the actual cavity, can make a significant contribution. Very narrow band signal detection using, for example 10 days trace record with about 50 Giga samples and 24 bit vertical resolution. This should return via FFT a μHz resolution and related thermal noise reduction. A phaselock method capable of reducing the relative phase noise down the μHz level has been presented and discussed. Higher order mode emitter and receiver cavities, possibly in one or in two LHC magnets were discussed and analyzed in terms of their axion radiation pattern (far field). Highly directional axion emitter and receiver structures may significantly increase the probability of detection.

Acknowledgements

The author would like to thank the CERN AB department management (P. Collier) and in particular the AB-RF group (E. Ciapala) for support as well as Steve Myers and R. Heuer for encouragement. Many thanks to A. Ringwald and J. Jäckel for a large number of hints and inspiring discussions and K. Zioutas for having brought the right people in the right moment together as well as having given very helpful comments.

References

[1] F. Hoogeveen, “Terrestrial axion production and detection using RF cavities”, Physics Letters B, Volume 288, Issues 1-2 (1992).

[2] J. Jaeckel, A. Ringwald, “A Cavity Experiment to Search for Hidden Sector Photons”, Physics Letters B 659:509-514 (2008)

[3] F. Caspers, J. Jaeckel, A. Ringwald, “Feasibility, engineering aspects and physics reach of microwave cavity experiments searching for hidden photons and axions”, IOP Publishing for SISSA (2009).

[4] Caspers et al., “Demonstration of 10-22 Watt signal detection methods in the microwave range at ambient temperatures”, CERN BE-Note 2009-026 (2009).

[5] T. Saad, “Microwave engineers handbook”.

[6] O. Dunkel, P. Legrand and P. Sievers, “A warm bore anticryostat for series magnetic measurements of LHC superconducting dipole and short straight section magnets”, LHC Project Report 685 (2003).

[7] Photonic Power Module PPM-5 from JDSU Company, `http://www.jdsu.com` (2010).

[8] Multipactor Calculator from ESA, `http://multipactor.esa.int/index.html` (2010).

CAST: Recent Results & Future Outlook

T. Papaevangelou[1], *S. Aune*[1], *K. Barth*[2], *A. Belov*[3], *S. Borghi*[2,*], *H. Bräuninger*[4], *G. Cantatore*[5], *J. M. Carmona*[6], *S. A. Cetin*[7], *J. I. Collar*[8], *T. Dafni*[6], *M. Davenport*[2], *C. Eleftheriadis*[9], *N. Elias*[2], *C. Ezer*[7], *G. Fanourakis*[10], *E. Ferrer-Ribas*[1], *H. Fischer*[11], *J. Franz*[11], *P. Friedrich*[4], *J. Galán*[6], *A. Gardikiotis*[12], *E. N. Gazis*[13], *T. Geralis*[10], *I. Giomataris*[1], *S. Gninenko*[3], *H. Gómez*[6], *E. Gruber*[11], *T. Guthörl*[11], *R. Hartmann*[14,†], *F. Haug*[2], *M. Hasinoff*[15], *D. H. H. Hoffmann*[16], *F. J. Iguaz*[6,24], *I. G. Irastorza*[6], *J. Jacoby*[17], *K. Jakovčić*[18], *D. Kang*[11,‡], *T. Karageorgopoulou*[13], *M. Karuza*[5], *K. Königsmann*[11], *R. Kotthaus*[19], *M. Krčmar*[18], *K. Kousouris*[10], *M. Kuster*[4,16,§], *B. Lakić*[18], *P. Lang*[16], *C. Lasseur*[2], *J. M. Laurent*[2], *A. Liolios*[9], *A. Ljubičić*[18], *V. Lozza*[5], *G. Lutz*[14,23], *G. Luzón*[6], *D. W. Miller*[8,¶], *A. Mirizzi*[19,‖], *J. Morales*[6,**], *T. Niinikoski*[2], *A. Nordt*[4,16,], *M. J. Pivovaroff*[20], *G. Raiteri*[5], *G. Raffelt*[19], *T. Rashba*[21], *H. Riege*[16], *A. Rodríguez*[6], *M. Rosu*[16], *J. Ruz*[6,2], *I. Savvidis*[9], *Y. Semertzidis*[12,††], *P. Serpico*[2], *P. S. Silva*[2], *S. K. Solanki*[21], *R. Soufli*[20], *L. Stewart*[2], *A. Tomás*[6], *M. Tsagri*[12,2], *K. van Bibber*[20], *T. Vafeiadis*[2,9], *J. Villar*[6], *J. K. Vogel*[11,20], *L. Walckiers*[2], *Y. Wong*[2], *S. C. Yildiz*[7], *K. Zioutas*[2,12]

1. IRFU, Centre d'Études Nucléaires de Saclay (CEA-Saclay), Gif-sur-Yvette, France
2. European Organization for Nuclear Research (CERN), Genève, Switzerland
3. Institute for Nuclear Research (INR), Russian Academy of Sciences, Moscow, Russia
4. Max-Planck-Institut für extraterrestrische Physik, Garching, Germany
5. Instituto Nazionale di Fisica Nucleare (INFN), Sezione di Trieste and Università di Trieste, Trieste, Italy
6. Instituto de Física Nuclear y Altas Energías, Universidad de Zaragoza, Zaragoza, Spain
7. Dogus University, Istanbul, Turkey
8. Enrico Fermi Institute and KICP, University of Chicago, Chicago, IL, USA
9. Aristotle University of Thessaloniki, Thessaloniki, Greece
10. National Center for Scientific Research "Demokritos", Athens, Greece
11. Albert-Ludwigs-Universität Freiburg, Freiburg, Germany
12. Physics Department, University of Patras, Patras, Greece
13. National Technical University of Athens, Athens, Greece
14. MPI Halbleiterlabor, München, Germany
15. Department of Physics and Astronomy, University of British Columbia, Vancouver, Canada
16. Technische Universität Darmstadt, IKP, Darmstadt, Germany
17. Johann Wolfgang Goethe-Universität, Institut für Angewandte Physik, Frankfurt am Main, Germany
18. Rudjer Bošković Institute, Zagreb, Croatia

[*] Present address: Department of Physics and Astronomy, University of Glasgow, Glasgow, UK
[†] Present address: PNSensor GmbH, München, Germany
[‡] Present address: Karlsruher Institut für Technologie (KIT), Karlsruhe, Germany
[§] Present address: European XFEL GmbH, Notkestrasse 85, 22607 Hamburg, Germany
[¶] Present address: Stanford University and SLAC National Accelerator Laboratory, Stanford, CA, USA
[‖] Present address: Institut für Theoretische Physik,Universität Hamburg, Hamburg, Germany
[**] Deceased
[††] Present address: Brookhaven National Laboratory, New York, USA

19. Max-Planck-Institut für Physik, Munich, Germany
20. Lawrence Livermore National Laboratory, Livermore, CA, USA
21. Max-Planck-Institut für Sonnensystemforschung, Katlenburg-Lindau, Germany

DOI: http://dx.doi.org/10.3204/DESY-PROC-2010-03/papaevangelou_thomas

The CAST (CERN Axion Solar Telescope) experiment is searching for solar axions by their conversion into photons inside the magnet pipes of an LHC dipole. The analysis of data taken so far has shown no signal above the background, thus implying an upper limit to the axion-photon coupling of $g_{a\gamma} < 0.85 \times 10^{-10} GeV^{-1}$ at 95% CL for $m_a < 0.02\, eV/c^2$. Ongoing measurements, with the magnet bores filled with a buffer gas (^3He), are improving the sensitivity of the experiment for higher axion masses towards 1 eV/c^2. Recent results, new ideas for Axion-Like Particle (WISPs) searches with CAST in the near future and the prospects of a new generation Helioscope are presented here.

1 Introduction

The CAST (CERN Axion Solar Telescope) experiment is using a decommissioned LHC dipole magnet to convert solar axions into detectable x-ray photons. Axions are light pseudoscalar particles that arise in the context of the Peccei-Quinn [1] solution to the strong CP problem and can be Dark Matter candidates [2]. Stars could produce axions via the Primakoff conversion of the plasma photons. CAST is pointing at our closest star, the Sun, aiming to detect solar axions. The detection principle is based on the coupling of an incoming axion to a virtual photon provided by the transverse field of an intense dipole magnet, being transformed into a real, detectable photon that carries the energy and the momentum of the original axion. The axion to photon conversion probability is proportional to the square of the transverse field of the magnet and to the active length of the magnet. Using an LHC magnet (9 T and 9.26 m long) improves the sensitivity by a factor 100 compared to previous experiments.

The CAST experiment has been taking data since 2003. During 2003 and 2004 the experiment operated with vacuum in the magnet bores (CAST phase I) and set the best experimental limit [3, 4] on the axion-photon coupling constant in the range of axion masses up to $0.02\, eV/c^2$. At this mass the sensitivity is degraded due to coherence loss.

In order to extend CAST sensitivity to higher axion masses, the experimental setup was upgraded in 2005 to operate the second phase of the experiment with the magnet bores filled with a buffer gas. The gas density has to be increased in appropriate steps to cover equally a possible range of axion masses above $0.02\, eV/c^2$. In the first part of the CAST phase II (2005-2006), ^{4}He was used as a buffer gas. During this time, the experiment scanned the range of axion masses from $0.02\, eV/c^2$ to $0.39\, eV/c^2$ and set the most restrictive limit on the axion-photon coupling constant for masses that are, for the first time, in the theoretically favored region [5], which has been used by the Particle Data Group (2010).

In 2007, the system was thoroughly upgraded to use ^{3}He as a buffer gas. The ongoing second part of CAST phase II started in 2008 with the goal to cover the range of axion masses up to $1.16\, eV/c^2$. So far, the experiment scanned the range up to $0.88\, eV/c^2$.

2 ^{3}He as a buffer gas

In the presence of a buffer gas the coherent axion to photon conversion condition is restored for a very narrow mass range, which depends on the gas density [5]. The precise knowledge and reproducibility of each density setting and the density homogeneity along the magnet bore during tracking are essential. Cooling the magnet with supperfluid ^{4}He at 1.8 K guaranties temperature stability along the cold bore. The amount of gas ejected into the magnet bores is measured precisely with a metering volume kept at stable temperature (typically 36 ^{o}C). These allow the reproduction of any desired density setting given the stable conditions of the superconductive magnets.

However, there are parts of the magnet bores, outside the magnetic field region, that are in higher temperatures. These temperatures can vary during tracking causing variations on the buffer gas density. In order to estimate the effect of those variations on the axion to photon conversion probability, a number of temperature and pressure sensors have been placed in several points of the magnet and the gas system. A series of Computational Fluid Dynamics (CFD) simulations with the sensors data as bounding conditions was performed and is still going on, both for the static and dynamic case (magnet movement).

Monitoring the evolution of the ^{3}He gas at CAST and comparing it to results from simulations have helped to understand the real nature of the gas, as well as effects such as buoyancy and convection. It has also revealed that CAST is now operating in conditions where the Van der Walls effects are significant; neglecting them can lead to deviations as large as 11%. The simulations performed have allowed the extraction of a precise formula for gas density calculation, being in agreement with experimental data within 200-300 ppm [6]. Also, they have verified that the desired density homogeneity across the magnet bore is achieved. Furthermore, they have allowed the precise knowledge of the gas density during tracking, which is essential for the data analysis.

3 First preliminary result from ^{3}He phase

During the 2007 shutdown, CAST replaced the TPC [7] and the conventional Micromegas [8] with new technology Micromegas detectors, built with the Bulk [9] or Microbulk [10] technology. The enhanced performance of the new detectors [11] in combination with the installation of shielding resulted in a reduction of the background level by a factor of 5-10 in comparison with the past situation. During September 2008 the Bulk detectors were replaced by the more stable Microbulks which showed a background level of $5 \times 10^{-6} s^{-1} cm^{-2} keV^{-1}$, equivalent to 1-2 counts per pressure setting. This performance, together with the already very low count rate of the CCD detector [12], makes interesting the use of an unbinned likelihood function in the analysis for the ^{3}He phase, instead of the binned version used in ^{4}He phase [5]. The unbinned likelihood function can be defined as:

$$log(L_{m_a}) \propto -R_T + \sum_i^N logR(t_i, E_i, d_i)$$

where the sum runs over each of the N detected counts and $R(t_i)$ is the event rate expected at the time t_i, energy E_i and detector d_i of the event i, while R_T is the integrated expected number of counts over all exposure time, energy and detectors:

$$R(t, E, d) = B_d + S(t, E, d)$$

being B_d the background rate of the detector d and $S(t, E, d)$ the expected rate from axions in detector d, which depend on the axion properties $g_{a\gamma}$ and m_a:

$$S(t, E, d) = \frac{d\Phi}{dE} P_{a\gamma} \epsilon_d$$

where $d\Phi/dE$ is the solar axion solar flux spectrum, $P_{a\gamma}$ the axion photon conversion probability in the CAST magnet and ϵ_d the detector efficiency.

Furthermore, the unbinned likelihood is more suitable for situations where the detection conditions are changing. The presence of a small ^{3}He leak during 2008 period makes the density of the cold bore to be continuously varying with time. Moreover the analysis of the gas behavior in this phase revealed that the effective cold bore density is affected by cold windows temperatures and convection which change during tracking movement. This effect is especially strong during 2008 data due to the configuration of the boundary conditions. In order to obtain a first exclusion limit on the mass region covered during 2008, the measured value of ^{3}He pressure (P_{gas}), corrected for the actual cryostat temperature, is assumed to be directly related to the core density, allowing in this approach to obtain the axion mass directly from the P_{gas} measurement. Then, R_T is calculated by using the time periods the detectors were in tracking conditions and obtaining the effective exposure time as a function of P_{gas} or what is equivalent the axion mass determined by the relation:

$$m_a = \sqrt{\frac{0.0201 P_{gas}}{1.8}}$$

Introducing into the unbinned likelihood the expected signal contribution for a given axion mass coming from the total exposure time of the 3 Micromegas detectors, and introducing the tracking counts measured by each detector in the region of sensitivity of the specific axion mass to be calculated, we have obtained a preliminary upper limit to $g_{a\gamma}$ by integration of the Bayesian probability from zero up to 95% of its area in $g^4_{a\gamma}$.

A preliminary limit has been derived [13] from the data taken in CAST in 2008 by the Micromegas detectors and is shown in Figure 1. The total exposure time was about 600 hours, covering axion masses between 0.39 and 0.65 eV/c^2. As soon as the analysis of the CCD data is completed the final combined limit of all detectors will be calculated and published.

4 Future outlook

CAST is planning to continue exploiting high axion masses with ^{3}He as buffer gas until July 2011. In case that no direct axion signal is observed, the CAST collaboration is preparing a proposal to CERN to extend its scientific program. Developments both in instrumentation and theoretical models, together with enhancements and additions to the existing CAST experimental equipment could enable, in the near-term future, best-in-class searches for several types of particles, including QCD-inspired axions, chameleons, paraphotons or any other exotic WISPs.

The possibility of a significant further reduction of the background level of the Micromegas detectors [11] by optimizing their design, would allow CAST to improve the ^{4}He and phase I results. In the first case the search would be oriented towards lowering the sensitivity for axion

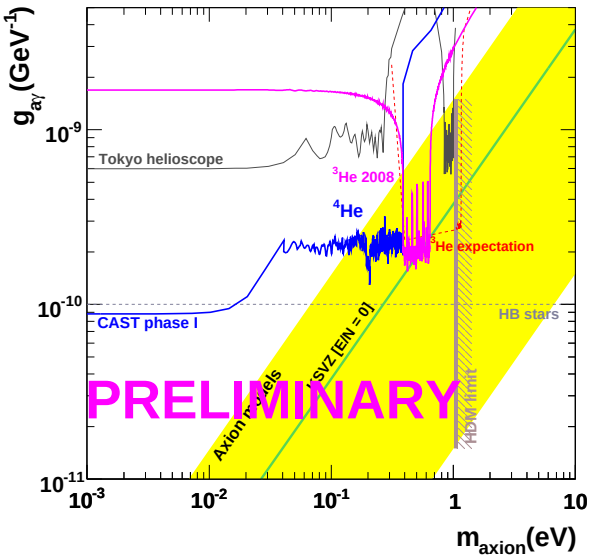

Figure 1: Preliminary exclusion limit (95% CL) from the three Micromegas detectors for axion masses between 0.39 and 0.65 eV/c^2 (2008 data).

masses in the range 0.02 to 0.39 eV/c^2 at the level of $10^{-10}GeV^{-1}$. In the second case, a sensitivity of the level of $g_{a\gamma} \approx 5 \times 10^{-11}GeV^{-1}$ for $m_a < 0.02\ eV/c^2$ could be achieved, after one year data tacking.

Returning to the vacuum phase and lowering the detector threshold at the level of 0.5 keV, CAST will become sensitive to solar chameleons [14], a dark energy candidate. This can be achieved in parallel with the axion searches, by using a new, low threshold *Frame Store* CCD [6] and transparent windows for the Micromegas detectors, constructed from nanotube materials [15].

The use of new techniques such as a Glan-Thompson Polarization Beam Splitter can exploit the nature of linearly polarized photons of axion origin. Provided we use very low background photo detectors, the CAST sensitivity for WISP searches in the visible energy range will be significantly enhanced. Furthermore, an extreme UV sensitive Micromegas can be used in order to cover the whole sub-keV range, together with the rest of the CAST detectors.

Besides the searches for WISP conversions in the presence of a magnetic field, CAST infrastructure can be used for parallel search for solar paraphotons (hidden-sector U(1) gauge bosons). CAST can be used for paraphoton searches either by using the magnet cold bores and the attached detectors or by mounting a dedicated paraphoton conversion vessel and photon detector onto the CAST magnet support structure [16].

In addition to considering various investigations for the near-term, the CAST collaboration has also begun consideration of a *next-generation axion helioscope* aiming to achieve at least an order of magnitude improvement in coupling constant sensitivity, compared to the result obtained by CAST. Such an experiment would require significant investments in developing the required X-ray optics and detectors and the design and construction of a new magnet, specifically optimized for axion searches.

5 Conclusions

CAST, during its 10 years of existence has put the strictest experimental limit on axion searches for a wide mass range, while currently is testing axion masses inside the region favored by QCD models. The first preliminary results of the ^{3}He data analysis show that high rest mass range ($\leq 1.16eV/c^2$) can be investigated with the targeted sensitivity. CAST has not observed a direct solar axion signal but has provided world class limits for axions and axion-like particles including paraphotons.

The CAST Colaboration is planning to start new searches for WISPs by mid-2011 when ^{3}He phase is going to be completed. Detector development and research on superconducting magnets in combination with the experience gained on solar axion searches can lead to more sensitive future helioscopes.

References

[1] R. D. Peccei and H. R. Quinn, Phys. Rev. Lett. **38**, 1440 (1977).

[2] P. Sikivie, Int. J. Mod. Phys. D3 S, 1 (1994) and Phys. Rev. Lett. **51**, 1415 (1983).

[3] K. Zioutas [CAST collaboration], "First results from the CERN Axion Solar Telescope", Phys. Rev. Lett. **94**, 121301 (2005) [hep-ex/0411033].

[4] S. Andriamonje [CAST collaboration], "An improved limit on the axion-photon coupling from the CAST experiment", JCAP **04**, 10 (2007) [hep-ex/0702006].

[5] E. Arik [CAST collaboration], "Probing the Axion models with CAST", JCAP 0902.008 (2009) [arXiv:0810.4482].

[6] T. Papaevangelou [CAST collaboration], "Status Report of the CAST Experiment", CERN-SPSC-2010-026; SPSC-SR-067.

[7] D. Autiero *et al.*, "The CAST Time Projection Chamber", New J. Phys **9**, 171, (2009) [hep-ex/0702189].

[8] P. Abbon *et al.*, "The Micromegas detector of the CAST experiment", New J. Phys **9**, 170, (2009) [hep-ex/0702190].

[9] Y. Giomataris *et al.*, "Micromegas in a bulk", Nucl. Instrum. Meth. A **560**. 2 (2006).

[10] S. Andriamonje *et al.*, "Developement and performance of Microbulk Micromegas detectors" JINST 5 P02001 (2010).

[11] S. Aune *et al.*, "An ultra-low-background detector for axion searches", J. Phys. Conf. Ser. **179**, 012015 (2009).

[12] M. Kuster *et al.*, "The X-ray telescope of CAST", New J. Phys **9**, 169, (2009) [hep-ex/0702188].

[13] J. Galán, PhD Thesis, in preparation.

[14] P. Brax and K. Zioutas, "Solar Chameleons", Phys. Rev. D **82**, 043007, (2010).

[15] A. G. Koutsioubas, N. Spiliopoulos, D. Anastassopoulos, A. A. Vradis and G. D. Priftis, J Appl. Phys. **103**, 094521 (2008) and Mat. Sc. Eng. B **165**, 270-273 (2009).

[16] S. N. Gninenko and J. Redondo, Phys. Lett. B **664**, 180 (2008).

Chapter 3

Astrophysics experiments searching for WISPs

ALPs in the Sky: New Bounds and Discovery Opportunities

Alessandro Mirizzi

II Institut für Theoretische Physik, Universität Hamburg, Luruper Chaussee 149, 22761 Hamburg, Germany

DOI: http://dx.doi.org/10.3204/DESY-PROC-2010-03/mirizzi_alessandro

Very light axion-like particles (ALPs) with a two-photon vertex are predicted in many extensions of the Standard Model. The two-photon coupling would induce the mixing with ALPs for photons emitted by distant astrophysical sources, and propagating in the large-scale cosmic magnetic fields. In this context, we discuss how current and upcoming astrophysical experiments, ranging from the cosmic microwave background to the high-energy gamma-rays, could probe the elusive ALPs in a region of their parameter space not accessible by laboratory experiments.

1 Introduction

Axion-like particles (ALPs) with a two-photon vertex are predicted in many extensions of the Standard Model (see [1] for a recent review). The $a\gamma\gamma$ coupling allows for ALP-photon conversions in electric or magnetic field. This effect is exploited by the ADMX experiment to search for axion dark matter, by CAST to search for solar axions, and by regeneration laser experiments. Due to their two-photon vertex, ALPs can also play an intriguing role in astrophysics. Indeed, photons emitted by distant sources and propagating through large-scale cosmic magnetic fields can mix with ALPs. As a consequence, two peculiar effects can arise. One is photon-ALP conversion (oscillation) and the other consists in the change of the polarization state of photons. Both these effects can be exploited to look for signatures of ALPs in astrophysical observations.

The outline of this talk is as follows. In Section 2 we review the mechanism of photon-ALP mixing in a magnetic field. In Section 3 we show how photon-ALP conversions in primordial magnetic fields in the Early Universe would have distorted the blackbody spectrum of the cosmic microwave background (CMB). Therefore, using the current high precision CMB spectral data one can obtain a strong bound on photon-ALP mixing. In Section 4 we discuss the impact of photon-ALP conversions on the polarization of distant gamma-ray bursts. Finally, in Section 5 we discuss about the impact of ALP conversions on the spectra of very high-energy gamma sources, in particular in relation with the surprising degree of transparency of the universe, recently measured by gamma-ray telescopes.

2 Photon-ALP conversions

ALPs and photons oscillate into each other in an external magnetic field due to the interaction term [2]

$$\mathcal{L}_{a\gamma} = -\frac{1}{4}\, g_{a\gamma} F_{\mu\nu} \tilde{F}^{\mu\nu} a = g_{a\gamma} \mathbf{E}\cdot\mathbf{B}\, a\,, \tag{1}$$

where $F_{\mu\nu}$ is the electromagnetic field tensor, $\tilde{F}_{\mu\nu} = \frac{1}{2}\epsilon_{\mu\nu\rho\sigma}F^{\rho\sigma}$ is its dual, a is the ALP field, and $g_{a\gamma}$ is the ALP-photon coupling. For a homogeneous magnetic field one may choose a coordinate system aligned with the field direction. The linear photon polarization state parallel to the transverse field direction $\mathbf{B}_T$ is denoted as $A_\parallel$ and the orthogonal one as $A_\perp$. Then, the probability for a photon emitted in the state $A_\parallel$ with energy ω to convert into an ALP after traveling a distance s is [2]

$$P_0(\gamma\to a) = \left|\langle A_\parallel(0)|a(s)\rangle\right|^2 = \sin^2(2\vartheta)\sin^2(\Delta_{\rm osc}s/2) = (\Delta_{a\gamma}s)^2\,\frac{\sin^2(\Delta_{\rm osc}s/2)}{(\Delta_{\rm osc}s/2)^2}\quad, \tag{2}$$

where the oscillation wavenumber is given by

$$\Delta_{\rm osc}^2 = (\Delta_{\rm pl}-\Delta_a)^2 + 4\Delta_{a\gamma}^2\,. \tag{3}$$

Here $\Delta_a = -m_a^2/2\omega$, $\Delta_{\rm pl} = -\omega_{\rm pl}^2/2\omega$, $\Delta_{a\gamma} = g_{a\gamma}|\mathbf{B}_T|/2$, and $\omega_{\rm pl}^2 = 4\pi\alpha\, n_e/m_e$ defines the plasma frequency, m_e being the electron mass and α the fine-structure constant.

It proves useful to define a *low critical energy*

$$E_L \equiv \frac{E\,|\Delta_a-\Delta_{\rm pl}|}{2\,\Delta_{a\gamma}} \simeq \frac{25\,|m^2-\omega_{\rm pl}^2|}{(10^{-13}{\rm eV})^2}\left(\frac{10^{-9}{\rm G}}{B_T}\right)\left(\frac{10^{-11}{\rm GeV}^{-1}}{g_{a\gamma}}\right){\rm keV} \tag{4}$$

In the energy range $E \gg E_L$ the photon-ALP mixing is maximal ($\vartheta \simeq \pi/4$) and the conversion probability becomes energy-independent. This is the so-called *strong-mixing regime*. Outside this regime the conversion probability turns out to be energy-dependent and vanishingly small.

Cosmic magnetic fields components have a quite complicated and poorly known morphology, so that it has become customary to suppose that they possess a domain-like structure with varying coherence lengths. The propagation over many random B-field domains is a truly 3-dimensional problem, because different photon polarization states play the role of $A_\parallel$ and $A_\perp$ in different domains. This is enough to guarantee that the conversion probability over many domains is an incoherent average over magnetic field configurations and photon polarization states. The probability after travelling over a distance $r \gg s$, where s is the domain size, is *on average* [3]

$$P_{\gamma\to a}(r) = \frac{1}{3}\left[1-\exp\left(-\frac{3P_0\,r}{2s}\right)\right], \tag{5}$$

with P_0 given by Eq. (2). As expected one finds that for $r/s\to\infty$ the conversion probability saturates, so that *on average* one third of all photons converts into ALPs. However, due to the stochastic behavior of the photon-ALP conversions in the random magnetic fields, on different lines of sight one can find $\mathcal{O}(1)$ variations with respect to the average value.

Finally, we mention that besides the conversion between photons and ALPs, there is a more subtle effect induced by the ALP two-photons vertex. Indeed, as a consequence of the loss of $\parallel$ photons into ALPs, the amplitude of the $\parallel$ mode with respect to the $\perp$ is depleted. This would lead to a rotation of the plane of polarization that can also lead to interesting signatures in astrophysical observations.

3 Resonant Conversions in the Early Universe

The presence of primordial magnetic fields would inevitably produce resonant conversions between photons and ALPs in the Early Universe, when the condition $m_{\rm a} = \omega_{\rm pl}$ is satisfied [4]. Depending on the ALP mass, these conversions could have taken place in different epochs during the thermal history of the Universe. For ALP masses ($m_a < 10^{-9}$ eV) undergoing resonant conversions after the recombination epoch, one can obtain constraints on this mechanism from the the spectral distortions induced on the CMB spectrum. Using the high precision CMB spectral data collected by the FIRAS instrument on board of the Cosmic Background Explorer, one gets as limit on the product of the ALP-photon coupling $g_{a\gamma}$ times the sky and polarization averaged magnetic field B [4]

$$gB < 10^{-13} - 10^{-11}\ \ {\rm GeV}^{-1}\ \ {\rm nG}\ . \tag{6}$$

For photon-ALP conversions occurring during the "weak-coupling" regime (10^{-9} eV $< m_a <$ 10^{-4} eV) the bound $gB < 10^{-11}{\rm GeV}^{-1}{\rm nG}$ occurs. Slightly weaker bounds were also derived for higher ALP masses.

Therefore, if a primordial magnetic field would eventually be found with values close to the current upper bound $B \simeq 1$ nG, the resulting CMB limit on the coupling $g_{a\gamma}$ for very light ALPs would overcome the barrier placed by current experimental and astrophysical bounds. Conversely, if ALPs will be eventually discovered improving the current sensitivity of the solar axion helioscope CAST, or with new techniques in laser experiments, this cosmological argument will provide a complementary constraint on the strength of the primordial magnetic field.

4 Polarization of cosmic gamma-ray bursts

Measuring the polarization of prompt gamma-ray burst (GRB) emission in the keV-MeV range represents one of the main challenges for high-energy astronomy of the next decade. Various polarimetric missions are currently being developed, which are expected to collect an all-sky rich sample of GRBs so as to allow for a meaningful statistical analysis of their polarization properties. As recently realized, important conclusions concerning the GRB emission models are expected to be drawn from these studies.

In [5] it has been shown that the existence of ALPs with parameters lying in experimentally allowed ranges drastically modifies the GRB polarization pattern. More specifically, cosmic magnetic fields of extragalactic, intracluster and Galactic origin along the line of sight to a GRB act as catalysts for significant photon-ALP mixing. In particular, due to the random structure of the extragalactic and intracluster magnetic fields, the amount of photon-ALP mixing strongly depends on the orientation of the line of sight. Therefore, starting with a given source polarization a broad statistical distribution is expected to be detected when observing GRBs from different directions in the sky. The observation of these peculiar broad distributions would hint at the existence of very light ALPs. In general, the presence of very light ALPs ($m_a < 10^{-13}$ eV) can play a role for values of the photon-ALP coupling constant $g_{a\gamma} < 10^{-11}$ GeV^{-1}, namely one order of magnitude lower than the current experimental limit set by the CAST experiment.

5 Transparency of the Universe to Very High-Energy photons

In the last recent years photon-ALP conversions have been proposed as a mechanism to avoid the opacity of the extragalactic sky to high-energy radiation due to pair production on the Extragalactic Background Light (EBL). At this regard, recent observations of cosmologically distant gamma-ray sources by ground-based gamma-ray telescopes have revealed a surprising degree of transparency of the universe to very high-energy (VHE) photons ($E \gtrsim 100$ GeV). Surprisingly, data seem to require a lower density of the EBL than expected and/or considerably harder injection spectra than initially thought. At this regard, oscillations between very high-energy photons and ALPs (with $m_a < 10^{-10}$ eV and $g_{a\gamma} \simeq 10^{-11}$ GeV^{-1}) in the random extragalactic magnetic fields [6] would represent an intriguing possibility to explain this puzzle through a sort of "cosmic light-shining through wall" effect.

It has been then realized [7] that the turbulent structure of the extragalactic magnetic fields would produce a stochastic behavior for the photon-ALP conversions along different lines of sight, producing both an enhancement or a suppression in the observable photon flux with respect to the expectations with only absorption. As a consequence, the most striking signature of the mixing with ALPs would be a reconstructed EBL density from TeV photon observations which appears to vary over different directions of the sky: consistent with standard expectations in some regions, but inconsistent in others. This effect is testable with the measurements of the new generation of Imaging Atmospheric Cherenkov Telescopes, and hopefully with the future Cherenkov Telescope Array.

Acknowledgments

A.M. acknowledges the organizers of the *PATRAS 2010* workshop for the kind hospitality in Zurich.

6 Bibliography

References

[1] J. Jaeckel and A. Ringwald, "The Low-Energy Frontier of Particle Physics," arXiv:1002.0329 [hep-ph].

[2] G. Raffelt and L. Stodolsky, "Mixing of the Photon with Low Mass Particles," Phys. Rev. D **37** (1988) 1237.

[3] A. Mirizzi, G. G. Raffelt and P. D. Serpico, "Photon axion conversion in intergalactic magnetic fields and cosmological consequences," Lect. Notes Phys. **741**, 115 (2008) [astro-ph/0607415].

[4] A. Mirizzi, J. Redondo and G. Sigl, "Constraining resonant photon-axion conversions in the Early Universe," JCAP **0908**, 001 (2009) [arXiv:0905.4865 [hep-ph]].

[5] N. Bassan, A. Mirizzi and M. Roncadelli, "Axion-like particle effects on the polarization of cosmic high-energy gamma sources," JCAP **1005** (2010) 010 [arXiv:1001.5267 [astro-ph.HE]].

[6] A. De Angelis, O. Mansutti and M. Roncadelli, "Evidence for a new light spin-zero boson from cosmological gamma-ray propagation?," Phys. Rev. D **76** (2007) 121301 [arXiv:0707.4312 [astro-ph]].

[7] A. Mirizzi and D. Montanino, "Stochastic conversions of TeV photons into axion-like particles in extragalactic magnetic fields," JCAP **0912**, 004 (2009) [arXiv:0911.0015 [astro-ph.HE]].

Axions and White Dwarfs

J. Isern[1,2], *S. Catalán*[3], *E. García–Berro*[4,2], *M. Salaris*[5], *S. Torres*[4,2]

[1]Institut de Ciències de l'Espai (CSIC), Campus UAB, 08193 Bellaterra, Spain
[2]Institut d'Estudis Espacials de Catalunya (IEEC), Ed. Nexus, c/Gran Capità, 08034 Barcelona, Spain
[3]Center for Astrophysics Research, University of Hertfordshire, College Lane, Hatfield AL10 9AB, UK
[4]Departament de Física Aplicada, Universitat Politècnica de Catalunya, c/Esteve Terrades 5, 08860 Castelldefels, Spain
[5]Astrophysics Research Institute, Liverpool John Moores University, 12 Quays House, Birkenhead, CH41 1LD, UK

DOI: http://dx.doi.org/10.3204/DESY-PROC-2010-03/isern_jordi

White dwarfs are almost completely degenerate objects that cannot obtain energy from the thermonuclear sources and their evolution is just a gravothermal process of cooling. The simplicity of these objects, the fact that the physical inputs necessary to understand them are well identified, although not always well understood, and the impressive observational background about white dwarfs make them the most well studied Galactic population. These characteristics allow to use them as laboratories to test new ideas of physics. In this contribution we discuss the robustness of the method and its application to the axion case.

1 Introduction

White dwarfs are almost completely degenerate objects that cannot obtain energy from the thermonuclear sources and their evolution is just a gravothermal process of cooling. Globally, the evolution of the luminosity of a white dwarf can be written as:

$$L + L_\nu + L_{\rm X} = -\int_0^{M_{\rm WD}} C_{\rm v}\frac{dT}{dt}\,dm - \int_0^{M_{\rm WD}} T\Big(\frac{\partial P}{\partial T}\Big)_{V,X_0}\frac{dV}{dt}\,dm + \quad (l_{\rm s}+e_{\rm s})\dot{M}_{\rm s} + \dot{\epsilon}_{\rm X} \qquad (1)$$

where the l.h.s. of this equation represents the sinks of energy, photons, neutrinos and any additional exotic term, while the r.h.s. contains the sources of energy, the heat capacity of the star, the work due to the change of volume, the contribution of the latent heat and gravitationl settling upon crystallization (the term $\dot{M}_{\rm s}$ is the rate of crystallization) and, finally, the last term represents any additional exotic source of energy [1]. There are two ways to test the theory of white dwarf evolution, namely, studying the white dwarf luminosity function and using the secular drift of the pulsation period of variable white dwarfs.

During the cooling process, white dwarfs experience some phases of pulsational instability powered by the κ- and the *convective driven*-mechanisms [2]. Depending on the composition

of the atmosphere variable white dwarfs are known as DOV, DBV and DAV. These stars also known as PG1159 or GW Vir stars, V777 He stars and ZZ Ceti stars respectively. Variable white dwarfs of different compositions occupy different regions in the Hertzsprung–Russell diagram. The value of the pulsation period indicates that these objects are experiencing g–mode non–radial pulsations, where the main restoring force is gravity. One of the main characteristics of these pulsations is that they experience a secular drift caused by the evolution of the temperature and radius. For qualitative purposes this drift can be approximated by [3]:

$$\frac{d\ln\Pi}{dt} \simeq -a\frac{d\ln T}{dt} + b\frac{d\ln R}{dt} \tag{2}$$

where a and b are constants of the order of unity that depend on the details of the model, and R and T are the stellar radius and the temperature at the region of period formation, respectively. This equation reflects the fact that, as the star cools down, the degeneracy of the plasma increases, the buoyancy decreases, the Brunt-Väisälä frequency becomes smaller and, as a consequence, the spectrum of pulsations gradually shifts to lower frequencies. At the same time, since the star contracts, the radius decreases and the frequency tends to increase. In general, DAV and DBV stars are already so cool (and degenerate) that the radial term is negligible and the change of the period of pulsation can be directly related to the change in the core temperature of the star. The timescales involved are of the order of $\sim 10^{-11}$ s/s for DOVs, $\sim 10^{-13}$ to $\sim 10^{-14}$ s/s for DBVs and $\sim 10^{-15}$ to $\sim 10^{-16}$ s/s for DAVs. Therefore, the measurement of such drifts provides an effective method to test the theory of cooling white dwarfs. This measurement is a difficult but feasible task, as it has been already proved in the case of G117–B15A, a ZZ Ceti star [4]. These properties allow to build a simple relationship [5, 6] to estimate the influence of an extra sink of energy, axions for instance, on the period drift of variable white dwarfs: $(L_{\rm X}/L_{\rm model}) \approx (\dot{\Pi}_{\rm obs}/\dot{\Pi}_{\rm model}) - 1$ where the suffix "model" refers to those models built using standard physics.

The white dwarf luminosity function is defined as the number density of white dwarfs of a given luminosity per unit of magnitude interval:

$$n(l) = \int_{M_{\rm i}}^{M_{\rm s}} \Phi(M)\,\Psi(t)\tau_{\rm cool}(l,M)\,dM \tag{3}$$

where t satisfies the condition $t = T - t_{\rm cool}(l,M) - t_{\rm PS}(M)$ and $l = -\log(L/L_\odot)$, M is the mass of the parent star (for convenience all white dwarfs are labeled with the mass of the main sequence progenitor), $t_{\rm cool}$ is the cooling time down to luminosity l, $\tau_{\rm cool} = dt/dM_{\rm bol}$ is the characteristic cooling time, $M_{\rm s}$ and $M_{\rm i}$ are the maximum and the minimum masses of the main sequence stars able to produce a white dwarf of luminosity l, $t_{\rm PS}$ is the lifetime of the progenitor of the white dwarf, and T is the age of the population under study. The remaining quantities, the initial mass function, $\Phi(M)$, and the star formation rate, $\Psi(t)$, are not known a priori and depend on the properties of the stellar population under study. The computed luminosity function is usually normalized to the bin with the smallest error bar, traditionally the one with $l = 3$, in order to compare theory with observations. Equation (3) shows that in order to use the luminosity function as a physical laboratory it is necessary to have good enough observational data and to know the galactic properties that are used in this equation (the star formation rate, the initial mass function and the age of the Galaxy). Fortunately, the bright branch of the luminosity function is only sensitive to the average characteristic cooling time of white dwarfs at the corresponding luminosity when the function is properly normalized. The

reason is twofold [7], on one hand the stellar population is dominated by low mass stars and on the other the lifetime of stars increases very sharply when the mass decreases. The result is that the old galactic populations are still producing bright white dwarfs and the number of such stars at each luminosity bin is the sum of the contributions of all the different episodes of star formation.

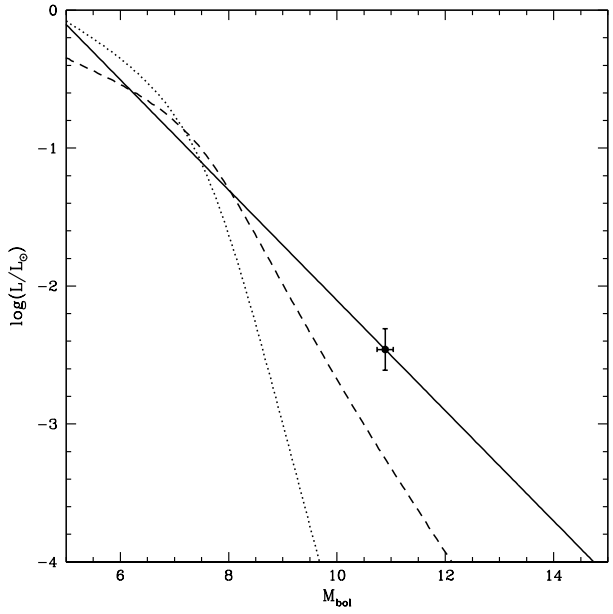

Figure 1: Power emitted in the form of photons (continuous line), neutrinos (dotted line) and axions (dashed line, arbitrary $g_{\rm aee}$) by a 0.6 $M_\odot$ white dwarf versus its bolometric magnitude, a function that monotonically increases with time. The cross represents the position of G115-B15A.

2 The axion case

We note that in white dwarf case only DFSZ axions have to be taken into account, since electron bremsstrahlung is the dominant process in white dwarf interiors. The axion emission rate under these conditions is given by [8]: $\dot{\epsilon}_{\rm ax} = 1.08 \times 10^{23} (g_{\rm aee}^2/4\pi)(Z^2 A)\, T_7^4 F(T,\rho)$ erg/g/s where F takes into account the Coulomb plasma effects, T_7 is the temperature in units of 10^7 K, Z and A are the atomic and mass numbers of the plasma components, respectively, and $g_{\rm aee}$ is the strength of the axion-electron Yukawa coupling. Figure 1 shows the energy losses of a typical white dwarf star. Since the neutrino emission is $\dot{\epsilon}_\nu \propto T^8$ and $L_{\rm phot} \propto T^{2.7}$ the luminosity function allows to disentangle the contribution of the different mechanisms of energy loss. When this method is applied to the luminosity function of white dwarfs the value of $g_{\rm aee}$ that best fits the luminosity function is 1.1×10^{-13}, but variations of a factor two are still compatible with the observations [9, 7]. Finally, the most recent analysis of G117-B15A shows that the value

of $g_{\rm aee}$ quoted here is compatible with the secular drift of the pulsation period, which gives support to the necessity to include an extra cooling term in the white dwarf models [10].

3 Conclusions

There are two independent evidences, the luminosity function and the secular drift of DAV white dwarfs, that these stars are cooling down more rapidly than predicted. The introduction of an additional sink of energy linked to the interaction of electrons with a light boson (axion, ALP,...) with an strength $g_{\rm aee} \sim 10^{-13}$ solves the problem satisfactorily. Of course, the remaining uncertainties, both observational and theoretical, still prevent to claim the existence of such interaction. A direct detection under laboratory conditions, like those of the CAST helioscope [11] or the shining through the wall experiments [12], could provide unambiguous evidences. In this sense, if the current result is interpreted as due to axions, such particles should have a mass, $m_{\rm a} \sim$ meV and should be coupled with photons with $g_{\rm a\gamma} \sim 10^{-12}$ GeV^{-1}.

Acknowledgments

This work has been supported by the MICINN grants AYA08-1839/ESP and AYA2008-04211-C02-01, by the ESF EUROCORES Program EuroGENESIS (MICINN grant EUI2009-04170), by SGR grants of the Generalitat de Catalunya and by the EU-FEDER funds.

References

[1] J. Isern, E. García-Berro, M. Hernanz, & R. Mochkovitch, "The physics of white dwarfs", Jour. Phys. Cond. Matter, **10**, 11263 (1998)

[2] L.G. Althaus, A.H. Córsico, J. Isern, & E. García-Berro, "Evolutionary and pulsational properties of white dwarfs", Astron. & Astrophys. Rev., in press (2010)

[3] D.E. Winget, C. J. Hansen, & H. M. Van Horn, "Do pulsating PG1159-035 stars put constraints on stellar evolution?", Nature, **303**, 781 (1983)

[4] S.O. Kepler *et al.*, "Measuring the evolution of the most stable optical clock G117-B15A", Astrophys. Jour., **634**, 1311 (2005)

[5] J. Isern, M. Hernanz, & E. García-Berro, "Axion cooling of white dwarfs", Astrophys. Jour., **392**, L23 (1992)

[6] J. Isern, & E. García-Berro, "White dwarfs as physics laboratories: the axion case", Mem. Soc. Astr. It., **79**, 545 (2008)

[7] J. Isern, S. Catalán, E. García-Berro, & S. Torres, "Axions and the white dwarf luminosity function", J. Phys.: Conf. Ser., **172**, 012005 (2009)

[8] M. Nakagawa, Y. Kohyama, & N. Itoh, "Axion bremsstrahlung in dense stars", Astrophys. Jour., **322**, 291 (1987)

[9] J. Isern, E. García-Berro, S. Torres, & S. Catalán, "Axions and the cooling of white dwarf stars", Astrophys. Jour., **682**, L109 (2008)

[10] J. Isern, E. García-Berro, L.G. Althaus, & A.H. Córsico, "Axions and the pulsation periods of variable white dwarfs revisited", Astron. & Astrophys., **512**, A86 (2010)

[11] T. Papaevangelou, "CAST, recent results results and future outlook", http: axion-wimp.desy.de and these proceedings.

[12] P. Arias, J. Jaeckel, J. Redondo, A. Ringwald "Improving the discovery potential of future light-shining-through-the-wall experiments", aerXiV:1009.1519 [hep-ph], http: axion-wimp.desy.de and these proceedings.

Signature of Solar Axions

Kenneth J. H. Phillips[1]

[1]Mullard Space Science Laboratory, University College London, Holmbury St Mary, Dorking, Surrey RH5 6NT, United Kingdom

DOI: http://dx.doi.org/10.3204/DESY-PROC-2010-03/phillips_kenneth

A summary of the standard solar model for the solar interior is given, with the present state of observational confirmation of the model from neutrinos and helioseismology. If there is a sizable flux of axions or axion-like particles from the solar core, it might result in the heating of magnetic rope structures in the tachocline in the interior or subtle X-ray signatures in the Sun's corona, or outer atmosphere. The intensities of certain X-ray lines with magnetic dipole transitions may also be affected.

1 The solar interior

Great strides in our understanding of the interior of the Sun have been made in the past thirty or so years through a number of developments. First, improved cross sections for nuclear reactions occurring at the Sun's core, where the temperature is approximately 15×10^6 K (15 MK), now give us fairly precise values for reaction rates. There is a complex series of such reactions, but the end result is the fusion, in a step-wise fashion, of four protons to form a single helium nucleus with energy released in the form of positrons, neutrinos, and thermal energy: $4p \rightarrow^4 \mathrm{He} + 2e^+ + 2\nu + 25$ MeV. The thermal energy generated is transported by photon diffusion through the inner part of the solar interior, out to a radius of about $0.7R_\odot$ (1 solar radius $= 1R_\odot = 696\,000$ km) where models predict a temperature of about 5 MK. At this level, there is an increase in the opacity of the gas, and the energy transfer is then by convection.

The structure of the solar interior has been modelled by applying known physical laws to the material of the Sun, in particular hydrostatic equilibrium and energy transfer (by both radiative and convective processes). The Sun is assumed to have been created by the collapse of an interstellar gas cloud with element abundances like those measured in the photosphere (Sun's surface layer where the energy escapes as radiation). The cloud is allowed to evolve, with hydrogen slowly converting to helium in the core region. After a time equal to the Sun's present age, the modelled Sun should resemble the actual Sun through its present radius and luminosity. Any deviations can be corrected by adjusting the Sun's chemical composition. Such is the *standard solar model* (SSM), long associated with the name of John Bahcall whose work on this subject has been well documented.

2 Testing the standard solar model: the tachocline

Since nothing can be directly observed below the photosphere (the opacity rapidly increases with depth), it might seem that the standard solar model cannot be easily observationally tested. However, there are two means available to solar physicists. The first is the observed flux of solar neutrinos at the Earth. The first experiments, particularly the Homestake mine experiment of Raymond Davies, indicated a roughly factor-of-three discrepancy between the predicted and observed neutrino flux, the observed being smaller. This has now been explained through the MSW effect.

The second test of the SSM is supplied by helioseismology: observations with spectrometers viewing Doppler shifts in sharp absorption lines in integrated sunlight show that there is a series of oscillations, identified as acoustic modes occurring over the whole Sun. These oscillations are due to sound waves travelling in the solar interior, generated by stochastic turbulence, with wave fronts moving through the solar interior in arc-like patterns. A cluster of modes is observed with frequencies of about 3 mHz. Each mode probes the interior at various depths, so giving a test of the radial variation of temperature and density predicted by the SSM. There was until 2005 highly impressive agreement of the observed mode frequencies with those predicted, but the adjustment of some element abundances [1] has vitiated this somewhat. This is still being investigated, but possibly fine adjustment of the abundances of other elements might restore the agreement.

The Sun is observed to rotate differentially (the photospheric period varies from 25 days near the equator to 34 days near the poles). Modes in the same direction as the solar rotation have a frequency that is slightly higher than those in the opposite direction: like spectral lines, then, there is a "rotational" splitting of the azimuthal mode frequencies. It provides a powerful way of examining the rotational speed of the solar interior at different depths. It is found that at a particular depth, near the boundary of the Sun's radiative and convective zones, there is a strong shear zone, with layers above rotating differentially but layers below rotating as a rigid body. This is the *tachocline*, and corresponds to where cooler material sinking down "overshoots". Helioseismology indicates that the tachocline is only 15 000 km thick, or $0.02R_\odot$.

3 Magnetic field in the tachocline

The Sun's magnetic field is manifested in particular structures, notably sunspot groups and associated regions above them in the high-temperature corona (temperature up to 5 MK), and in a general field most obvious near the poles at times of few sunspots. Zeeman splitting of spectral lines shows that sunspot fields can attain 0.4 T, but there are also field concentrations all over the Sun's surface, with strengths of up to 0.1 T. The continual generation of the magnetic field every eleven years (the solar cycle) is attributed to a dynamo operating in the solar interior. It is deduced that the dynamo cannot operate in the convective zone since the rope-like structures that the field takes on will rise by magnetic buoyancy. On the other hand, the radiative zone is practically isolated from the convective zone so any magnetic field there is not likely to appear at the Sun's surface. The seat of the dynamo is therefore thought to be the tachocline, which is convectively stable apart from the overshoot of convective currents above this level. The strength of the field in the tachocline has been much discussed: previous estimates from theoretical models indicated around 1 T. However, fields of this magnitude do not explain the latitude distribution of sunspots. Choudhuri [2] and others have persuasively

argued for much larger fields, up to 10 T, in the tachocline; only then do model calculations reproduce the observed distribution of sunspot locations.

4 Implications for solar axions

The case has been made for large numbers of axions or axion-like particles (ALPs) to be produced in the solar core [9, 10]. The probability of conversion to X-ray photons by the inverse Primakoff effect is proportional to $g^2B^2l^2$ where g is the coupling constant, B the magnetic field strength, and l a length scale. For laboratory measurements, l is of order meters, but if there is interaction with solar magnetic fields l is in the range $100 - 10\,000$ km. Thus, if axions are produced at the Sun's core, with average energy $\approx$ few keV, interactions with the Sun's magnetic field could proceed resulting in observable X-ray signatures and this in turn might give a useful upper limit to g. Zioutas et al. [9] suggested there might be a halo of axions gravitationally captured resulting in X-ray emission. Carlsson & Tseng [3] discuss the possibility of axions interacting with the Sun's general field and strong sunspot fields by the inverse Primakoff effect. They predict that there would be an observable modulation in the X-ray emission as a large sunspot rotates across the solar disk; the field orientation does not seem to be considered by them, but this is important as the sunspot field below the photosphere is largely radial, and so the as the axion–magnetic field interaction will be reduced.

Interaction of axions with the field in the tachocline region, now considered to be 10 T and so much larger than sunspots or the general field, might produce some perturbation in the SSM. There would be substantial heating of this region and so possibly an increase of convective activity. The field in the tachocline would most likely be in the form of rope-like structures, with the length of the rope parallel to the solar equator, so the convective activity may appear in bands of latitude near where sunspots occur. The length scales l are likely to be around 10 000 km. The general field of the Sun is most apparent during solar minimum and is approximately dipole-like. Interaction of axions with the general field above the equator, which is almost parallel to the Sun's surface and so perpendicular to the axion flow, might lead to patches of dim X-ray emission near the apparent Sun's centre. Such effects have been looked for with the Soft X-ray Telescope on *Yohkoh* (operational 1991–2000), but so far nothing resembling this has been found [6]. The flux of 3–6 keV X-rays calculated on the assumption of $g \approx 10^{-10}$ GeV^{-1} and light ($\lesssim 2 \times 10^{-6}$ eV) axions, viz. ≈ 400 photons m^{-2} s^{-1} keV^{-1} [3], is close to measured estimates [4] from the *RHESSI* solar X-ray spacecraft during periods of low activity between 2005 and 2006. However, solar X-ray activity has been considerably less since then [5]. The SphinX instrument on the Russian *CORONAS-PHOTON* spacecraft [8] measured 1–15 keV X-ray flux levels 20 times less than the flux in an equivalent band in 2005–2006. It may therefore be possible to constrain the axion fluxes to much lower limits when the SphinX results are fully analyzed.

Other signatures for solar axions or ALPs include nuclear and atomic M1 (magnetic dipole) transitions. The most widely-cited in this context has been the 14.4 keV line formed when ^{57}Fe nuclides are thermally excited inside the Sun ([7]). Upper limits to the flux of this line can be set from solar X-ray spectrometers such as *RHESSI*. No feature has ever been observed at 14.4 keV, imposing an upper limit to the line flux of ≈ 10 photons m^{-2} s^{-1}. Some lines due to M1 atomic transitions are notable in the solar X-ray spectrum. They include lines emitted by flares of He-like ions such as Fe^{+24} and Ca^{+18}, with transitions $1s^2\,{}^1S_0 - 1s2p\,{}^3P_2$, close to an intercombination line ($1s^2\,{}^1S_0 - 1s2p\,{}^3P_1$). Anomalies in the intensities of these

lines have been noted but are thought to be due to the intercombination line rather than the M1 line. However, the M1 line at 1.7096 nm emitted by active regions due to Ne-like Fe (Fe^{+16}), transition $2p^6\,{}^1S_0 - 2p^6 3d\,{}^3P_2$, has an intensity that varies with time compared with the nearby $2p^6\,{}^1S_0 - 2p^6 3d\,{}^3P_1$ (wavelength 1.7050 nm). The changes with time are subtle but are unexplained (for example by high densities). An axion explanation is unlikely but detailed calculations must be done to see what the possible effects are.

5 Conclusions

The possible flow of axions or ALPs from the solar core might give rise to observable effects that could lead to useful limits on the coupling constant, the length scales being much larger than are obtainable in the laboratory. These effects include the heating of magnetic rope-like structures in the tachocline (region of convective overshoot just beneath the convective zone of the solar interior) and X-ray emission in and around the solar corona. There are also possibly interesting anomalies in observed X-ray spectral lines due to magnetic dipole transitions: axion explanations are unlikely but calculations need to be done that assess their likelihood.

Acknowledgments

I am very grateful to Dr Konstantin Zioutas for his invitation to participate in this Workshop, and to the Workshop organizers for financial assistance.

References

[1] M. Asplund, N. Grevesse, A. J. Sauval, C. Allende Prieto and R. Blomme, "Line formation in solar granulation - VI," Astron. and Astrophys. **431**, 693 (2005).

[2] A. R. Choudhuri, "The evolution of loop structures", Solar Phys. **123**, 217 (1989).

[3] E. D. Carlsson and L.-S. Tseng, "Pseudoscalar conversion and X-rays from the Sun," Phys. Letters B **365**, 193 (1996).

[4] I. G. Hannah, G. J. Hurford, H. S. Hudson, R. P. Lin and K. van Bibber, "First limits on the 3–200 keV X-ray spectrum of the quiet Sun using *RHESSI*," Astroph. J., **659**, L77 (2007).

[5] I. G. Hannah, H. S. Hudson, G. J. Hurford and R. P. Lin, "Constraining the hard X-ray properties of the quiet Sun with new *RHESSI* observations," [arXiv:1009.2918v2 [astro.ph.SR]]

[6] H. Hudson, *RHESSI* Science Nugget No. 50, "Solar X-rays from axions": http://sprg.ssl.berkeley.edu/~tohban/nuggets (2007).

[7] S. Moriyama, "Proposal to search for a monochromatic component of solar axions using ^{57}Fe," Phys. Rev. Letts **75**, 3222 (1995).

[8] J. Sylwester, M. Kowalinski, S. Gburek, M. Siarkowski, S. Kuzin, F. Farnik, F. Reale and K. J. H. Phillips, "The Sun's X-ray emission during the recent solar minimum," EOS **91**, No. 8 (2010).

[9] K. Zioutas, K. Denneri, L. DiLella, D. H. H. Hoffmann, J. Jacoby and Th. Papaevangelou, "Quiet-Sun X-rays as signature for new particles," Astroph. J. **607**, 575 (2004).

[10] K. Zioutas, M. Tsagri, Y. Semertzidis, Th. Papaevangelou, T. Dafni and V. Anastassopoulos, "Axion searches with helioscopes and astrophysical signatures for axion(-like) particles", New J. Phys. **11**, 105020 (2009).

EBL data and limits: Implications for Axion Search

Tanja M. Kneiske
Experimentalphysik, University of Hamburg, Luruper Chaussee 148, Hamburg, Germany

DOI: http://dx.doi.org/10.3204/DESY-PROC-2010-03/kneiske_tanja

One way to search for axion like particle (ALP) is to study the absorption in extragalactic gamma-ray sources. The change of a high-energy photon to an ALP could prevent the absorption due to pair production with ambient infrared photons. The knowledge of these diffuse low energy photon fields are therefore one of the key elements in such a search. In the following the different methods are explained to get limits and data for the extragalactic background light (EBL) to show the current status in this field. The purpose of this article is to show that up to now there is no disagreement between observations of the EBL flux and absorption of gamma-ray photons from extragalactic sources. Only future detections of high redshifted gamma-ray sources could lead to non-standard physics.

1 Data & limits

The extragalactic background light is the optical to infrared part of the local component of the cosmic radiation fields (for a review see [1]). Direct emission from stars and reprocessed light by the interstellar medium can explain most of the observed flux, but there are still uncertainties, which give room for other contributions [2]. There are basically two types of observations constraining the EBL flux, direct observations (Figure 1; green symbols) and galaxy number counts (Figure 1; blue symbols).

1.1 Galaxy number counts

Galaxy counts are a good method to estimate a strict lower limit for the EBL flux from galaxies. The idea is to count in a deep field the observed galaxies according to their luminosity. The integrated light of all counted galaxies is a certain contribution to the EBL. Most of the data derived in this way are much smaller than the direct observations and model predictions since the samples are flux limited and they have been derived only from a small part of the sky. A better estimate is if the results are extrapolated for the whole sky. This can only be done if the deep field represents an average and cosmological representative part of the universe. Therefore recent observations and number counts are not based on one deep field but on two or more. The choice of the deep fields and their dimensions are also very important. The deep fields are chosen to lie in a direction without bright foreground galaxies, stars and clusters. The line of sight includes also only low cirrus infrared emission, low extinction and low hydrogen column densities. To avoid an over- or underprediction due to the large-scale structure a combination with wide fields are important. They are not as deep but cover a larger area at the sky averaging voids and filaments of the cosmic web. Lower limits shown Figure 1 using this method are from the Hubble Space Telescope (HST) (solid blue squares) [3], the SPITZER data in the near IR

(open blue triangles) [4], the lower limits in the far infrared derived from Herschel (filled blue circles) [5] and by AKARI (blue X) [6]. A technique to get even deeper galaxy count images is to use galaxy cluster lenses as has been done with ISO (cyan filled triangles) [7], [8] and Herschel (Cyan filled circles) [9]. Another way of deriving good lower limits is the stacking analysis of deep fields. Using a source catalogue of observed galaxies at 24 microns [10] has looked for a combined signal from all sourced at 70 and 160 microns where the galaxies were not observable as single sources. This has been updated in [11] (open blue triangles). All the derived data, even if they are not published as that, are to be handled as lower limits, due to the detection technique. It is always possible that the surveys are missing faint galaxies or stars and galaxies at higher redshift. As a result it seems that the far infrared background is close to being resolved by recent observatories, since the number counts are on the same flux level as the direct observations.

1.2 Direct observations

A different way of observing the EBL flux is the direct observations. Here the sky is searched for a radiation component, which is independent of direction and place of observation. The biggest problem with this method is that the EBL flux is very small compared to the dominating foreground emission like the zodiacal light. It is reflected sunlight by a ring of dust particles around the sun. Venus and the earth are inside the ring and so also inside the dust emission. Although the zodiacal light is not completely isotropic detailed models of the location and type of dust is needed to estimate this component (see [1] and refs. therein). In the far infrared the interstellar medium can also play a role and DIRBE data have been analyzed by different authors to estimate its influence (open green circles) [12]. So despite great efforts to study the foreground emission contamination of data from IRTS (Infrared Telescope in Space [13] and DIRBE (Diffuse infrared Background Explorer, [14] are still under discussion. More recent data from AKARI [6] show a good agreement with the older observations. Since it is not clear if all foreground emission have been removed all the direct observations have to be seen as upper limits.

1.3 EBL limits from AGN observations

Besides the direct ways of detecting the EBL flux there is the method of using the effect of EBL photons on the high-energy spectra of extragalactic gamma-ray sources. This indirect method is based on the pair-production process, which takes place between the ambient infrared photons and the relativistic gamma-rays. The search for absorption features in AGN at GeV and TeV energies is a possibility to study the EBL flux avoiding the problems stated above. But here another uncertainty comes into play. To calculate from the observed AGN spectra the EBL density the physics of the AGN needs to be known. Right now there are several theories, which could explain the multi-wavelength behavior of AGN spectra. But since AGN are complex objects where hadrons and electrons accelerated to relativistic energies meet thermal emission from the interstellar medium of the host galaxies and the gas and dust close to their cores, it is very hard to develop a model which can describe AGN completely. Each AGN also needs to be treated on its own, since even belonging to the same class of objects like blazars they can look quite differently. Making only very general and almost model independent assumptions about the gamma-ray spectrum upper limits on the EBL flux can be derived by Cherenkov telescope observations of blazars[15] (dashed red line), [16] (solid red line), [17] (solid red line), [18](short

dashed line)). Using observed gamma-ray spectra by FERMI more optical limits could be derived [19] (red triangles down). Interestingly the limits from AGN observations came close to the lower limits from number counts. But right now the upper limits are within the errors about a factor of two above the lower limits and are therefore still in agreement. Only if the AGN upper limits fall below the lower limits from number counts, one has to re-think about the assumptions going into the limits. There awould be basically two possibilities then; AGN are different from the model predictions used or some process prevent the high energy photons from being absorbed.

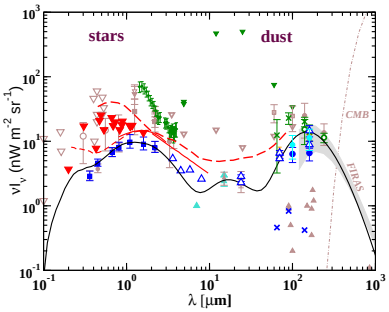

Figure 1: Extragalactic background light flux: data and limits (description and refs. see text). The black line is the lower limit EBL model [23] which gives a physically correct description of the lower limit data, including redshift evolution.

2 Implications for axions and axion like particles

Assuming that the EBL lower limit flux has been measured correctly and that the AGN physics is understood there are several theoretical ideas, which could alter the pair production process on large scales in the universe. One is the conversion of photons into axions or ALPs. If such a particle is converted back to a gamma-ray photon before it reaches earth is would be detected together with the unabsorbed emission. The gamma-ray spectrum would look less absorbed than it should be and the resulting upper limit on the EBL flux could be below the number counts [20], [21]. However all the absorption features including high 3C279, can be explained by standard physics in the photon-photon pair production framework. But there are some discrepancies, which are so small that they can still be explained by observational and theoretical uncertainties, but could also hint towards some disagreement in the standard picture. To model the lower limit number counts a very low cosmic star formation rate (CSFR) needed. Data of the CSRF are highly model dependent and scatter almost within one order of magnitude. Since the star formation cannot be observed directly the data are calculated from galaxy number counts, the same that are used to derive the EBL data. To infer the CSFR a conversion factor is needed [22]. The CSFR, which is used to fit the EBL lower limit data, lies below the average data. So the lower-limit EBL star formation is already underestimating the amount of stars observed in the universe. A factor of two more star formation in the universe would describe the CSFR data much better, but it also leads to an EBL flux on the same level as the AGN upper limits.

Only a slight change of the limits could lead to question standard physics.

Acknowledgements

TK acknowledge the support of a grant from the LEXI Hamburg - "Cluster of Excellence: Connecting Particles with the Cosmos".

References

[1] M.G. Hauser & E. Dwek, "The Cosmic Infrared Background: Measurements and Implications" Ann. Rev. A&A, **39**, 249 (2001)

[2] T.M. Kneiske, K. Mannheim, & D. Hartmann, "1. Implications for gamma-ray absorption: Evolution for the metagalactic radiation field" A & A, **386**, 1 (2002)

[3] P. Madau & L.Pozzetti, "Deep galaxy counts, extragalactic background light and the stellar baryon budget" Mon. Not. Roy. Astro. Soc. **312**, L9 (2000)

[4] G.G. Fazio *et al.* "Number Counts at 3-10microns from the Spitzer Space Telescope" Astrophys. Journal Supl. **154**, 39 (2004)

[5] S. Berta *et al.* "Dissecting the cosmic infra-red background with Herschel/PEP" A&A, **518**, 30 (2010)

[6] S. Matsuura *et al.* "Detection of the Cosmic Far-Infrared Background in the AKARI Deep Field South" Astrophys. Journal (sub) (2010) [arXiv:1002.3674 [astro-ph]]

[7] B. Altieri *et al.* "An ultra-deep ISOCAM observation through a cluster-lens" A&A, **343**, 65 (1999)

[8] L. Metcalfe *et al.* "An ISOCAM survey through gravitationally lensing galaxy clusters." A&A, **407**, 791 (2003)

[9] B. Altieri *et al.* "Herschel deep far-infrared counts through Abel 2218 cluster-lens" A&A, **518**, L17 (2010)

[10] H. Dole *et al.* "The CIB resolved by Spitzer. Contributions of mid-infrared galacies to the far infrared background" A&A, **451**, 2 (2006)

[11] M. Bethermin *et al.* "Spitzer deep and wide legacy mid- and far-infrared number counts and lower limits of the CIB" A&A, **512**, 78 (2010)

[12] G. LaGache *et al.* "First detection of the warm ionised medium. Implications for the CFIB" A&A, **354**, 247 (2000)

[13] T. Matsumoto *et al.* "IRTS Observations of the NIR EBL" Astrophys. Journal **626**, 31 (2005)

[14] M.G. Hauser *et al.* "The COBE Diffuse Infrared Background Search for the CIB. Limits and detections." Astrophys. Journal **508**, 25 (1998)

[15] D. Mazin & M. Raue "New limits on the density of the EBL in the opical to the infrared from the optical to the infrared spectra of all known TeV blazars" A & A **471**, 439 (2007)

[16] Aharonian *et al.* "A low level EBL as revealed by gamma-rays from blazars" Natur **440**, 1018 (2006)

[17] Aharonian *et al.* "New constraints on the mid-IR EBL from the HESS discovery of VHE gamma-rays from 1ES0229+200" A & A **475**, 9 (2007)

[18] The MAGIC Collaboration "Very-High-Energy Gamma Rays from a Distan Quasar: How Transparent is the Universe?" Science **5884**, 1752 (2008)

[19] J. Yang & J. Wang "Constraining the EBL From TeV Blazars" A & A (accepted) [arXiv:1006:4897] (2010).

[20] A. Mirizzi & D. Montanino "Stochastic conversions of TeV photons into axion-like particles in the extralgactic magnetic fields" Journal of Cosm. Astrop. Phys. **12**, 004 (2009)

[21] A. de Angelis, O. Mansutti & M. Roncadelli "ALPs, cosmic magnetic fields and gamma-ray astrophysics" Phys. Lett. B **659**, 5

[22] A.M. Hopkins & J.F. Beacom "On the Normalization of the Cosmic Star Formation History" Astrophys. Journal **651**, 142 (2006)

[23] T.M. Kneiske & H. Dole "A lower-limit flux for the EBL" A & A **515**, 19 (2010)

Signatures for Solar Axions/WISPs

Konstantin Zioutas[1,2], *Theodoros Vafeiadis*[1,2,3], *Mary Tsagri*[1]*, *Yannis K Semertzidis*[4], *Thomas Papaevangelou*[5], *Theopisti Dafni*[6]†*and Vassilis Anastassopoulos*[1]

[1]University of Patras, Patras, Greece
[2]European Organization for Nuclear Research (CERN), CH-1211 Genève 23, Switzerland
[3]University of Thessaloniki, Thessaloniki, Greece
[4]Brookhaven National Laboratory, NY-USA
[5]IRFU, Centre d' Études Nucléaires de Saclay, Gif-sur-Yvette, France
[6]Laboratorio de Física Nuclear y Astropartículas, Universidad de Zaragoza, Zaragoza, Spain

DOI: http://dx.doi.org/10.3204/DESY-PROC-2010-03/zioutas_konstantin

Standard solar physics cannot account for the X-ray emission and other puzzles, the most striking example being the solar corona mystery. The corona temperature rise above the non-flaring magnetized sunspots, while the photosphere just underneath becomes cooler, makes this mystery more intriguing. The paradoxical Sun is suggestive of some sort of exotic solution, axions being the (only?) choice for the missing ingredient. We present atypical axion signatures, which depict solar axions with a rest mass $m_{ax} \simeq 17\,meV/c^2$. Then, the Sun has been for decades the overlooked harbinger of new particle physics.

1 Introduction

The ∼5800 K temperature of the solar photosphere naturally decreases outwards. Beyond a height of ∼500 km, i.e., in the chromosphere, the beginning of a mysterious behaviour appears. The atmospheric temperature, instead of decreasing, starts rising again, up to 1-2 MK, and this all of a sudden within only ∼100 km. How this temperature behaviour can happen steadily, and all over the entire Sun, is dubbed the solar corona heating problem, *one of the most perplexing and unresolved problems in astrophysics to date* [1]. The phenomenology of the solar atmosphere makes this mystery even more enigmatic. For example, the unnaturally high-temperature upper solar atmosphere becomes even hotter above non-flaring magnetized locations, like the puzzling dark sunspots, reaching about 5-10 MK [2], while the underlying surface of the sunspots gets relatively cooler, reaching occasionally ∼3000 K, instead of the ambient ∼5800 K. The temperature difference between two neighbouring solar layers, i.e., that of the photosphere and that of the corona, with the chromosphere sandwiched in between, widens. How can this additional and intriguing behaviour of the magnetized Sun fit conventional thinking? Obviously, the solar magnetic field, is the ingredient adding *somehow* to the solar corona mystery. This finding is a second fingerprint of the corona's mystery, with the first being the formation of the surprisingly strong temperature inversion across the so-called transition region. Furthermore,

*Present address: European Organization for Nuclear Research (CERN), CH-1211 Genève 23, Switzerland
†E-mail: tdafni@unizar.es

following conventional reasoning, we still do not know how magnetic energy is converted into thermal energy of the corona [3].

The solar corona mystery is not an isolated one, but rather ubiquitous throughout the solar-type stars in the Universe. Astonishingly, the Sun's radiation spectrum deviates strongly from that of a black body, and this reflects the whole mystery. For comparison, an almost perfect black body spectrum is exhibited by the CMB radiation of the infant Universe (3000 K). Therefore, the question arises as to why the Sun behaves only partly as a perfect black body and how it manages to keep its tiny outer atmosphere, packed so close to its surface, at such an unnaturally high temperature. Note that the Sun is permeated spatiotemporally with unpredictably varying magnetic fields, which is the cause of many puzzling solar phenomena, while the early Universe had diminishingly small magnetic fields. This difference is essential from the axion point of view, since the axion-photon oscillation probability, as most solar phenomena, shows a striking B^2-dependence. One should bear in mind that no stellar theory expects a Sun-like star to emit any measurable quantity of X-rays, as we witness since decades with the Sun.

To the best of our knowledge, in recent times, no other solar problem has defied explanation for so long, e.g., take the solution of the solar neutrino deficit problem. It is logical to conclude that the mysterious coronal behaviour must be the manifestation of hidden new (solar) physics. Other solar phenomena associated with the mysterious 11-year clock, like flares, coronal mass ejections, sunspots, spicules, etc. raise also serious questions about their (not much less) mysterious origin, thus further suggesting a (common?) exotic solution.

2 Solar/Stellar axion manifestation

How can the solar behaviour be related to exotica like axions? The production of axions inside the Sun's core was widely accepted soon after their theoretical invention, constraining also their coupling strength to matter following the non-observation of additional star ageing effects [2]. An extra energy escape from their hot core into space should have made them appear older than they actually are. In fact, stellar evolution arguments constrain the allowed escaping solar energy into axions to the ‰-level. Nevertheless, this is still a quite large percentage compared to the solar observations under consideration as being due to or triggered by new exotica. For example, the unexpected quiet Sun X-ray emission makes only $\sim 10^{-7}$ of its total energy output, while present X-ray missions detect solar fluxes at the level of $\sim 10^{-14}$. This demonstrates the enormous potential solar observations have to unravel new physics, with the axion scenario inspiring the most, since (most) puzzling solar phenomena correlate with the magnetic field. Therefore, axion involvement in stars can have far reaching consequences, even if it causes only faint emission of radiation, since this leaves no signs of premature ageing.

Encouraged by the Sun's groundbreaking impact in the past in nuclear and astroparticle physics, it was natural to be attracted by the Sun's puzzling and inspiring behaviour, which depicts axion involvement. While we refer only to solar axions, the cause of the multifaceted and unpredictable Sun is not necessarily due to one single process by one single particle's involvement, though in certain cases exotic scenarios remain the only choice. Observations at extreme conditions, like the non-flaring quiet Sun during solar minimum or an isolated active/flaring solar region, could favour the showing-up of one exotic component against other(s), if any.

We refer throughout this work to axions, but we consider them as being representative of any other exotica dubbed WISPs (Weakly Interacting Slim Particles), which can couple similarly to ordinary matter, e.g., intriguing scalar particles like the chameleons, which are potential

candidates for the cosmic dark energy. While the QCD-inspired axion implies a particle with one rest mass and one coupling constant, WISPs do not have to follow this constraint, e.g. massive solar axions of the Kaluza–Klein type [4].

3 Solar axion signatures

For the last 15 years, the search for axions in solar X-rays has mostly been oriented towards a very light axion (rest mass $\ll 10^{-4}\,\mathrm{eV/c^2}$) [2]. But, if its mass is (far) above this range, any search should fail, and this is the case so far. Therefore, this work addresses a much higher axion rest mass range ($\sim$20 meV/c^2), albeit not intentionally but being observationally driven: if axions play a certain role in the Sun's workings, then some strange phenomena should show up, at least occasionally, i.e., with known physics being unable to provide an explanation. In fact, this is what happens so strikingly, since the Sun is full of mysteries.

We focus here on derived atypical solar axion signatures related to magnetic fields. For example, for the solar corona mystery, massive solar axions of the Kaluza–Klein type have been suggested as the potential source of the steady solar X-ray emission component [4]. The very thin solar corona is rather similarly hot ($\sim$1-10 MK) as the hot solar core ($\sim$16 MK), and therefore it requires an energy input, which has been elusive and has kept the corona mystery alive for several decades, even though there is no luck of proposed models. Note, the corona density changes dynamically, e.g., by factor up to $\sim$10-100 [5]. Then, within the axion scenario, the observed solar corona reflects the balance between inwards directed radiation pressure from the spontaneous decay of massive axions of the Kaluza–Klein type or any other massive, radiatively-decaying WISPs, while out-streaming axions being magnetically converted to X-rays exert an additional but outwards directed radiation pressure. To show the dynamical character of the Sun, it is worth mentioning, for example, the mysterious solar spicules, which cover about 1% of the Sun's surface; their plasma density reaches values of $\sim 10^{11}/\mathrm{cm}^3$, which are also of potential interest for axion-photon oscillations.

Figure 1 shows the directly measured "excess" X-rays from the quietest to the flaring Sun (see Figure 10 in [2]). Here we update the first intensity calculations presented in [2]. Thus, a magnetic-field-related X-ray emission, be it transient be it steady, can be, in principle, axion in origin. The maximum conversion rate of out-streaming axions near the magnetized solar surface was estimated to be $P_{\mathrm{a}\to\gamma} \approx 10^{-12}$ (see section 3 in [2]). For comparison, assuming even that the entire quiet Sun soft X-ray luminosity measured recently by the SPhinX detector ($\mathrm{L}_x \approx 10^{21}$ erg/s) is due to converted axions, this requires an even smaller conversion rate (10^{-13}). Furthermore, since only $\sim$1% of the complex magnetism of the quiet Sun is seen [6], this leaves room for much larger conversion efficiencies ($\sim 10^{-8}$), i.e. an X-ray brightness of $10^3\,\mathrm{erg/cm^2/sec}$ can still be axion related, which is not small. In addition, the fading solar magnetic field during the 2009 solar minimum was correlated with a 100 times weaker soft X-ray emission than during the previous solar minimum measured by the SPhinX mission [8]. But, the only $\sim$25% decrease of the solar magnetic field cannot justify a 100-fold X-ray luminosity decrease, following a B^2-dependence. But if, for example, the conversion occurs deeper inside the photosphere, some X-rays are absorbed, or, in any case they become more red-shifted and might evade observation. These measurements show that the calculated maximum axion conversion in [2] was (very) conservative. Moreover, there is room for still larger conversion, which could account also for larger X-ray surface brightness from flares: the rarity of such events may eventually reflect the not so easily achievable 'fine tuning' of magnetic field and plasma

density. While the aim of this work is not to explain all solar X-ray phenomena exclusively by axions, this might be the case to a larger extent than anticipated so far (given the mentioned uncertainties).

In addition, Figure 2 shows the B^2 dependence of the deficit IR emission above the magnetized sunspots. If this is due to the disappearance of photons into axions, it implies also an overlooked strong solar axion source at low energies with far reaching implications in solar axion research. Finally, Figure 3 explains how one may make visible new signatures, hidden in the solar irradiance spectrum, using the normalised residuals from a pure black body distribution.

4 Conclusions

We present observational evidence in favour of the solar axion scenario. Both massive and light axions are required, in order to explain the celebrated solar coronal heating mystery and unexpected (transient) X-ray activity. The suggested axion scenario does not exclude the involvement of other WISPs (or the synergy with conventional phenomena). For example, the solar chameleon might be a potential candidate. This work is observationally driven. The accumulating axion signatures, when considered coherently all together, increase their combined significance in favour of solar axions as being at the origin of often miraculous solar behaviour. Nevertheless, each finding reflects an axion signature in its own right. On top of every other argument, we keep in mind that such a large amount of X-rays is anyhow not expected to be emitted by a cool star like the Sun, and this is what triggered this work.

References

[1] P. Antolin, K. Shibata, T. Kudoh, D. Shiota and D. Brooks, "Magnetic Coupling between the Interior and Atmosphere of the Sun," Astroph. Space Sc. Proc. Part 2 pp.277-280 (2010) [eprint astro-ph/0903.1766].

[2] K. Zioutas, M. Tsagri, Y. K. Semertzidis, T. Papaevangelou, T. Dafni and V. Anastassopoulos, "Axion Searches with Helioscopes and astrophysical signatures for axion(-like) particles," New J. Phys. **11** 105020 (2009) and references therein.

[3] H. P. Warren et al., "Evidence for Steady Heating: Observations of an Active Region Core with Hinode and TRACE," ApJ **711** p.228 (2010).

[4] L. DiLella, P. Pilaftsis, G. Raffelt and K. Zioutas, "Search for solar Kaluza-Klein axions in theories of low-scale quantum gravity," Phys. Rev. D **62** 125011 (2000); L. Di Lella and K. Zioutas "Observational evidence for gravitationally trapped massive axion (-like) particles," Astropart. Phys. **13** p.145 (2003).

[5] M. Aschwanden, "Physics of the Solar Corona," Ed. Springer pp.24-26 (2004).

[6] J. T. Bueno, N. Shchukina and A. A. Ramos, "A substantial amount of hidden magnetic energy in the quiet Sun ," Nature **430** p.326 (2004).

[7] M. Battaglia, L. Fletcher, A. O. Benz, "Observations of conduction driven evaporation in the early rise phase of solar flares," A.& A. **498** 891 (2009).

[8] J. Sylwester, M. Kowalinski, S. Gburek, M. Siarkowski, S. Kuzin, F. Farnik, F. Reale, K. J. H. Phillips, "The Sun's X-ray Emission During the Recent Solar Minimum," Eos Trans. AGU, **91** (#8) p.73 (2010).

[9] G. Peres, S. Orlando, F. Reale, R. Rosner and H. Hudson "The Sun as an X-Ray Star. II. Using the Yohkoh/Soft X-Ray Telescope-derived Solar Emission Measure versus Temperature to Interpret Stellar X-Ray Observations," ApJ. **528** 537 (2000).

[10] W. Livingston, M. Penn, "Are Sunspots Different During This Solar Minimum?," Eos Trans. AGU **90** (#30) p.257 (2009). `http://www.leif.org/EOS/2009EO300001.pdf`.

[11] W. Livingston, private communication, 2010.

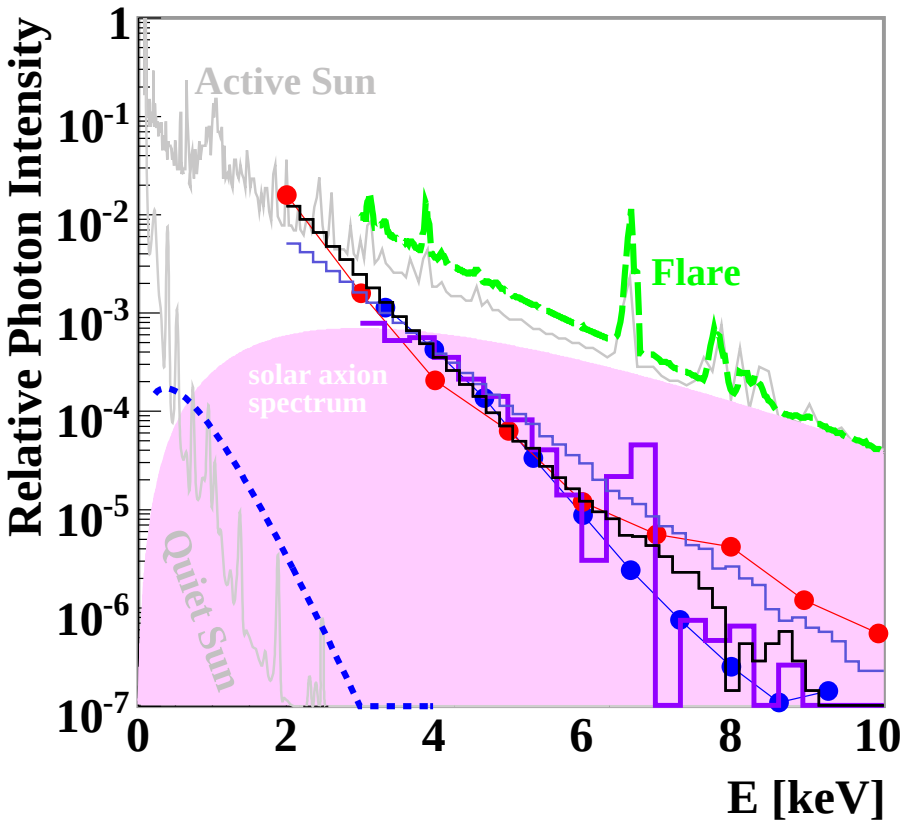

Figure 1: Reproduced spectra from directly measured solar X-rays from: a) the main phase of a large flare with T∼20 MK [7] (green dashed), b) a flare with RESIK and RHESSI (red dots), c) preflaring periods after having subtracted the main X-ray flare component from the original spectra [7] (purple histogram), d) non-flaring active regions with T≈6 MK, i.e. sunspots (blue dots), e) non-flaring quiet Sun, with T≈ 2.7 MK, at solar minimum with SPhinX (blue dashed line) [8]; this is also supported by the recent findings that in the Quiet Sun regions stronger magnetic fields occur in deeper layers than in the ARs [2], implying more down-comptonization and giving rise to a larger slope. The initial broad solar axion spectrum is also shown shadowed (pink dashed line). Two GEANT4 simulated spectra following multiple Compton scattering from a depth of ∼350 km and ∼400 km are also shown for comparison (thin histograms), where the estimated plasma frequency, i.e., also the axion rest mass, is ∼17 meV/c^2. The uncertainty is a factor of ∼2, since the density changes by factor of ∼4 between the ∼300 km and ∼1000 km depth. Note the strong deviations of the indirectly derived spectra (grey lines) in the past [9] of the non-flaring quiet Sun at solar minimum and that of the active Sun at solar maximum below ∼ 1 keV (SPhinX measurements). The spectra are not to scale.

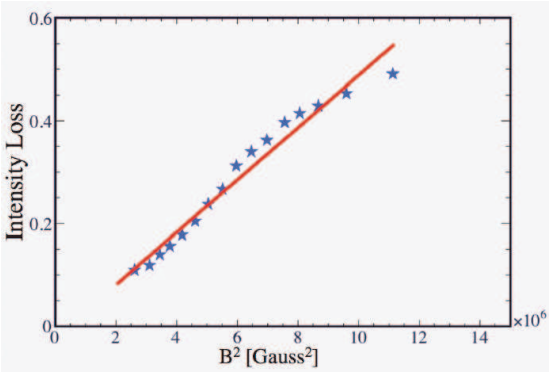

Figure 2: The observed infrared (IR) intensity in the darkest position of sunspot cores (i.e., umbrae) is plotted vs. $\mathbf{B}^2$, as derived from a total number of 1392 sunspots [10, 11]. The measurements were performed from 1992 to 2009. The red line shows the $\mathbf{B}^2$-dependence as a guide. It is not a fit to the IR intensity loss data. An example: intensity loss of 0.4 means that the number of IR photons is reduced by 40% (with zero being the reference quiet Sun value) [11]. (Courtesy W. Livingston, NOAO/NSO, Tucson, Arizona.)

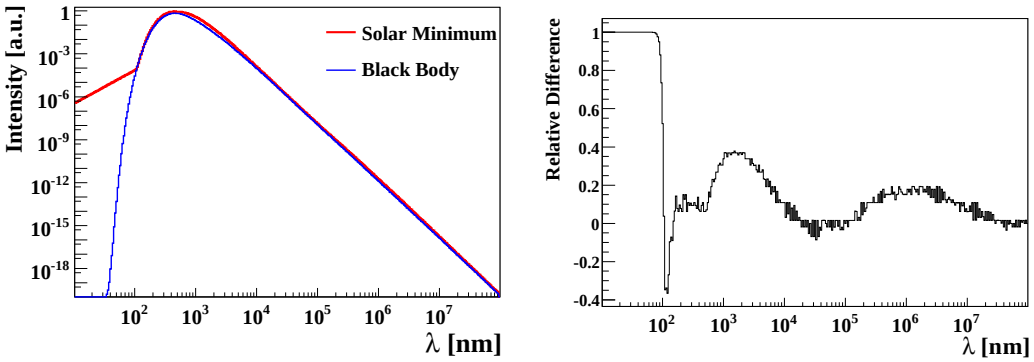

Figure 3: ((**Left**) The approximated solar radiation spectrum during solar minimum (red line) and the black body spectrum for T=5800 K (blue line). (**Right**) The normalized relative difference between the two spectra can be used to unravel non-thermal contributions, whatever their origin. The residuals below ∼100 nm correspond to the hot corona excess. Residuals at $\sim 10^6$ nm might be a contamination of the CMB radiation, though the peak appears too broad towards shorter wavelengths to be eventually explained exclusively by CMB (either directly or reflected from the Sun). The origin of the excess around ∼2000–3000 nm is real, but it is not yet identified. (Courtesy Marlene DiMarco/ UCAR Office of Education and Outreach/2009.)

Producing Chameleons in the Sun

Philippe Brax,

Institut de Physique Théorique, CEA, IPhT, CNRS, URA 2306,
F-91191Gif/Yvette Cedex, France.

DOI: http://dx.doi.org/10.3204/DESY-PROC-2010-03/brax_philippe

We present a mechanism whereby chameleons can be produced in the strong magnetic field of the solar tachocline. A small fraction of the resulting chameleons can be back-converted into photons which would naturally have a spectrum in the soft X-ray region. The remaining chameleons are energetic enough to penetrate into helioscopes and could trigger a photonic X-ray signal.

1 Introduction

Chameleon fields [1] can be responsible for the late time acceleration of the expansion of the universe while preserving gravity locally. Chameleons can disturb the growth of structures on large scales and even lead to testable predictions for Casimir experiments and optical cavity experiments. In the latter case, the physics of chameleons is extremely similar to axion physics. It is well known that axions may modify the burning rate of stars. In a similar fashion, chameleons may lead to an enhanced dissipation of energy in the sun. On the other hand, chameleons have a density dependent mass which hampers their creation by the Primakoff effect in very dense environments, hence cutting the spectrum of created chameleons below their mass threshold. In most circumstances, this prevents their appearance apart from a depleted number of very energetic ones. Fortunately, chameleons feel the presence of the surrounding plasma and this interaction may be resonant when the mass of the chameleons (almost) coincides with the plasma frequency. In this case, the plasma becomes almost transparent to chameleons which can therefore be produced in an enhanced manner. Now it happens that the chameleon mass varies inside the sun as the density changes from the inner sun to the solar surface. When the mass of the chameleon varies (almost) like the matter density, the whole solar interior becomes transparent to chameleons. If produced deep inside the sun in the tachocline, a region of intense magnetic field, these chameleons escape the sun producing a soft X-ray chameleon flux which can eventually reach the earth. Of course, along their path from the inner sun to the outer sun, chameleons can be back-converted into photons. This process is a second order effect which is therefore suppressed compared to the chameleon creation inside the sun. If the back-converted photons are produced deep inside the sun, the smallness of the photonic mean free path implies that these photons contribute as a small perturbation to the radiative transfer with negligible effects. On the other hand, back-converted photons at the surface of the sun have a long enough mean free path to escape the sun. Moreover their spectrum is a mirror image of the photon spectrum in the tachocline (modulo a transfer function corresponding to the creation and then disappearance of the intermediate chameleons). This spectrum is predominantly in

the soft X-ray band. It happens that we can impose that the back-converted photons saturate the Sphinx bound on the luminosity of the quiet sun. Of course, this is a strong prior and the back-converted photons could be contributing to a much smaller fraction of the soft X-ray flux. Once chameleons have been emitted by the sun, they reach the earth and again some of the chameleons do not penetrate inside the atmosphere which acts as a first barrier to the incoming chameleon flux. Due to the low density of the earth atmosphere, most chameleons go through and could even penetrate inside helioscopes when their energy is greater than the chameleon mass in dense materials such a lead. In this case, the remaining chameleons could be converted into X-ray photons. These photons would then be detectable by helioscope detectors provided their number exceeds the detector sensitivity. In the following, we will give a numerical example where all these conditions are met. The study of the parameter space, for which the back-converted photons in the outer sun do not exceed the Sphinx bound and the number of soft X-ray photons produced in the helioscope pipes is large enough to overcome the detector noise, is in progress.

2 Chameleon Production

Chameleons are particles which couple to matter in such a way that their effective potential becomes matter density dependent

$$V_{\rm eff}(\phi) = V(\phi) + e^{\beta\phi/M_{Pl}}\rho \tag{1}$$

This potential has a density dependent minimum $\phi_{\rm min}$. This is the vacuum of the theory in a given environment. The density-dependent minimum is such that the mass of the scalar field becomes also density dependent. We will mainly focus on inverse power law models defined by

$$V(\phi) = \Lambda^4 + \frac{\Lambda^{4+n}}{\phi^n} + \dots \tag{2}$$

where we have neglected higher inverse powers of the chameleon field. We will choose $\Lambda = 2.4\ 10^{-12}$GeV to lead to the acceleration of the universe on large scales. The potential has a minimum located at $\phi_{\rm min} = (\frac{nM_{\rm Pl}\Lambda^{4+n}}{\beta\rho})^{1/(n+1)}$ where ρ is the total non-relativistic matter density. The chameleon rest mass at the minimum is $m^2 \approx \beta\frac{e^{\beta\phi_{\rm min}/M_{\rm Pl}}\rho}{M_{\rm Pl}}\frac{n+1}{\phi_{\rm min}}$. Chameleons also couple to photons in a way akin to the axion coupling

$$S_{EM} = -\int d^4x\sqrt{-g}\frac{e^{\phi/M_\gamma}}{4}F^2 \tag{3}$$

implying that the effective matter density in the effective potential is

$$\rho = \rho_m + \frac{m_{\rm Pl}}{\beta M_\gamma}\frac{B^2}{2} \tag{4}$$

The chameleon mixes with photons when a constant magnetic field is present. We find that the chameleons couple to the polarisation orthogonal to the constant magnetic field. The chameleon mixes with the orthogonal polarisation of the photon, resulting in an effective momentum

$$k^2(\omega) = \omega^2 - (m^2 - \frac{B^2}{M_\gamma^2} - \omega_{\rm pl}^2)(\frac{\cos\theta + 1}{2\cos 2\theta}) \tag{5}$$

where ω is the initial frequency of the incoming photons. This depends on the mixing angle which is given by

$$\tan 2\theta = \frac{2\omega B}{M_\gamma(m^2 - \frac{B^2}{M_\gamma^2} - \omega_{\rm pl}^2)} \tag{6}$$

and the plasma frequency is $\omega_{\rm pl}^2 = \frac{4\pi\alpha_{EM}n_e}{m_e}$. Electro-neutrality implies that in the sun $n_e = \frac{\rho_m}{m_p}$, where m_p is the proton mass. The chameleons propagate when $k^2 > 0$ and are forbidden to propagate when $k^2 < 0$. The thermal photons inside the fully ionised inner sun evolve as free particles for a length equal to their mean free path λ. The chameleon production rate is obtained from the transition probability

$$P_{\rm chameleon}(\omega) \approx \frac{1}{2}\theta^2. \tag{7}$$

This is the conversion probability of one photon into a chameleon over the length of one mean free path. During one second, the photons experience N interactions inside the rather static solar magnetic field, where $N = \frac{1}{\lambda}$ in reduced units with $c = \hbar = 1$. The probability of creating one chameleon per second out of one thermal photon is then $P_{\rm total}(\omega) = NP_{\rm chameleon}(\omega)$ as $P_{\rm chameleon} \ll 1$. For the thermal photons, we assume a Planckian distribution $p_\gamma(\omega) = \frac{\omega^2}{\pi^2\bar{n}}\frac{1}{e^{\frac{\omega}{T}}-1}$ where the average number of photons at temperature T is $\bar{n} = \frac{2\zeta(3)}{\pi^2}T^3$, implying that the chameleon spectrum is

$$\Phi_{\rm cham}(\omega) = p_\gamma(\omega)P_{\rm total}(\omega)n_\gamma \tag{8}$$

where n_γ is the photon flux corresponding to the number of photons going through a sphere of radius R from the centre of the sun. We take it to be a constant in the magnetic region near the tachocline we are considering.

The photons which can be suddenly created in the photosphere from the chameleon flux are such that they will not thermalise and escape relatively quickly after their creation with a spectrum reflecting directly the nature of the chameleon production spectrum inside the sun. The flux of back-converted photons in the photosphere from chameleons created in the tachocline region ($R \sim 0.7R_{\rm sun}$) is then

$$\Phi_{\rm photon}(\omega) \approx \frac{1}{2}\theta_{\rm outer}^2\Phi_{\rm cham}(\omega) \tag{9}$$

where $\theta_{\rm outer}$ is the mixing angle in the photosphere.

3 Phenomenology

A first constraint on the chameleon production is the Sphinx direct observation of the quiet sun X-ray brightness which specifies that the photon energy flux in the range of energies larger than ~ 1 keV is about $10^{-3}{\rm erg/s\cdot cm^2}$. A second constraint is the non-observation of photons by the CAST experiment which also restricts the parameter space (β, M_γ, n) of the model.

For instance, these constraints can be satisfied when $M_\gamma = 10^{5.8}$ GeV. A strong enough resonance in the outer sun can be obtained with $\beta = 10^{7.09218}$ and $n = 8.7$. For these values, we have presented the spectrum of the chameleon flux out of the sun in Fig. 1. These chameleons go through the earth atmosphere. Similarly they would enter the CAST magnet. There, in the pipes, the chameleons can be back-converted into photons via the inverse Primakoff effect. Now,

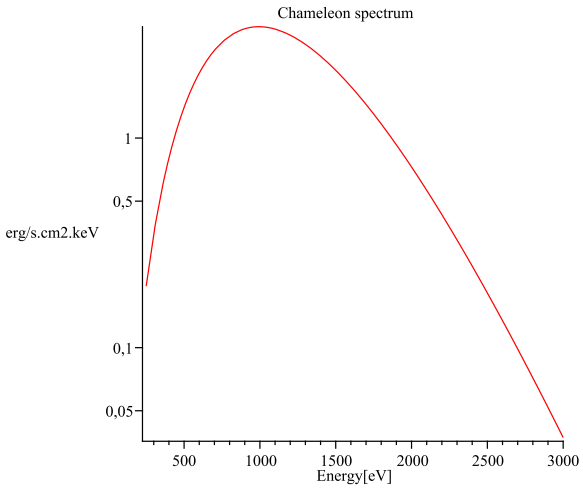

Figure 1: The energy spectrum of the emitted chameleons. Energies are expressed in eV and the spectrum in erg/s·cm^2·keV. The coupling is chosen to be $M_\gamma = 10^{5.8}$ GeV and the magnetic field in the lower convection region is B=30 T which is the solar chameleon source. The integrated flux at the solar surface is 4 erg $\cdot$ s^{-1} $\cdot$ cm^{-2}.

the spectrum of the regenerated X-ray photons can be evaluated using $B_{\rm cast} = 9$ T, taking the length of the magnetic region to be $L_{\rm cast} = 9.26$ m, the diameter of the pipes $d = 43$ mm and the pressure in the vacuum pipes less than 10^{-6} mbar ($T \approx 1.8$ K). We can calculate the rate of excess photon production and we find $N_\gamma \approx 0.04$ photon per hour. The CAST experiment has taken data with vacuum in the magnetic pipes for $\sim$ 200 hours and the noise level is 0.13 photon per hour in the 1-7 keV band. The number of converted photons represents a 1.5 σ effect and therefore it could not have been seen. A better performing CAST experiment has the potential to observe such an X-ray excess. The situation would improve drastically with a new CAST configuration, where we assume the following specifications: $B = 6$ T, $L = 15$ m and aperture surface 0.15 m^2. In this case, the number of photons per hour becomes $N_\gamma = 12$ in the keV region. With a noise level of 4 photons per hour, a 5 σ detection would only take 3 hours of solar tracking.

In conclusion, the fact that chameleon models for some values of the parameters can be within the CAST ball-park is encouraging. A thorough study of the parameter space would certainly be valuable and help putting new bounds on chameleon couplings.

References

[1] See P. Brax and K. Zioutas, Phys. Rev. D **82** (2010) 043007 [arXiv:1004.1846 [astro-ph.SR]] and references therein.

Evidence for an axion-like particle from blazar spectra?

Marco Roncadelli[1], *Alessandro De Angelis*[2], *Giorgio Galanti*[3], *Massimo Persic*[4]

[1]INFN, Sezione di Pavia, via A. Bassi 6, I – 27100 Pavia, Italy
[2]Dipartimento di Fisica, Università di Udine, Via delle Scienze 208, I – 33100 Udine, and INAF and INFN, Sezioni di Trieste, Italy
[3]Dipartimento di Fisica, Università di Pavia, and INFN, Sezione di Pavia, Via A. Bassi 6, I – 27100 Pavia, Italy
[4]INAF, via G.B.Tiepolo 11, I-34143 Trieste, Italy, and INFN, Sezioni di Trieste, Italy

DOI: http://dx.doi.org/10.3204/DESY-PROC-2008-02/roncadelli_marco

Observations with the Imaging Atmospheric Cherenkov Telescopes H.E.S.S., MAGIC, CANGAROO III and VERITAS have shown that the Universe is more transparent than expected to gamma rays above 100 GeV. As a natural explanation, the DARMA scenario has previously been proposed, wherein photons can oscillate into a new very light axion-like particle and vice-versa in the presence of cosmic magnetic fields. Here we demonstrate that the most recent observations further support the DARMA scenario.

1 Introduction

A generic prediction of many extensions of the Standard Model of particle physics – including four-dimensional theories, compactified Kaluza-Klein models and superstring theories – is the existence of very light axion-like particles (ALPs). They are defined by the low-energy effective lagrangian

$$\mathcal{L}_{\rm ALP} \;=\; \frac{1}{2}\,\partial^\mu a\,\partial_\mu a - \frac{1}{2}\,m^2\,a^2 - \frac{1}{4M}\,F^{\mu\nu}\,\tilde{F}_{\mu\nu}\,a\;, \qquad (1)$$

where $F^{\mu\nu}$ is the electromagnetic field strength, $\tilde{F}_{\mu\nu}$ is its dual, a denotes the ALP field whereas m stands for the ALP mass. Accordingly, it is assumed $M \gg G_F^{-1/2}$ and $m \ll G_F^{-1/2}$ ($G_F^{-1/2} \simeq 250\,\text{GeV}$ is the Fermi constant). The standard axion is the most well known example of ALP, but as far as *generic* ALPs are concerned the parameters M and m are to be regarded as *independent*.

While extremely elusive in laboratory experiments, ALPs can give rise to dramatic astrophysical effects owing to the characteristic $\gamma\gamma a$ vertex in $\mathcal{L}_{\rm ALP}$. Correspondingly, ALPs can be emitted by astronomical objects of various kinds, and the present situation can be summarized as follows. The negative result of the CAST experiment designed to detect ALPs emitted by the Sun yields the bound $M > 0.86 \cdot 10^{10}\,\text{GeV}$ for $m < 0.02\,\text{eV}$. Moreover, theoretical considerations concerning star cooling via ALP emission provide the generic bound $M > 10^{10}\,\text{GeV}$, which for $m < 10^{-10}\,\text{eV}$ gets replaced by the stronger one $M > 10^{11}\,\text{GeV}$ even if with a large uncertainty. The same γ-γ-a vertex produces an off-diagonal element in the mass matrix for the

photon-ALP system in the presence of an external magnetic field **B**. Therefore, the interaction eigenstates differ from the propagation eigenstates and photon-ALP oscillations show up.

A few years ago, it was realized that photon-ALP oscillations in cosmic magnetic fields – the so-called DARMA scenario [1] – can provide a natural explanation for the anomaluosly large transparency of the Universe above 100 GeV observed since 2006 by the Imaging Atmospheric Cherenkov Telescopes (IACTs) H.E.S.S., MAGIC, CANGAROO III, VERITAS, and further confirmed by subsequent observations.

Our aim is to show that the most recent observations of blazars at redshift $z > 0.3$ beautifully fit within the DARMA scenario, thereby providing further support in favour of the existence of an ALP with M slightly larger than 10^{11} GeV and m slightly smaller than 10^{-10} eV. Remarkably enough, this claim can be tested with some detectors originally devised to search for non-baryonic dark matter [2].

2 Extragalactic background light

Photons from distant sources scatter off background photons permeating the Universe, thereby disappearing into electron-positron pairs and so giving rise to a cosmic opacity. The corresponding cross section $\sigma(\gamma\gamma \to e^+e^-)$ peaks where the very high energy (VHE) photon energy E and the background photon energy ϵ are related by $\epsilon \simeq (500\,\mathrm{GeV}/E)\,\mathrm{eV}$. As far as IACT observations are concerned, the cosmic opacity is dominated by the interaction with diffuse background photons with $0.005\,\mathrm{eV} < \epsilon < 5\,\mathrm{eV}$, usually called extragalactic background light (EBL). Owing to the absorption process in question, photon propagation is controlled by the optical depth $\tau(E, z)$, with z denoting the source redshift. Within the standard Big Bang model we have $E(z) = E_0(1+z)$ and $\epsilon(z) = \epsilon_0(1+z)$, with E_0 and ϵ_0 referring to the present ($z = 0$). Therefore, the observed photon spectrum $\Phi_{\rm obs}(E_0, z)$ of a source at z is related to the emitted one $\Phi_{\rm em}(E(z))$ by

$$\Phi_{\rm obs}(E_0, z) = e^{-\tau_\gamma(E_0,z)}\ \Phi_{\rm em}\left(E_0(1+z)\right)\ . \tag{2}$$

Note that $\tau_\gamma(E_0, z)$ increases with z, since a greater source distance entails a larger probability for a beam photon to be absorbed.

Given the fact that all blazars observed so far by IACTs lie in the energy band $0.2\,\mathrm{TeV} < E_0 < 2\,\mathrm{TeV}$, we restrict our attention to this energy range from now on, in which blazar data are fitted as $\Phi_{\rm obs} \propto E^{-\Gamma_{\rm obs}}$. The results for all VHE blazars observed to date by IACTs are exhibited in Fig. 1, where the corresponding observed spectral indices $\Gamma_{\rm obs}$ are plotted *vs.* the source redshift z for all sources reported in Table 1 of ref. [3] plus three more recently detected ones, namely PKS 1424+240 at $z < 0.66$, S5 0716+714 at $z = 0.31$ and 3C66A at $z = 0.444$.

It is generally assumed that $\Phi_{\rm em} \propto E^{-\Gamma_{\rm em}}$ for $E > 100\,\mathrm{GeV}$, and so Eq. (2) yields

$$\Gamma^{\rm CP}_{\rm obs}(z) \propto \Gamma_{\rm em} + \tau_\gamma(E_0, z)\ , \tag{3}$$

up to a negligible additional term with a logarithmic z-dependence and z-independent factors, where CP means that this result follows from conventional physics alone.

A key ingredient in the evaluation of $\tau_\gamma(E_0, z)$ is the EBL spectral number density, which depends on the adopted model for the EBL. We choose the one of Franceschini, Rodighiero and Vaccari (FRV) [4]. A convenient analytic fit is to the corresponding EBL spectral number density at $z = 0$ is

$$n_\gamma(\epsilon_0, 0) \simeq 10^{-3}\,\alpha\left(\frac{\epsilon_0}{\mathrm{eV}}\right)^{-2.55}\ \mathrm{cm}^{-3}\,\mathrm{eV}^{-1}\ , \tag{4}$$

with $0.5 < \alpha < 3$. Besides redshifting all energies in proportion of $1 + z$, the cosmic expansion dilutes the EBL by a factor $(1+z)^3$. In addition, the EBL spectral energy distribution changes because of the intrinsic evolution of the galactic population over cosmic times. A quantitative analysis shows that the EBL photon number density acquires an extra factor $(1 + z)^{-1.2}$ as long as $z \leq 1$. Altogether, we get $n_\gamma(\epsilon(z), z) \simeq (1 + z)^{0.8}\ n_\gamma(\epsilon_0, 0)$. We expect the EBL photon absorption to be negligible for nearby blazars ($z < 0.03$), and so we suppose that observations of these sources do yield $\Phi_{\rm em}(E)$. We find $\Gamma_{\rm em} \simeq 2.4$ on average. We further assume that all VHE observed blazars have an emission spectrum with basically the *same* slope[1]. Then resulting values of $\Gamma^{\rm CP}_{\rm obs}(z)$ for $0.5 < \alpha < 3$ lie between the two dotted lines in Fig. 1.

As it is clear from Fig. 1, the actually observed spectral index $\Gamma_{\rm obs}(z)$ increases more slowly than $\Gamma^{\rm CP}_{\rm obs}(z)$ for redshifts $z > 0.2$. Moreover, the observed values cannot be explained for $z > 0.3$ by the EBL model of FRW even for α as low as 0.5. Being $\tau_\gamma(E_0, z)$ a monotonically increasing function of z, we interpret the conflict between $\Gamma_{\rm obs}(z)$ and $\Gamma^{\rm CP}_{\rm obs}(z)$ shown in Fig. 1 as calling for a departure from the conventional view.

A suggested way out of this difficulty relies upon the modification of the standard Synchro-Self-Compton (SSC) emission mechanism. One option invokes strong relativistic shocks [5]. Another rests upon photon absorption inside the blazar [6]. While successful at substantially hardening the emission spectrum, these attempts fail to explain why *only* for the most distant blazars does such a drastic departure from the conventional view show up.

3 DARMA scenario and its predictions

The spirit of the DARMA scenario [1] is quite different. Implicit in previous considerations is the hypothesis that photons propagate in the standard way throughout cosmological distances. We suppose instead that photons-ALP oscillations occur in the presence of cosmic magnetic fields, whose existence at the nanogauss level has been suggested by AUGER observations [7]. Once ALPs are produced close enough to the source, they travel *unimpeded* throughout the Universe and can convert back to photons before reaching the Earth. Since ALPs do *not* undergo EBL absorption, the effective optical depth gets *reduced*, thereby leading to a *reduction* of the predicted observed spectral index $\Gamma^{\rm DARMA}_{\rm obs}(z)$ in this context.

Owing to the notorious lack of information about the morphology of cosmic magnetic fields, one usually supposes that they have a domain-like structure [8]. That is, $\mathbf{B}$ ought to be constant over a domain of size $L_{\rm dom}$ equal to its coherence length, with $\mathbf{B}$ randomly changing its direction from one domain to another but keeping approximately the same strength. As explained elsewhere [7], it looks plausible to assume the coherence length in the range $1-10\,$Mpc. Correspondingly, the inferred strength lies in the range $0.3 - 1.0\,$nG [7].

Following the same computational procedure as in ref. [1], we evaluate the probability $P_{\gamma\to\gamma}(E_0, z)$ that a photon remains a photon after propagation from the source to us when allowance is made for photon-ALP oscillations as well as for photon absorption by the EBL. As a consequence, Eq. (2) becomes

$$\Phi_{\rm obs}(E_0, z) = P_{\gamma\to\gamma}(E_0, z)\ \Phi_{\rm em}\left(E_0(1 + z)\right) \tag{5}$$

so that Eq. (3) gets replaced by

$$\Gamma^{\rm DARMA}_{\rm obs}(z) \propto \Gamma_{\rm em} - \ln P_{\gamma\to\gamma}(E_0, z)\ , \tag{6}$$

[1]Note that no assumption is being made about the intensity of the VHE emission, so that we are absolutely *not* supposing VHE blazars to be standard candles.

again up to a negligible additional term with a logarithmic z-dependence and z-independent factors. Assuming $m < 10^{-10}\,\mathrm{eV}$ and $M \simeq 4 \cdot 10^{11}\,\mathrm{GeV}$ as in ref. [1] and adopting the same EBL model as before as well as $\Gamma_{\mathrm{em}} \simeq 2.4$, the resulting values of $\Gamma_{\mathrm{obs}}^{\mathrm{DARMA}}(z)$ for $0.5 < \alpha < 3$ lie between the two solid lines in Fig. 1.

Clearly, there is no problem to slightly lower the latter regions so as to achieve a perfect agreement with observations. We have also checked that the same result remains practically unaffected within the range $10^{11}\,\mathrm{GeV} < M < 10^{13}\,\mathrm{GeV}$.

More details and additional references can be found in ref. [3].

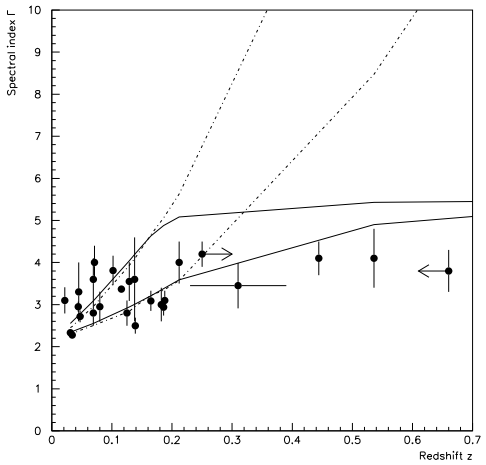

Figure 1: The observed values of the spectral index for all blazars detected so far in the VHE band are represented by big dots and corresponding error bars. Superimposed on them is the predicted behaviour of the observed spectral index within two different scenarios. In the first one (area between the two dotted lines) $\Gamma_{\mathrm{obs}}^{\mathrm{CP}}$ is computed in terms of conventional physics in the FRV model of the EBL. In the DARMA scenario (area between the two solid lines) $\Gamma_{\mathrm{obs}}^{\mathrm{DARMA}}$ is evaluated within the proposed photon-ALP oscillation mechanism as based on the same FRV model of the EBL.

References

[1] A. De Angelis, M. Roncadelli and O. Mansutti, Phys. Rev. **D76** 121301 (2007).

[2] F. T. Avignone III, R. J. Creswick and S. Nussinov, Phys. Lett. B 681 122 (2009).

[3] A. De Angelis, O. Mansutti, M. Persic and M. Roncadelli, Mon. Not. R. Astron. Soc. **394** L21 (2009).

[4] A. Franceschini, G. Rodighiero and M. Vaccari, Astron. Astrophys. **487** 837 (2008).

[5] F. W. Stecker, M. G. Baring and E. J. Summerlin, Astrophys. J. **667** L29 (2007). F. W. Stecker and S. T. Scully, Astron. Astrophys **478** L1 (2008).

[6] F. Aharonian, D. Khangulyan and L. Costamante, Mon. Not. R. Astron. Soc. **387** 1206 (2008).

[7] J. Abraham *et al.* [Pierre Auger Collaboration], Science **318** 939 (2007). A. De Angelis, M. Persic and M. Roncadelli, Mod. Phys. Lett. **A23** 315 (2008).

[8] P. P. Kronberg, Rept. Prog. Phys. **57** 325 (1994). D. Grasso and H. Rubinstein, Phys. Rep. **348** 163 (2001).

Hidden Photons from the Sun

Davide Cadamuro and Javier Redondo

Max Planck-Institute für Physik, Föhringer Ring 6, D-80805 München, Germany

DOI: http://dx.doi.org/10.3204/DESY-PROC-2010-03/redondo_javier

A brief account of the phenomenon of photon oscillations into sub-eV mass hidden photons is given and used to estimate the flux and properties of these hypothetical particles from the Sun. A new generation of dedicated helioscopes, the Solar Hidden Photon Search (SHIPS) in the Hamburg Observatory amongst them, will cover a vast region of parameter space.

A Hidden Photon (HP) is the gauge boson of a local $U(1)$ hidden symmetry. This kind of symmetries arise very frequently in many popular extensions of the Standard Model, especially in String Theory [1]. Known particles have no direct interaction with HPs (hence the name hidden) but couplings can still be generated through radiative corrections or gravity. In particular, HPs could be really not so hidden, because very massive particles with both electric and hidden charge can generate kinetic mixing with the standard photon [2],

$$\mathcal{L}_{mix} = -\frac{1}{4}\chi A_{\mu\nu}B^{\mu\nu} \ , \tag{1}$$

where $A_{\mu\nu}$ and $B_{\mu\nu}$ are the photon and HP field strengths. In this case, the natural value of the dimensionless kinetic mixing coupling χ is that of a quantum correction. Since the hidden gauge coupling can be very small, see e.g. [3], and there can be cancellations between different mediator contributions, there is no clear minimum for χ. Values in the $10^{-16} \sim 10^{-3}$ range have been predicted in the literature [3, 4]. Moreover, HPs can become massive via Higgs and/or Stueckelberg mechanisms [5].

This very weak interaction makes HPs perfect candidates for the dark sector that current cosmology and astrophysics are revealing. They have been proposed as Dark Matter (DM) candidates [6] and as mediating Dark Forces between DM particles [7]. On the other hand, if their mass is in the meV range, their cosmological relic abundance could also provide the extra radiation favoured by the recent WMAP-7 results [8].

The presence of the kinetic mixing term signals that the photon (A_μ) and the HP (B_μ) fields are not orthogonal. Since the photon is by definition an interaction eigenstate (couples to the electric charge) and the HP is in general massive, the kinetic mixing *misaligns* the interaction (A, S) and propagation eigenstates $(\tilde{A}, B)$. The photon can be written in terms of propagation eigenstates as

$$A_\mu = \tilde{A}_\mu - \sin\chi B_\mu \simeq \tilde{A}_\mu - \chi B_\mu \ . \tag{2}$$

Most importantly, the state orthogonal to it, i.e.

$$S_\mu = B_\mu + \chi\tilde{A}_\mu \ , \tag{3}$$

is completely sterile to electromagnetic interactions.

The *misalignment* between interaction and propagation eigenstates is well know to produce flavour oscillations, i.e. photons (γ) will convert into sterile states (γ') –and vice-versa– as they freely propagate with a probability [9]

$$P(\gamma \to \gamma') = 4\chi^2 \sin^2\left(\frac{m_{\gamma'}^2 L}{4\omega}\right), \tag{4}$$

where $m_{\gamma'}$ is the HP mass, L is the length of the path covered and ω is the photon energy.

The oscillation mechanism previously described is presently the best known ally to search for ∼meV mass HPs by means of the so called Light Shining through Walls (LSW) experiments [9, 10]. The experimental setup consists of a photon source and a photon detector separated by a thick shielding. Due to the very low probability of photon to HP conversion, very powerful sources, as high intensity lasers, and very sensitive photon detectors are necessary.

The most remarkable source of photons to be exploited could be our Sun itself. Most importantly, it can be an astounding source of hidden photons as well, if they are produced in $\gamma \to \gamma'$ oscillations of the photons populating its interior [9, 11, 12]. Solar Neutrino flux data constrain an exotic "invisible" solar luminosity to be less than 10% of the solar photon luminosity [13] ($L_\odot \simeq 3.84 \times 10^{26}$ W). These HPs can be searched for with helioscopes such as CAST and SUMICO, built for the search of solar axions. Solar HPs can easily travel all along to the Earth, entering an optically thick vacuum vessel in which the inverse oscillation process $\gamma' \to \gamma$ will recreate solar photons that could in principle be easily detected. A 1 m^2 Helioscope like CAST could detect the hidden photons emitted by the Sun inside a solid angle of about $(150 \times 10^9)^{-2}$ sr, which means that the Sun could be providing up to 140 W of HPs without contradicting the solar dynamics.

Photon→HP oscillations inside the Sun are strongly affected by matter effects. A complex refraction index n is normally defined to account for the refractive and absorptive properties of a medium

$$-2\omega^2(n-1) \equiv m_\gamma^2 + i\omega\Gamma\,. \tag{5}$$

The optical properties of the solar plasma depend mainly on the electron density $n_e(R)$, which in the Sun is a decreasing function of the radius R, through the plasma frequency ω_p

$$\omega_p^2(R) = m_\gamma^2(R) = \frac{4\pi\alpha}{m_e} n_e(R)\,. \tag{6}$$

Taking into account these considerations, it is possible to derive a very simple expression for the probability of a photon to convert into a HP inside the Sun and subsequently escape [12]

$$P(\gamma(\text{in}) \to \gamma'(\text{out})) = \frac{m_{\gamma'}^4(R)}{\left(m_\gamma^2(R) - m_{\gamma'}^2\right)^2 + \left(\omega\Gamma(R)\right)^2}\,. \tag{7}$$

The dependence of m_γ on n_e given by (6) makes the last equation quite interesting for our discovery purpose. The interior of the Sun has indeed a very high electron density ($n_e \simeq 10^{25}$ cm^{-3}) which corresponds to a rather large photon mass $m_\gamma \simeq 300$ eV. In this region the production of HPs of very small mass will be extremely suppressed.

Moving away from the solar centre the electron density decreases, allowing eventually the effective photon mass to be equal to HP mass at a certain R_*, i.e. $m_\gamma(R_*) = m_{\gamma'}$. Since the Sun is a weakly coupled plasma (except for absorption lines and very small frequencies one has

$\omega\Gamma \ll m_\gamma^2$), the resonant production of HPs in a thin spherical shell is very much enhanced and generally dominates over the emission from the rest of the Sun. In the sharp resonance approximation, i.e. considering the HPs production only in this tiny shell whose thickness can be approximated by $\Delta R \simeq \omega\Gamma(dm_\gamma^2/dR)^{-1}$, it is possible to linearise the Sun density profile to obtain an analytical HP flux $\Phi_{\gamma'}$,

$$\begin{aligned}\frac{d\Phi_{\gamma'}}{d\omega} &= \frac{1}{4\pi R_{earth}^2}\int_0^{R_\odot} 4\pi R^2 dR \frac{1}{\pi^2}\frac{\omega\sqrt{\omega^2-m_{\gamma'}^2}}{e^{\omega/T}-1}\frac{\chi^2 m_{\gamma'}^4}{\left(m_\gamma^2-m_{\gamma'}^2\right)^2+(\omega\Gamma)^2}\Gamma \\ &\simeq \frac{2}{\pi^2}\frac{R^2}{R_{earth}^2}\frac{\chi^2 m_{\gamma'}^4}{\omega\frac{dm_\gamma^2}{dR}}\frac{\omega\sqrt{\omega^2-m_{\gamma'}^2}}{e^{\omega/T}-1}\Bigg|_{R=R_*} . \end{aligned} \tag{8}$$

Interestingly, in this approximation the flux does not depend on the absorption coefficient.

From the Earth, HPs emitted from the resonant shell will appear most prominently in a ring of radius R_* in the Sun. This could be in principle be used to measure the HP mass through the estimate of R_* and m_γ.

In particular, for HPs in the sub-eV mass range, the resonance would happen in the outer layers of Sun and the radius R_* becomes practically equal to the solar radius $R_\odot$, where the plasma is not fully ionized. Unfortunately, the presence of bounded electrons makes things more complicated and spoils the simple picture we have described. A gas with bounded electrons can be modelled as a superposition of damped oscillators, from which the index of refraction can be written as

$$-2\omega^2(n-1) = m_\gamma^2 + i\omega\Gamma = \frac{4\pi\alpha n_e}{m_e}\sum_j \frac{f_j}{\omega^2-\omega_j^2+i\omega\gamma_j} , \tag{9}$$

where ω_j is the frequency of the j-th oscillator, f_j is the fraction of electrons that can be excited in that frequency and $\gamma_j = 2\alpha\omega\omega_j/(3m_e)$ is the free-radiator damping constant. Of course, in a plasma like our Sun, corrections to this simple picture such as thermal and pressure broadening have in principle to be included. For light of frequency ω far from the absorption lines it is possible to split the sum over resonances into a IR ($\omega_k \ll \omega$) and a UV part ($\omega_k \gg \omega$),

$$m_\gamma^2 \simeq \frac{4\pi\alpha n_e}{m_e}\left(\sum_{IR} f_j - \sum_{UV} f_j\left(\frac{\omega}{\omega_j}\right)^2\right) . \tag{10}$$

The net effect of bounded electrons is to decrease m_γ^2 with respect to the naive fully-ionized plasma case. Therefore, the resonance displaces inwards the Sun with respect to the position it should have in the fully ionized model. Moreover, this displacement is frequency dependent so that the HPs emission ring is somewhat broadened with a tendency of higher frequencies to be emitted from the ring's interior. The emission of HPs with frequencies corresponding to strong absorption lines will be widespread in the ring, first because Γ is bigger and $\Delta R \propto \Gamma$ but also because on-resonance the contribution of the oscillator to n is purely imaginary and the real part changes sign very steeply.

We are currently working on a detailed code to compute the hypothetical flux of HPs from the Sun taking into account the detailed properties of the index of refraction in the solar plasma. The resulting fluxes are crucial to interpret correctly the outcome of a number of on-going helioscope experiments looking for solar hidden photons such as possible parasitic

experiments of the CAST and SUMICO axion searches and a dedicated experiment at the Hamburg Observatory, the solar hidden photon search (SHIPS). The order of magnitude derived from (8) is however most promising. Everything points towards an improvement of more than one order of magnitude in sensitivity for χ with respect to the current CAST limit [12], exploring a vast unknown territory in parameter space, which in particular contains the region which could explain the WMAP-7 preference for an extra radiation-like component of the universe [8].

References

[1] M. Goodsell and A. Ringwald, Fortsch. Phys. **58** (2010) 716 [arXiv:1002.1840 [hep-th]].

[2] B. Holdom, Phys. Lett. B **166**, 196 (1986).

[3] M. Goodsell, J. Jaeckel, J. Redondo and A. Ringwald, JHEP **0911**, 027 (2009) [arXiv:0909.0515 [hep-ph]].

[4] K. R. Dienes, C. F. Kolda and J. March-Russell, Nucl. Phys. B **492**, 104 (1997) [arXiv:hep-ph/9610479] ; S. A. Abel, M. D. Goodsell, J. Jaeckel, V. V. Khoze and A. Ringwald, JHEP **0807**, 124 (2008) [arXiv:0803.1449 [hep-ph]] ; M. Bullimore, J. P. Conlon and L. T. Witkowski, arXiv:1009.2380 [hep-th].

[5] M. Ahlers, J. Jaeckel, J. Redondo and A. Ringwald, Phys. Rev. D **78**, 075005 (2008) [arXiv:0807.4143 [hep-ph]].

[6] J. Redondo and M. Postma, JCAP **0902**, 005 (2009) [arXiv:0811.0326 [hep-ph]] ; M. Pospelov, A. Ritz and M. B. Voloshin, Phys. Rev. D **78**, 115012 (2008) [arXiv:0807.3279 [hep-ph]].

[7] N. Arkani-Hamed, D. P. Finkbeiner, T. R. Slatyer and N. Weiner, Phys. Rev. D **79**, 015014 (2009) [arXiv:0810.0713 [hep-ph]].

[8] J. Jaeckel, J. Redondo and A. Ringwald, Phys. Rev. Lett. **101**, 131801 (2008) [arXiv:0804.4157 [astro-ph]]; E. Komatsu *et al.*, arXiv:1001.4538 [astro-ph.CO].

[9] L. B. Okun, Sov. Phys. JETP **56**, 502 (1982) [Zh. Eksp. Teor. Fiz. **83**, 892 (1982)].

[10] J. Jaeckel and A. Ringwald, Phys. Lett. B **659**, 509 (2008) ; F. Caspers, J. Jaeckel and A. Ringwald, JINST **4**, P11013 (2009) ; J. Jaeckel and J. Redondo, Europhys. Lett. **84**, 31002 (2008) ; M. Ahlers, H. Gies, J. Jaeckel, J. Redondo and A. Ringwald, Phys. Rev. D **76** (2007) 115005 and Phys. Rev. D **77** (2008) 095001 ; J. Jaeckel, J. Redondo and A. Ringwald, Europhys. Lett. **87**, 10010 (2009) ; R. Cameron *et al.*, Phys. Rev. D **47**, 3707 (1993) ; M. Fouche *et al.*, Phys. Rev. D **78**, 032013 (2008) ; A. Afanasev *et al.*, Phys. Lett. B **679**, 317 (2009) ; K. Ehret *et al.*, Phys. Lett. B **689**, 149 (2010) .

[11] V. Popov, Europhys. Lett. **15**, 7-10 (1991);

[12] J. Redondo, JCAP **0807**, 008 (2008) [arXiv:0801.1527 [hep-ph]] ; S. N. Gninenko and J. Redondo, Phys. Lett. B **664**, 180 (2008) [arXiv:0804.3736 [hep-ex]].

[13] P. Gondolo and G. Raffelt, Phys. Rev. D **79**, 107301 (2009) [arXiv:0807.2926 [astro-ph]].

Photon-axion oscillations and the transparency of the universe

Alessandro Mirizzi[1], *Daniele Montanino*[2]

[1]Institut für Theoretische Physik, Universität Hamburg, Luruper Chaussee 149, 22761 Hamburg, Germany
[2]Dipartimento di Fisica, Università del Salento, Italy & Istituto Nazionale di Fisica Nucleare sez. di Lecce, Italy

DOI: http://dx.doi.org/10.3204/DESY-PROC-2010-03/montanino_daniele

Universe should be opaque to photons with energy $\geq$ TeV due scattering on the extragalactic background light during their propagation. However, a surprisingly high degree of transparency of the universe has been observed. In order to explain this fact, the conversion between photons and hypothetical axion-like particles in the turbulent extragalactic magnetic field has been invoked. We have derived new equations to calculate the mean survival probability of the photons. We have also found that the photon transfer functions on different lines of sight could have relevant deviations with respect to the mean value, producing both an enhancement or a suppression in the observable photon flux.

1 Introduction

Axion-like particles (ALP's) with a two-photon vertex are predicted in many extensions of the Standard Model. Pseudoscalar ALP's couple with photons through the effective coupling $g_{a\gamma}\tilde{\mathbf{F}}\mathbf{F}a$, where a is the ALP field with mass m_a, $\mathbf{F}$ and $\tilde{\mathbf{F}}$ are the electromagnetic field-strength tensor and its dual, and $g_{a\gamma}$ the ALP-photon coupling. As a consequence of this coupling, ALP's and photons do oscillate into each other in an external magnetic field.

ALP's could play an intriguing role in astrophysics. Indeed, photons emitted by distant sources and propagating through cosmic magnetic fields can oscillate into ALP's. In particular, in the last recent years photon-ALP conversions have been proposed as a mechanism to avoid the opacity of the extragalactic sky to high-energy radiation due to pair production on the Extragalactic Background Light (EBL) [1, 2, 3]. At this regard, recent observations of cosmologically distant gamma-ray sources by ground-based gamma-ray telescopes have revealed a surprising degree of transparency of the universe to very high-energy (VHE) photons ($E > 100$ GeV). Oscillations between very high-energy photons and ALP's could represent an intriguing possibility to explain this puzzle. In fact, if VHE photons are converted into ALP's and then regenerated, they should not suffer absorption effects while they propagate as ALP's. We have worked out simple equations that describe the mean and the variance of the photon transfer function in the random structure of the intergalactic magnetic field without a montecarlo simulation [4].

2 VHE $\gamma - a$ mixing

The evolution equation for photon moving in the x_3 direction can be written as

$$\frac{\partial}{\partial x_3}\begin{pmatrix} A_1 \\ A_2 \\ a \end{pmatrix} = -i\mathcal{H}\begin{pmatrix} A_1 \\ A_2 \\ a \end{pmatrix},$$

where, in the presence of absorption and in the high energy limit ($E \geq 100$ GeV) the (no longer hermitian) hamiltonian $\mathcal{H}$ can be written as

$$\mathcal{H} = \begin{bmatrix} -i\frac{\Gamma_\gamma(E)}{2} & 0 & \frac{g_{a\gamma}B_T}{2}c_\phi \\ 0 & -i\frac{\Gamma_\gamma(E)}{2} & \frac{g_{a\gamma}B_T}{2}s_\phi \\ \frac{g_{a\gamma}B_T}{2}c_\phi & \frac{g_{a\gamma}B_T}{2}s_\phi & 0 \end{bmatrix}.$$

Here $\mathbf{B}_T = \mathbf{B} - B_3\mathbf{e}_3$ is the transverse component of the external magnetic field, $c_\phi \equiv \cos\phi = \mathbf{B}_T \cdot \mathbf{e}_1/B_T$, and Γ_γ is the absorption rate for the pair production process $\gamma^{\rm VHE}\gamma^{\rm bkg} \to e^+e^-$, where $\gamma^{\rm bkg}$ is a background (EBL) photon. We stick in the hypothesis that $m_a < 10^{-10}$ eV so that the axion mass term in the hamiltonian can be neglected.

3 Mean photon transfer function

Very high-energy gamma-rays propagate in the extragalactic magnetic fields during their route to the Earth which presumably have a turbulent structure. Let us now consider the propagation of photons in many domains of equal size l ($\simeq 1$ Mpc in our case) in which the magnetic field has (constant) random values and directions. Along a given line of sight, the angles ϕ are randomly distributed in $[0, 2\pi)$. During their path with a total length L, photons cross $k = 1, \ldots n$ domains ($n = L/l$) representing a given random realization of B_k and ϕ_k. Since we cannot know this particular configuration, we perform an ensemble average over all the possible realizations on the $1, \ldots n$ domains. Since we have to perform averages on the random configurations of the intergalactic magnetic field, it is convenient to stick in the formalism of the density matrix. Defining this ensemble average as $\bar{\rho}_n = \langle\rho_n\rangle_{1\ldots n}$, we have

$$\bar{\rho}_n = \langle e^{-i\mathcal{H}_n l} \cdot \bar{\rho}_{n-1} \cdot e^{i\mathcal{H}_n^\dagger l}\rangle_n .$$

Expanding $\mathcal{H}$ at second order and performing the ensemble average, we finally arrive at a system of two coupled differential equations ($dy = P_{a\gamma}dx_3/l$) [4]

$$\frac{d}{dy}\begin{pmatrix} T_\gamma \\ T_a \end{pmatrix} = \begin{bmatrix} -\alpha - \frac{1}{2} & 1 \\ \frac{1}{2} & -1 \end{bmatrix}\begin{pmatrix} T_\gamma \\ T_a \end{pmatrix}, \tag{1}$$

where we have used the approximation $\bar{\rho}_n - \bar{\rho}_{n-1} \simeq l\partial_{x_3}\bar{\rho}(x_3)$. Here $T_\gamma \equiv I_\gamma(y)/I_\gamma(0) = \bar{\rho}_{11} + \bar{\rho}_{22}$ (since the two polarization states are indistinguishable) and $T_a = \bar{\rho}_{aa}$ are the mean transfer functions for the photon and for the ALP respectively; $P_{a\gamma} = g_{a\gamma}^2|\mathbf{B}|^2l^2/6$ is the average photon-ALP conversion probability in each domain (in absence of absorption) and finally $\alpha = \Gamma_\gamma l/P_{a\gamma}$ is the ratio between the absorption probability and the conversion probability. In realistic astrophysical situations both $P_{a\gamma}$ and α are functions of the distance, due to the redshift dependence of the extragalactic magnetic field and of the EBL.

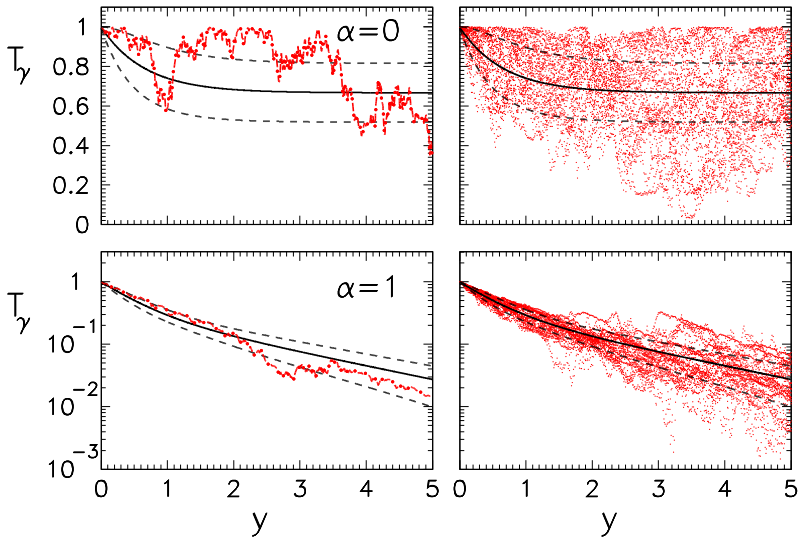

Figure 1: Photon transfer function $T_\gamma(y)$ for $\alpha = 0$ (the upper panels) and $\alpha = 1$ (lower panels) for a given random realization of the magnetic field (left) and for 20 realizations (right).

In particular, in the case of strong absorption ($\alpha \gg 1$) from Equation (1) we obtain $T_\gamma \propto (\Gamma_\gamma)^{-2}$. Using the approximate power–law spectrum for the EBL we observe that the transfer function would drop as a power of the energy (rather than exponentially as expected without ALP mixing). Moreover, also the attenuation of the transfer function with the distance is less than in the case of absence of conversions. In fact, in this case we have $T_\gamma \propto e^{-\Gamma_\gamma x/\alpha}$, in which the argument of the exponential is suppressed by a factor α with respect to the no-conversion case. Thus this effect would explain the high transparency of the universe.

In [4] we have also calculated the root mean square δT_γ for the distribution of the transfer function in different random realizations of the magnetic field. This result is useful to estimate the uncertainty associated with the averaging procedure. In Figure 1 we compare the transfer function $T_\gamma(y)$ (continuous lines) calculated from Eq. (1) with those calculated for a given random realization of the magnetic field along the photon line of sight, with and without absorption (left panels) and for 20 realizations (right panels). For comparison we have also shown the dispersion around the mean $T_\gamma \pm \delta T_\gamma$ (dashed lines).

4 Results

In Figure 2 we show the photon transfer function as function of the energy for four different values of the redshift of the emitting source. We have used a realistic EBL model [5] which provides a strict lower-limit flux for the extragalactic background light which gives us the maximal possible transparency compatible with the standard expectations, so that an evidence of a greater transparency would have to be attributed to nonstandard effects in the photon propagation. We see that in absence of ALP conversions the photon transfer function would be strongly suppressed at energies above $E \geq 100$ GeV, the stronger the suppression the larger

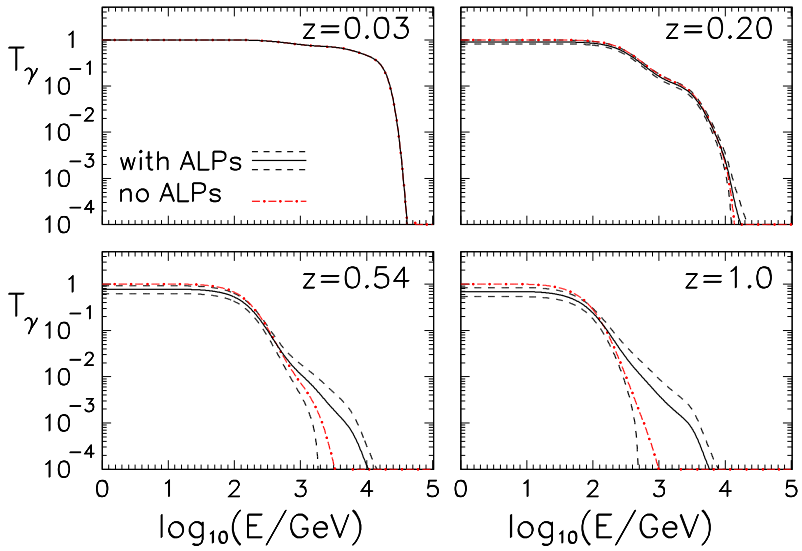

Figure 2: VHE photons transfer function T_γ in function of the observed photon energy E, for different values of the redshift z.

the redshift. We also realize that the spread in the possible values of T_γ would make difficult to infer strong conclusions about ALP mixing observing only few sources. To test this effect we would need to collect data from sources along different directions in the sky in order to perform a study of the photon energy distributions, from which we could hope to infer possible hints of ALP's. A further signature of these stochastic conversions would be the detection of peculiar direction-dependent dimming effects in the diffuse photon radiation observable in GeV range, testable with the FERMI (previously called GLAST) experiment.

References

[1] A. De Angelis, O. Mansutti and M. Roncadelli, "Evidence for a new light spin-zero boson from cosmological gamma-ray propagation?," Phys. Rev. D **76**, 121301 (2007).

[2] A. De Angelis, O. Mansutti and M. Roncadelli, "Axion-Like Particles, Cosmic Magnetic Fields and Gamma-Ray Astrophysics," Phys. Lett. B **659**, 847 (2008).

[3] A. De Angelis, O. Mansutti, M. Persic and M. Roncadelli, "Photon propagation and the VHE gamma-ray spectra of blazars: how transparent is the Universe?," Mon. Not. R. Astron. Soc. **394**, L21 (2009).

[4] A. Mirizzi and D. Montanino, "Stochastic conversions of TeV photons into axion-like particles in extragalactic magnetic fields," JCAP **0912** (2009) 004.

[5] T. M. Kneiske and H. Dole, "A strict lower-limit EBL: Applications on gamma-ray absorption," AIP Conf. Proc. **1085**, 620 (2009).

Chapter 4

Direct Detection of WIMPs

Direct Dark Matter Detection: Overview and Update

Louis E. Strigari[1]

[1]Kavli Institute for Particle Astrophysics and Cosmology,
Stanford University, Stanford CA, 94305

DOI: http://dx.doi.org/10.3204/DESY-PROC-2010-03/strigari_louis

A series of modern experimental efforts aim for direct detection of particle dark matter in the Galactic halo. In this contribution, principles of direct detection are discussed in the context of modern experiments. Recent theoretical analysis on the extraction of particle properties and Galactic halo properties are reviewed, as well as astrophysical limits to direct dark matter detection.

1 Introduction

It is well-established that our Galaxy, as well as external galaxies, contains a substantial amount of dark matter that is deduced primarily via gravitational effects. Null results from searches for gravitational microlensing along the line-of-sight towards the Magellanic clouds imply that no more than $\sim 10\%$ of the Galactic dark matter halo is comprised of compact objects such as planets or low-mass stars [1, 2]. The dominant component of the dark matter must be smooth enough as to not cause an excess of microlensing events, and nearly cold and collisionless so as to satisfy constraints from the large scale distribution of galaxies and the Cosmic Microwave Background [3].

Cold, collisionless Weakly-Interacting Massive Particles (WIMP) in thermal equilibrium in the early Universe may freeze-out with a relic abundance of order the observed dark matter density, $\Omega_{\rm DM} = 0.227^{+0.015}_{-0.016}$. Elastic scattering processes between WIMPs and quarks may lead to observable signals in low background underground detectors [4]. It is therefore prudent to search for particles with these properties to determine whether they constitute a significant fraction of the mass of the Galactic halo.

This contribution reviews principles, results, and future prospects for direct searches of WIMP dark matter particles. It is intended to provide a theoretical overview and framework for the various experimental results discussed at this meeting. For details on each of the experiments, please see the respective presentations [1] and proceeding contributions.

2 Principles

WIMP-nucleus scattering in direct detection experiments is non-relativistic, described by incoming WIMP velocities of order $(v/c) \sim 10^{-3}$. The energy deposited to the nucleus in the

[1]http://axion-wimp.desy.de/e80839/

interaction is $\sim 1-10$ keV, much less than the typical nuclear binding energy scale of MeV per nucleon. Even though the energy deposited to the nucleus is small, experiments are primarily sensitive to the high velocity tail of the distribution of WIMPs in the halo.

In terms of fundamental interactions, it is most standard to assume that WIMP-nuclei elastic scattering is described by a momentum-independent contact interaction. For standard scalar, fermionic, and vector dark matter construction of non-relativistic operators then leads to the WIMP-nucleus cross section (See e.g. [5] for a recent analysis and review). More general dark matter models can be considered, e.g. inelastic dark matter [6] or dark matter with momentum-dependent interactions.

The lightest neutralino of supersymmetry has been extensively studied as a dark matter candidate. See Refs. [7] for general reviews of supersymmetric dark matter candidates. Though a wide range of cross sections are predicted in neutralino models, experimental limits and theoretical considerations point to the "zeptobarn" scale as characteristic for spin-independent cross sections [8]. Modern experimental limits are quickly approaching this regime of sensitivity.

The observed recoil spectrum due to WIMP interactions is given by the integral $dR/dE_R = N_T\rho_\chi/m_\chi \int_{v_{\rm min}}^{v_E} d^3v v f(v) d\sigma/dE_R$, where N_T is the number of targets, ρ_χ is the local WIMP density, and m_χ is the WIMP mass. The minimum velocity for scattering is $v_{\rm min}$ and the escape velocity is v_E. The differential cross section scales as $d\sigma/dE_R \propto v^{-2}$, so that the rate is simply parameterized as proportional to the integral over the WIMP velocity distribution as $\int dv f(v)/v$.

3 Recent Results

The final results from the CDMS experiment, and also first results from ZEPLIN III [9] and EDELWEISS II [10], are beginning to exclude WIMP cross sections predicted in the canonical Constrained Minimal Supersymmetric Standard Model (CMSSM) [13, 14]. The first results from the XENON100 experiment achieve a cross section sensitivity of $\sim 3 \times 10^{-44}$ cm^2 at a WIMP mass of ~ 40 GeV [12].

Due to the results of the CoGent [16] and DAMA [15] experiments, there has been recent interest in WIMPs in the relatively low-mass range ~ 10 GeV [18]. A new low threshold analysis from CDMS with a trigger threshold of 2 keV excludes parameter space associated with possible low mass WIMP signal interpretations by DAMA/LIBRA and CoGeNT [11]. The CDMS analysis reduces their energy thresholds by identifying the relevant electron recoil backgrounds. The first results from XENON100 may be sensitive to this low mass regime depending on the energy resolution of the scintillation efficiency at low nuclear recoils [19].

4 Future Prospects

A direct detection of particle dark matter would represent a scientific achievement of profound importance. Though at the present stage direct dark matter detection experiments operate as "discovery" experiments, it is worthwhile to consider the scientific gain a positive signal would entail. A new laboratory would be opened up that allows to probe the fundamental interactions of particle physics, and also a new field of "dark matter astronomy" will be born.

The limits discussed above assume a canonical dark matter halo model described by a smooth maxwellian distribution function with a local dark matter density of 0.3 GeV cm^{-3} and a Galactic escape velocity of 544 km/s. A series of recent papers has explored how these

limits and future signals will change depending on the properties of the Galactic dark matter distribution [20]. Several authors have also revisited the constraints on the local dark matter density given astrophysical data [21]. Though our knowledge of the distribution of local dark matter from astrophysical observations is impressive, it is unlikely it in of itself constitute a strong enough prior when attempting to determine the WIMP mass.

Ultra-high resolution simulations of Galaxy-mass dark matter halos have determined, at their resolution limits of $\sim 10^3$ $M_\odot$, the smooth versus clumpy mass and velocity distribution in the Galactic halo [22]. Numerical simulations that include baryonic effects have particle resolutions over two orders of magnitude larger [24]. Though the smooth component of the velocity distribution is most significant, these simulations show deviations from standard Maxwellian models, particularly at high velocity tail close to the escape velocity. Deviations of the smooth distribution from maxwellian behavior can be analytically understood starting from cosmologically-motiaved density profiles, under simplifying assumptions [25].

Current direct detection experiments operate under the principle of zero astrophysical backgrounds. However, this will be possible only up to a certain sensitivity level. Irreducible signals from coherent scattering of solar neutrinos [26] limit the extraction of dark matter-nucleon cross sections below 10^{-46} cm^2 at energies below ~ 7 keV for Ge and below ~ 5 keV for Xe [27]. At lower cross sections of $\sim 10^{-48}$ cm^2 neutrino signals from atmospheric and diffuse supernova become significant over the entire energy recoil range where a WIMP signal is expected.

References

[1] C. Alcock *et al.* [MACHO Collaboration], "The MACHO project: Microlensing results from 5.7 years of LMC observations," Astrophys. J. **542**, 281-307 (2000). [astro-ph/0001272].

[2] T. Lasserre [EROS Collaboration], "Not enough stellar mass machos in the galactic halo," Astron. Astrophys. **355**, L39-L42 (2000). [astro-ph/0002253].

[3] D. N. Spergel *et al.* [WMAP Collaboration], "First year Wilkinson Microwave Anisotropy Probe (WMAP) observations: Determination of cosmological parameters," Astrophys. J. Suppl. **148**, 175-194 (2003). [astro-ph/0302209].

[4] M. W. Goodman, E. Witten, "Detectability of Certain Dark Matter Candidates," Phys. Rev. **D31**, 3059 (1985).

[5] J. Fan, M. Reece, L. -T. Wang, "Non-relativistic effective theory of dark matter direct detection," [arXiv:1008.1591 [hep-ph]].

[6] D. Tucker-Smith, N. Weiner, "Inelastic dark matter," Phys. Rev. **D64**, 043502 (2001). [hep-ph/0101138];

[7] G. Jungman, M. Kamionkowski, K. Griest, "Supersymmetric dark matter," Phys. Rept. **267**, 195-373 (1996). [hep-ph/9506380]; G. Bertone, D. Hooper, J. Silk, "Particle dark matter: Evidence, candidates and constraints," Phys. Rept. **405**, 279-390 (2005). [hep-ph/0404175].

[8] J. L. Feng, D. Sanford, "Heart of Darkness: The Significance of the Zeptobarn Scale for Neutralino Direct Detection," [arXiv:1009.3934 [hep-ph]].

[9] V. N. Lebedenko *et al.* [ZEPLIN-III Collaboration], "Limits on the spin-dependent WIMP-nucleon cross-sections from the first science run of the ZEPLIN-III experiment," Phys. Rev. Lett. **103**, 151302 (2009). [arXiv:0901.4348 [hep-ex]].

[10] E. Armengaud, C. Augier, A. Benoit *et al.*, "First results of the EDELWEISS-II WIMP search using Ge cryogenic detectors with interleaved electrodes," Phys. Lett. **B687**, 294-298 (2010). [arXiv:0912.0805 [astro-ph.CO]].

[11] , *et al.* [CDMS Collaboration], "Results from a Low-Energy Analysis of the CDMS II Germanium Data," [arXiv:1011.2482 [astro-ph.CO]].

[12] E. Aprile *et al.* [XENON100 Collaboration], "First Dark Matter Results from the XENON100 Experiment," Phys. Rev. Lett. **105**, 131302 (2010). [arXiv:1005.0380 [astro-ph.CO]].

[13] J. R. Ellis, K. A. Olive, Y. Santoso *et al.*, "Update on the direct detection of supersymmetric dark matter," Phys. Rev. **D71**, 095007 (2005). [hep-ph/0502001].

[14] R. Trotta, F. Feroz, M. P. Hobson *et al.*, "The Impact of priors and observables on parameter inferences in the Constrained MSSM," JHEP **0812**, 024 (2008). [arXiv:0809.3792 [hep-ph]].

[15] R. Bernabei, P. Belli, F. Cappella *et al.*, "New results from DAMA/LIBRA," Eur. Phys. J. **C67**, 39-49 (2010). [arXiv:1002.1028 [astro-ph.GA]].

[16] C. E. Aalseth *et al.* [CoGeNT Collaboration], "Results from a Search for Light-Mass Dark Matter with a P-type Point Contact Germanium Detector," [arXiv:1002.4703 [astro-ph.CO]].

[17] D. S. Akerib *et al.* [CDMS Collaboration], "A low-threshold analysis of CDMS shallow-site data," [arXiv:1010.4290 [astro-ph.CO]].

[18] D. Hooper, J. I. Collar, J. Hall *et al.*, "A Consistent Dark Matter Interpretation For CoGeNT and DAMA/LIBRA," [arXiv:1007.1005 [hep-ph]].

[19] J. I. Collar, D. N. McKinsey, "Comments on 'First Dark Matter Results from the XENON100 Experiment'," [arXiv:1005.0838 [astro-ph.CO]].

[20] A. M. Green, "Determining the WIMP mass from a single direct detection experiment, a more detailed study," JCAP **0807**, 005 (2008). [arXiv:0805.1704 [hep-ph]]; L. E. Strigari, R. Trotta, "Reconstructing WIMP Properties in Direct Detection Experiments Including Galactic Dark Matter Distribution Uncertainties," JCAP **0911**, 019 (2009). [arXiv:0906.5361 [astro-ph.HE]]; A. H. G. Peter, "Getting the astrophysics and particle physics of dark matter out of next-generation direct detection experiments," Phys. Rev. **D81**, 087301 (2010). [arXiv:0910.4765 [astro-ph.CO]]; M. Pato, O. Agertz, G. Bertone *et al.*, "Systematic uncertainties in the determination of the local dark matter density," Phys. Rev. **D82**, 023531 (2010). [arXiv:1006.1322 [astro-ph.HE]].

[21] R. Catena, P. Ullio, "A novel determination of the local dark matter density," JCAP **1008**, 004 (2010). [arXiv:0907.0018 [astro-ph.CO]]; M. Weber, W. de Boer, 'Determination of the Local Dark Matter Density in our Galaxy," [arXiv:0910.4272 [astro-ph.CO]].

[22] M. Vogelsberger, A. Helmi, V. Springel *et al.*, "Phase-space structure in the local dark matter distribution and its signature in direct detection experiments," [arXiv:0812.0362 [astro-ph]];

[23] M. Kuhlen, N. Weiner, J. Diemand *et al.*, "Dark Matter Direct Detection with Non-Maxwellian Velocity Structure," JCAP **1002**, 030 (2010). [arXiv:0912.2358 [astro-ph.GA]].

[24] F. S. Ling, E. Nezri, E. Athanassoula and R. Teyssier, "Dark Matter Direct Detection Signals inferred from a Cosmological N-body Simulation with Baryons," JCAP **1002**, 012 (2010) [arXiv:0909.2028 [astro-ph.GA]].

[25] M. Lisanti, L. E. Strigari, J. G. Wacker *et al.*, "The Dark Matter at the End of the Galaxy," [arXiv:1010.4300 [astro-ph.CO]].

[26] B. Cabrera, L. M. Krauss, F. Wilczek, "Bolometric Detection Of Neutrinos," Phys. Rev. Lett. **55**, 25 (1985).

[27] J. Monroe, P. Fisher, "Neutrino Backgrounds to Dark Matter Searches," Phys. Rev. **D76**, 033007 (2007). [arXiv:0706.3019 [astro-ph]]; L. E. Strigari, "Neutrino Coherent Scattering Rates at Direct Dark Matter Detectors," New J. Phys. **11**, 105011 (2009). [arXiv:0903.3630 [astro-ph.CO]]; A. Gutlein, C. Ciemniak, F. von Feilitzsch *et al.*, "Solar and atmospheric neutrinos: Background sources for the direct dark matter search," Astropart. Phys. **34**, 90-96 (2010). [arXiv:1003.5530 [hep-ph]].

Results from DAMA/LIBRA

R. Bernabei[1], *P. Belli*[1], *F. Cappella*[2], *R. Cerulli*[3], *C.J. Dai*[4], *A. d'Angelo*[2], *H.L. He*[4], *A. Incicchitti*[2], *X.H. Ma*[4], *F. Montecchia*[1,5], *F. Nozzoli*[1], *D. Prosperi*[2,*], *X.D. Sheng*[4], *R.G. Wang*[4], Z.P. Ye[4,6]

[1]Dip. di Fisica, Università di Roma "Tor Vergata" and INFN, sez. Roma "Tor Vergata", I-00133 Rome, Italy
[2] Dip. di Fisica, Università di Roma "La Sapienza" and INFN, sez. Roma, I-00185 Rome, Italy
[3] Laboratori Nazionali del Gran Sasso, I.N.F.N., I-67010 Assergi, Italy
[4] IHEP, Chinese Academy, P.O. Box 918/3, Beijing 100039, China
[5] Lab. Sperim. Policentrico di Ingegneria Medica, Università di Roma "Tor Vergata"
[6] University of Jing Gangshan, Jiangxi, China
[*] deceased

DOI: http://dx.doi.org/10.3204/DESY-PROC-2010-03/cerulli_riccardo

The 250 kg highly radiopure NaI(Tl) DAMA/LIBRA experiment and the former DAMA/NaI (first generation experiment with $\simeq$ 100 kg exposed mass) have released so far the results obtained cumulatively over 13 annual cycles. Their total exposure of 1.17 ton $\times$ yr gives a model independent evidence of the presence of Dark Matter (DM) particles in the galactic halo at 8.9 σ C.L. on the basis of the DM annual modulation signature.

The DAMA project at the Gran Sasso National Laboratory of the I.N.F.N. is focused on the development and use of low background scintillators for the investigation of many rare processes [1, 2, 3, 4, 5, 6, 7, 8, 9, 10, 11, 12, 13, 14, 15, 16]. In particular, DAMA/LIBRA is investigating the presence of DM particles in the galactic halo by exploiting the model independent DM annual modulation signature [17] based on the Earth motion around the Sun, which is moving in the Galaxy. The flux of the DM particles crossing the Earth is expected to be larger around $\sim$ 2 June (when the Earth orbital velocity is summed to the one of the solar system with respect to the Galaxy) and smaller around $\sim$ 2 December (when the two velocities are subtracted). This signature is very effective and allow the test of a large number of DM candidates, a large interval of cross sections and of halo densities. In particular, the signal must simultaneously satisfy all the following requirements: the rate must contain a component modulated according to a cosine function (1) with one year period (2) and a phase that peaks roughly around $\simeq$ 2 June (3); this modulation must only be found in a well-defined low energy range, where DM particle induced events can be present (4); it must apply only to those events in which just one detector of many actually "fires" (*single-hit events*), since the DM particle multi-interaction probability is negligible (5); the modulation amplitude in the region of maximal sensitivity must be $\lesssim$7% for usually adopted halo distributions (6), but it can be larger in case of some possible scenarios such as e.g. those in refs. [18, 19]. Only systematic effects or side reactions able to simultaneously fulfil all these requirements and to account for the whole observed modulation amplitude could mimic this signature; thus, no other effect investigated so far in the field of rare processes offers a so stringent and unambiguous signature.

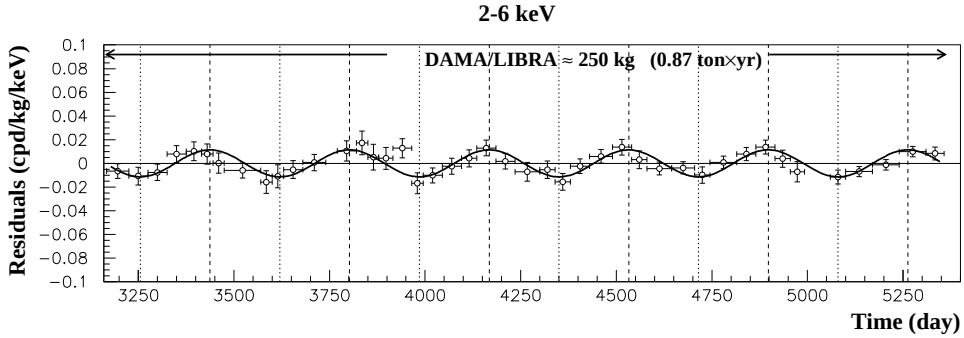

Figure 1: Model-independent result: residual rate of the *single-hit* events, measured by DAMA/LIBRA,1-6 in (2 – 6) keV range as a function of the time. The experimental points present the errors as vertical bars and the associated time bin width as horizontal bars. The superimposed curve is the function $A\cos\omega(t-t_0)$ with $T=\frac{2\pi}{\omega}=1$ yr, $t_0=152.5$ day (June 2^{nd}) and with modulation amplitudes, A, equal to the central values obtained by best fit over the DAMA/LIBRA and DAMA/NaI cumulative exposure (1.17 ton × yr). The dashed vertical lines correspond to the maximum expected for the DM signal (June 2^{nd}), while the dotted vertical lines correspond to the minimum [20].

The DAMA/LIBRA set-up [14] is composed by a sensitive part made of 25 highly radiopure NaI(Tl) crystal scintillators placed in a 5-rows by 5-columns matrix; the detectors' responses range from 5.5 to 7.5 photoelectrons/keV, allowing the experiment to set the software energy threshold at 2 keV (here and hereafter keV means keV electron equivalent), while the hardware threshold of each photomultiplier (PMT) is at single photoelectron (each detector is equipped with two low background PMTs working in coincidence); energy calibration with X-rays/γ sources are regularly carried out down to few keV in the same conditions as the production runs.

The DAMA/LIBRA data released so far corresponds to six annual cycles for an exposure of 0.87 ton×yr [15, 20]. Considering these data together with those previously collected by DAMA/NaI over 7 annual cycles (0.29 ton×yr), the total exposure collected over 13 annual cycles is 1.17 ton×yr; this is orders of magnitude larger than the exposures typically collected in the field.

Several analyses to investigate the model-independent DM annual modulation signature have been performed (see ref. [15, 20] and references therein); here just few arguments are mentioned. In particular, Fig. 1 shows the time behaviour of the experimental residual rates of the *single-hit* events collected by DAMA/LIBRA in the (2–6) keV energy interval. The superimposed curve is the cosinusoidal function: $A\cos\omega(t-t_0)$ with a period $T=\frac{2\pi}{\omega}=1$ yr and with a phase $t_0=152.5$ day (June 2^{nd}), and modulation amplitude, A, obtained by best fit over the seven cycles of DAMA/NaI [4, 5] and the six of DAMA/LIBRA [15, 20]. When the period and the phase parameters are also released in the fit, values well compatible with those expected for a DM particle induced effect are obtained; in the (2–6) keV energy interval it results: $A=(0.0116\pm0.0013)$ cpd/kg/keV, $T=(0.999\pm0.002)$ yr and $t_0=(146\pm7)$ day. The analysis of the *single-hit* residual rate favours the presence of a modulated cosine-like behaviour with proper features at 8.9 σ C.L..

A Fourier analysis on the the (2–6) keV *single-hit* residuals has been performed in order

to extract the modes of the modulation. The principal mode of the obtained power spectrum is consistent with a frequency corresponding to a period of 1 year; the same analysis in other energy region shows instead only aliasing peaks. Thus, a clear modulation is present at low energy while it is absent at energies just above, as expected for the anual modulation signature.

The measured energy distribution has been investigated in energy regions not of interest for DM. The data analyses have allowed to exclude the presence of a background modulation in the whole energy spectrum at a level much lower than the effect found in the lowest energy region for the *single-hit* events [15, 20].

A further analysis show that while a clear modulation is present in the (2–6) keV *single-hit* events, amplitudes well compatible with zero are obtained for the *multiple-hits* events in the same energy range. Similar results were previously obtained also for the DAMA/NaI case [5]. Thus, again evidence of annual modulation with proper features, as required by the DM annual modulation signature, is present in the *single-hit* residuals (events class to which the DM particle induced events belong), while it is absent in the *multiple-hits* residual rate (event class to which only background events belong). Since the same identical hardware and the same identical software procedures have been used to analyse the two classes of events, the obtained result offers an additional strong support for the presence of DM particles in the galactic halo further excluding any side effect either from hardware or from software procedures or from background [15, 20].

It has been also verified that the measured modulation amplitudes are statistically well distributed over all the crystals, over all the annual cycles and energy bins [15, 20].

It is also worth to mention the results of the analysis performed by releasing the assumption of a phase $t_0 = 152.5$ day in the procedure of maximum likelihood to evaluate the modulation amplitudes from the data of the seven annual cycles of DAMA/NaI and the six annual cycles of DAMA/LIBRA. The obtained results confirm that a modulation amplitude is present in the lower energy intervals for single hit events and that the period and the phase agree with those expected for DM induced signals [15, 20].

As previously done for DAMA/NaI [4, 5], Careful investigations on absence of any significant systematics or side reaction effect in DAMA/NaI and in DAMA/LIBRA have been quantitatively carried out and reported in details in ref. [4, 5, 15, 22, 23, 24] and references therein. No systematics or side reactions able to mimic the signature (that is, able to account for the measured modulation amplitude and simultaneously satisfy all the requirements of the signature) has been found or suggested by anyone over more than a decade.

In conclusion, DAMA/LIBRA has confirmed the presence of an annual modulation satisfying all the requirements of the DM annual modulation signature, as previously pointed out by DAMA/NaI; in particular, the evidence for the presence of DM particles in the galactic halo is cumulatively supported at 8.9 σ C.L.. As regards the corollary investigation on the nature of the DM candidate particle(s) and related astrophysical, nuclear and particle physics scenarios, it has been shown that the obtained model independent evidence can be compatible with a wide set of possibilities; see for example [2, 4, 5, 6, 7, 8, 9, 10, 11, 15]. Many other interpretations of the annual modulation results are available in literature (as e.g. [18, 25, 26, 27, 28, 29, 30, 31, 32, 33, 34], etc.); others are open. For discussions about the comparison between this result and the results obtained by other experiments see ref. [4, 5, 15, 36, 37]

References

[1] R. Bernabei et al., *Il Nuovo Cim.* **A112**, 545 (1999).

[2] R. Bernabei et al., *Phys. Lett.* **B389**, 757 (1996); R. Bernabei et al., *Phys. Lett.* **B424**, 195 (1998); R. Bernabei et al., *Phys. Lett.* **B450**, 448 (1999); P. Belli et al., *Phys. Rev.* **D61**, 023512 (2000); R. Bernabei et al., *Phys. Lett.* **B480**, 23 (2000); R. Bernabei et al., *Phys. Lett.* **B509**, 197 (2001); R. Bernabei et al., *Eur. Phys. J.* **C23**, 61 (2002); P. Belli et al., *Phys. Rev.* **D66**, 043503 (2002).

[3] R. Bernabei et al., *Eur. Phys. J.* **C18**, 283 (2000).

[4] R. Bernabei el al., *La Rivista del Nuovo Cimento* **26** n.1, 1 (2003).

[5] R. Bernabei et al., *Int. J. Mod. Phys.* **D13**, 2127 (2004).

[6] R. Bernabei et al., *Int. J. Mod. Phys.* **A21**, 1445 (2006).

[7] R. Bernabei et al., *Eur. Phys. J.* **C47**, 263 (2006).

[8] R. Bernabei et al., *Int. J. Mod. Phys.* **A22**, 3155 (2007).

[9] R. Bernabei et al., *Eur. Phys. J.* **C53**, 205 (2008).

[10] R. Bernabei et al., *Phys. Rev.* **D77**, 023506 (2008).

[11] R. Bernabei et al., *Mod. Phys. Lett.* **A23**, 2125 (2008).

[12] R. Bernabei et al., *Phys. Lett.* **B408**, 439 (1997); P. Belli et al., *Phys. Lett.* **B460**, 236 (1999); R. Bernabei et al., *Phys. Rev. Lett.* **83**, 4918 (1999); P. Belli et al., *Phys. Rev.* **C60**, 065501 (1999); R. Bernabei et al., *Il Nuovo Cimento* **A112**, 1541 (1999); R. Bernabei et al., *Phys. Lett.* **B515**, 6 (2001); F. Cappella et al., *Eur. Phys. J.-direct* **C14**, 1 (2002); R. Bernabei et al., *Eur. Phys. J.* **A23**, 7 (2005); R. Bernabei et al., *Eur. Phys. J.* **A24**, 51 (2005); R. Bernabei et al., *Astrop. Phys.* **4**, 45 (1995); R. Bernabei, in *The identification of Dark Matter*, World Sc. Pub., Singapore, 1997, pp. 574.

[13] DAMA web page: `http://people.roma2.infn.it/dama`

[14] R. Bernabei et al., *Nucl. Instr. & Meth.* **A592**, 297 (2008).

[15] R. Bernabei et al., *Eur. Phys. J.* **C56**, 333 (2008).

[16] R. Bernabei et al., *Eur. Phys. J.* **C62**, 327 (2009).

[17] K. A. Drukier et al., *Phys. Rev.* **D33**, 349 (1986); K. Freese et al., *Phys. Rev.* **D37**, 3388 (1988).

[18] D. Smith and N. Weiner, *Phys. Rev.* **D64**, 043502 (2001); D. Tucker-Smith and N. Weiner, *Phys. Rev.* **D72** 063509 (2005); D. P. Finkbeiner et al, *Phys. Rev.* **D80**, 115008 (2009).

[19] K. Freese et al., *Phys. Rev.* **D71**, 043516 (2005); *Phys. Rev. Lett.* **92**, 111301 (2004).

[20] R. Bernabei et al., *Eur. Phys. J.* **C67**, 39 (2010).

[21] F. S. Ling, P. Sikivie and S. Wick, *Phys. Rev.* **D70**, 123503 (2004).

[22] R. Bernabei et al., AIP Conf. Proceed. **1223**, 50 (2010), arXiv:0912.0660[astro-ph.GA].

[23] R. Bernabei et. al, *J. Phys.: Conf. Ser.* **203**, 012040 (2010) (arXiv:0912.4200); http://taup2009.lngs.infn.it/slides/jul3/nozzoli.pdf, talk given by F. Nozzoli.

[24] R. Bernabei et. al, arXiv:1007.0595

[25] A. Bottino, N. Fornengo, and S. Scopel, *Phys. Rev.* **D67**, 063519 (2003); A. Bottino, F. Donato, N. Fornengo, and S. Scopel, *Phys. Rev.* **D69** 037302 (2003); *Phys. Rev.* **D78**, 083520 (2008); A. Bottino, F. Donato, N. Fornengo, S. Scopel, arXiv:0912.4025.

[26] R. Foot, *Phys. Rev.* **D78**, 043529 (2008).

[27] Y. Bai and P.J. Fox, arXiv:0909.2900

[28] K. Belotsky, D. Fargion, M. Khlopov and R.V. Konoplich, *Phys. Atom. Nucl.* **71**, (2008) 147.

[29] E.M. Drobyshevski et al., *Astrohys. & Astronom. Trans.* **26:4**, 289 (2007); *Mod. Phys. Lett.* **A23**, 3077 (2008).

[30] Nima Arkani-Hamed et al., *Phys. Rev.* **D79**, 015014 (2009).

[31] Daniele S.M. Alves et al., arXiv:0903.3945.

[32] D. Hooper, Lisa Goodenough, arXiv:1010.2752; D. Hooper et al., arXiv:1007.1005.

[33] Spencer Chang, Rafael F. Lang, Neal Weiner, arXiv:1007.2688.

[34] Spencer Chang, Neal Weiner, Itay Yavin, arXiv:1007.4200.

[35] Sarah Andreas, Andreas Ringwald, arXiv:1008.4519 and this Proceedings.

[36] R. Bernabei et al., ISBN 978-88-95688-12-1, pages 1-53 (2009) Exorma Ed. (arXiv:0806.0011v2).

[37] J.I. Collar and D.N. McKinsey, arXiv:1005.0838; arXiv:1005.3723; J.I. Collar, arXiv:1006.2031.

DRIFT: Background Reduction and Spin-Dependent Limits

Daniel Walker on behalf of the DRIFT collaboration

Department of Physics and Astronomy, University of Sheffield, S3 7RH, UK

DOI: http://dx.doi.org/10.3204/DESY-PROC-2010-03/walker_daniel

The DRIFT (Directional Recoil Identification From Tracks) collaboration operates a $1m^3$ directional dark matter search experiment, based on a low pressure gaseous negative ion time projection chamber (NI-TPC) in the Boulby Underground Laboratory. Recent progress includes the addition of CF_4 to the target volume, and a series of background reduction work. A preliminary limit on the spin-dependent WIMP-proton interaction cross-section is presented from a non-blind analysis of 47.2 days live time with a $0.8m^3$ 30 Torr CS_2 - 10 Torr CF_4 target. The preliminary limit has a minimum of 1.1pb for a 100GeV WIMP.

1 Introduction

Dark matter halo models suggest that WIMPs may exist in the form of an isothermal sphere encompassing the Milky Way, providing an explanation for flat galactic rotation curves [1]. The interaction of WIMPs with baryonic matter is expected to be such that particle detectors of sufficient sensitivity should be able to detect the rare low energy nuclear recoils that would result (~ 1 keV at < 1 event/kg/day). The basis of directional detection lies in the assumption of a finite Galactic orbital velocity of our Solar System, $\sim 220 kms^{-1}$ relative to the WIMP velocity distribution in the Galactic halo. There is hence a WIMP 'wind' experienced for a detector in the Solar System, with a preference for nuclear recoils with velocities opposite to the orbital motion through the Galaxy. This WIMP 'wind' will have both an annual and a sidereal variation as shown in Figure 1. Over the course of a sidereal day the direction of this will oscillate, a very powerful signature that will be difficult for any terrestrial background to mimick [2]. The DRIFT collaboration is attempting to utilise this powerful discriminant against terrestrial backgrounds through the development of a directionally sensitive dark matter detector.

2 DRIFT Overview

The DRIFT-II detector is described in detail in [3]. DRIFT-II is a $1m^3$ low pressure gaseous negative ion time projection chamber (NI-TPC). WIMP-nucleon interactions in the 40 Torr CS_2-CF_4 target gas are expected to create ionisation tracks a few millimetres in length. The orientation of these tracks would be biased in the direction opposite to that of the incoming WIMPs [4]. In DRIFT, the drifted tracks are negative ions, which reduces diffusion up to drift

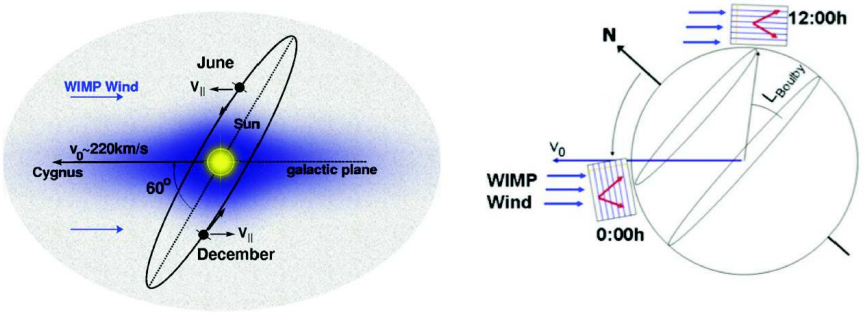

Figure 1: The WIMP 'Wind' and its annual (left) and sidereal (right) variation.

distances of 50 cm. CS_2 is electronegative, thus primary ionisation electrons quickly attach to CS_2 molecules producing a track of negative CS_2 ions. Compared with electrons drifted alone these heavy ions give far less diffusion, down to thermal levels. This preserves the track's directional information.

3 Backgrounds

The current dominating background in the underground DRIFT-II detector is from events termed radon progeny recoils (RPRs). Radon gas (^{222}Rn and ^{220}Rn) is present in the DRIFT detector target volume, emitted from trace levels of U and Th in the detector components. ^{222}Rn is unstable and decays to ^{218}Po, emitting a 5.49 MeV alpha particle, which gives an ionisation track in the detector volume of length $\sim$ 400mm. Because of the long track length, these events can be discriminated with high efficiency, and hence have negligible effect. $\sim$ 80% of the time, the decay product is ^{218}Po$^+$, an unstable, charged atom. In the electric field this drifts to the surface of the 20μm stainless steel central cathode wires [5]. The ^{218}Po$^+$ atom then decays via emission of a 6.11 MeV alpha particle. In stainless steel this has a range of 14μm, and hence due to the geometry of the wire, this gives a 37% chance of the alpha becoming embedded in the cathode wire, with only the recoil atom (^{218}Po) being detected in the fiducial volume. The detection of a nuclear recoil of energy $\sim$ 100keV can potentially mimick the signal expected from a WIMP nuclear recoil. In addition, the radon decay chain results in ^{210}Pb plating out onto the surface of the cathode wires. Being unstable, with a half life of 22.3 years, this can be a further source of RPR background events, even after any radon inside the detector volume has been eliminated.

The first step in reducing this background is the removal of radon from the detector volume. It was found from radon emanation tests that RG58 coaxial cables (PVC coated) and ribbon cables (also PVC coated) were the dominant source of radon emanation. As suitable replacements, PTFE coated coaxial signal cables and FEP coated ribbon cables were found. After these replacements, the total number of Rn atoms per second emitted by all detector components was found to have been reduced from 0.95 ± 0.06 to 0.09 ± 0.03.

In a further step to remove any radon, in March 2008 the 1m^2 central cathode was etched in nitric acid to remove long lived radon progeny (^{210}Pb). Subsequent analysis of data from

before and after this procedure showed that the level of background events was reduced further by a factor of 6.7 ± 1.0.

4 Spin-Dependent WIMP-Proton Limit

In order to set a limit for spin-dependent WIMP interactions, a target material of 30 Torr CS_2 - 10 Torr CF_4 was chosen. This maximises the fluorine content, which has nuclei of spin 1/2 [6]. Negative ion drift and detector stability is maintained via this mixture [7]. A total of 47.2 days live time data with a continuous flow of this gas mixture was taken, this flow being to minimise radon in the gas. This yields 1.47 kg·days of fluorine fiducial mass. Preliminary limits on the SD WIMP-proton cross-section were produced using the zero background signal region and the WIMP detection efficiency. These limits are shown in Figure 2. Note that this analysis is not blind, as the signal region was chosen after an analysis of the data and background study. A fully blind analysis is planned with further data that is currently being taken.

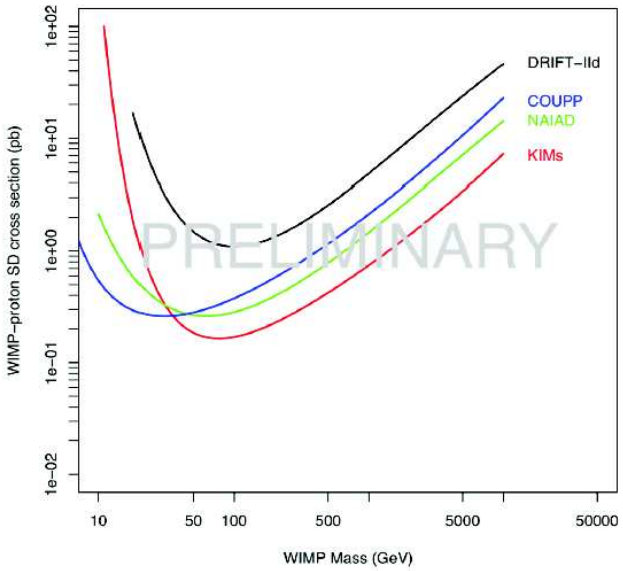

Figure 2: Preliminary limits on spin-dependent WIMP-proton coupling from 47.2 days live time with a $0.8m^3$ fiducial volume of 30 Torr CS_2 - 10 Torr CF_4 in the DRIFT-IId detector underground at Boulby Mine.

5 Thin Film Cathode

The RPR background discussed above results from unstable radon progeny on the surface of the central cathode wires that recoil into the fiducial volume. The alpha that should easily distinguish this event from signal becomes embedded in the central cathode wire. One way to

reduce this background is to make the cathode more transparent to alphas in order to reject these events via detection of this alpha.

Several potential cathodes were modelled, and a 0.9μm mylar sheet, evaporation coated with aluminium was found to be a suitable material. It was expected that $\sim 1\%$ of decays on the surface would result in a recoil that would be indistinguishable from a WIMP recoil, compared with 37% of radon progeny decays on the wire cathode. This suggests a potential reduction in background by a factor of ~ 40.

After testing at Occidental College, a 1m^2 cathode was installed on the detector at Boulby mine in March 2010. Preliminary analysis of data taken shows a reduction in background by a factor ~ 15, suggesting there may be other backgrounds within the RPR region introduced by the thin film cathode. A study is currently underway to understand these backgrounds for the proposed blind analysis.

Acknowledgments

We would like to acknowledge the support of Cleveland Potash Ltd, operators of Boulby Mine, NSF and STFC.

References

[1] J. D. Vergados, "Theoretical directional and modulated rates for direct supersymmetric dark matter detection," Phys. Rev. D **67**, 103003 (2003).

[2] B. Morgan, A. M. Green, and N. J. C. Spooner, "Directional statistics for realistic weakly interacting massive particle direct detection experiments," Phys. Rev. D **71**, 103507 (2005).

[3] G. J. Alner, et al., "The DRIFT-II dark matter detector: Design and commissioning," Nucl. Instrum. Meth. A **555**, 173 (2005).

[4] D. P. Snowden-Ifft, C. J. Martoff, and J. M. Burwell, "Low pressure negative ion time projection chamber for dark matter search," Phys. Rev. D **61**, 101301 (2000).

[5] S. Burgos, et al., "Track reconstruction and performance of DRIFT directional dark matter detectors using alpha particles," Nucl. Instrum. Meth. A, **584**, 114 (2008).

[6] J. Ellis, and R. A. Flores, "Elastic supersymmetric relic-nucleus scattering revisited," Phys. Lett. B **263**, 259 (1991).

[7] K. Pushkin, and D. P. Snowden-Ifft, "Measurements of W-value, mobility and gas gain in electronegative gaseous CS2 and CS2 gas mixtures," Nucl. Instrum. Meth. A **606**, 569 (2009).

XMASS

Masaki Yamashita for the XMASS collaboration

Kamioka Observatory, ICRR, University of Tokyo,
456 Higashi-Mozumi, Kamioka-cho, Hida, Gifu, 506-1205 , Japan

DOI: http://dx.doi.org/10.3204/DESY-PROC-2010-03/yamashita_masaki

The goal of XMASS experiment aims at the direct dark matter, the solar neutrinos from pp and ^{7}Be and neutrino less double beta decay (^{136}Xe) with ton scale fiducial volume of liquid xenon detector. In the current stage, we focus on the the direct detection of dark matter in the form of WIMPs (Weakly Interacting Massive Particles) via their elastic scattering off xenon nuclei with 800 kg detector at Kamioka in Japan. XMASS 800 kg detector will achieve a sensitivity down to 10^{-45} cm^2 of WIMP-nucleus cross section for the spin independent case. The status of experiment will be review and discussed here.

1 Introduction

XMASS is a multi-purpose of ultra pure liquid xenon detector for the underground physics. Its targets are dark matter search, low energy solar neutrinos and neutrinoless double beta decay with ton scale fiducial volume [1]. The project was funded for the 800 kg detector mainly for the dark matter search prior to the final stage. Based on the results and experiences which will be obtained by this 800 kg detector, the final detector will be employed for the study of low energy solar neutrinos and the further investigation of dark matter. WIMPs populating the halo of our galaxy can be detected directly via their interactions with nuclei in terrestrial detectors. XMASS is a dark matter detector, with the aim of observing the small energy (∼10 keV or less) released after a WIMP scatters off a Xe nucleus. Liquid xenon has a large scintillation photon yield of 46,000 photons/MeV, which is as good as NaI(Tl) scintillator. This enables us to achieve the detection of small energy signals. The Key idea of the background reduction in XMASS is self-shielding, to use detector liquid xenon itself as a shield to reduce gamma rays background. Due to its high atomic number (Z=54) and high density of liquid xenon (3g/cm3), the compact detector with relatively small size can be constructed. Using the outer region of liquid xenon as shield for gamma rays, extremely low background environment can be achieved in the detector center region for the purpose of detecting rare events from WIMPs or neutrinos.

2 XMASS 800 kg Detector

The XMASS 800 kg detector was installed in the new experimental hall at Kamioka in Japan. This experimental hall, 15 m wide and 21m deep and 15m height, was completed in August, 2008. Fig.1 shows and the installation of the water tank, ϕ 10 m × 10m, which was completed in March, 2009. The spherical liquid xenon detector was installed in the water tank in fall,

2010. The detector employs a single phase technology and observes only scintillation lights emitted by the interaction of dark matter. The total amount of liquid xenon for active volume is about 850 kg and the total mass of liquid xenon in the detector is 1080 kg. The 642 hexagonal photomultiplier tubes (PMTs), R10789 Hamamatsu, are mounted in an approximately spherical shape with an average radius of 40 cm of xenon as shown in Fig. 1. PMTs photo-cathode give about 64.4% coverage of the inner surface of the detector. The actual shape of the structure holding PMTs is called Pentakis-dodecahedron which consists of 12 pentagonal pyramids and each pyramid is made by 5 triangles. The purification of xenon in gas phase is performed by SAES getter at the 30L/min of flow rate during the filling with two 200W pulse tube refrigerators. The recirculation of xenon in liquid phase is also possible at a few L/min (LXe) of flow rate for the purification ,if necessary.

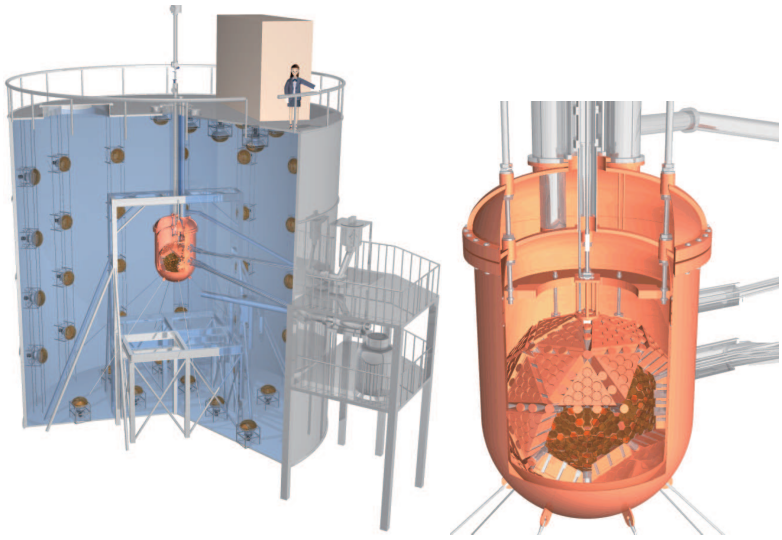

Figure 1: The water tank is used for the radiation shield (Left). The size of the tank is ϕ10 mm $\times$10 m, the detector was installed in the center of it and 20 inch PMTs in the water will be used for the active veto for the cosmic ray events. 850 kg of liquid xenon will be surrounded by 642 ultra low radioactive PMTs. (Right) The double wall detector vessel made of the OFHC is about 1.2 m in inner diameter to hold liquid xenon with the vacuum insulation. The average radius of liquid xenon is about 40 cm.

3 Background and Sensitivity

The key technology to reduce the radioactive background at low energy for XMASS experiment is to use "self-shield" as mentioned above. The clean core of liquid xenon volume will be used as sensitive volume by eliminating the volume near the wall which is suffered from the gamma rays background from the outside. The main component of radioactive background is expected to come from the PMTs. The activity level of PMT is designed to be 1/10 of R8778, giving 0.704 mBq/PMT for uranium-chain, 1.51 mBq/PMT for thorium-chain, <5.1 mBq/PMT for 40K, and 2.92 mBq/PMT for ^{60}Co including the base. The Monte Carlo simulation was performed

to estimate the background from PMTs and its rate is about 0.1 count/day/kg/keV in the active volume and less than 10^{-4} count/day/kg/keV will be achieved by 20 cm fiducial volume cut(100 kg sensitive volume) from the PMT windows.

Requirements for the internal background are ^{238}U $< 10^{-14}$g/g, ^{232}Th $< 2\times10^{-14}$g/g and ^{85}Kr < 1 ppt in liquid xenon. ^{238}U and ^{232}Th daughters in liquid xenon are measured using the Bi-Po coincidence method by the prototype detector. Assuming radioactive equilibrium, ^{238}U is $(9\pm6)10^{-14}$g/g and ^{232}Th is less than 23×10^{-14}g/g. As for ^{85}Kr, 3.3±1.1 ppt was achieved by a distillation tower purification system which was developed by XMASS [2]. These radioactive contaminations are near the goal of requirements, within factor 10. The purification system for the 800 kg detector will be installed for removing radon by the filter which is under studying. The distillation tower for Kr was built to achieve $<$ 1ppt with about 4m length of the tower column and about 1.2 ton of xenon gas was processed in September 2010 for 10 days by this tower.

With 10^{-4} count/day/kg/keV background level, the sensitivity of WIMP-nucleon cross section for the spin independent case will be 10^{-45} cm^2 at 100 GeV/c^2 WIMP mass(Fig.2) for 5 years exposure. This sensitivity is more than one order of magnitude higher than the current best limit by CDMSII and XENON10 as shown in Fig. 2.

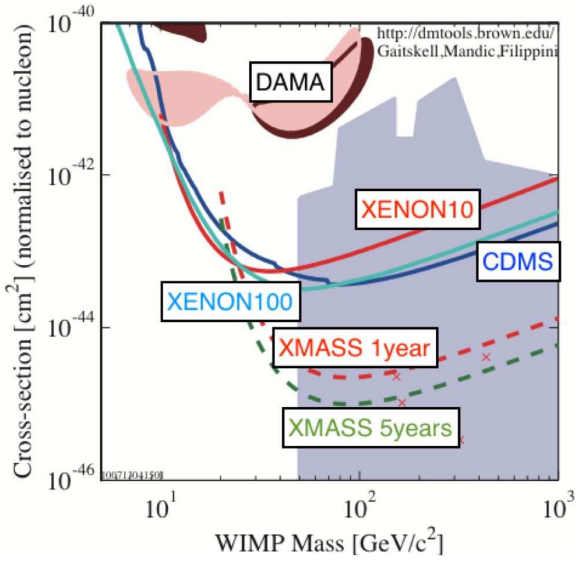

Figure 2: The expected sensitivity of WIMP-nucleus cross section as a function of WIMP mass. For 5 years exposure, the sensitivity will be reach to 10^{-45} cm^2. DAMA/LIBRA [3], CDMSII [4], XENON10 [5] and XENON100 [6] results are also shown here.

4 Conclusion and Summary

The construction of XMASS 800 kg detector was completed in fall, 2010 and the water shield is ready to be used for the active veto for cosmic-rays. After the commissioning run, the data taking will be started in late 2010.

References

[1] Y. Suzuki *et al*, [hep-ph/0008296].

[2] K. Abe *et al.*, Astroparticle Physics **31** (2009) 290.

[3] C. Savage et al., JCAP 0904, 010 (2009).

[4] Z. Ahmed et al., [arXiv:0912.3592].

[5] J. Angle et al. (XENON10), Phys. Rev. Lett. 100, 021303 (2008).

[6] E. Aprile et al. (XENON100), [arXiv:1005.0380].

Latest results of the direct dark matter search with the EDELWEISS-II experiment

Gilles Gerbier[1] *for the EDELWEISS collaboration*

[1]IRFU/SPP, CEA Saclay, , 91191 Gif s Yvette, France

DOI: http://dx.doi.org/10.3204/DESY-PROC-2010-03/gerbier_gilles

The EDELWEISS-II experiment uses cryogenic heat-and-ionization Germanium detectors in order to detect the rare interactions from WIMP dark matter particles of local halo. New-generation detectors with an interleaved electrode geometry were developped and validated, enabling an outstanding gamma-ray and surface interaction rejection. We present here preliminary results of a one-year WIMP search carried out with 10 of such detectors in the Laboratoire Souterrain de Modane. A sensitivity to the spin-independent WIMP-nucleon cross-section of 5×10^{-8} pb was achieved using a 322 kg.days effective exposure. We also present the current status of the experiment and prospects to improve the present sensitivity by an order of magnitude in the near future.

1 The Edelweiss II set up and the detectors

Weakly Interacting Massive Particles (WIMPs) are a class of particles now widely considered as one of the most likely explanation for the various observations of dark matter from the largest scales of the Universe to galactic scales. The collisions of WIMPs on ordinary matter are expected to generate mostly elastic scatters off nuclei, characterised by low-energy deposits (<100 keV) with an exponential-like spectrum, and a very low interaction rate, currently constrained at the level of 1 event/kg/year. Detecting these events requires an ultralow radioactivity environment as well as detectors with a low energy threshold and an active rejection of the residual backgrounds [1].

EDELWEISS-II is a low-background experiment using cryogenic Germanium detectors aiming at the direct observation of the local WIMPs which may constitute the dark matter of our Milky Way. The main EDELWEISS-II setup is located at the Laboratoire Souterrain de Modane (LSM), where the 4800 m water-equivalent rock overburden reduces the cosmic muon flux down to 5 $\mu/\mathrm{m}^2/\mathrm{day}$. Germanium detectors are hosted within a reversed geometry dilution cryostat which may host up to 40 kg of detectors down to 20 mK. A 20 cm thick lead shield surrounds the detectors, with its inner parts made of roman lead, in order to attenuate the external γ/β radioactivity. A 50 cm thick polyethylen shielding protects detectors against the external flux of fast neutrons. A muon veto made of plastic scintillators with a coverage of more than >98% tags neutrons produced by the residual flux of muons which have been interacting mostly in the lead shield. Additional background monitorings are achieved by a Radon level detector near the cryostat, measurements of the thermal neutron flux inside the shielding with a ^{3}He-gas detector, and studies of muon-induced neutrons with a Gd-loaded liquid scintillator outside the shielding.

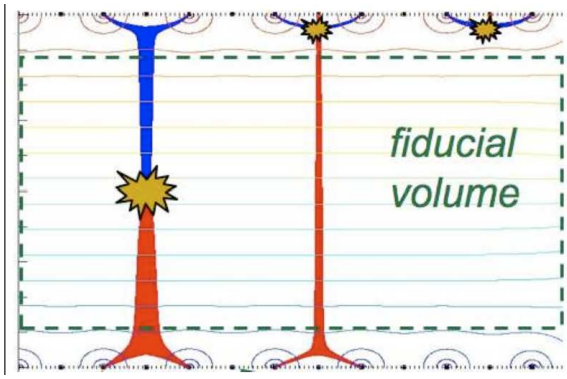

Figure 1: Sectional view illustrating the principle of an ID detector. The interleaved electrodes on the top and bottom of the Germanium crystal create an electric field whose equipotential lines are represented in thin lines. The charge propagation is represented under very simplified assumptions in blue (electrons) and red (holes) for three different interaction positions within the crystal. The distribution of the collected charges in the different electrodes enables to discriminate interactions taking place within the fiducial volume.

EDELWEISS detectors are ultrapure germanium crystals equipped with a dual heat and ionization measurement in order to discriminate induced electronic recoils from potential WIMP induced nuclear recoils, a technology with proven rejection efficiency since the beginning of the 2000s [2]. The heat sensors are NTD thermometers glued on the surface of each detector, while the ionization is measured using electrodes polarized at a few volts. The ionization yield for nuclear recoils is well-measured and is a factor $\sim$3 lower with respect to electron recoils in the energy region of interest, enabling a complete event-by-event discrimination for the bulk of γ-ray radioactivity. However, when an interaction takes place near the surface of the detector, the charge collection is incomplete and difficult to control. In particular, the local radioactivity from residual ^{210}Pb, a daughter of Radon which is present on all surfaces, generates such surface events. Deficit of charge collection can be such that some of them cannot be discriminated from potential WIMP-induced signals.

In order to reject these events, new-generation detectors called "ID" (InterDigit) were developped. The principle of these detectors is shown on Fig. 1 : a set of interleaved electrodes forming concentric rings modifies the electric field topology near the crystal surface, and therefore the repartion of charges induced by near-surface events. This allows to tag specifically near-surface interactions and to define a well-controlled fiducial volume for each detector. Note that this strategy to reject surface backgrounds is different from the one used within the CDMS experiment [3], which relies on the use of more complex phonon sensors.

The discrimination against surface events for ID detectors was experimentally proven at a level of 10^5 using β-ray sources placed in front of a 200 g ID bolometer [4]. Fiducial interactions are selected down to low energies by requiring both a perfect charge balance between the signals of the top and bottom collecting electrodes, and the absence of charge deposits on the field shaping electrodes. This dual rejection provides a strong redundance, and enables the detector operation even when charges cannot be read on one of the field shaping electrodes. The rejection quality was found to be independent of the intensity of the applied voltages.

The fiducial volume of ID detectors may be estimated using a simple electrostatic modelling

of the detectors, and has been also measured in real WIMP-search conditions using the 9.0 keV and 10.3 keV γ-ray lines from the decays of the ^{65}Zn and ^{68}Ge isotopes, homogeneously distributed within the crystals due to cosmogenic activation. Comparing the intensity of these lines before and after the fiducial selection provides a measurement of the fiducial mass : for 400 g ID detectors, this mass is (166±6) g. Simulations show that it is primarily determined by the guard regions that are equipped with independent plain electrodes on the edges of the crystals.

2 WIMP search with one year data

A WIMP search was carried out using ten 400 g ID detectors within the EDELWEISS-II setup, mostly between April 2009 and May 2010. Here we present a preliminary analysis of the full data set, using nine out of the ten bolometers, corresponding roughly to a doubling of the exposure with respect to the first 6 months of WIMP search which were already published in [5].

Stable cryogenic conditions at 18 mK were maintained over the whole year without any major interruption. Around 90% of the electronics channels were working, enabling the use of nine detectors over the ten installed in the cryostat for a first blind WIMP search. External gamma-ray and neutron calibrations were carried out for all detectors. The data was processed using two independent reconstruction pipelines, both of them making use of optimal filtering in order to adapt to the different noise conditions encountered. The average baseline resolutions were of $\sim$ 1.2 keV FWHM for heat channels and $\sim$ 0.9 keV FWHM for ionizations. Baseline noise measurements are used in order to automatically select good periods of data taking, with an 80% efficiency. A χ^2 cut is also applied to reject misreconstructed events. WIMPs are then searched among fiducial events, using the ionization yield to discriminate gamma-rays with a 99.99% rejection efficiency. In order to reject neutron-induced recoils, events in coincidence between bolometers and also with the muon veto are also rejected. Furthermore, a WIMP search energy threshold was also set a priori at 20 keV in this analysis, so that the search efficiency is independent of the energy. After all cuts, an effective exposure of 322 kg$\times$days is obtained. This analysis procedure is strictly identical to the one published in [5].

The WIMP-gamma discrimination diagram obtained after the fiducial cut is presented on Fig. 2(left). Four events are observed in the band, but with a large gap with no event between 23 and 175 keV. Using the standard Yellin prescription [6], this enables to improve the EDELWEISS sensitivity by a factor of 2 with respect to the published limit, as shown on Fig. 2 (right). A limit on the spin independent WIMP-nucleon cross-section of 5×10^{-8} pb is set for a WIMP mass of 80 GeV. A final analysis of this data set is under way, which aims mostly at optimizing the cumulated exposure using our improved knowledge of these new detectors.

From the Fig. 2(left), first hints of a residual background start to appear in the data from these detectors : three events are present in the nuclear recoil band near the analysis threshold, between 20 and 23 keV, while two other outliers are present near the nuclear recoil band at higher energies. Note that all these events are well-reconstructed, and comfortably above the noise level of the detectors. Background studies are currently ongoing to fully understand their origin.

Preliminary upper limits may be derived for the known residual gamma, beta and neutron backgrounds, using calibrations, radioactivity measurements as well as simulations. Overall, less than 1.6 events (90% CL) of known origin are expected for this WIMP search.

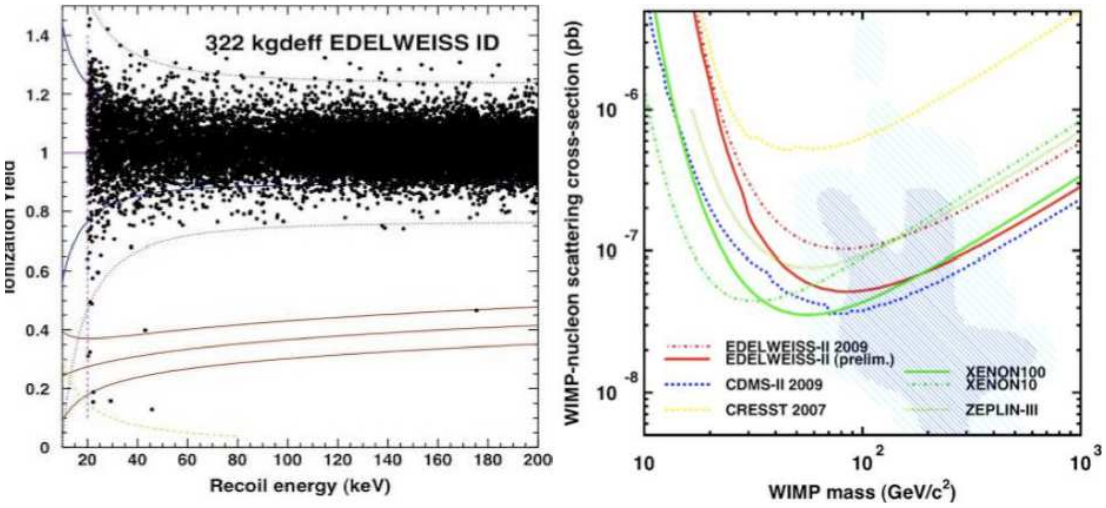

Figure 2: Left: Ionization yield vs energy for all fiducial interactions taking place in a WIMP search corresponding to a 322 kg×days exposure. Right: The corresponding limit on the WIMP-nucleon cross-section (continuous red line) is compared to other experiments.

Figure 3: Picture of an 800 g Full InterDigit bolometer.

3 Improved detectors, prospects

New detectors have been built with interleaved electrodes surrounding the cylindrical part of the crystal, hence their name Full InterDigit (FID). A first series of four 800 g and two 400 g FIDs were built, one of them been shown on Fig. 3. Using the FID design with an unprecedented mass of 800 g, will increase significantly the fiducial mass for a given detector. The currently commissionned 800 g detectors at LSM have six charge readout channels and two NTD sensors, enabling an additional redundancy. After the validation of these "FID800" detectors, it is planned to upgrade several parts of the EDELWEISS-II setup (shieldings, cryostat, cabling) in order to reduce the gamma and neutron backgrounds and lower the energy thresholds. Then 40 such detectors will be installed, allowing to reach a 3000 kg×days exposure within a few months in 2012, with a potential WIMP-nucleon cross-section sensitivity at the level of 5×10^{-9} pb.

As a conclusion, the EDELWEISS collaboration has carried out a one-year WIMP search with new-generation ID detectors. The achieved sensitivity of 5×10^{-8} pb for a WIMP mass of 80 GeV is at the same level as the recently published CDMS and XENON100 sensitivities to the standard neutralino-like WIMP models. Optimized detectors are now on the way to be validated in order to improve the current sensitivity by an order of magnitude within the coming years.

References

[1] K. Nakamura *et al.* [Particle Data Group], "Review of particle physics," J. Phys. G **37** (2010) 075021, see also "Particle Dark Matter", edited by G. Bertone, Cambridge University Press, 2010.

[2] A. Benoit et al., Phys. Lett. B **513** (2001), 15 [arXiv:astro-ph/0106094].

[3] D.S. Akerib et al., Phys. Rev. Lett. **96** (2006), 011302 [arXiv:astro-ph/0509259].

[4] A. Broniatowski et al., Phys. Lett. B **681** (2009), 305 [arXiv:0905.0753].

[5] E. Armengaud et al., Phys. Lett. B **687** (2010), 294 [arXiv:0912.0805].

[6] S. Yellin, Phys. Rev. D **66** (2002) 032005.

Towards a ton scale LAr WIMP Detector

Christian Regenfus on behalf of the ArDM collaboration

Physik-Institut der Universität Zürich, CH–8057 Zürich, Switzerland

DOI: http://dx.doi.org/10.3204/DESY-PROC-2010-03/regenfus_christian

ArDM is a prototype for a ton scale liquid argon WIMP-detector designed to record scintillation light and ionisation charge from recoiling nuclei down to a threshold of 30 keV$_r$. The detector uses the dual-phase principle to suppress background by the charge-to-light ratio, the scintillation time structure, and the topology of individual events. Design and developments of the detector components were strongly driven by scalability. The entire assembly is currently commissioned on surface at CERN. This allows for the test of principle functionalities, implementation of missing components, and preparation for the installation in the underground site. The project is briefly reviewed, with emphasis on selected features of the liquid argon technology.

1 Introduction

Prime candidates for the dark matter in our universe are a unknown kind of stable elementary particles which remained as a cold thermal relic from the big bang, so called weakly interacting massive particles (WIMPs). Their coupling strength to normal matter is estimated from their actual (gravitational) abundance and inferred to be situated at the weak scale. Direct detectability via weak neutrino-like couplings were first calculated in the 1980's [1] and predict nuclear recoils in a earth based detector with a decreasing energy spectrum of up to roughly 100 keV$_r$ depending on the (unknown) WIMP mass, target composition and thermal distribution of the WIMPs (halo models). The cross section of WIMPs is equally unknown. Scattering rates in a ton liquid argon detector are estimated from present searches [2] not to exceed a few recoils per day at a threshold of 30 keV$_r$. This has to be confronted with the background rates present in such a kind of detector. An order of 1 kHz of electronic recoils is expected just from the ^{39}Ar content in natural argon from the atmosphere [3]. However, recently it was demonstrated that argon extracted from liquified dwell gases contains substantially less of this radioactive isotope [4]. Liquid argon is particularly well suited for electronic background discrimination due to its large light and charge yields and the large difference in decay times of the fast and slow scintillation components (ionisation density effect [5]). Furthermore in detectors of the size described here background from neutrons imitating WIMP interactions can be estimated by statistical means [6, 7] from background neutron interaction multiplicities and their energy distributions.

The goal of the ArDM project[8] is to design, assemble and operate a dual-phase ton scale liquid argon detector with independent ionisation and scintillation readout, and to demonstrate the required performance. This is achieved in a staged approach with the upcoming installation of the experiment at the Canfranc underground site in the Pyrenees.

2 Experimental overview

A WIMP interaction in liquid argon leading to a 30 keV$_r$ nuclear recoil produces about 300 VUV photons (128 nm), together with a few ionisation charges, the latter number depending strongly on the strength of the electric field [9]. Recoiling electrons in the same energy range produce about 4 times more light [10] and exhibit several hundreds of ionisation charges. Figure 1 shows the conceptual layout of the experiment with free charges drifting to the top of the detector, while the light is wave shifted on the side walls and reflected down to an array of PMTs at the bottom (diffusion cell design[7]). The vertical electric field (up to 3 kV/cm) prevents some electrons from recombination and sweeps them upwards. It is provided by field shaping ring electrodes coupled to a diode-capacitor charge pump system (Greinacher/Cockroft-Walton circuit) which is fully immersed in the liquid argon [11]. Charges drifting to the interface are extracted into the gas by a strong electric field and swept towards a Large Electron Multiplier (LEM, [12]) and a segmented anode for 2D position reconstruction. The 3D image of the event is obtained by the drift time.

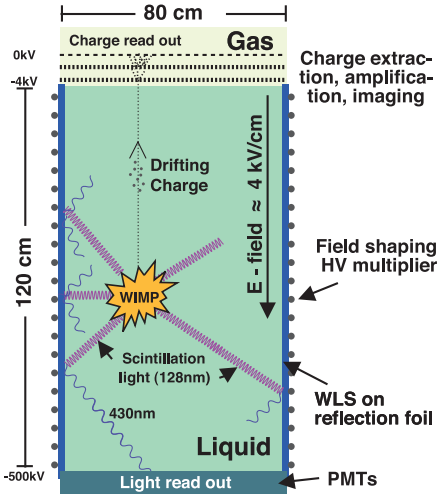

Figure 1: Conceptual design

The 128 nm VUV scintillation light is emitted isotropically from any interaction point in the fiducial volume and converted into blue light (420 nm) by a thin deposit of tetra-phenyl-butadiene (TPB) on Teflon fabric reflector foils (Tetratex). The shifted and reflected light is collected at the bottom of the cryostat by 14 hemispherical 8" photomultiplier tubes immersed in the liquid (Hamamatsu type R5912-02MOD, featuring bialkali photocathodes with Pt underlay). Each PMT is soldered from its leads onto a 3 mm thick printed circuit board providing both the mechanical footing and the voltages for cathode and dynodes by means of passive electronic components. A TPB deposition on the PMT surface is also performed to improve direct VUV light detection. To optimise the performance of the light readout in ArDM, a range of reflectors and TPB deposition combinations were investigated in small setups, where argon scintillation light was generated by radioactive sources in gas at normal temperature and pressure. Detailed descriptions of the developments for the light readout system can be found in [13, 14, 15]. The current choice of main reflectors consists of 254 μm thick Tetratex foils which have nearly 100% diffuse Lambertian reflectance. A coating density of 1 mg/cm^2 of TPB was evaporated onto these foils and 0.05 mg/cm^2 onto the glass windows for the PMTs.

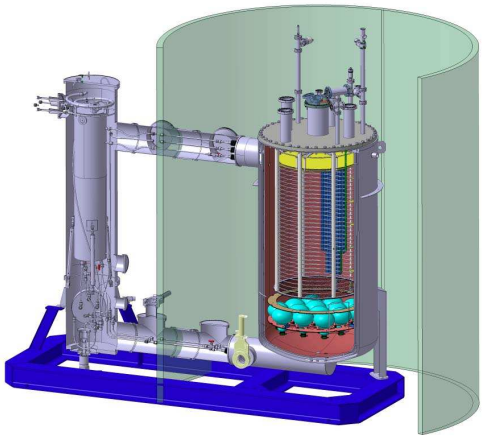

Figure 2: Experimental setup

Presently a 1400 kg (850 kg fiducial) LAr vessel is installed on the surface at CERN. Figure 2 shows the 3D sketch of the main components of this setup. The liquid argon in the fiducial

volume (right dewar) is conditioned by a cryogenic purification system (left dewar) separated from the detector to allow for insertion of a neutron shield (indicated by the open cylinder).

So far two test runs were performed, one in single-phase light collection mode and very recently also a second one in double-phase mode with charge extraction and collection on a prototype anode. The surface operation is needed to systematically test all functionalities, complete and upgrade subcomponents and prepare the whole experiment for its final installation in an underground location where physics runs under low cosmogenic background conditions can be performed. Some results and conclusions from the first test run are briefly discussed in the following chapter, while data from the double-phase operation is still under analysis.

3 Recent achievements

A first four weeks engineering run with liquid argon took place in May 2009 dedicated to explore the operational parameters of the system and to test a preliminary light readout setup of 7 PMTs. The run was preceded by a careful assessment of the requirements of the cryogenic system and the related safety issues. A first brief review on results can be found in [20] and a more comprehensive review in [21].

A main point of interest was at first the cleanliness of the setup. Despite a not yet operative recirculation system, good and stable purity of the liquid argon was observed in terms of scintillation yields. From the measured life time τ_2=1.54 μs of the slow scintillation component (triplet excimer states [1]), an upper limit for N_2 and O_2 impurities of 0.1 ppm was estimated (see [22, 23] for details). Hence we found the detector satisfactorily tight and clean.

Further important point of study was the light readout system in respect to yield and energy threshold. As mentioned above only 7 out of 14 Hamamatsu cryogenic PMTs were installed in this first evaluation run. No problems were found in operating the devices at liquid argon temperature. All dark count rates were in the expected ranges ($<$ 10 kHz). Gain fluctuations over the four weeks of cryogenic operation were smaller than 15% and seemed to be correlated on all 7 devices. The exact source could not be identified but probably was due to small temperature or pressure fluctuations. The gain of each PMT is monitored offline from single photons in the event tails and corrected for in the data. The light yield was determined by measuring the response of the detector to photons from radioactive line sources (e.g. ^{22}Na). For this purpose source spectra recorded at different heights were compared to the corresponding spectra from GEANT4 Monte Carlo simulations. Considerable effort was put in the buildup of a modular software framework for data reconstruction and these simulation (all based on C++). Finally using only a handful of common parameters the MC spectra were describing the measured spectra in all regions better than 10% (see [21] for details).

Wave shifting efficiency ($\approx$ 100%), the diffuse reflection coefficient (95%) and the quantum efficiency of the PMTs (18.5 - 22%) were all consistent with values found during the development of the light readout components [14, 15]. A final light yield of just under 1 p.e./keV$_{ee}$ was estimated for the detector with no electric field, a complete set of PMTs and the LEM installed. Since the light yield for nuclear recoils is lower due to quenching, typically 25% that for electrons in the few 10 keV range [10], we expect from these measurements to detect 30 keV$_r$ nuclear recoils with an average signal of 6 photoelectrons and a resolution of about 40%. For completeness, the energy distribution for events passing trigger conditions of at least two coincident photoelectrons within 10 ns shows that reconstructing events down to a few 10th of keV is feasible.

[1] The literature value for the life time of the triplet excimer state in liquid argon is $\approx$1.6μs

4 Scintillation light R&D in liquid argon

The interaction of particles with liquid argon is governed by a complex interplay of collisions, excitation and ionisation of argon atoms, recombination of charges and ions, as well as the formation of molecular states (excimers) with possible collisions among the participating partners at different stages in the temporal evolution of the interactions. The yields for the final observables, scintillation light and ionisation charge, are not known very precisely for low energy nuclear recoils and are difficult to determine. For this reason we investigate these numbers and their statistical behaviour by means of a monochromatic neutron source at a small liquid argon cell in one of our laboratories at CERN [16]. This research project also contains the development of methods for data reconstruction and Monte Carlo simulations. The project forms part of the development program of the european consortium DARWIN, a design study for a next generation multiton liquid Xe and Ar facility [17].

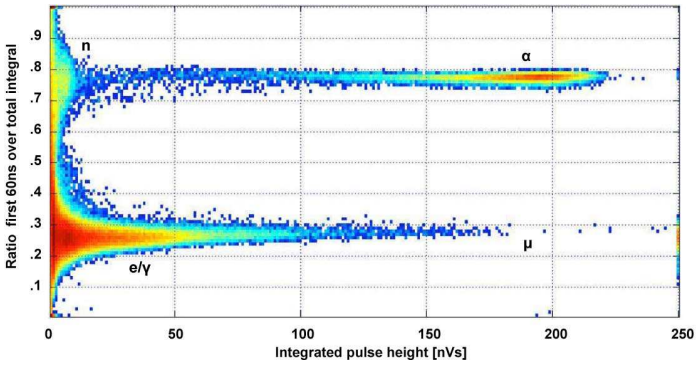

Figure 3: Pulse shape variable versus light yield in LAr

As an example fig. 3 shows the effect of different ionisation densities (pulse shapes) from data taken in a small liquid argon cell in the laboratory with different radioactive sources. Two characteristic bands of high and low ionisation density events can be identified as nuclear and electronic recoil bands [2]. Shown is the fraction of the prompt ($\leq$50 ns) to the total light for interactions created by scattered neutrons or alpha particles in the upper branch and scattered photons or muons in the lower branch respectively (pulse shape separator). Using a likelihood based discrimination method a minimum value of about 10^3 was achieved to suppress electronic recoil events from the nuclear recoil band for E_r>30 keV$_r$ in a test chamber in the laboratory [18, 19]. Our task is to optimise these methods for the case of a large liquid argon target as is the case for ArDM.

5 Outlook

Further work will be performed to complete the detector with the final charge readout and another test run on the surface is planned for the upcoming months. However many parameters to be tested now require low background environmental conditions and will be carried out after installation in the underground location.

Acknowledgements

This work was supported by ETH Zürich, the University of Zürich, and the Swiss National Science Foundation (SNF).

[2] apparently α-particles exhibit the same pulse shape as nuclear recoils (under study)

References

[1] M. Goodman and E. Witten, *Detectability of certain dark-matter candidates, weak neutrino-like couplings*, Phys. Rev. D **31**, 3059 (1985)

[2] K. Nakamura *et al.* (Particle Data Group), *The Review of Particle Physics*, J. Phys. G **37**, 075021 (2010)

[3] P. Benetti *et al.*, *Measurement of the specific activity of ^{39}Ar in natural argon*, NIM A **574** 83 (2007)

[4] D.-M. Mei *et al.*, *Prediction of Underground Argon Content for Dark Matter Experiments*, arXiv:0912.5368v1 [nucl-ex] (2009)

[5] A. Hitachi *et al.*, *Effect of ionization density on the time dependence of luminescence from liquid argon and xenon*, Phys. Rev. B **27** 9 5279 (1983)

[6] L. Kaufmann, *Detector Performance and Background Studies for the ArDM Experiment*, PhD thesis, ETH Zürich (2008)

[7] C. Regenfus, *The Argon Dark Matter Experiment (ArDM)*, Proceedings of the 4th Patras workshop on Axions, WIMPs and WISPs, DESY Hamburg Germany, DESY-PROC-2008-02 (2008)

[8] A. Rubbia, *ArDM: A ton-scale liquid argon experiment for direct detection of dark matter in the universe*, J. Phys. Conf. Ser. **39** 129 (2006)

[9] R. Chandrasekharan, *Design of the Light Readout for the ArDM Experiment*, PhD thesis, ETH Zürich No. 16985 (2006)

[10] D. Gastler *et al.*, *Measurement of scintillation efficiency for nuclear recoils in liquid argon*, arXiv:1004.0373v1 [physics.ins-det] (2010)

[11] S. Horikawa *et al.*, *Feasibility of high-voltage systems for a very long drift in liquid argon TPCs*, arXiv:1009.4908v1 [physics.ins-det] (2010)

[12] P. Otyugova, *Development of a LEM based Charge Readout System for the ArDM Experiment*, PhD thesis, ETH Zürich No. 17704 (2008)

[13] C. Regenfus, *Detection of VUV scintillation light in one ton of liquid argon*, Proceedings of the 6th Int. workshop (IDM2006) Rhodes, Greece, p. 325, World Scientific (2007)

[14] V. Boccone et al., *Development of wavelength shifter coated reflectors for the ArDM argon dark matter detector*, JINST **4** P06001 (2009)

[15] V. Boccone, *Development of the Light Readout for the ArDM Dark Matter Search*, PhD thesis, UZH Zürich (2010)

[16] see: `http://cern.ch/regenfus/zunf.htm`

[17] see: `http://darwin.physik.uzh.ch`

[18] W. Lippincott *et al.*, *Scintillation time dependence and pulse shape discrimination in liquid argon*, Phys. Rev. C **78** 035801 (2008)

[19] W. Lippincott *et al.*, *Erratum: Scintillation time dependence and pulse shape discrimination in liquid argon*, Phys. Rev. C **81** 039901(E) (2010)

[20] C. Regenfus, *The Argon Dark Matter Experiment*, Proceedings of TAUP2009, arXiv:0912.2962v1 [phys.ins-det] (2009)

[21] C. Amsler *et al. First results on light readout from the 1-ton ArDM liquid argon detector for dark matter searches*, JINST **5** P11003 (2010)

[22] C. Amsler *et al. Luminescence quenching of the triplet excimer state by air traces in gaseous argon*, JINST **3** P02001 (2008)

[23] R. Acciarri *et al. Effects of nitrogen and oxygen contaminations in liquid argon*, NIM A **607** 169 (2009)

XENON100

Uwe Oberlack[1] *and Marc Schumann*[2] *for the XENON100 collaboration*

[1]Institute of Physics, Johannes Gutenberg University Mainz, D-55128 Mainz, Germany,
[2]Physics Institute, University of Zürich, CH-8057 Zürich, Switzerland

DOI: http://dx.doi.org/10.3204/DESY-PROC-2010-03/oberlack_uwe

The XENON100 Dark Matter experiment, installed in the Laboratory Nazionali del Gran Sasso (LNGS, Italy), is searching for WIMP type Dark Matter particles scattering off a 62 kg liquid xenon target in a dual phase (liquid/gas) time projection chamber. The analysis of 11.2 live days of background data taken during a commissioning run in fall 2009 leads to the first science result of XENON100: No events are observed in a pre-defined fiducial volume of 40 kg mass, excluding spin-independent WIMP-nucleon scattering cross sections above 3.4×10^{-44} cm^2 (at 100 GeV/c^2). Below 80 GeV/c^2, this is the most sensitive exclusion limit so far, constraining the interpretation of DAMA and CoGeNT being due to spin-independent, elastic interactions of light mass WIMPs.

1 Introduction

Indirect astronomical observations at all cosmological length scales suggest that a large amount of the matter content of the Universe is dark, i.e. invisible over the whole electromagnetic spectrum [1]. There are strong indications that this Dark Matter is made up from yet-unknown, heavy, non-relativistic (cold) particles that build large scale cosmological structures. A well motivated candidate is the WIMP (Weakly Interacting Massive Particle), a stable particle arising naturally in many theories beyond the Standard Model, such as supersymmetry or theories with extra dimensions [2].

In experiments, WIMPs are expected to interact with the target nuclei (nuclear recoil interactions) because they are neutral, whereas the main background comes from electromagnetic interactions of gammas and electrons with the atomic electrons (electronic recoil interactions). From the assumed WIMP mass and velocity distribution one expects to measure a steeply falling, featureless nuclear recoil spectrum at energies of a few keV only. The predicted rates are tiny, much less than one interaction per kg and day of exposure. Therefore, the experiments have to reduce their background as much as possible in order to be sensitive to WIMPs.

2 XENON100

The XENON collaboration uses liquid xenon (LXe) as target material. Xenon is a heavy target ($A \sim 131$) which enhances the sensitivity for spin-independent WIMP-nucleon scattering. Being an efficient scintillator ($\lambda = 178$ nm), xenon also serves as detector material. It's high density ($\rho \sim 3$ g/cm^3) allows to build compact detectors with excellent self shielding capabilities. Furthermore, xenon has no long-lived radioactive isotopes, and small admixtures of the

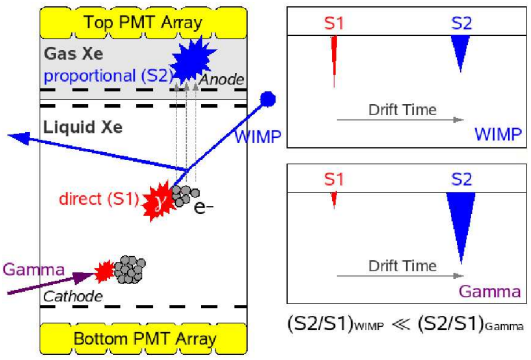

Figure 1: Double-phase LXe TPC: An interaction generates prompt scintillation light (S1) and ionizes the target. The ionization electrons are drifted upwards and extracted into the gas phase where they generate proportional scintillation (S2). The S2 light pattern, together with the drift time of the electron cloud, is used to reconstruct the event vertex. The S2/S1 ratio differs for nuclear and electronic recoil interactions and is used for signal/background discrimination.

radioactive ^{85}Kr can be removed to the ppt level [3].

Liquid xenon detectors provide 3-dimensional interaction vertex reconstruction and signal to background discrimination when operated as a dual-phase (liquid/gas) time projection chamber (TPC), see Fig. 1: An interaction in the LXe generates prompt scintillation light (the S1 signal) and ionizes the target. The ionization electrons are drifted towards the liquid gas interface by a strong electric field. Here, the electrons are extracted into the gas phase and accelerated towards the anode while generating proportional scintillation light (S2). Both signals, S1 and S2, are detected by two arrays of photosensors, one immersed in the liquid for optimal light collection, and one located in the gas phase above the target. The position of the interaction can be reconstructed using the S2 signal distribution on the top array (x, y) and the time difference between prompt S1 and delayed S2 signal (z). Due to their different track densities in the medium, the ratio S2/S1 can be used to discriminate between signal (nuclear recoil interactions) and background (electronic recoils).

XENON100 is the current detector at the 100 kg scale within the phased program of the XENON collaboration. It follows the XENON10 phase which has proven that liquid xenon detectors are able to deliver very competitive results [4]. XENON100 has a total mass of 161 kg of LXe, out of which 62 kg are in the cylindrical target volume which is viewed by two arrays of Hamamatsu R8520 photomultipliers from above (98 PMTs) and below (80 PMTs). The remaining 99 kg of LXe are surrounding the target in 4π. This volume is instrumented with another 64 PMTs and acts as an active veto. The whole detector is installed inside a passive shield in order to reduce the background from ambient gamma rays and neutrons.

Background All materials considered for XENON100 were screened with high purity germanium spectrometers in order to determine their intrinsic radioactivity. Only materials with a reasonable radioactivity were accepted for the detector construction. All measured radioactivity values are used as input parameters for a detailed Monte Carlo model of the detector and the result of the simulation agrees remarkably well with the measured background spectrum over the full energy range [6]. In a fiducial volume of 30 kg mass, XENON100's background rate in the low energy range is 5.3×10^{-3} events keVee^{-1}kg^{-1}day^{-1} (electron recoil equivalent energy) when the active LXe veto is employed. This is a factor 100 lower than XENON10, thus achieving one of the design goals of XENON100. In fact, XENON100 is currently the experiment with the lowest background level of all running dark matter detectors, more than two orders of magnitude below any other experiment at low energies.

Data Analysis and Result XENON100 is installed underground at Laboratori Nazionali del Gran Sasso (LNGS, Italy) since spring 2008. After extensive calibrations and studies to characterize the detector response, first science data has been taken in fall 2009. This article summarizes the results of this run, which have been published in [5].

In order to use the $\log_{10}$(S2/S1) parameter to discriminate between electronic and nuclear recoils, the low energy response of the detector to these interactions was calibrated using the Compton continuum of ^{60}Co and elastic neutron interactions from an ^{241}AmBe source, respectively. The two populations are well separated and lead to a discrimination of $> 99\%$ at 50% nuclear recoil acceptance.

Based on the cut acceptance and the expected recoil spectrum from WIMPs, the energy region of interest for the first Dark Matter analysis has been chosen from 4–20 PE (S1 signal). This region has to be converted to a nuclear recoil equivalent energy scale (given in keVnr) which takes into account the reduced scintillation yield for nuclear recoil interactions ("quenching"). This conversion is based on the measurement $\mathcal{L}_{\text{eff}}$(keVnr) of the scintillation efficiency of nuclear recoils relative to interaction of 122 keV gamma rays, measured by various groups in dedicated experiments. However, at low energies the results differ more than expected from the stated error bars. For a recent discussion of the systematics of these measurements, see [7]. Therefore, we have chosen to employ a statistical approach to this data to derive a best fit description (with a flat extrapolation below 5 keVnr) and a lower 90% CL-contour (with a conservative logarithmic extrapolation). We give our results for both cases in order to reflect the current uncertainties.

The data leading to the first XENON100 results were taken in stable conditions in October and November 2009. Altogether 11.2 life days of data have been used for the analysis. The data has not been blinded, however, the analysis has been performed in a quasi-blind way and all cuts and selections were developed on calibration data only.

The WIMP search region between 4 and 20 PE corresponds to 8.7–32.6 keVnr (best fit $\mathcal{L}_{\text{eff}}$).

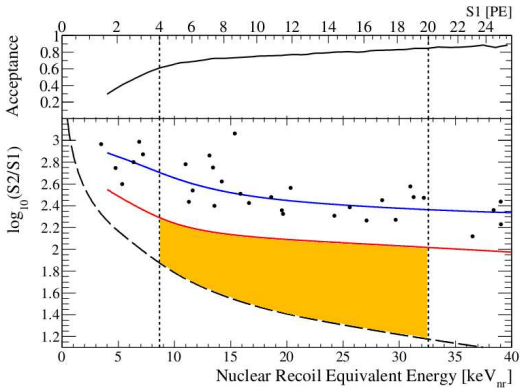

Figure 2: In $\log_{10}$(S2/S1) space, used for discrimination between signal and background, all remaining events are well above the nuclear recoil median (red). No event falls in the predefined WIMP search region (yellow).

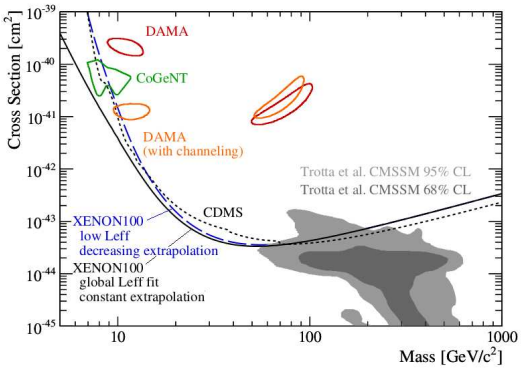

Figure 3: The limit on the spin independent WIMP-nucleon cross section derived from the first XENON100 data. The exclusion plot shows the 90% CL exclusion contours for the two $\mathcal{L}_{\text{eff}}$ cases described in the text.

The upper bound in $\log_{10}$(S2/S1) space was the median of the nuclear recoil band from the neutron calibration, the lower bound a software threshold of S2 > 300 PE. A simple cylindrical fiducial volume with 40 kg of xenon was chosen for this analysis, and < 0.2 background events were expected in this volume for the given exposure.

Only events with a single S2 peak (single scatter events) were selected for the WIMP analysis, since the interaction probability of WIMPs is far too small to scatter in the detector twice.

The positions of the events remaining in the fiducial volume in $\log_{10}$(S2/S1) space are shown in Fig. 2. All events are well separated from the WIMP search region. This figure is the most remarkable result of this analysis: It demonstrates that LXe detectors can be indeed used for background-free WIMP searches. The upper part of Fig. 2 gives the energy dependent acceptance function not taking into account the 50% acceptance from $\log_{10}$(S2/S1)-based electronic recoil discrimination.

Fig. 3 shows the limits from this analysis, calculated for the two choices of $\mathcal{L}_{\text{eff}}$ as discussed above, assuming an isothermal WIMP halo. The acceptance-corrected exposure, weighted by a spectrum of a 100 GeV/c^2 WIMP, is 172 kg×days. For WIMP masses below 80 GeV/c^2, this result places the lowest limit so far. At light WIMP masses, DAMA [8] and CoGeNT [9] are constrained even assuming the conservative $\mathcal{L}_{\text{eff}}$.

3 Outlook

The previous section summarized the first Dark Matter results of XENON100, derived from 11.2 life days of data taken during a commissioning run in fall 2009 [5]. In the meantime, about 10× more science data has been acquired and a blind analysis is ongoing. The ultimate sensitivity of XENON100 for spin-independent WIMP-nucleon scattering, based on the background predictions from Monte Carlo simulations, is $\sigma = 2 \times 10^{-45}$ cm^2 (at 100 GeV/c^2) for an exposure of 200 life days and a fiducial mass of 30 kg.

The XENON collaboration is already in the design phase for XENON1T: This future detector will employ a LXe double-phase TPC with a fiducial mass of 1000 kg in a large water Cherencov muon veto to achieve a sensitivity of a few 10^{-47} cm^2. A large fiducial volume cut, together with careful material selection and LXe purification, will further decrease the background by a factor 100 in order to explore the WIMP parameter space down to lower cross sections than XENON100, or to confirm a possible WIMP detection.

References

[1] K. Nakamura et al. (Particle Data Group), *J. Phys.* **G 37**, 075021 (2010) and references therein.

[2] G. Bertone G (ed.), *Particle Dark Matter*, Cambridge University Press, Cambride (2010).

[3] K. Abe et al. (XMASS), *Astropart. Phys.* **31**, 290 (2009).

[4] J. Angle et al. (XENON10), *Phys. Rev. Lett.* **100**, 021303 (2008);
J. Angle et al. (XENON10), *Phys. Rev. Lett.* **101**, 091301 (2008).

[5] E. Aprile et al. (XENON100), *Phys. Rev. Lett.* **105**, 131302 (2010),

[6] E. Aprile et al. (XENON100), `arXiv:1101.3866` (2011).

[7] A. Manalaysay, `arXiv:1007.3746` (2010).

[8] C. Savage et al., *J. Cosmol. Astropart. Phys.* **4**, 10 (2009).

[9] C.E. Aalseth et al. (CoGeNT) `arXiv:1002.4703` (2010).

Chapter 5

Indirect detection of WIMPs

Indirect Detection of WIMPs: Principles and Techniques

Christopher Savage[1]

[1]The Oskar Klein Centre for Cosmoparticle Physics, Department of Physics, Stockholm University, AlbaNova, SE-10691 Stockholm, Sweden

DOI: http://dx.doi.org/10.3204/DESY-PROC-2010-03/savage_christopher

The various main methods for indirectly inferring the presence of Weakly Interacting Massive Particles (WIMPs) as the unknown dark matter in the universe are examined. Indirect detection techniques include detecting cosmic-ray contributions from WIMP annihilation in the galactic halo, particularly in the positron, anti-proton, and gamma-ray spectra. WIMPs can also be captured in massive bodies such as stars, producing neutrinos or, in more extreme cases, modifying the luminosity or evolution of the star, both of which provide additional means of indirectly detecting the presence of WIMPs.

1 Introduction

The unknown dark matter in the universe could be composed of a new, massive stable particle; just such a particle with weak-scale coupling would freeze out during the early universe with a relic density of the right scale to account for the dark matter. There are theoretically motivated candidates for these Weakly Interacting Massive Particles (WIMPs), such as a Dirac neutrino and, perhaps one of the most favored dark matter candidates, the neutralino found in many supersymmetric theories [1].

There are three general areas in which WIMPs as dark matter can be probed. They can be produced in accelerators such as the Large Hadron Collider; interactions of relic WIMPs with ordinary matter can be directly observed in a detector (direct detection); or WIMPs can be more indirectly inferred, primarily through detecting the products or impact of relic WIMPs that annihilate elsewhere, such as in the galactic halo or in stars. Here, we examine the principles and techniques behind the most common methods for indirectly detecting WIMPs. Experimental results for indirect detection can be found elsewhere in these proceedings.

We break down the indirect detection methods into two areas: observation of cosmic-rays created by WIMP annihilations in galactic halos (Sec. 2) and signatures from WIMP capture in massive bodies such as stars (Sec. 3).

2 Cosmic rays

Annihilation of WIMPs in the dark matter halo produces high energy particles that contribute to various cosmic-ray spectra; observation of these high energy particles would be an indication of WIMP dark matter [2]. However, many other sources of cosmic rays exist, not all of which

are well understood or modelled. These backgrounds present difficulties in identifying any high energy particles as arising from WIMP annihilations. Some of the clearest expected signatures of WIMP annihilations in light of these backgrounds are unique features that might arise in the positron, anti-proton, and gamma-ray spectra. In the case of gamma-rays, which do not diffuse under the galactic magnetic field as do the positrons and anti-protons, the direction the gamma-rays arrive from indicates where they were produced; the mapping of gamma-ray sources provides another possible means to detect WIMP annihilations as WIMP annihilations can occur with a different spatial distribution than background sources.

2.1 Positrons

Positron backgrounds are mainly secondaries from cosmic-ray collisions with interstellar matter that is expected to produce a smooth continuum for the positron flux spectra. Annihilation of WIMPs directly to electrons and positrons would provide a sharp peak (broadened by propagation effects) in the spectrum that is at odds with the expected background and would provide a clear signature for WIMPs. However, direct annihilation to positrons is typically loop suppressed and is not expected to be a significant decay channel. Annihilation of WIMPs to W's, however, will lead to a broader peak from the leptonic W decays. This peak should provide an observable WIMP signature above the background continuum. Other annihilation channels can also produce positrons, but these channels generally give a continuum spectrum not distinguishable from the background. The positron spectrum is examined by experiments such as HEAT [3] and PAMELA [4].

2.2 Anti-protons

Anti-proton backgrounds are also mainly secondaries from cosmic-ray collisions with interstellar matter, producing a smooth continuum. However, collisions energetic enough to produce anti-protons are unlikely to produce low speed anti-protons (kinetic energies of $\sim$1 GeV or less) due to a kinematic suppression, so the background spectrum is expected to fall rapidly at low energies. Anti-protons produced during hadronization processes of WIMP annihilations are expected to also yield a continuum spectrum; however, low energy anti-protons are not suppressed in this production mechanism. Thus, an anti-proton spectrum that does not fall at low energies would provide a signature for WIMPs. The anti-proton spectrum is examined by experiments such as BESS [5], CAPRICE [6], and AMS [7].

2.3 Gamma-rays

Unlike the positrons and anti-protons, gamma-rays are uncharged and travel mainly unimpeded from their source to a gamma-ray detector. Thus, in addition to the gamma-ray flux spectrum, the spatial distribution of gamma-ray sources can be used to identify WIMP cosmic-ray contributions. The background spectrum for gamma-rays is expected to be a continuum only. Annihilation of WIMPs directly to gammas or a gamma + Z will produce a mono-energetic peak or a peak + continuum, respectively, though both annihilation channels are usually loop suppressed and not significant. Internal bremsstrahlung processes will provide a hard spectrum that can also offer a signature for WIMPs. Other channels that produce gammas produce a continuum similar to the background. The spatial resolution for gamma-rays allows spectra to be observed from different sources. The backgrounds depend on the observational target. The

galactic center, with its high WIMP density, should produce a high signal, but the backgrounds are also expected to be high there. Dwarf galaxies and subhalos, on the other hand, would have a much smaller signal, but the backgrounds would also be low (possibly giving a better signal-to-noise ratio). In addition, spatial variations in the spectra can provide further mechanisms for extracting WIMP contributions to cosmic rays. Gamma-rays are examined by experiments such as EGRET [8], HESS [9], and Fermi [10].

3 Capture in massive bodies

WIMPs can become captured within massive bodies such as stars and planets, primarily through scattering off of nuclei, providing several possible signatures of WIMP dark matter. The process proceeds as follows: WIMPs within the dark matter halo of a galaxy will pass through a star (or planet), occasionally scattering off of a nucleus. Some WIMPs that undergo such scatters will lose enough energy that they become gravitationally bound to the star. Subsequent orbits through the star will lead to additional scatters and loss of energy, resulting in the WIMP that falls towards to the center of the star. As a population of such WIMPs grows at the center of the star, they will annihilate with each other, producing (most significantly) neutrinos and heat. The former (neutrinos) can pass through the star and possibly be observed by a neutrino detector if the source is close enough. The latter (heat) can lead to several observable effects, depending on the circumstances, from changes in the chemical abundances in a star, moderate increases in the stellar luminosity, to a wholesale change in a star's formation and evolution.

3.1 Neutrinos from the Sun/Earth

The Sun and Earth are the only two massive bodies near enough that the neutrino flux from WIMP annihilations at their centers could potentially be detected [11]. Of these two bodies, the Sun is expected to provide a more easily detected flux of neutrinos as the small size of the Earth leads to a small capture rate with the further issue that the small capture rate typically requires a period much longer than the age of the Earth for a large enough population of WIMPs to accumulate at the center to efficiently annihilate. The Sun, however, is likely to have accumulated enough WIMPs at its center that the annihilation rate has come to equilibrium with the capture rate and the population size has become stable. Searches for WIMP annihilation neutrinos from the Sun and Earth are (or will be) undertaken by neutrino detection experiments such as Super-Kamiokande [12], IceCube/DeepCore [13], and ANTARES [14].

3.2 WIMP burners and dark stars

At the galactic center, where the WIMP density (and therefore capture rate) increases, the heat from the annihilations in the center of a star might be significant enough to increase the luminosity or modify the evolution of a star; such objects are referred to as "WIMP burners" [15]. The effects are expected to be most notable in smaller, dimmer objects such as white dwarfs or low mass stars that are in close orbits around the galaxy's central black hole. In the case of white dwarfs, the relative boost in luminosity could be large; in addition, white dwarfs in eccentric orbits about the black hole could have a luminosity that varies as they pass through regions of higher and lower WIMP densities. Low mass main sequence stars near the black hole might achieve longer lifetimes and undergo a modified track in the HR diagram.

In the early universe, the first protostellar halos collapsed to produce the population III stars. Adiabatic contraction of these halos would lead to high dark matter densities. In the case of WIMPs, the increased density would lead to WIMP annihilations. For high enough densities, the heat from the annihilations would halt the collapse of the baryons before the baryon densities were sufficient to begin the nuclear fusion process. The result would be a massive, stable body ("dark star") powered by WIMP annihilation instead of fusion [16]. Even after the dark matter density is depleted enough to allow the star to further collapse and initiate fusion, WIMP annihilation can contribute a large amount of energy for a long period of time, significantly altering the evolution of these population III stars. These stars may be more massive, have a different luminosity versus temperature relationship, and be far longer lived than standard population III stars. These early universe objects may be observable by the Hubble and James Web Space Telescopes.

Acknowledgments

CS is grateful for financial support from the Swedish Research Council (VR) through the Oskar Klein Centre and thanks A Putze for useful discussions.

References

[1] G. Jungman, M. Kamionkowski and K. Griest, Phys. Rept. **267**, 195 (1996) [arXiv:hep-ph/9506380].

[2] J. Silk and M. Srednicki, Phys. Rev. Lett. **53**, 624 (1984); J. R. Ellis, R. A. Flores, K. Freese, S. Ritz, D. Seckel and J. Silk, Phys. Lett. B **214**, 403 (1988); V. Berezinsky, A. Bottino and G. Mignola, Phys. Lett. B **325**, 136 (1994) [arXiv:hep-ph/9402215]; P. Gondolo and J. Silk, Phys. Rev. Lett. **83**, 1719 (1999) [arXiv:astro-ph/9906391].

[3] S. Coutu *et al.*, Astropart. Phys. **11**, 429 (1999) [arXiv:astro-ph/9902162].

[4] O. Adriani *et al.* [PAMELA Collaboration], Nature **458**, 607 (2009) [arXiv:0810.4995 [astro-ph]].

[5] T. Maeno *et al.* [BESS Collaboration], Astropart. Phys. **16**, 121 (2001) [arXiv:astro-ph/0010381].

[6] M. Boezio *et al.* [WiZard/CAPRICE Collaboration], Astrophys. J. **561**, 787 (2001) [arXiv:astro-ph/0103513].

[7] M. Aguilar *et al.* [AMS Collaboration], Phys. Rept. **366**, 331 (2002) [Erratum-ibid. **380**, 97 (2003)].

[8] S. D. Hunter *et al.*, Astrophys. J. **481**, 205 (1997).

[9] F. Aharonian *et al.* [H.E.S.S. Collaboration], Phys. Rev. Lett. **97**, 221102 (2006) [Erratum-ibid. **97**, 249901 (2006)] [arXiv:astro-ph/0610509].

[10] A. A. Abdo *et al.* [Fermi LAT Collaboration], Phys. Rev. Lett. **103**, 251101 (2009) [arXiv:0912.0973 [astro-ph.HE]].

[11] J. Silk, K. A. Olive and M. Srednicki, Phys. Rev. Lett. **55**, 257 (1985); K. Freese, Phys. Lett. B **167**, 295 (1986).

[12] S. Desai *et al.* [Super-Kamiokande Collaboration], Phys. Rev. D **70**, 083523 (2004) [Erratum-ibid. D **70**, 109901 (2004)] [arXiv:hep-ex/0404025].

[13] J. Ahrens *et al.* [IceCube Collaboration], Astropart. Phys. **20**, 507 (2004) [arXiv:astro-ph/0305196]; C. Wiebusch and f. t. I. Collaboration, arXiv:0907.2263 [astro-ph.IM].

[14] E. Aslanides *et al.* [ANTARES Collaboration], arXiv:astro-ph/9907432.

[15] P. Salati and J. Silk, Astrophys. J. **338**, 24 (1989); I. V. Moskalenko and L. L. Wai, Astrophys. J. **659**, L29 (2007) [arXiv:astro-ph/0702654]; M. Fairbairn, P. Scott and J. Edsjo, Phys. Rev. D **77**, 047301 (2008) [arXiv:0710.3396 [astro-ph]].

[16] D. Spolyar, K. Freese and P. Gondolo, Phys. Rev. Lett. **100**, 051101 (2008) [arXiv:0705.0521 [astro-ph]]; F. Iocco, Astrophys. J. **677**, L1 (2008) [arXiv:0802.0941 [astro-ph]]; K. Freese, D. Spolyar and A. Aguirre, JCAP **0811**, 014 (2008) [arXiv:0802.1724 [astro-ph]].

Understanding Cosmic Rays and Searching for Dark Matter with PAMELA

Roberta Sparvoli[1,2]*, for the PAMELA Collaboration*

[1]University of Rome "Tor Vergata", Rome, Italy
[2]INFN Section of Rome "Tor Vergata", Rome, Italy

DOI: http://dx.doi.org/10.3204/DESY-PROC-2010-03/sparvoli_roberta

After four years of data taking in space, the experiment PAMELA is showing very interesting features in cosmic rays that might change our basic vision of their mechanisms of production, acceleration and propagation in the galaxy. In addition, PAMELA measurements of cosmic antimatter fluxes are setting strong constraints to the nature of dark matter. In this paper PAMELA main results will be briefly reviewed.

1 PAMELA physics goals and instrument description

PAMELA was conceived as a cosmic ray observatory placed at 1 Astronomical Unit; its 70 degrees, 350–610 km quasi–polar elliptical orbit, indeed, makes it particularly suited for studying cosmic rays of galactic, heliospheric and trapped nature.

PAMELA best capabilities are expressed in the high–precision spectral measurement of antiprotons and positrons, and in the search for antinuclei in the cosmic radiation, over a wide energy range. Besides the study of cosmic antimatter, the high–identification capabilities of the instrument allow light nuclei and their isotopes, at least up to Z=8, to be identified. This provides complementary data, besides antimatter abundances, to test models for the origin and propagation of galactic cosmic rays, and to investigate the nature of dark matter.

The instrument is installed inside a pressurized container attached to the Russian Resurs–DK1 Earth observation satellite that was launched into Earth orbit by a Soyuz–U rocket on June 15^{th} 2006 from the Baikonur cosmodrome in Kazakhstan. The mission is foreseen to last till at least December 2011.

The PAMELA apparatus comprises the following subdetectors: a time–of–flight system, a magnetic spectrometer, an anticoincidence system, an electromagnetic imaging calorimeter, a shower tail catcher scintillator and a neutron detector. The timing resolution of the TOF system allows albedo–particle identification and mass discrimination below 1 GeV/c. The magnetic spectrometer consists of a 0.43 T permanent magnet and a silicon tracking system, composed of 6 planes of double–sided microstrip sensors. The acceptance of the spectrometer, which also defines the overall acceptance of the PAMELA experiment, is 21.5 cm^2sr and the spatial resolution of the tracking system is better than 4 μm up to a zenith angle of 10°, corresponding to a maximum detectable rigidity (MDR) exceeding 1 TV. The electromagnetic calorimeter ha 16.3 X_0 and 0.6 $\lambda 0$, and allows topological discrimination between electromagnetic and hadronic showers, or non–interacting particles. More technical details about the PAMELA instrument

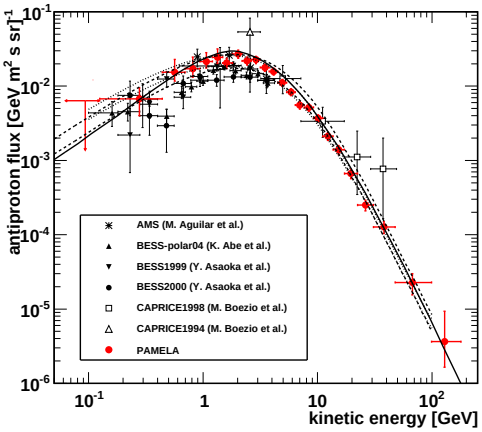

Figure 1: The antiproton energy spectrum at the top of the payload compared with contemporary measurements [3, 4, 5, 6, 7] and theoretical calculations for a pure secondary production [8, 9].

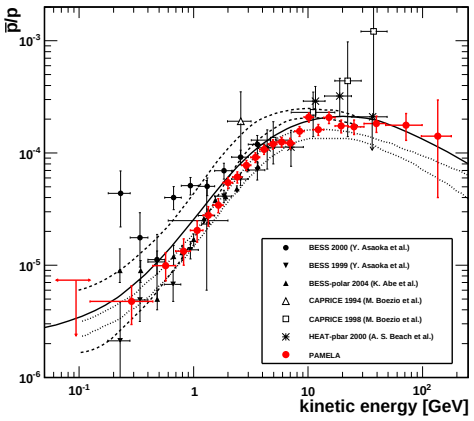

Figure 2: The antiproton-to-proton flux ratio at the top of the atmosphere compared with contemporary measurements [3, 4, 5, 6, 10] and theoretical calculations for a pure secondary production [11, 12, 9].

and launch preparations can be found in [1].

PAMELA was first switched on June 21st 2006 and it has been collecting data continuosly since July 11th 2006. To date, about 1600 days of data have been analyzed, corresponding to more than two billion recorded triggers and about 20 TB data.

2 PAMELA results: Antiprotons

In 2009 the PAMELA collaboration presented the antiproton-to-proton flux ratio in the kinetic energy range between 1.5 and 100 GeV [2], and this was found to follow the expectations from secondary production calculations. In 2010 we extended the data set collected, and we obtained the antiproton absolute spectrum from 60 MeV to 180 GeV - the widest energy range ever achieved - and the antiproton-to-proton flux ratio across the same energy interval [14]. Figure 1 shows the antiproton energy spectrum and figure 2 shows the antiproton-to-proton flux ratio measured by PAMELA along with other recent experimental data and theoretical calculations assuming pure secondary production of antiprotons during the propagation of cosmic rays in the galaxy. The curves were calculated for solar minimum, which is appropriate for the PAMELA data taking period, using the force field approximation [13].

The PAMELA results reproduce the expected peak around 2 GeV in the antiproton flux (due to the kinematic constraints on the antiproton production) and are in overall agreement with pure secondary calculations. The experimental uncertainties are smaller than the spread in the different theoretical curves and, therefore, provide important constraints on parameters relevant for secondary production calculations. Comments about a possible exotic contribution compatible with PAMELA antiproton data are given in [14].

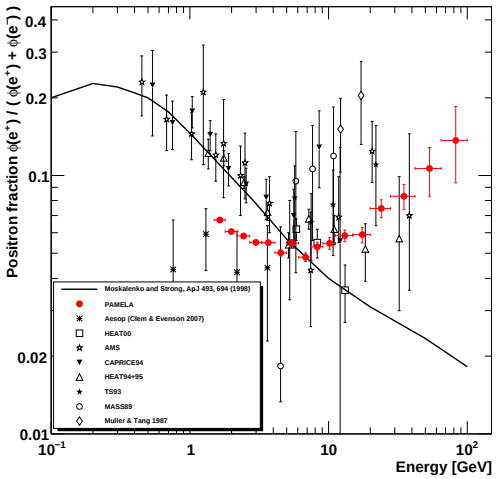

Figure 3: The positron fraction measured by the PAMELA experiment, compared with other recent experimental data [15], and a theoretical calculation [16].

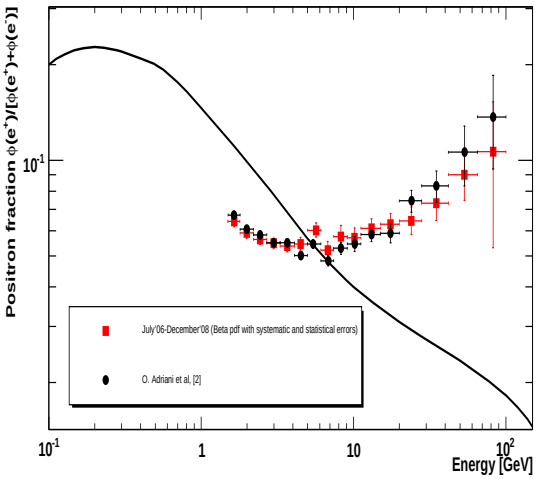

Figure 4: The positron fraction obtained using a beta-fit with statistical and systematic errors summed in quadrature (red) [17], compared with the fraction reported in fig. 3.

3 PAMELA results: Positrons

The positron to all electron (i.e. electron + positron) ratio measured by the PAMELA experiment is given in fig. 3, compared with other recent experimental results and with a theoretical calculation [15]. The data, covering the energy range 1.5 - 100 GeV, show two clear features. At low energies, below 5 GeV, the PAMELA results are systematically lower than data collected during the 1990's; this can be convincingly explained by effects of charge-dependent solar modulation. At high energies, above 10 GeV, data show a positron fraction increasing significantly with energy, contradicting the expectations.

Results published in [15] refer to data collected by PAMELA between July 2006 and February 2008. Afterwards, we analyzed a larger data set and we applied a different statistical methodology [17] for the determination of the background in the positron sample.

Fig. 4 shows the positron fraction obtained through a beta-fit with statistical and systematic errors summed in quadrature, compared with the PAMELA positron fraction of fig. 3. The new experimental results are in agreement with what reported in [15] and confirm both solar modulation effects on cosmic-rays with low rigidities and an anomalous positron abundance above 10 GeV. Various hypotheses about the nature of this exciting and unexpected increase at high energy have been proposed. The most interesting is connected with the annihilation of dark matter, even if astrophysical sources such as pulsars could contribute in part to the observed flux of positrons. A review of possible hypothesys is given in [18].

It is worth to note that a physical process creating a positron from a zero charge system also implies the creation of a corresponding electron. Therefore an exotic source of positrons in our Galaxy is presumably also a source of electrons. PAMELA collaboraton is working to provide measurements of the electron, positron and "all-electron" spectra. Results will be ready for

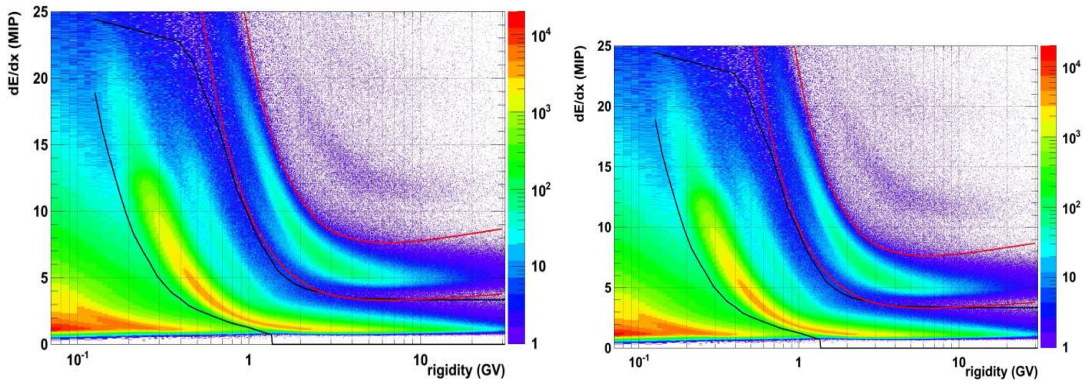

Figure 5: Left: Energy loss in tracker vs. tracker rigidity for positively charged particles. The proton and helium bands are clearly visible: the black and red lines represent the cuts used to select protons and heliums. Right: Capability of the Time-Of-Flight scintillators to separate the different charges as a function of velocity (beta), from proton to Oxygen.

publication by Fall 2010.

4 PAMELA results: Astrophysics Background

An accurate theoretical modeling of the fluxes of secondary species as antiprotons and positrons, produced by interaction of cosmic rays nuclei with the interstellar medium, is the starting point to highlight the presence of components produced by exotic sources such as dark matter. PAMELA is measuring with good precision and high statistics protons, ^{4}He, Carbon and Oxygen (primaries) together to ^{3}He, Li, Be, B (secondaries). These data constrain existing production and propagation models, providing detailed information on the galactic structure and the various mechanisms involved.

Figure 5, left, shows the energy loss in the PAMELA tracker versus the rigidity for positively charged particles. The proton and helium bands are clearly visible. On the right, instead, the capability of the TOF scintillators to separate the different charges, from proton to oxygen, is shown. Proton, helium and light nuclei fluxes measured by PAMELA are currently in publication, and they cannot be reported in this paper. However, by the end of 2010 PAMELA will have released to the scientific community the most comprehensive collection of cosmic matter and antimatter data ever acquired in space, across the widest energy range.

References

[1] Picozza P. et al., Astropart. Phys. 27, 296 (2007).

[2] Adriani O. et al., Phys. Rev. Lett. 102 , 051101 (2009).

[3] Boezio M. et al., Astrophys. J. 487, 415 (1997).

[4] Boezio M. et al., Astrophys. J. 561, 787 (2001).

[5] Asaoka Y. et al., Phys. Rev. Lett. 88, 051101 (2002).
[6] Abe K. et al., Phys. Lett. B 670, 103 (2008).
[7] Aguilar M. et al, Phys. Rep. 366, 331 (2002).
[8] Donato F. et al., Astrophys. J. 563, 172 (2001).
[9] Ptuskin V. S. et al., Astrophys. J. 642, 902 (2006).
[10] Beach A. S. et al., Phys. Rev. Lett. 87, 271101 (2001).
[11] Simon M., Molnar A. and Roesler S., Astrophys. Journal 499, 250 (1998).
[12] Donato F. et al., Phys. Rev. Lett. 102, 071301 (2009).
[13] Gleeson, L. J. and Axford, W. I., Astrophys. J. 154, 1011 (1968).
[14] Adriani O et al., arXiv:1007.0821, Phys. Rev. Lett. 105, 121101 (2010).
[15] Adriani O. et al., Nature 458, 607 (2009).
[16] Moskalenko I. V. and Strong A. W. , Astrophys. J. 493, 694 (1998).
[17] Adriani O. et al., Astropart. Phys. 34, 1 (2010).
[18] Boezio M. et al., New Journal of Physics 11, 105023 (2009).

Light Asymmetric Dark Matter

Mads T. Frandsen[1], *Subir Sarkar*[1]

[1]Rudolf Peierls Centre for Theoretical Physics, University of Oxford,
1 Keble Road, Oxford OX1 3NP, UK

DOI: http://dx.doi.org/10.3204/DESY-PROC-2010-03/frandsen_mads

Stable relic particles of mass around 5 GeV with an intrinsic matter-antimatter asymmetry would naturally provide the dark matter. They do not annihilate after being captured by the Sun and the capture rate is exponentially enhanced if they have self-interactions (of the right order to solve the excessive substructure problem of collisionless cold dark matter). Such particles can significantly affect heat transport in the Sun and may solve the 'Solar composition problem' — the predicted small changes in low energy neutrino fluxes are potentially measurable by Borexino and the proposed SNO+ and LENS experiments.

1 Asymmetric Dark Matter

An asymmetry in dark matter similar to that in baryons would naturally explain why their observed abundances are of the same order of magnitude [1]. Technicolour models of electroweak symmetry breaking [2] provide a TeV mass candidate for asymmetric Dark Matter (ADM) in the form of the lightest neutral technibaryon [3, 4]. Other stable Techni-Interacting Massive Particles (TIMPs) may be pseudo Nambu-Goldstone bosons of 'walking' technicolour interactions and thus much lighter [5]. There has recently been renewed interest in GeV-scale ADM from new strong dynamics [6, 7], motivated by putative signals in dark matter detectors [8].

If the dark matter is sufficiently strongly self-interacting that there is no significant *symmetric* relic abundance today (as for baryons), the relic density of the dark matter χ is given simply by $\Omega_\chi \sim (m_\chi \mathcal{N}_\chi / m_{\rm B} \mathcal{N}_{\rm B}) \Omega_B$ where $\mathcal{N}_{{\rm B},\chi}$ are the respective asymmetries. If $\mathcal{N}_{\rm B} \sim \mathcal{N}_\chi$ (e.g. if both asymmetries are created by leptogenesis) then the required abundance is obtained for a 5 GeV particle as shown in Fig.1 — this also shows how the required relic abundance is achieved again for $\sim$ TeV mass ADM due to the Boltzmann suppression factor [3, 4].

If ADM arises from a strongly coupled gauge theory, then there is naturally a conserved $U(1)$ global symmetry (like B number in QCD) which guarantees stability of the lightest $U(1)$ charged object. A 'dark baryon' from a QCD-like strongly interacting sector but with a mass of about 5 GeV is thus a natural candidate for ADM. The self-interaction cross-section of such a neutral particle can be estimated by scaling up the neutron self-scattering cross-section of $\sim 10^{-23}$ cm^2 as: $\sigma_{\chi\chi} = (m_{\rm n}/m_\chi)^2 \sigma_{\rm nn}$. The self-annihilation cross-section will be of the same order which ensures that the relic thermal (symmetric) abundance is negligible.

2 ADM and the Sun

In contrast to candidates for cold dark matter (CDM) which have a relic thermal abundance determined by 'freeze-out' from chemical equilibrium, ADM does not annihilate upon capture in astrophysical bodies such as the Sun, leading to a build up of its concentration. In particular, self-interactions of the order above can lead to an *exponential* increase of the ADM abundance in the Sun as it orbits around the Galaxy, accreting dark matter [9, 10].

ADM does not have the usual indirect signatures e.g. there will be no high energy neutrino signal from annihilations in the Sun. Instead ADM will alter heat transport in the Sun thus affecting low energy neutrino fluxes. This had been proposed as a solution to the 'Solar neutrino problem' [11, 12, 13]. Although the solution is now understood to be neutrino oscillations [14], small changes induced by accreted CDM particles may account [10, 15] for the current discrepancy [16] between helioseismological data and the revised 'Standard Solar Model' (SSM).

2.1 Capture of self-interacting ADM by the Sun

The capture rate for χ particles with *both* an asymmetry and self-interactions is governed by $\mathrm{d}N_\chi/\mathrm{d}t = C_{\chi\mathrm{N}} + C_{\chi\chi}N_\chi$, where $C_{\chi\mathcal{N}}$ is the usual rate of capture of CDM particles by scattering off nuclei (dominantly protons) within the Sun, while $C_{\chi\chi}$ is the rate of self-capture through scattering off already captured χ particles. Hence the number of captured particles grows exponentially for $t \gtrsim C_{\chi\chi}^{-1}$. However the effective cross-section for self-captures cannot increase beyond πr_χ^2 where $r_\chi \simeq 0.13 R_\odot \sqrt{m_\mathrm{N}/m_\chi}$ is the scale-height of the region where they are gravitationally trapped [11]. The linear growth by contrast can continue up to the 'black disk' limit i.e. $\pi R_\odot^2$, as seen in Fig.1. In both cases there is an additional enhancement due to 'gravitational focussing' [11, 17]. Ejection of captured particles by recoil effects in the self-scattering can be neglected [9] and 'evaporation' is negligible for $m_\chi \gtrsim 3.7$ GeV [17].

The ADM capture rate is proportional to the χ-nucleon cross-section which is constrained by direct detection experiments such as CDMS-II [18], XENON10/100 [19] and CoGeNT [20] to be $\sigma_{\chi\mathrm{N}}^{\mathrm{SI}} \lesssim 2 \times 10^{-40}$ cm^2 for spin-independent interactions and $m_\chi = 5$ GeV. For spin-dependent interactions the constraints are considerably weaker, and the strongest bound of $\sigma_{\chi\mathrm{N}}^{\mathrm{SD}} \lesssim 10^{-36}$ cm^2 for this mass is set by PICASSO [21]. The self-capture rate in the Sun is proportional to the self-interaction cross-section which is unconstrained by direct detection.

Self-interacting CDM was proposed [22] to account for observations of galactic and subgalactic structure on scales $\lesssim$ a few Mpc which are not in accord with numerical simulations using collisionless cold particles. The discrepancy can be solved if CDM has a mean free path against self-interactions of $\lambda \sim 1$ kpc $- 1$ Mpc corresponding to a self-scattering cross-section between $s_{\chi\chi} \sim 8 \times 10^{-22}$ and $\sim 8 \times 10^{-25}$ cm^{2}GeV^{-1} [22]. A detailed analysis sets an upper limit of $s_{\chi\chi} \lesssim 10^{-23}$ cm^{2}GeV^{-1} [23], while a study [24] of the colliding 'Bullet cluster' of galaxies implies a stronger bound of $\sim 2 \times 10^{-24}$ cm^{2}GeV^{-1}, which we adopt for our calculations below.

If χ has a magnetic moment, photon exchange will give rise to both spin-independent and spin-dependent interactions with nucleons as has been investigated in a model of a 5 GeV 'hidden baryon' interacting with the photon through mixing with a hidden photon [7]. Since the photon couples *only* to the proton in direct detection experiments, the experimental limit on $\sigma_{\chi\mathrm{N}}^{\mathrm{SI}}$ is degraded for this model to $\sim 8 \times 10^{-40}$ cm^2 [10]. Such a cross-section can easily be achieved in this model and will moreover be accompanied by spin-*dependent* interactions which can be bigger and would be particularly relevant for heat transport in the Sun. Hence we adopt a cross-section of $\sigma_{\chi\mathrm{N}}^{\mathrm{SD}} \sim 4 \times 10^{-39}$ cm^2 as an example.

3 Helioseismology and Solar neutrinos

Fig. 1 shows the growth of the number of captured ADM particles in ratio to the number of baryons in the Sun, including the 'gravitational focussing' factor of $(v_{\rm esc}(r)/\bar{v})^2$ [17] and setting $r = R_\odot$ or r_χ ($\simeq 0.07 R_\odot$ for $m_\chi = 5$ GeV) as appropriate.

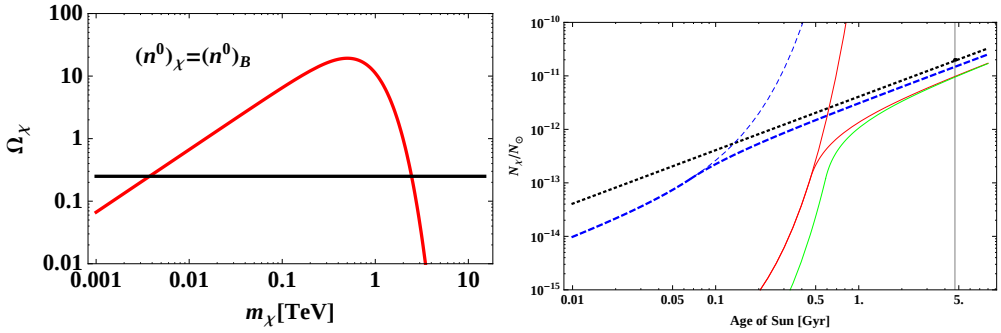

Figure 1: Left: The relic density of ADM as a function of its mass. Right: Growth of the relative abundance of 5 GeV mass ADM particles in the Sun until its present age (vertical line) for $s_{\chi\chi} = 2 \times 10^{-24}{\rm cm}^2{\rm GeV}^{-1}$ and $\sigma_{\chi N}/{\rm cm}^2 = 2 \times 10^{-40}$ (green line), 10^{-39} (red line) and 10^{-36} (blue line); also shown is the 'black disk' limit (dotted line) for the Sun.

Due to the self-captures the limiting abundance $N_\chi/N_\odot \sim 10^{-11}$ is almost independent of the actual scattering cross-section as seen in Fig.1. Such an ADM fraction in the Sun can affect the thermal transport and Solar neutrino fluxes [11, 12] which are in fact well accounted for (taking neutrino oscillations into account) by the Standard Solar Model (SSM) [26] with the 'standard' Solar composition [27]. The SSM used to be in excellent agreement with helioseismology [28], however the recent revision of the Solar composition [29] means that it no longer reproduces the sound speed and density profile, resulting in a 'Solar composition problem' [16]. We find that the presence of ADM in the Sun can alleviate this problem and precision measurements of Solar neutrino fluxes can constrain the properties of self-interacting ADM [10].

A simple scaling argument gives for the luminosity carried by the ADM [11]:

$$L_\chi \sim 4 \times 10^{12} L_\odot \frac{N_\chi}{N_\odot} \frac{\sigma_{\chi{\rm N}}}{\sigma_\odot} \sqrt{\frac{m_{\rm N}}{m_\chi}} \,, \tag{1}$$

where $L_\odot \sim 4 \times 10^{33} {\rm ergs\,s}^{-1}$. When the ADM mean free path $\lambda_\chi (= 1/n_\odot \sigma_{\chi{\rm N}})$ is large compared to the scale-height r_χ then the energy transfer is *non-local* [11]. This is the case when $\sigma_{\chi{\rm N}} \ll \sigma_\odot$ where $\sigma_\odot \equiv (m_{\rm N}/M_\odot) R_\odot^2 \sim 4 \times 10^{-36}$ cm^2 is a critical scattering cross-section. The resulting variation of the Solar luminosity $\delta L(r) \equiv L_\chi(r)/L_\odot(r)$ is shown in Fig.2 assuming $\sigma_{\chi{\rm N}} = 4 \times 10^{-39}$ cm^2 (i.e. $10^{-3}\sigma_\odot$) and $N_\chi = 2 \times 10^{-11} N_\odot$ from Fig. 1. Note that the luminosity scales linearly with both $\sigma_{\chi{\rm N}}$ and $N_\chi/N_\odot$.

The ADM temperature T_χ is fixed by requiring that the energy absorbed in the inner region ($T(r) > T_\chi$) is equal to that released in the outer region ($T(r) < T_\chi$), such that $L_\chi(R_\odot) = 0$. This approximation overestimates the energy transfer by a small factor [30, 31] but is sufficiently accurate for the present study. From the radiative transport equation it follows that a small variation of the Solar luminosity is equivalent to an *opposite* small variation in the effective

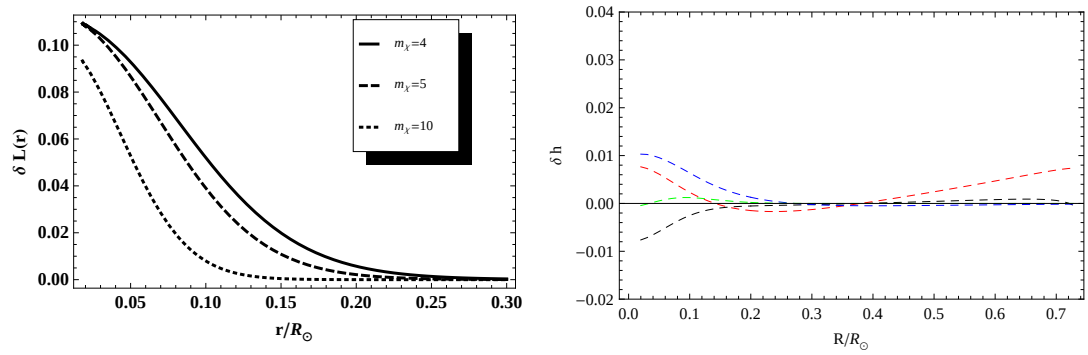

Figure 2: Left: Radial variation of $\delta L(r) \equiv L_\chi(r)/L_\odot(r)$ due to ADM. Right: Effect of 5 GeV ADM with $\sigma_{\chi \mathrm{N}} = 4 \times 10^{-39}$ cm^2 on the Solar temperature (black), pressure (red), mass fraction (blue), and luminosity (green), as computed using the linear Solar model [34].

radiative opacity: $\delta L(r) \sim -\delta\kappa_\gamma(r) \equiv -\kappa_\chi(r)/\kappa_\gamma(r)$ [32]. The effect of such a localised opacity variation in the region $r \lesssim 0.2 R_\odot$ has been studied by a Monte Carlo simulation [33] and results in excellent agreement obtained using a linear approximation to the solar structure equations [34]. Fig. 2 shows that the opacity modification due to a 5 GeV ADM with a relative concentration of 10^{-11} is roughly equivalent to the effect of a 10% opacity variation. In general, to have an observable effect on neutrino fluxes requires $\sigma_{\chi \mathrm{N}} N_\chi / \sigma_\odot N_\odot \gtrsim 10^{-14}$.

It is possible through helioseismology to determine the mean variations of the sound speed profile $\langle \delta c/c \rangle$ as well as the boundary of the convective zone R_{CZ} which is determined to be $(0.713 \pm 0.001) R_\odot$, while the SSM with the revised composition [29] predicts a significantly higher value. Lowering the opacity in the central region of the Sun with ADM also lowers the convective boundary. The 10% opacity variation shown in Fig. 2 leads to a $\sim 0.7\%$ reduction in R_{CZ} [34] and thus *restores* the agreement with helioseismology. The sound speed and density profiles, which are presently underestimated in the region $0.2 R_\odot \lesssim r \lesssim R_{\mathrm{CZ}}$, would also be corrected by the opacity modification displayed in Fig. 2.

The modification of the luminosity profile extends into the neutrino producing region. Precision measurements of different neutrino fluxes can thus test the ADM model and determine its parameters. The ADM mass determines the scale height r_χ, hence the relative modifications of individual neutrino fluxes, while the cross-section determines the capture rate and thereby the overall modification. Both Monte Carlo simulations [33] and the 'linear solar model' [34] show that the variation of neutrino fluxes with respect to localised opacity changes in the neutrino producing region ($r \lesssim 0.2 R_\odot$) scales approximately as $\delta\Phi_{\mathrm{B}} \sim 1.5\delta\kappa$ and $\delta\Phi_{\mathrm{Be}} \sim 0.7\delta\kappa$. The opacity variation in Fig. 2 leads to variations $\delta\Phi_{\mathrm{B}} = -17\%, \delta\Phi_{\mathrm{Be}} = -6.7\%$ and $\delta\Phi_{\mathrm{N}} = -10\%, \delta\Phi_{\mathrm{O}} = -14\%$ [34]. Measurements of the ^{8}B flux by Super-Kamiokande [35], SNO [36] and Borexino [37] are precise to 10% while the expectations vary by up to 20% depending on whether the old [27] or the new [29] composition is used [28]. For the ^{7}Be flux, the theoretical uncertainty is 10%, while Borexino aims to make a measurement precise to 3% [38]. SNO+ aims to make a first measurement of the pep and CN-cycle fluxes [39], while LENS may be sensitive to the commensurate small increase in the pp neutrino flux [40].

Numerical simulations of Solar evolution with ADM [41, 42] indicate similar reductions of the neutrino fluxes but smaller effects on helioseismology. This is under investigation.

4 Conclusions

Intriguingly a 5 GeV 'dark baryon' would naturally a) have the required relic abundance if it has an initial asymmetry similar to that of baryons, b) have a self-interaction cross-section of the right order to suppress excessive sub-structure on galactic scales, c) modify the deep interior of the Sun, restoring agreement between the standard Solar model and helioseismology, and d) be consistent with recent hints of signals in direct detection experiments. Such a 5 GeV ADM particle would lower the Solar neutrino fluxes which ought to be measurable by the Borexino and (forthcoming) SNO+ and LENS experiments. Thus this model is predictive and falsifiable.

References

[1] G. B. Gelmini, L. J. Hall & M. J. Lin, Nucl. Phys. B **281**, 726 (1987).

[2] S. Weinberg, Phys. Rev. D **19**, 1277 (1979); L. Susskind, Phys. Rev. D **20**, 2619 (1979).

[3] S. Nussinov, Phys. Lett. B **165**, 55 (1985); R.S. Chivukula & T.P. Walker, Nucl. Phys. B **329**, 445 (1990);

[4] S.M. Barr, R.S. Chivukula & E. Farhi, Phys. Lett. B **241**, 387 (1990).

[5] S. B. Gudnason, C. Kouvaris & F. Sannino, Phys. Rev. D **73**, 115003 (2006); C. Kouvaris, Phys. Rev. D **76**, 015011 (2007); T. A. Ryttov & F. Sannino, Phys. Rev. D **78**, 115010 (2008); F. Sannino & R. Zwicky, Phys. Rev. D **79**, 015016 (2009); R. Foadi, M.T. Frandsen & F. Sannino, Phys. Rev. D **80**, 037702 (2009); M.T. Frandsen & F. Sannino, Phys. Rev. D **81**, 097704 (2010); A. Belyaev *et al.*, arXiv:1007.4839 [hep-ph].

[6] D.B. Kaplan, Phys. Rev. Lett. **68**, 741 (1992); D. Hooper, J. March-Russell & S. M. West, Phys. Lett. B **605**, 228 (2005); D.E. Kaplan, M.A. Luty & K.M. Zurek, Phys. Rev. D **79**, 115016 (2009); G.D. Kribs *et al.*, Phys. Rev. D **81**, 095001 (2010); H. An *et al.*, JHEP **1003**, 124 (2010),

[7] H. An *et al.*, Phys. Rev. D **82**, 023533 (2010).

[8] J. Kopp, T. Schwetz and J. Zupan, arXiv:0912.4264; M. Farina, D. Pappadopulo and A. Strumia, arXiv:0912.5038; A. L. Fitzpatrick, D. Hooper and K. M. Zurek, arXiv:1003.0014.

[9] A.R. Zentner, Phys. Rev. D **80**, 063501 (2009).

[10] M.T. Frandsen & S. Sarkar, Phys. Rev. Lett. **105**, 011301 (2010)

[11] D.N. Spergel & W.H. Press, Astrophys. J. **294**, 663 (1985); Astrophys. J. **296**, 679 (1985).

[12] J. Faulkner & R.L. Gilliland, Astrophys. J. **299**, 994 (1985).

[13] R.L. Gilliland *et al.*, Astrophys. J. **306**, 703 (1986).

[14] For a review, see: J.N. Bahcall & C. Pena-Garay, New J. Phys. **6**, 63 (2004).

[15] see talk by F. Villante: http://taup2009.lngs.infn.it/slides/jul1/villante.pdf

[16] C. Pena-Garay & A. Serenelli, arXiv:0811.2424.

[17] A. Gould, Astrophys. J. **321**, 560 & 571 (1987).

[18] Z. Ahmed *et al.* Science **327**, 1619 (2010); D. S. Akerib *et al.* arXiv:1010.4290 [astro-ph.CO]; Z. Ahmed *et al.* arXiv:1011.2482 [astro-ph.CO].

[19] J. Angle *et al.* Phys. Rev. D **80**, 115005 (2009); E. Aprile *et al.* Phys. Rev. Lett. **105**, 131302 (2010).

[20] C. E. Aalseth *et al.*, arXiv:1002.4703.

[21] S. Archambault *et al.*, Phys. Lett. B **682**, 185 (2009).

[22] D.N. Spergel & P.J. Steinhardt, Phys. Rev. Lett. **84**, 3760 (2000).

[23] B.D. Wandelt *et al.*, arXiv:astro-ph/0006344.

[24] S.W. Randall *et al.*, Astrophys. J. **679**, 1173 (2008).

[25] K. Griest & D. Seckel, Nucl. Phys. B **283**, 681 (1987).

[26] J.N. Bahcall, A.M. Serenelli & S. Basu, Astrophys. J. **621**, L85 (2005).

[27] N. Grevesse & A.J. Sauval, Space Sci. Rev. **85**, 161 (1998).

[28] For a review, see: A.M. Serenelli, arXiv:0910.3690.
[29] M. Asplund *et al.*, Ann. Rev. Astron. Astrophys. **47**, 481 (2009).
[30] A. Gould & G. Raffelt, Astrophys. J. **352**, 669 (1990).
[31] D. Dearborn, K. Griest & G. Raffelt, Astrophys. J. **368**, 626 (1991).
[32] A. Bottino *et al.*, Phys. Rev. D **66**, 053005 (2002).
[33] G. Fiorentini & B. Ricci, Phys. Lett. B **526**, 186 (2002);
[34] F.L. Villante & B. Ricci, Astrophys. J. **714**, 944 (2010).
[35] J.P. Cravens *et al.*, Phys. Rev. D **78**, 032002 (2008).
[36] B. Aharmim *et al.*, Phys. Rev. Lett. **101**, 111301 (2008).
[37] G. Bellini *et al.*, Phys. Rev. D **82**, 033006 (2010).
[38] C. Arpesella *et al.* Phys. Rev. Lett. **101**, 091302 (2008).
[39] W.C. Haxton and A.M. Serenelli, Astrophys. J. **687**, 678 (2008).
[40] R. S. Raghavan, J. Phys. Conf. Ser. **120**, 052014 (2008).
[41] D.T. Cumberbatch *et al.*,Phys. Rev. D **82**, 103503 (2010).
[42] M. Taoso *et al.*, Phys. Rev. D **82**, 083509 (2010).

Chapter 6

New ideas and Developments, Visions, Large Laboratories

An adjustable Cosmological Constant

Jihn E. Kim

Department of Physics and Astronomy and Center for Theoretical Physics,
Seoul National University, Seoul 151-747, Korea

DOI: http://dx.doi.org/10.3204/DESY-PROC-2010-03/kim_jihn

After showing the axion couplings, I review the Hawking type solution of the cosmological constant problem, present a (probably) correct way to calculate the probability amplitude, and show that the Kim-Kyae-Lee self-tuning model allows a finite range of parameters for the $\overline{\Lambda} = 0$ to have a singularly large probability, approached from the AdS side.

1 Axion couplings

Since this is an axion conference, I present first the axion couplings with the current status and then discuss on the cosmological constant (CC). The axion couplings are given in [1] for the KSVZ [2] and DFSZ axions [3]. We show the current cosmological and astrophysical bounds in Fig. 1. Theortical expectations are also shown. In particular, we insert one line [4] from a superstring model calculation from a Z_{12-I} compactification [5]. This is a calculation from a theory with an ultra violet completion with all fermions of the full theory is taken into account.

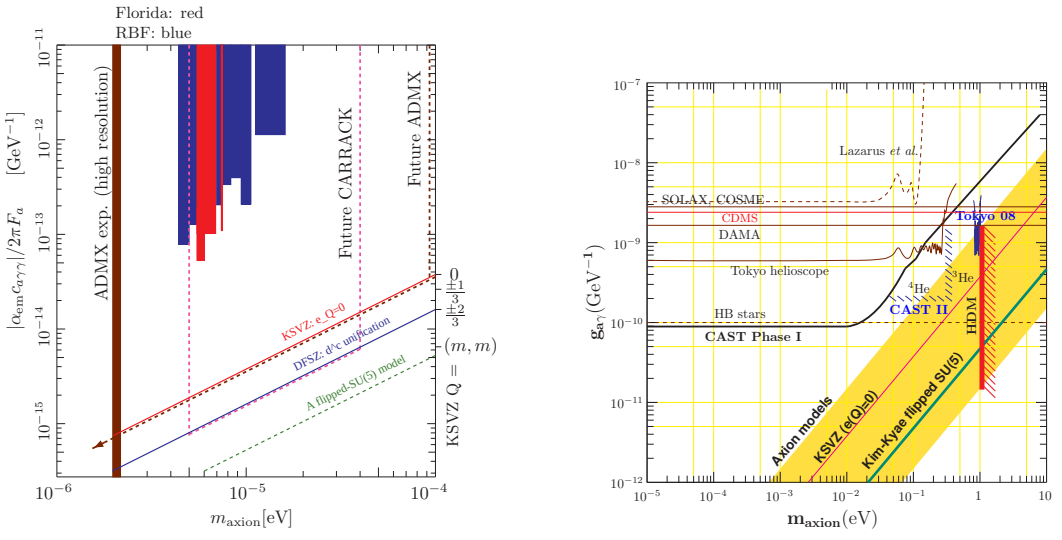

Figure 1: (a) The cosmological bounds and axion models, and (b) the astrophysical bounds.

2 Cosmological constants

Now, I present the idea on the solution of the CC problem in models with extra dimensions published in [6, 7].

Recently, Nicoli commented (cited in [7]) that the Einstein equation is inconsistent from the outset because the left-hand side (LHS) and the right-hand side (RHS) of the Einstein equation $R_{\mu\nu} - \frac{1}{2}Rg_{\mu\nu} = 8\pi G_N T_{\mu\nu}$ are logically different. The LHS is exactly determined by the continuous space-time geometry, and the RHS is contributed by particle quanta which have roots in the probabilistic interpretation of quantum mechanics. So, any discussion in the Planck era is speculative and not yet well formulated, and the present CC solutions are speculative. But they are welcome if it is not contradicted outrageously from the present perspective on the fundamental physics. In this spirit I present an idea with a specific action toward a CC solution.

One question on the determination of the CC is at which energy scale and *temperature* the CC is required to vanish. Out of the mass hierarchy scales in particle physics, from $M_P = 2.44\times 10^{18}$ GeV down to $T \approx 10^{-4}$ eV, the scale where the CC is determined must be known. Note that there are two other issues related to the CC constant. After the first inflationary scenario with the R and R^2 terms [8], the inflationary paradigm has been formulated with a scalar field called the *inflaton* [9]. Presumably, the beginning of inflation with the inflaton starts at a temperature when the vacuum energy was much above the electroweak scale [9]. The vanishing CC solution at the zero temperature must be in harmony with this inflation of the early Universe. Another CC related issue is the current acceleration of the Universe which is known as the dark energy (DE) problem [10]. The current DE is not exactly zero but of order $(0.002\ \text{eV})^4$. The vanishing CC solution must be in harmony with this tiny DE also. If there exists a CC solution, it is better to address these other problems.

When we consider quantum mechanics, we talk in terms of the probability amplitude: The initial state $|I\rangle$ transforming to a final state $|F\rangle$. In this spirit, Baum and Hawking [11] considered the Euclidian action, only with the Ricci scalar R and the CC term Λ. If the topology change of the metric is considered, we must know the full gravity equation, in which case an exponential of exponential function may be obtained [12]. But, here we do not delve into an exponential of an exponential. The Euclidian action integral was found to have the form $e^{-\tilde{I}_E} = e^{3\pi M_P^2/\Lambda}$. Hawking considered a scalar field in terms of $A_{\mu\nu\rho}$ (or the field strength $H_{\mu\nu\rho\sigma}$).

In this scenario, the quantity to calculate is the action. Even if we understand the CC in this way, we must address the following: (*i*) How do we assign the initial state?, (*ii*) How does the needed primary inflation come about in this scenario?, and (*iii*) How does it fit to the current DE?

With extra dimensions, there exists the no-go theorem for self-tuning solutions under some plausible conditions such that one employs the usual kinetic energy term and assumes the existence of Lorentz symmetry and 4D gravity for a large distance separation [13]. So, we try to go beyond using the standard kinetic energy (KE) term. In this regard, we note the self-tuning model by Kim, Kyae and Lee (KKL) [14]. The KKL model is worked out in the Randal-Sundrum II setup [15], with a nonstandard KE term of the field strength H_{MNPQ}: $\sim 1/H^2$ [14],

$$-I_E = \int d^5x_E\sqrt{g_{(5)}}\left(\tfrac{1}{2}R_{(5)} - \tfrac{2\cdot 4!}{H^2} - \Lambda_b - \Lambda_1\delta(y)\right) = \int dy \int d^4x_E \left\{ -\Psi^4\Lambda_1\delta(y) + \tfrac{1}{2}R\Psi^2 + 4\Psi^3\Psi'' + 6\Psi^2(\Psi')^2 + \tfrac{2\cdot 4!\Psi^4}{H^2} - \Psi^4\Lambda_b \right\}. \quad (1)$$

The KE term with H^2 is not developing a VEV in the low energy limit, i.e. in the long wavelength limit $(\partial_\mu A^{\nu\rho\sigma}) \to 0$. So, even with $\langle H^2 \rangle = 0$, H^2 can be moved to the denominator, $\frac{1}{H^2}$, with $\langle H^2 \rangle \neq 0$. The self-tuning solution of (1) was found in [14]. It is easy to show the existence of the nearby dS and AdS solutions also. With this self-tuning solution, we illustrate our idea of the CC solution.

3 The wave function of the universe

One way of doing quantum cosmology is to solve the Wheeler-DeWit equation with an appropriate boundary condition. The obtained wave function of the universe is independent of time. It is a videotape containing all the information of the universe. There are many videotapes satisfying the Wheeler-DeWit equation [7]. The probability to obtain a certain videotape is given by the wave function of the universe. If one obtains a videotape, he can run it in a film motion-picture projector with a certain definition of time to see how the videotape, containing all the fundamental constants of physics, evolves in the classical regime.

This idea of quantum cosmology must be recast with extra dimensions and branes. The KKL solution has a remarkable property as noted in [16] that the vanishing CC solution is not allowed for the parameter range of $|\Lambda_1| \geq \sqrt{-6\Lambda_b}$, since the boundary condition at the brane $(\beta'/\beta)_{y=0^+} = -\Lambda_1/6$ cannot be satisfied, which is shown in the LHS figure of Fig. 2.

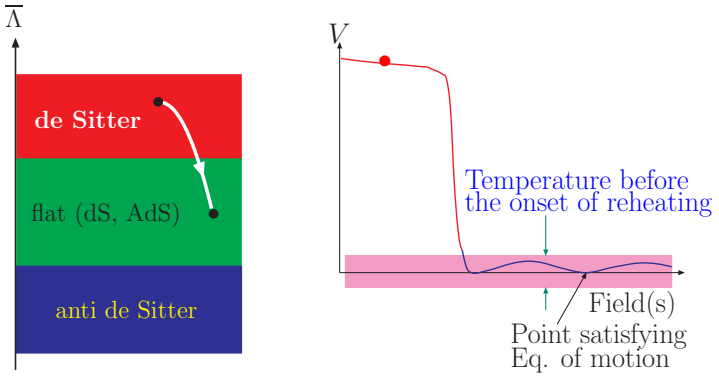

Figure 2: (a) Brane world parameters. The initial inflation takes place for $|\Lambda_1| > \sqrt{-6\Lambda_b}$. (b) The initial inflation and the recent acceleration. In the lavender band, the CC solution is swamped and the wave function of the universe is not exactly choosing the equilibrium point.

We start with a finite range of parameter of Λ_1 in the top region of the LHS side figure of Fig. 2. Next, the particle physics action at the brane may change Λ_1 such that it falls into the central region where all the possibilities are open: flat, dS and AdS solutions. Then the inflationary period might end. This state in the central region is our initial condition.

The number of e-foldings during inflation is about 60, or the scale factor increases by a factor 10^{26}. So, the brane Lagrangian for inflation is tuned to satisfy this condition. Then, the initial temperature T_i drops to $10^{-26}T_i$ before the inflaton reheats up the universe. At this supercooled state before reheating, we define the initial state for the probability calculation. This initial state must be fuzzy enough to allow $(0.002\text{ eV})^4$ vacuum energy, even if our probability calculation dictates the vacuum energy should be zero. Then, we require $10^{-26}T_i$ be greater than 0.002

eV, namely T_i should be greater than 2×10^{14} GeV. Namely, we let the fuzziness of our CC solution cannot be accurate down to order $(0.002 \text{ eV})^4$, which is depicted in Fig. 2.

4 Calculation of probability amplitude in the KKL model

If particle physics Lagrangian does not contribute to the action integral, it is sufficient to consider the R and Λ terms only as Hawking has done. His basic argument was on the size of the Euclidian volume, suppressed by $1/\Lambda$. The dS space volume is finite, the flat space volume is infinite, and the AdS space volume is even more infinite. If we consider the particle physics Lagrangian, as in the self-tuning model of KKL, the $1/\overline{\Lambda}^2$ term contributes and the AdS volume wins [6]. This may change Hawking's view completely.

Here, I discuss what has been discussed on the H^2 Lagrangian in the Hawking type calculation, present a (probably) correct way to calculate the amplitude, and show that the KKL self-tuning model allows a finite range of parameters for which $\overline{\Lambda} = 0^-$ has the singularly large probability [6].

Hawking presented the first calculation, using H^2 term in the Lagrangian [11]. Since then, there has been discussions on which value of the H^2 term must be used in the action integral. A surface term $\epsilon^{\mu\nu\rho\sigma} H_{\mu\nu\rho\sigma}$ has been noted, which does not change the equation of motion. It turned out that it amounts to changing the sign of H^2 term in the action integral [17], from which Duff concluded that the probability amplitude for $\overline{\Lambda} = 0$ is least probable with $H_{\mu\nu\rho\sigma}$. But, Wu [17] obtained the opposite result from that of Duff. This is because of the treatment on the surface term, which does not affect the equation of motion. If we follow Duff's method, it has the effect of changing the sign of $1/H^2$ term inside the action integral with the surface term neglected, from $\int d^5x_E \sqrt{g_{(5)}}(2 \cdot 4! \Psi^4/H^2)$ to $\int d^5x_E \sqrt{g_{(5)}}(-2 \cdot 4! \Psi^4/H^2)$. Thus, it raises an important question, "Which method should we choose?" To our view, the confusion arises from taking a specific vacuum in their calculation [17]. As in the θ-vacuum of QCD, we have the α-vacuum of antisymmetric tensor field $H_{\mu\nu\rho\sigma}$. Duff took one extremum point corresponding to $\alpha = \pi$ and Wu took another vacuum corresponding to $\alpha = 0$, and they obtained different results even though both satisfied equations of motion. As an illustration, we may consider α-vacuum with the H^2 kinetic energy term. For two antisymmetric indices from μ, ν, ρ, and σ, there are six $({}_4C_2 = 6)$ independent second rank antisymmetric gauge functions, for which $A_{\mu\nu\rho}$ transforms as $A_{\mu\nu\rho} \to A_{\mu\nu\rho} - \partial_\mu \Lambda_{\nu\rho} - \partial_\nu \Lambda_{\rho\mu} - \partial_\rho \Lambda_{\mu\nu}$; so we consider the maps of $S_3 \to S_3$. Namely, there exists one type of instanton solution.

Now, we can construct a gauge invariant α-vacuum, following the θ-vacuum construction of QCD, $|\alpha\rangle = \sum_{n=-\infty}^{+\infty} |n\rangle e^{in\alpha}$. In the α-vacuum, after integrating out the H^2 field, what Duff chose is $\alpha = \pi$ and what Wu chose is $\alpha = 0$. However, in the α vacuum any value of α is allowed, i.e. not restricted to $\alpha = 0$ and π.

Now, this α-vacuum is defined with the $1/H^2$ term. We calculate the action integral for $\alpha = 0$ and π with the $1/H^2$ term and for any α the action integral is between them. If one makes α a dynamical field as the QCD axion, then α is cosmologically settled to 0.

Finally, we find that there exist the parameter space where $\overline{\Lambda} = 0^-$ dominates, which is the proposed CC solution. A more detailed discussion can be found in [6].

Acknowledgements

This work is supported in part by the Korea Res. Found., Grant No. KRF-2005-084-C00001.

References

[1] J. E. Kim, "Constraints on very light axion from cavity experiments," Phys. Rev. D **58**, 055006 (1998); J. E. Kim and G. Carosi, "Axions and the strong CP problem," Rev. Mod. Phys. **82**, 557 (2010).

[2] J. E. Kim, "Weak interaction singlet and strong CP invariance," Phys. Rev. Lett. **43**, 103 (1979); M. A. Shifman, V. I. Vainstein, and V. I. Zakharov, "Can confinement ensure natural CP invariance of strong interactions?," Nucl. Phys. B **166**, 4933 (1980).

[3] M. Dine, W. Fischler and M. Srednicki, "A simple solution to the strong CP problem with a harmless axion," Phys. Lett. B **108**, 199 (1981); A. P. Zhitnitskii, "Possible suppression of axion-hadron interactions," Yad. Fiz. **31**, 497 (1980) [Sov. J. Nucl. Phys. **31**, 260 (1980)].

[4] K.-S. Choi, I.-W. Kim and Jihn E. Kim, "String compactification, QCD axion and axion-photon-photon coupling," JHEP **03**, 116 (2007) [hep-ph/0612107].

[5] J. E. Kim and B. Kyae, "Flipped SU(5) from Z_{12-I} orbifold with Wilson line," Nucl. Phys. B **770**, 47 (2007) [hep-th/0608086].

[6] J. E. Kim, "Cosmological constant is probably adjustable in brane worlds," Phys. Rev. D **81**, 123018 (2010) [arXiv:0912.2733[hep-th]].

[7] J. E. Kim, "Self-tuning of the cosmological constant," arXiv:1009.5071[hep-th].

[8] A. A. Starobinsky, "Relic gravitation radiation spectrum and initial state of the Universe,"JETP Lett. **30**, 682 (1979).

[9] A. H. Guth, "The inflationary Universe: A possible solution to the horizon and flatness problems," Phys. Rev. D **23**, 347 (1981); A. D. Linde, "A new inflationary Universe scenario: A possible solution of the horizon, flatness, homogeneity, isotropy and primordial monopole problems," Phys. Lett. B **108**, 389 (1982); A. Albrecht and P. J. Steinhardt, "Cosmology for grand unified theories with radiatively induced symmetry breaking," Phys. Rev. Lett. **48**, 1220 (1982).

[10] S. Perlmutter *et al.* (Supernova Cosmology Project Collaboration), "Measurements of Ω and Λ from 42 high redshift supernovae," Astrophys. J. **517**, 565 (1999); A. G. Riess *et al.* (Supernova Search Team Collaboration), "Observational evidence from supernovae for an accelerating universe and a cosmological constant," Astron. J. **116**, 1009 (1998).

[11] E. Baum, "Zero cosmological constant from minimum action," Phys. Lett. B **133**, 185 (1983); S. Hawking, "The cosmological constant is probably zero," Phys. Lett. B **134**, 403 (1984).

[12] S. R. Coleman,"Why there is nothing rather than something: A theory of the cosmological constant," Nucl. Phys. B **310**, 643 (1988).

[13] C. Csaki, J. Erlich, C. Grojean, and T. Hollowood, "General properties of the selftuning domain wall approach to the cosmological constant problem," Nucl. Phys. B **584**, 359 (2000) [hep-th/0004133].

[14] J. E. Kim, B. Kyae and H. M. Lee, "Randall-Sundrum model for selftuning the cosmological constant," Phys. Rev. Lett. **86**, 4223 (2000) [hep-th/0011118]; "Selftuning solution of the cosmological constant problem with antisymmetric tensor field," Nucl. Phys. B **613**, 306 (2001) [hep-th/0101027].

[15] L. Randall and R. Sundrum, "An alternative to compactification," Phys. Rev. Lett. **83**, 4690 (1999) [hep-th/9906064].

[16] J. E. Kim, "Inflation with blowing up solution of cosmological constant problem," JHEP **0301**, 042 (2003) [hep-th/0210117].

[17] M. J. Duff, "The cosmological constant is possibly zero, but the proof is probably wrong," Phys. Lett. B **226**, 36 (1989); Z. C. Wu, "The cosmological constant is possibly zero, and the proof is possibly right," Phys. Lett. B **659**, 891 (2008).

Torsion Pendulum Searches for WISPs

S.A. Hoedl[1], *E.G. Adelberger*[1], *B.R. Heckel*[1]

[1]University of Washington, Seattle, WA, USA

DOI: http://dx.doi.org/10.3204/DESY-PROC-2010-03/hoedl_seth

Torsion pendulums are powerful instruments to probe for new gravitational scale physics. Here we review two torsion pendulums that provide limits on scalar and pseudoscalar WISPs.

1 Introduction

Torsion pendulum experiments have unprecedented sensitivity to fifth-forces. The Eöt-Wash group at the University of Washington has developed a technique that converts an oscillating force or acceleration acting on a pendulum into an oscillating rotation that is observed with an auto-collimator. Most of our torsion balance experiments have angular noise of about 1 nano-rad/$\sqrt{\text{day}}$. That noise corresponds to a force on each atom in the pendulum equivalent to the electrostatic repulsion force between two electrons separated by 100 light-years. With this level of sensitivity, our torsion pendulums probe many interesting questions such as:

- Are there forces much weaker than gravity?
- Is there a force that couples to B-L number?
- Is there a non-gravitational force between luminous matter and dark matter?
- Are there *large* extra-dimensions?
- Is there a preferred frame in space?
- Are the light scalar particles of string theory hidden by a self-interaction process?
- Are there weakly interacting scalars or pseudoscalars?

A recent review[1] summarizes our research on these and other questions. Here we focus only on our results that are relevant for very light and weakly interacting scalar and pseudoscalar particles.

2 Testing the gravitational inverse square law

There are a number of theoretical reasons to expect that the gravitational inverse square law (ISL) is modified at short distances. The fat graviton [3] and models with extra time dimensions [4] would *weaken* gravity at short distances. The extra space dimensions of M theory

would *strengthen* gravity at short distances [5]. In addition, testing the ISL constrains forces generated by the exchange of scalar or vector particles. The coupling of these particles to photons can also be probed. For example, through a second-order process (see Fig. 1), a massive *scalar* that couples to two photons will modify gravity at short distances [2] according to:

$$V_G(r) = -G\frac{m_1 m_2}{r}\left(1 + g^2_{\phi\gamma\gamma}\frac{9\alpha^2_{EW}}{16\pi^3 G}\left[\frac{Z}{A}\right]_1\left[\frac{Z}{A}\right]_2 e^{-r/\lambda_\phi}\right),$$

where G is Newton's constant, α_{EW} is the fine-structure constant, $g_{\phi\gamma\gamma}$ is the coupling of the scalar to two photons, λ_ϕ is the Compton wavelength of the scalar and Z/A is the proton number to atomic number ratio for each body.

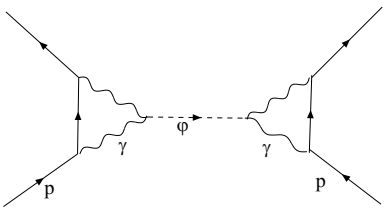

Figure 1: The fenymann diagram illustrating the ISL experiment's sensitivity to a scalar-photon coupling.

Our most recent ISL pendulum [6] consisted of a torsion pendulum, the "detector," suspended above a rotating pair of disks, the "attractor." (See Fig. 2). The active part of the detector was a 1 mm thick molybdenum disk that had 42 holes machined in a 21-fold rotationally symmetric pattern. 42 holes were also machined into each disk of the attractor. However, the lower attractor disk was thicker and made of tantalum. In addition, the holes machined into the lower disk were displaced by $\pi/21$ rad from the holes in the upper attractor disk so that the Newtonian torque created by the upper disk canceled the Newtonian torque created by the lower disk when the pendulum was approximately 100 μm above the attractor.

We parameterize a deviation from the ISL by looking for a potential of the form:

$$V(r) = -G\frac{m_1 m_2}{r}\left(1 + \alpha \cdot e^{-r/\lambda}\right),$$

where λ and α parameterize respectively the range and strength of a Yukawa deviation. Figure 3 plots our most recent 2-σ exclusion bounds on α as a function of λ. Reference [7] discusses some particle physics implications of these results. For a scalar mass of 1 meV/c^2, our results constrain the coupling strength $g_{\phi\gamma\gamma} \leq 1.6 \times 10^{-17}$ GeV^{-1}. Note that this constraint is 10^{11} times smaller than the coupling that was claimed to explain the dichroism and birefringence of the vacuum initially observed by the PVLAS collaboration [8].

3 Looking for pseudoscalars

As discussed elsewhere in these proceedings, a number of extensions to the standard model predict the existence of light pseudoscalar particles. Typically, these particles correspond to a spontaneously broken symmetry. They are also predicted by string theories [9]. The axion is the most well developed pseudoscalar and several experimental searches, a number of which are discussed in these proceedings, are actively underway. Here we refer to any pseudoscalar as an axion-like particle (ALP).

Most ALP searches employ the Primakoff vertex to look for either the conversion of an ALP into a photon or a photon into an ALP in the presence of a static magnetic field. Alternatively,

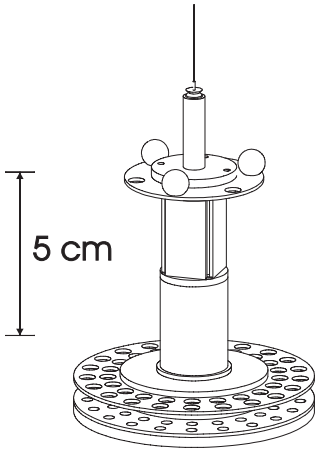

Figure 2: A scale drawing of the ISL pendulum.

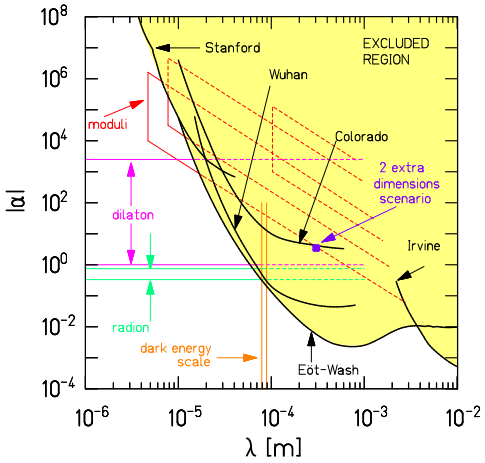

Figure 3: 2-σ constraints on deviations from the ISL.

if an ALP couples with both a scalar and pseudoscalar vertex to nucleons and electrons respectively, then the ALP will mediate a parity and time violating force between polarized and unpolarized matter given by the potential [10]:

$$V(\hat{\sigma},\hat{r}) = \frac{\hbar^2}{8\pi m_e}\left(\frac{g_s^N g_p^e}{\hbar c}\right)(\hat{\sigma}\cdot\hat{r})\left(\frac{1}{\lambda_{\rm ALP} r}+\frac{1}{r^2}\right)e^{-r/\lambda_{\rm ALP}},$$

where r is the electron-atom separation vector, $\lambda_{\rm ALP} = m_{\rm ALP}/\hbar c$ is the Compton wavelength of the ALP, $\hat{\sigma}$ and m_e are the spin unit-vector and mass of the polarized electron respectively, g_p^e is the ALP pseudo-scalar coupling constant to a polarized electron and g_s^N is the ALP scalar coupling constant to a nucleon. If the ALP is sufficiently massive, the ALP mediated force will be macroscopic and possibly accessible with a torsion pendulum. Although this ALP search method is only sensitive to a particular type of ALP, it has three distinct advantages over more conventional techniques: it does not rely on cosmological or astrophysical sources of ALPS, it is sensitive to ALPs that do not couple to photons, and most critically, it simultaneously probes a wide mass range.

To probe the astrophysically and cosmologically allowed mass range, the so-called "Axion-Window," we constructed a dedicated torsion pendulum [11] sensitive to the parity and time violating (PTV) force (see Fig. 4). This apparatus consisted of two parts: a split toroidal electromagnet that provided the source of polarized electrons and a planar torsion pendulum suspended between the two magnet halves that provided the source of unpolarized nucleons. The magnet halves were fixed to the apparatus and the pendulum was free to rotate about the fiber axis. A change in the equilibrium angle when the magnetic field reversed direction from the clockwise to counter-clockwise orientation would be a signature of the PTV force.

Spurious signals associated with the strong magnetic field (3.6 kG) and the finite magnetic susceptibility of the silicon dominated the data. However, the ALP mediated force has a unique signature: it must strengthen as the pendulum approaches either magnet half. Thus,

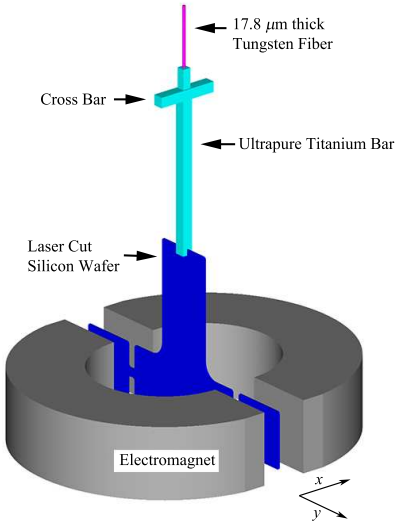

Figure 4: A diagram of the ALP pendulum.

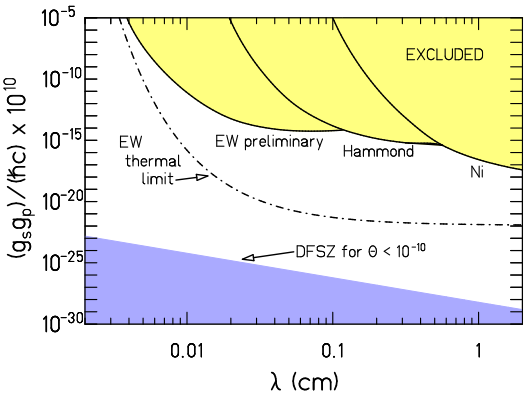

Figure 5: The 2-σ exclusion plot on an axion mediated force.

by measuring the PTV force at different pendulum positions, we could distinguish an ALP force from spurious signals. No evidence for the ALP force was observed. Figure 5 shows our constraints.

Acknowledgments

This work was primarily supported by NSF grant PHY0653863 and secondarily via DOE support for the Center for Experimental Nuclear Physics and Astrophysics at the University of Washington.

References

[1] E.G. Adelberger *et al.*, Progress in Particle and Nuclear Physics **62** 102 (2009).

[2] A. Dupays *et al.* Phys. Rev. Lett. **98** 131802 (2007).

[3] R. Sundrum, Phys. Rev. **D69**, 044014 (2004).

[4] G. Dvali, G. Gabadadze and G. Senjanovic, arXiv:hep-ph/9910207 (1999).

[5] N. Arkani-Hamed, S. Dimopoulis and G.R. Dvali, Phys. Lett. **B436** 257 (1998).

[6] D.J. Kapner *et al.*, Phys. Rev. Lett. **98** 021101 (2007).

[7] E.G. Adelberger *et al.*, Phys. Rev. Lett. **98** 131104 (2007).

[8] E. Zavattini *et al.* Phys. Rev. Lett. **96** 110406 (2006).
E. Zavattini *et al.* Phys. Rev. **D77** 032006 (2007).

[9] P. Svrcek and E. Witten, JHEP **06** 051 (2006).

[10] J. Moody and F. Wilczek, Phys. Rev. **D30** 130 (1984).

[11] S. Hoedl *et al.* submitted to Phys. Rev. Lett.

Spectroscopic Bounds on New Physics

Joerg Jaeckel, Sabyasachi Roy

Institute for Particle Physics Phenomenology,
Durham University, Durham DH1 3LE, United Kingdom

DOI: http://dx.doi.org/10.3204/DESY-PROC-2010-03/roy_sabyasachi

We use atomic spectra to extend pure Coulomb's law tests to larger masses. We interpret these results in terms of constraints for hidden sector photons. With existing data the bounds for hidden photons are not improved. However we find that our atomic spectra bounds are an especially clean and model-independent complement to existing ones from other methods. We also show that data from future tests of true muonium and muonic atoms could produce atomic spectra bounds which probe untested parameter space.

1 Introduction

We use atomic spectroscopy of ordinary and exotic atoms to test Coulomb's law with high precision on atomic length scales [1, 2]. This in turn allows us to constrain new particles such as hidden photons [1, 4, 5] which arise naturally in a variety of extensions of the standard model [4, 6, 7] (see also [8] for a review)[1] [2].

Hidden photons cause a deviation from Coulomb's law,

$$V(r) = -\frac{Z\alpha}{r}(1 + e^{-m_{\gamma'} r}\chi^2) \tag{1}$$

where $m_{\gamma'}$ is the mass of the hidden photon and χ is the kinetic mixing [6]. Note that independent of the particle interpretation, our bounds can more generally constrain deviations from Coulomb's law by a Yukawa type potential.

In the small and large mass limits we recover the original $\frac{1}{r}$ form potential. It is only in the intermediate mass regions that we expect to see measurable deviations to Coulomb's Law. Hence we expect our bounds to drop off at low and high energies.

2 Spectroscopic bounds

We adapt the method presented in Ref. [9], where the Lamb shift in atomic hydrogen is used to bound minicharged particles.

At first order in perturbation theory the energy shift of a state $|\psi_n\rangle$ is given by

$$\delta E_n^{(1)} = \langle \psi_n \mid H' \mid \psi_n \rangle = \langle \psi_n \mid \delta V \mid \psi_n \rangle. \tag{2}$$

[1] Note that we can also produce bounds for minicharged particles [3, 9, 10]. However they turn out to be relatively weak.

[2] Spectroscopy can also constrain Unparticles (see e.g. [11]).

We then impose that $\delta E_n^{(1)}$ must be smaller than the uncertainty in the transition [3] [4]. This constrains δV.

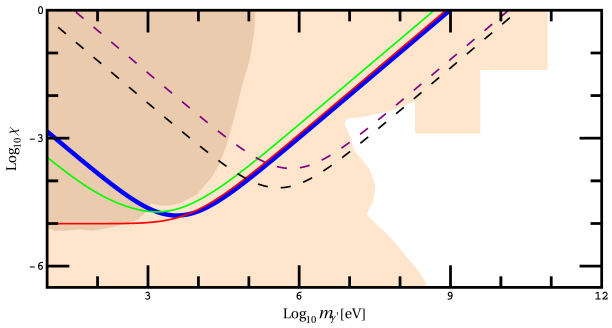

Figure 1: Bounds on hidden photons. The thick blue curve is from the $2s_{1/2}-2p_{1/2}$ transition in atomic hydrogen. The red curve shows the naive bound from $1s_{1/2}-2s_{1/2}$ in atomic hydrogen. It behaves incorrectly at small $m_{\gamma'}$. The thin joined (green) curve is correctly renormalised by combining $1s_{1/2}-2s_{1/2}$ with $2s_{1/2}-8s_{1/2}$. The colour filled regions are existing bounds. Those from pure Coulomb's law tests are the darker section (brown) [1, 2]. The lower dashed curve (black) shows a speculative bound from $2s_{1/2}-2p_{1/2}$ in true muonium, using only theoretical values. The upper dashed curve (purple) uses experimental data from muonic hydrogen to form another speculative bound. Both speculative curves penetrate untested parameter space.

We find that a naive application of this method fails. Transitions between states with different values of the principal quantum number n do not exhibit the correct drop off for small masses. For example the naive $1s_{1/2}-2s_{1/2}$ bound from atomic hydrogen is plotted as the dotted red curve in Fig. 1. We can understand the physical reasoning for this from Eq. (1). At small masses our perturbation reduces to a term that has the form of a Coulomb potential, but with an extra factor $(1+\chi^2)$, which we have not absorbed into α. In other words we have forgotten to properly (re-)normalise the coupling α. We do this by treating α as a unknown instead of a constant, and using a second transition to solve for it. We can then produce properly renormalised bounds which are functions of two transitions and not one. Fig. 1 shows a correctly renormalised bound (thin, joined, green) using $1s_{1/2}-2s_{1/2}$ and $2s_{1/2}-8s_{1/2}$ transitions in atomic hydrogen.

Note that Lamb shift [5] bounds renormalise trivially and can therefore be formed using only one measurement (see [3]). The $2s_{1/2}-2p_{1/2}$ bound from atomic hydrogen is the thick blue joined curve in 1. The bound drops off correctly for small masses.

Other transitions involving higher excited states in atomic hydrogen are considered. However these do not form good bounds, mainly due to high experimental uncertainties (see [3]).

We then apply the method to other atomic systems. The idea is that other atomic systems may have advantages over atomic hydrogen. For example in pure QED systems like muonium

[3] We conservatively estimate the "uncertainty" by adding absolute values of the experimental and theoretical errors (see [3]).

[4] Charge radii of nuclei are a major source of uncertainty. These radii must be determined from an independent source. Moreover, to avoid even partial degeneracies (which weaken the bound at short length scales), the determination of the radius should be obtained at high momentum transfer. Hence we use electron scattering values.

[5] A Lamb shift is defined by the energy difference between two states with the same n, j.

and positronium, we can assume a point-like nucleus [12]. This eliminates large uncertainties from finite nuclear size effects. Smaller uncertainties strengthen our bounds, as can be seen from Eq. 2.

However in many cases theoretical uncertainties are larger. For example hadronic orbiting particles also interact with the nucleus via the strong interaction, which causes huge theoretical and experimental uncertainties (see [3]).

Also many of these atoms have larger reduced masses or smaller Bohr radii than atomic hydrogen, shifting our bounds to higher masses and towards the unexplored region.

All relevant transitions in hydrogen-like atoms were examined to see whether the advantages outweigh the disadvantages. We found overall that we could not improve upon our original atomic hydrogen bounds using existing data [6].

Our best bounds (the light green and thick dark blue lines in Fig. 1) do not penetrate new parameter space for hidden photons. However they do improve upon previous Coulomb's law tests (brown region in 1) in the sense that they extend the excluded region to higher masses. This is a non-trivial improvement as Coulomb based bounds are especially clean and model independent [3, 2]. We often find that other competing bounds are more model dependent; for example fixed target bounds assume a 100 % branching ratio for hidden photons to decay into charged standard model particles. If this assumption is wrong, then the bounds are weakened or possibly invalidated (see [3]).

Finally we investigate the discovery potential of future experiments.

For example, a recent article suggests that true muonium ($\mu^+ \mu^-$) could be produced and studied in the near future. The reduced mass is ~ 100 times greater than atomic hydrogen, and for a pure QED system we expect small theoretical errors. Since no experimental data is available, we produce a speculative bound using an estimate of the theoretical error (lower dashed, black in Fig. 1). This penetrates new parameter space, but one still needs to obtain a coherent experimental result.

The reduced mass of muonic atoms are ~ 200 times larger than atomic hydrogen. In references [14, 15] the $2s^{F=1}_{1/2} - 2p^{F=2}_{3/2}$ difference in muonic hydrogen is calculated as a function or the proton radius r_p . If we substitute in the most precise current value of $r_p = 0.8768(69)$ fm, from atomic spectra [16], we obtain $E_{th} = -205.984(062)$ meV. The theoretical uncertainty alone is quite high. Moreover this also deviates from the recently measured experimental value of $-206.295000(3)$ meV [15] by around 5σ. This discrepancy is bad for producing bounds, but could be taken as a potential signal for new physics. We considered if the hidden photon could be used to explain this anomaly [17]. However this is ruled out by Lamb shift measurements in atomic hydrogen (see [3]).

However we can form a speculative bound (upper dashed, purple in Fig. 1) from just experimental uncertainty. This bound penetrates new parameter space. If an independent and sufficiently precise value of r_p could be determined – consistent with the muonic hydrogen extraction – this speculative bound could be turned into a real one.

[6] This is actually a slight simplification. The Lamb shift bound for the $Z = 2$ hydrogen-like ion is marginally stronger than the corresponding one for atomic hydrogen. This is because the r_p anomaly causes a high level of theoretical uncertainty in atomic hydrogen and weakens the bound considerably. No such anomaly exists for measurements of alpha particle charge radius, and the helium-like hydrogen Lamb shift gives us a slightly stronger bound. However the general trend is for bounds to weaken as the nuclear charge Z increases. We expect this trend to re-established as soon as the r_p anomaly is resolved; the atomic hydrogen bound should then be the strongest.

3 Conclusion

We have used atomic spectroscopy of ordinary and exotic atoms to constrain deviations from Coulomb's law. A fully renormalised method was developed, which provides correctly shaped constraints for high and low masses. We interpreted these constraints as bounds on hidden photons and found that pure Coulomb bounds were extended to higher masses. This is a non-trivial improvement as Coulomb based bounds are especially clean and model-independent, and provide complementary information to existing ones, which are often more model dependent. We also find that new parameter space for hidden photons could be penetrated using future data from exotic atoms.

Acknowledgements

The authors would like to thank A. Lindner, J. Redondo and A. Ringwald for interesting discussions and useful comments.

References

[1] Popov, V., Tr. J. of Physics **23**, 943 (1999).

[2] Karshenboim, S. G., Phys. Rev. Lett. **104**, 220406 (2010) [arXiv:1005.4859 [hep-ph]]; Karshenboim, S. G., [arXiv:1005.4872 [hep-ph]].

[3] Jaeckel, J. and Roy, S., (2010) [arXiv:1008.3536 [hep-ph]].

[4] Okun, L.B., Sov. Phys. **56**, (1982).

[5] Pospelov, M., Phys. Rev. **D80**, 095002 (2009) [arXiv:0811.1030 [hep-ph]].

[6] Holdom, B., Phys. Lett. **57**, (1986).

[7] Dienes, K. R., Nucl. Phys. B **492**, 104 (1997); Abel, S. A. and Schofield, B. W., Nucl. Phys. **B685**, 150 (2004) [arXiv:0311051 [hep-th]]; Abel, S. A., Jaeckel, J., and Khoze, V. V. and Ringwald, A., Phys. Lett. **B666**, 66 (2008) [arXiv:0608248 [hep-ph]]; Abel, S. A., Goodsell, M. D., Jaeckel, J. and Khoze, V. V. and Ringwald, A., JHEP **07**, (2008) [arXiv:0803.1449 [hep-ph]]; Goodsell, M., and Jaeckel, J., and Redondo, J. and Ringwald, A., JHEP **11**, 027 (2009) [arXiv:0909.0515 [hep-ph]].

[8] Jaeckel, J. and Ringwald, A., (2010) [arXiv:1002.0329 [hep-ph]].

[9] Gluck, M., Rakshit, S. and Reya, E., Phys. Rev. **D76**, 091701 (2007) [arXiv:0703140 [hep-ph]].

[10] Jaeckel, J., Phys. Rev. Lett. **103**, 080402 (2009) [arXiv:0904.1547 [hep-ph]].

[11] Thalapillil, A. M., Phys. Rev. **D81**, 035001 (2010). [arXiv:0906.4379 [hep-ph]].

[12] Jungmann, K. P., (2004) [arXiv:0404013 [nucl-ex]].

[13] Brodsky, S. J., Lebed, R. F., Phys. Rev. Lett. **102**, 213401 (2009) [arXiv:0904.2225 [hep-ph]].

[14] Eides, M. I., Grotch, H. and Shelyuto, V. A., Phys. Rept. **342**, 63 (2001) [arXiv:0002158 [hep-ph]]; Pachucki, K., Phys. Rev. A **53**, 2092 (1996); Pachucki, K., Phys. Rev. A **60**, 3593 (1999); Borie, E., Phys. Rev. A **71**, 032508 (2005); Martynenko, A. P., Phys. Rev. A **71**, 022506 (2005); Martynenko, A. P., Phys. of Atom. Nuclei **71**, 125 (2008).

[15] Pohl, R. et. al., Nature **466**, 213 (2010).

[16] Mohr, P.J, Taylor, B.N and Newell, D.B., Rev. Mod. Phys. **80**, 633 (2007).

[17] Falkowski, A, `http://resonaances.blogspot.com/2010/07/muonic-hydrogen-and-dark-forces.html`.

Underground Laboratories

Lucia Votano[1]

[1]Gran Sasso National Laboratory, SS 17 bis km 18+910, 67100 Assergi(AQ), Italy

DOI: will be assigned

Underground Laboratories are the main infrastructures for astroparticle and neutrino physics. Searches for rare events like $2\beta0\nu$ or proton decay, study of weak interactions from cosmic or artificial neutrinos, detection of dark matter candidates and nuclear astrophysics studies require low-background environments that can only be achieved in a shielded underground environment. Thanks to the reduction in the cosmic ray flux and c.r.-spallation induced neutrons, the rock coverage provides the necessary low background environment to investigate these processes. The most important underground laboratories all over the world together with their future projects will be reviewed.

1 Introduction

Going back over the scientific path of these last 30 years, it's worth mentioning the impressive growth of astroparticle physics, a research field which connects elementary particle physics, astrophysics and cosmology. The community of researchers involved has considerably grown and dimensions, complexity and technology of the experimental apparata have increased as well. Underground laboratories are the main infrastructures devoted to astroparticle physics; underground experiments have produced the first clear evidence of physics beyond the standard model (SM), the discovery on the flavor lepton changing by using neutrino natural sources. Neutrinoless $\beta\beta$ decay, direct detection of dark matter particles, proton decay are all weak and rare processes that require very impressive efforts to be observed. Underground laboratories with low radioactive background environments are the ideal places where experiments aiming to discover such processes can be performed.

2 Backgrounds for underground Physics

The challenge towards greater sensitivities in underground experiments turns into a continuous fight against radioactive background. The depth of the laboratory and the nature of the rocks around specifically characterize each facility. Background main sources are:

- Flux of high-energy muons induced by cosmic rays interactions decreases as depth increases while the angular dependence is due to the surface profile.
- At low energies, neutrons are generated by α particles and fission processes of Uranium and Thorium in the rocks: this contribution depends on the site but it is independent on depth.

- At higher energies, neutrons (energy up to GeV) are generated by muon spallation processes: this contribution is related to the site depth.
- Radioactive radon concentration in the air depends on local geology, but increases in closed halls. This can only be tuned by proper ventilation.
- Cosmogenic processes may produce radioactive nuclides.
- Concrete around the detector, supports, shielding, electrical connections, etc. contribute to the radioactive background.

3 Overview of underground laboratories

All the main sites available for astroparticle physics are reported in figure 1: Features of some of the main underground laboratories and facilities will be now taken into account.

Figure 1: Worldwide map of underground physics laboratories.

3.1 European facilities

- The INFN Gran Sasso National Laboratory (LNGS) is the largest underground laboratory and it is a worldwide facility for scientists - presently over 900 from 30 different Countries - working in one of the fifteen experiments currently in operation. LNGS (see figure 2) is near the town of L'Aquila and at about 120 kilometres from Rome. The underground facilities are located on one side of the ten-kilometre long highway tunnel crossing the Gran Sasso massif. They consist of three large experimental halls, each about 100 m long, 20 m wide and 18 m high and linked by service tunnels, for a total volume of about 180000 m^3. The average 1400 m rock coverage (3400 m.w.e.) gives a reduction factor of one million in the cosmic ray flux; moreover, the neutron flux is thousand times less than the one on the surface. LNGS scientific program is quite rich and includes: CNGS Project (CERN neutrinos to Gran Sasso) for OPERA and ICARUS experiments; dark matter search (DAMA-LIBRA, CRESST2, XENON, WARP); neutrinoless double beta decay (COBRA, CUORE, GERDA); neutrinos from Sun and geoneutrinos (BOREXINO);

neutrinos from galactic Supernova explosion (LVD); nuclear astrophysics (LUNA2). A special facility is dedicated to low radioactivity measurements.

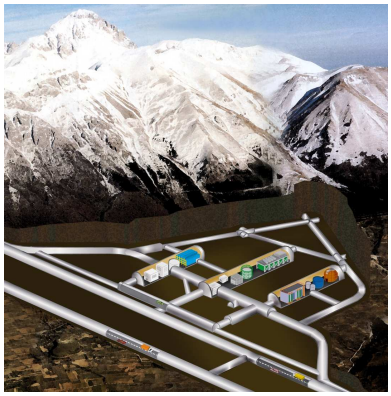

Figure 2: Sketch of the internal site of the Gran Sasso National Laboratory in Italy.

- Laboratoire Subterrain de Modane in France is running since 1982. The available volume for the experimental apparata is about 5000 m^3 while the rock overburden is 1700 m (4800 m.w.e.). The Laboratory houses two main detectors: NEMO3 (neutrinoless double beta decay) and EDELWEISS (dark matter), plus a low radioactivity counting facility. A huge expansion of the lab of 60000 m^3 is planned ('Ulisse project'), profiting of the construction of a new tunnel approved by French and Italian Governments.

- Underground structures of the Laboratorio Subterráneo de Canfranc were completed in 2005 though, due to several design and construction defects, repairs were needed. Surface infrastructures are under construction and the Lab will be completed by the end of this year. Its entrance is horizontal via one of the tunnels and access must be notified to the freeway tunnel control. The available volume for underground physics is about 9000 m^3, while maximum rock coverage is 850 m (2500 m.w.e.). The scientific plan for astroparticle physics includes experiments on dark matter (ANAIS and ROSEBUD) and on neutrinoless double beta decay (NEXT and BiPo, ancillary to superNEMO).

- The Boulby Palmer Laboratory is located in United Kingdom inside a potash mine 1100 m (2800 m.w.e.) deep under a flat surface. The salt environment limits the cavities width to about 5 m. The area for experiments is about 7000 m^3. The scientific program is focused on dark matter search: ZEPLIN III now running and DRIFT II in *R&D* phase. There are low radioactivity measurements and geophysics research. There is an excellent potential for expansion but the future is uncertain.

3.2 Asian facilities

- The Kamioka Observatory is located inside the Kamioka mine in Japan at a depth of about 1000 m (2700 m.w.e.). It was established in 1983 in order to host the Kamiokande experiment; the present observatory which belongs to the Institute for Cosmic Ray Research (ICRR) was established in 1995 after the completion of the excavation for the Super-Kamiokande project, the largest underground experiment presently devoted to T2K. The

present facility also contains KamLand and the XMASS experiment devoted to dark matter detection by using a single-phase liquid xenon detector. The research activities include neutrinoless $\beta\beta$ decay (Candles) and gravitational waves search (CLIO). To face the request from experimental collaborations for more space, the underground laboratory will be further extended.

- The Yangyang Underground Laboratory (Y2L) in Korea hosts KIMS experiment, and the China JingPing Laboratory (CJPL) in China hosts CDEX experiment; both Labs are planning expansions of their experimental area.

3.3 North America Laboratory

- The Canadian underground laboratory Snolab, located two kilometres below the surface in the Vale Inco Creighton Mine (near Sudbury), is an expansion of the facility constructed for the SNO solar neutrino experiment. Excavation and installation of the basic infrastructures of the new experimental halls and the outfitting in Phase I areas are complete. The experimental programme includes solar neutrinos, dark matter searches, neutrinoless $\beta\beta$ decay and the detection of neutrinos from Supernova. The SNO+ experiment will use the SNO detector filled with liquid scintillator; DEAP-I and PICASSO are currently operational and devoted to dark matter searches.

- Soudan Underground Laboratory (SUL) is located in the Soudan underground mine State Park and it is run by University of Minnesota. There are two major experiments, MINOS on the NUMI long baseline neutrino beam and CDMS devoted to dark matter searches.

- The proposed Deep Underground Science (physics, biology, and geology) and Engineering Laboratory (DUSEL) should be realized inside the Homestake mine in South Dakota. Due to the rich scientific program, Laboratory spaces will be built separately for biology, geology and physics. The two experimental sites for physics will be about 1450 m (3300 m.w.e.) and 2200 m (5000 m.w.e.) deep (see figure 3).

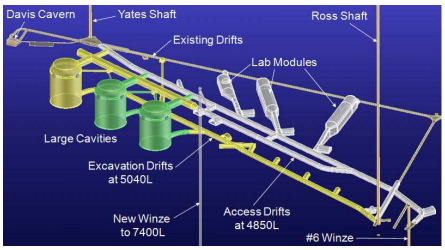

Figure 3: Layout of DUSEL in South Dakota (US).

4 Conclusion

Underground physics has therefore a glorious past but also a very bright future ahead. It will continue to significantly contribute to discovering fundamental laws that rule Nature and at the same time to unveil the mystery of the constituents of the Universe and its evolution.

WISP Perspectives at DESY

Joachim Mnich

Deutsches Elektronen-Synchrotron, Notkestraße 85, D-22607 Hamburg, Germany

DOI: http://dx.doi.org/10.3204/DESY-PROC-2010-03/Mnich_Joachim

The strategy concerning experiments at DESY searching for Weakly Interacting Slight Particles (WISPs) is sketched. Small and medium sized particle physics experiments at DESY provide interesting complementarity to LHC and ILC activities in several respects. Hence the DESY management is committed to support WISP searches also in future.

Particle physics activities at DESY contributes to understand the deepest structure of matter and the fundamental constituents and forces reigning the Universe. DESY has decided to concentrate its forces mainly on the high energy frontier. After the shutdown of HERA in summer 2007 (data analysis is still carried on) a large fraction of experimental particle physics at DESY concentrates on LHC related activities thereby exploiting DESY's expertise in planning, constructing and operating large complex facilities. In addition preparations towards a future International Linear Collider are ongoing.

In the recent years it became evident, that the competences and the technical infrastructure at DESY provide also opportunities for interesting small and medium sized particle physics experiments which are difficult to realize elsewhere. Most notably in this respect are the OLYMPUS (http://web.mit.edu/olympus/) and ALPS [1] activities. The search of ALPS at the "low energy frontier complements DESY's engagement at LHC to look for physics beyond the Standard Model at the TeV energy scale.

Besides its impact on physics the DESY management supports such activities due to several considerations:

- Small and medium scale experiments offer the opportunity to have on-site experimental particle physics activities at DESY in the LHC era.
- With experiments like ALPS DESY gets into contact to previously detached physics communities. The success of ALPS would not have been possible without the close collaboration with the laser and optics experts driving the large interferometers searching for gravitational waves. Such contacts broaden the DESY perspective and might lead to exciting new ideas also in future.
- Experiments like ALPS take place on a moderate time and budget scale. They allow young scientists to contribute to all stages of an experiment. This might be interesting for physicists not necessarily attracted by very large international collaborations.

ALPS has been a first step at DESY in this direction. It started only in 2007 and is meanwhile at the forefront of sensitivity in the search for WISPs [1]. However, due to the challenging

international competition DESY has to increase efforts in order to stay competitive. Hence the DESY management supports the planning and first steps towards an ALPS-II, leading to a Technical Design Report.

Other similar activities are the SHIPS experiment (looking for hidden photons from the sun [2]) and HIPS [3], which could tackle GeV dark forces. With the collaboration in the large LHC experiments, the IceCube detector at the south pole, the ILC preparation and a whole series of smaller projects as ALPS, HIPS, SHIPS and OLYMPUS, experimental particle physics at DESY has a broader spectrum than ever before.

References

[1] K. Ehret, "ALPS at DESY," these proceedings.

[2] J. Redondo, "Hidden Photons from the Sun," these proceedings.

[3] S. Andreas, "Current status of sub-GeV hidden particle searches," these proceedings.

List of Authors

List of Participants

Afanasev, Andrei – Hampton U/Jefferson Lab.
Albuquerque, Ivone – University of Sao Paulo
Allkofer, Yves – Universität Zürich
Anastassopoulos, Vassilis – University of Patras
Andreas, Sarah – DESY
Antoniadis, Ignatios – CERN
Arias, Paola – DESY
Arneodo, Francesco – LNGS Assergi
Avignone, Frank – University of South Carolina
Baker, Keith – Yale University
Balakishiyeva, Durdana – University of Florida, Gainesville
Baudis, Laura – Universität Zürich
Behrens, Annika – Universität Zürich
Bertolucci, Sergio – CERN
Bertone, Gianfranco – Universität Zürich and IAP
Brax, Philippe – CEA Saclay
Burdman, Gustavo – University of Sao Paulo
Cadamuro, Davide – MPI für Physik, München
Cantatore, Giovanni – University of Trieste
Caspers, Fritz – CERN
Cerulli, Riccardo – LNGS Assergi
Chung, Dan – University of Wisconsin, Madison
Creus, William – CERN
Davenport, Martyn – CERN
Döbrich, Babette – University of Jena
Edwards, Blair – Rutherford Laboratory
Ehret, Klaus – DESY
Engel, Andreas – Universität Zürich
Everett, Lisa – University of Wisconsin, Madison
Ferrella, Alfredo Davide – Universität Zürich
Frandsen, Mads – Oxford University
Gerbier, Gilles – CEA France
Giomataris, Ioannis – CERN
Hoedl, Seth – University of Seattle
Horns, Dieter – DESY
Irastorza, Igor – University of Zaragoza
Isern, Jordi – CSIC-IEEC
Jaeckel, Joerg – IPPP/Durham University
Jimenez, Raul – University of Barcelona
Katsanevas, Stavros – CNRS, Paris
Kim, Jihn E. – Seoul University
Kneiske, Tanja – Universität Hamburg

Lindner, Axel – DESY
Manalaysay, Aaron – Universität Zürich
Marrodán Undagoitia, Teresa – Universität Zürich
Mirizzi, Alessandro – DESY
Mnich, Joachim – DESY
Montanino, Daniele – Università di Salento
Montaruli, Teresa – University of Wisconsin, Madison
Moore, Ben – Universität Zürich
Moortgat, Filip – ETH Zürich
Newman, Seth – University of South Carolina
Oberlack, Uwe – Universität Mainz
Papaevangelou, Thomas – CERN
Phillips, Kenneth – University College London
Raffelt, Georg – MPI für Physik, München
Redondo, Javier – MPI für Physik, München
Regenfus, Christian – Universität Zürich
Ringwald, Andreas – DESY
Roncadelli, Marco – INFN, Pavia
Sabyasachi, Roy – IPPP/Durham University
Savage, Chris – University of Stockholm
Schumann, Marc – Universität Zürich
Servant, Geraldine – CERN
Siemko, Andrzej – CERN
Slocum, Penny – Yale University
Sparvoli, Roberta – University of Rome
Strigari, Louie – Stanford University
Verde, Licia – ICREA& ICC Barcelona
Votano, Lucia – LNGS Assergi
Walker, Daniel – University of Sheffield
Wester, William – Fermilab
Wikström, Gustav – University of Geneva
Williams, Peter – Daresbury Laboratory
Yamashita, Masaki – University of Tokyo
Zioutas, Konstantin – University of Patras

76 participants